# INVESTIGATING THE ROLE OF HISTIDINE IN MYC-DRIVEN TUMOURIGENESIS

**Ersa Gjelaj**

Department of Immunology and Inflammation,
Imperial College London (Crick)

*Supervisor:*
Dr. Mariia Yuneva

A thesis submitted for the degree of
Doctor of Philosophy

October 2024

## Statement of Originality

I Ersa Gjelaj confirm that the work presented in this thesis is my own. Where information has been derived from other sources, I confirm that this has been indicated in the thesis.

# Copyright

This thesis is licensed under a Creative Commons Attribution-Non Commercial-Share Alike 4.0 International License (CC BY-NC-SA 4.0).

Under this license, you may copy and redistribute the material in any medium or format. You may also create and distribute modified versions of the work. This is on the condition that: you credit the author and do not use it, or any derivative works, for a commercial purpose, and any adaptations must be distributed under the same license.

When reusing or sharing this work, ensure you make the licence terms clear to others by naming the licence and linking to the licence text. Where a work has been adapted, you should indicate that the work has been changed and describe those changes.

Please seek permission from the copyright holder for uses of this work that are not included in this licence or permitted under UK Copyright Law.

To view a copy of this license, visit https://creativecommons.org/licenses/by-nc-sa/4.0/.

# Abstract

The *MYC* oncogene reprograms cellular metabolism to fulfil the biosynthetic demands of cancer cells. A key aspect of this process involves the uptake of essential amino acids through the L-type amino acid transporter (LAT1), which is crucial for MYC-driven glutamine metabolism and tumour formation. LAT1 is an obligate antiporter, transporting amino acids across the membrane by exchanging an intracellular amino acid for an extracellular one. Given that glutamine, a bidirectional LAT1 substrate, serves as a primary fuel for the Krebs cycle, the heightened demand for glutamine in MYC-driven cancer cells could impact LAT1 function. Identifying how MYC-transformed cells maintain LAT1 activity during extensive glutamine catabolism could unveil potential metabolic vulnerabilities. This research reveals histidine as the primary bidirectional LAT1 substrate in Myc-driven mammary tumour cells and emphasizes the essential role of histidine in maintaining amino acid homeostasis. Our results demonstrate that Myc-driven mammary tumours exhibit increased histidine levels and uptake, influenced by glutamine availability. We show that histidine availability sustains LAT1-transport activity, mTORC1/4EBP1 signalling, and protein translation, providing Myc-driven tumour cells with a proliferative advantage. Under histidine scarcity, Myc- and Atf4-dependent upregulation of specific amino acid transporters, including Lat1, maintains essential amino acid levels and supports proliferation. We establish that histidine contributes to Myc-driven tumour growth and propose that dietary histidine restriction could be a viable treatment strategy on its own or in combination with other drugs. Together, these results identify histidine availability as a metabolic vulnerability in glutamine-addicted cancers and underscore its important role in maintaining amino acid homeostasis in Myc-driven cancer cells.

# Acknowledgement

I want to express my most sincere gratitude to everyone who has supported and guided me throughout the process of completing this thesis. First and foremost, I am immensely thankful to my PhD supervisor, Mariia Yuneva, whose contagious enthusiasm for science has been profoundly impactful. Her invaluable guidance and unwavering encouragement have been instrumental in shaping this work. I would also like to thank the members of the Yuneva lab, both past and present: Amy, Asad, Giulia, Josep, Michael, Shravan, Weigang, Avinash, Andy, Brinnie, Chandan, Lili, Peter, Richard, Sam, Wei C., Wei D., and Yulia. Thank you for the last 4 years, what I have learned from everyone is invaluable, and I am incredibly excited to see the amazing work that each of you will continue to contribute. I would also like to express my gratitude to our extended metabolism family, the Anastasiou lab, for their expertise and support, and Antonia for being a constant support system as we journeyed through life as PhD students in cancer metabolism.

I could not have done this without the support of my thesis committee, Holger Auner, Alex Gould, James Macrae, and Cristina Lo Celso. Their expertise and guidance have been instrumental to my work, and I consistently left every thesis committee feeling motivated and excited to do science.

I want to thank the science technology platforms and services at the Francis Crick Institute for their support throughout this project. In particular, the Metabolomics STP has been integral to this work. My sincere thanks go to James Macrae and Paul Driscoll, especially, for his expertise and efforts, which have had a tremendous impact on this project. I am also grateful to the Biological Research Facility, Saidu Sesay and Adebambo Adekoya, and everyone who contributed to supporting the animal work in this thesis. I would also like to thank the Experimental Histopathology, Flow Cytometry, Bioinformatics and Biostatistics STPs for their technical assistance and guidance. Finally, I wish to acknowledge the hard work of those who ensure smooth day-to-day operations and maintain a

safe and supportive environment at the Crick. Being able to do this PhD in such an exceptional environment is a privilege I immensely appreciate.

I would not be where I am today without the sacrifices of my parents, Halil and Kozeta; they are my harbour, and I could not have navigated this PhD journey without them. To my sisters, Mimi and Alba, who I adore, thank you for being constant sources of motivation and joy. To my dearest friends, thank you for always being there for me, even when oceans separate us. A heartfelt thanks to Frank for sacrificing his weekends to sit in the Crick with me, your support has been invaluable. Finally, I want to thank my dog, Lulu, for being the biggest cutie pie, always offering the sweetest cuddles and goofiest faces.

Over the final years of this degree, we have witnessed an ongoing human rights catastrophe that has deprived countless children and young adults in Gaza of their futures as potential scientists, thinkers, and leaders. I would be remiss not to acknowledge this profound loss of both human life and potential in Palestine. This work is dedicated to the students who will never have the opportunity to study, learn, and contribute- whose brilliance the world will never get to see.

# Table of Contents

*Abstract……* ..... *4*

*Acknowledgement* ..... *5*

*Table of Contents* ..... *7*

*Table of figures* ..... *12*

*List of tables…* ..... *17*

*Abbreviations* ..... *18*

*Chapter 1. Introduction* ..... *21*

**1.1 Breast Cancer** ..... **21**

1.1.1 Overview of Subtypes ..... 22

1.1.2 Triple Negative Breast Cancer ..... 24

**1.2 MYC** ..... **28**

1.2.1 MYC in cancer ..... 29

1.2.2 MYC in TNBC ..... 31

1.2.3 Targeting MYC Therapeutically ..... 33

1.2.4 Myc-driven metabolic rewiring ..... 34

**1.3 SLC7A5/LAT1** ..... **44**

1.3.1 SLC transporters ..... 44

1.3.2 LAT1 Structure and Function ..... 49

1.3.3 Glutamine in LAT1 Function ..... 53

1.3.4 Histidine in LAT1 Function ..... 54

**1.4 Histidine and its role in cancer** ..... **55**

1.4.1 Histidine Metabolism ..... 55

1.4.2 Histidine Metabolism in Cancer ..... 56

**1.5 Thesis Aims** ..... **58**

*Chapter 2. Materials & Methods* ..... *59*

**2.1 Reagents and Chemicals** ..... **59**

**2.2 Cloning** ..... **64**

2.2.1 CRISPR-Cas9 ..... 64

2.2.2 Plasmid Construction for Protein Overexpression ..... 66

2.2.3 Transformation and Amplification of Plasmids ..... 68

**2.3 Cells and *in vitro* experimental procedures ..... 68**
2.3.1 Cells ..... 68
2.3.2 Generating Stable Knockdown Cell Lines ..... 70
2.3.3 Generating Stable Knockout Cell Lines ..... 70
2.3.4 Generating Stable Overexpression Cell Lines ..... 71
2.3.5 Small Molecule Inhibitors ..... 72
2.3.6 Proliferation Assays ..... 72
2.3.7 SUnSET ..... 72
2.3.8 BrdU-PI Cell Cycle Analysis ..... 72
2.3.9 Immunofluorescence ..... 74
**2.4 Mouse models and *in vivo* experimental procedures ..... 75**
2.4.1 Mouse Models ..... 75
2.4.2 Tumour initiation by Mammary Fat Pad Injection ..... 75
2.4.3 Diets ..... 76
2.4.4 JPH203 Preparation and Administration ..... 77
2.4.5 Stable-isotope Labelling ..... 78
2.4.6 IVIS Bioluminescence Imaging ..... 78
2.4.7 Tumour Interstitial Fluid Collection ..... 79
2.4.8 In vivo SUnSET ..... 79
2.4.9 Immunohistochemistry and Analysis ..... 79
2.4.10 Cytokine Array ..... 80
2.4.11 IFNγ Assay ..... 81
**2.5 Tumour Slice Culture ..... 81**
2.5.1 Tissue Processing ..... 81
2.5.2 Culture Conditions ..... 81
**2.6 Metabolomics for LC-MS ..... 82**
2.6.1 Tissue ..... 82
2.6.2 Cells ..... 83
2.6.3 Protein Quantification from MeOH:Chloroform Lysates ..... 84
2.6.4 Media/Serum ..... 84
2.6.5 LC-MS Data Analysis ..... 85
**2.7 Quantitative Real-Time PCR ..... 86**
2.7.1 RNA Extraction ..... 86
2.7.2 Reverse Transcription ..... 86
2.7.3 qPCR ..... 87
**2.8 Immunoblotting ..... 87**

2.8.1 Cell and tissue lysis ..... 87
2.8.2 SDS-PAGE ..... 88
**2.9 Computational Analysis ..... 89**
2.9.1 RNA-seq Data Analysis ..... 89
**2.10 Quantification and Statistical Analysis ..... 91**
***Chapter 3. MYC-driven mammary tumours have an increased demand for histidine 93***
**3.1 Introduction ..... 93**
**3.2 Lat1 mRNA and protein levels are significantly upregulated in Myc-driven mammary gland tumours. ..... 95**
**3.3 Myc-driven mammary gland tumours have increased histidine uptake. 98**
**3.4 Histidine is primarily catabolised in the liver of healthy animals. ..... 101**
**3.5 Myc-driven tumour cells do not catabolise histidine. ..... 105**
**3.6 Discussion ..... 108**
***Chapter 4. Glutamine availability influences histidine requirement.....113***
**4.1 Introduction ..... 113**
**4.2 Myc-driven cancer cells depend on exogenous glutamine for central carbon metabolism and proliferation. ..... 115**
**4.3 Exogenous glutamine limitation increases cellular requirement for histidine. ..... 119**
**4.4 Glutamine Synthetase levels are negatively correlated with histidine requirement in BC cell lines. ..... 123**
**4.5 The ectopic overexpression of GS in Myc-driven tumour cell lines did not maintain glutamine pools. ..... 127**
**4.6 Glutamine compensates for histidine limitation. ..... 130**
**4.7 Myc-driven mammary gland tumours depend on exogenous glutamine for tumour growth ..... 131**
**4.8 Discussion ..... 135**

*Chapter 5. Histidine is the preferred LAT1 exchange factor in Myc-driven cancer cells139*

**5.1 Introduction ..... 139**

**5.2 Histidine is exchange for amino acids through LAT1..... 142**

**5.3 Histidine is the preferred LAT1 exchange substrate in Myc-driven tumour cells. ..... 155**

**5.4 Interrogating the role of asparagine during amino acid starvation..... 163**

**5.5 Histidine preloading primes cells for increased mTORC1/4E-BP1 signalling. ..... 168**

**5.6 Assessing histidine exchange in tumours. ..... 182**

**5.7 Discussion ..... 200**

*Chapter 6. Histidine availability is a targetable metabolic vulnerability in Myc-driven tumourigenesis .....206*

**6.1 Introduction ..... 206**

**6.2 Histidine is important in maintaining amino acid homeostasis..... 210**

**6.3 Myc and Atf4-mediated transcription facilitates SLC transporter response to histidine limitation..... 218**

**6.4 LAT1 inhibition does not reduce tumour burden in Myc- or ErbB2-driven mammary gland tumours. ..... 226**

**6.5 Histidine is required for Myc-dependent mammary tumourigenesis. .. 229**

**6.6 Dietary histidine limitation invokes systemic changes in metabolism.237**

6.6.1 Amino acid profiles are altered in mice fed a histidine reduced diet. ..... 237

6.6.2 Rewiring of glutamine metabolism ..... 241

**6.7 Dietary histidine limitation is less effective in immunocompromised mice. 246**

**6.8 Discussion ..... 254**

*Chapter 7. Discussion .....263*

**7.1 MYC-driven metabolic reprogramming: glutamine utilisation and LAT1 substrates..... 264**

**7.2 Histidine in mTORC1/4E-BP1 activation in MYC-dependent cancers .. 265**

**7.3 Implications for histidine in AA homeostasis in MYC-dependent cancers 267**

**7.4 Therapeutic targeting of histidine: dietary restriction, transport inhibition in MYC-dysregulated breast cancer and beyond ..... 271**

**7.5 Limitations ..... 274**

**7.6 Future Directions..... 276**

**7.7 Concluding Remarks ..... 277**

***Reference List .....279***

***Appendix .....305***

# Table of figures

Figure 1-1. Molecular subtypes within clinical subtypes of breast cancer.....23
Figure 1-2 The percentage of MYC amplified tumours within each subtype.....33
Figure 1-3. MYC-regulated metabolic pathways in cancer[46]. .....35
Figure 1-4. Glutamine as a nitrogen donor[122].....38
Figure 1-5. Mechanisms of mTORC1 activation via amino acids.....43
Figure 1-6. Prominent structures associated with members of the SLC transporter superfamily. .....46
Figure 1-7. Overview of SLC transporter amino acid exchange mechanisms. .....47
Figure 1-8. Simplified schematic of histidine metabolism.....56
Figure 3-1. Myc-driven MGTs have increased expression of Slc7a5/Lat1.....97
Figure 3-2. Myc-driven MGTs have increased uptake of histidine. .....99
Figure 3-3. Other transporters may compensate for LAT1 inhibition in Myc-driven MGTs. .....100
Figure 3-4. Histidine metabolism is tissue-specific.....104
Figure 3-5. Histidine is not catabolised in MYC-driven MYAZ tumour cells. .....107
Figure 4-1.ErbB2 is lost from MMTV-ErbB2 MGT-derived tumour cell lines.....117
Figure 4-2.Myc-driven tumour cells are glutamine auxotrophs. .....118
Figure 4-3.Myc-driven tumour cells use glutamine as the primary fuel for the Krebs cycle.....119
Figure 4-4. Glutamine limitation increases histidine uptake in Myc-driven cancer cells.....121
Figure 4-5.Cells cultured in low glutamine have increased histidine efflux. .....122
Figure 4-6.GS expression positively correlates with glutamine independence. ....125
Figure 4-7.Glutamine dependent BC cells have increased histidine uptake. .....127
Figure 4-8.Overexpression of GLUL did not confer glutamine independence in Myc-driven tumour cells.....128
Figure 4-9.GLUL/GS overexpression did not compensate for glutamine limitation. .....129
Figure 4-10. Glutamine can rescue proliferation under histidine limitation. .....131
Figure 4-11.Myc-driven MGTs rely on dietary glutamine. .....132

Figure 4-12. MGTs from mice fed a QDD maintain glutamine levels and Krebs cycle intermediates. ..... 134
Figure 4-13. MGTs from mice fed a QDD did not have increased histidine uptake. ..... 135
Figure 5-1.Histidine is effluxed from the cell in Myc-dependent tumour cells. ..... 144
Figure 5-2. Histidine preloaded cells have increased uptake of specific amino acids. ..... 146
Figure 5-3.Histidine preload increases uptake of specific amino acids in TNBC cell lines. ..... 148
Figure 5-4. Histidine exchange is mediated through a stereoselective transporter. ..... 150
Figure 5-5. Histidine is a bidirectional LAT1 substrate that facilitates uptake of EAAs. ..... 152
Figure 5-6. Histidine exchange can be blocked by pharmacological inhibition of LAT1. ..... 155
Figure 5-7. Histidine is a more efficient LAT1 substrate than glutamine. ..... 157
Figure 5-8. Glutamine is used to fuel the Krebs cycle even during amino acid starvation. ..... 158
Figure 5-9. Glutamine is used for NEAA biosynthesis during amino acid starvation. ..... 159
Figure 5-10. Histidine is used as the preferential LAT1 exchange substrate at physiological levels. ..... 162
Figure 5-11. Asparagine levels increase during amino acid starvation in a glutamine-independent manner. ..... 164
Figure 5-12. Asparagine is released through proteolysis. ..... 166
Figure 5-13. Genes enriched in asparagine codons are associated with GO terms involving the plasma membrane. ..... 167
Figure 5-14. Histidine availability enhances mTORC1/4E-BP1 signalling in Myc-dependent cancer cells. ..... 170
Figure 5-15. mTORC1 activation is dependent on LAT1. ..... 172
Figure 5-16. Histidine preload enhances protein translation. ..... 175
Figure 5-17. Amino acid-starved cells have increased transcription of ribosomal biogenesis genes. ..... 179
Figure 5-18. Histidine preload does not significantly increase cell replication. ..... 182

Figure 5-19. Overnight fasting in mice results alters amino acid profiles in serum. .....184
Figure 5-20. A single bolus of histidine is unable to increase histidine levels in fasted mice. .....185
Figure 5-21. Similar metabolic changes are observed in fasted tumours and amino acid starved tumour cells. .....188
Figure 5-22. mTORC1 signalling was unaffected in fasted mice. .....190
Figure 5-23. Histidine availability enhances mTORC1/4E-BP1 signalling and protein translation in MGT *ex vivo* cultures. .....193
Figure 5-24. LAT1 KO cells have reduced leucine uptake and proliferation. .....196
Figure 5-25. LAT1 was not knocked out efficiently in vivo .....199
Figure 6-1. Regulation of ATF4 translation by the ISR. .....207
Figure 6-2. Histidine limitation induces expression of ASCT2. .....211
Figure 6-3. Histidine limitation enhances transcription of amino acid transporters. .....213
Figure 6-4. Intracellular amino acid levels increase under histidine limitation. .....215
Figure 6-5. Histidine and leucine deprivation induce macroautophagy and proteasomal degradation to similar extents. .....218
Figure 6-6. Transcriptional response to histidine limitation is only partially dependent on Myc. .....219
Figure 6-7. Transcriptional response to histidine limitation is partially dependent on Atf4. .....221
Figure 6-8. Histidine limitation induces Myc and Slc transporters in Myc-low cells. .....222
Figure 6-9. Transcriptional response to histidine limitation is partially dependent on Atf4 in 67NR cells. .....224
Figure 6-10. Histidine limitation sensitizes 67NR cells to LAT1 inhibition. .....225
Figure 6-11. LAT1 inhibition is insufficient to inhibit Myc-driven tumour growth. ..228
Figure 6-12. A histidine deficient diet results in significant weight loss. .....230
Figure 6-13. A 25% histidine diet significantly reduces serum histidine without affecting body weight. .....232
Figure 6-14. The HRD significantly attenuates Myc-driven mammary tumourigenesis. .....234

Figure 6-15. The HRD impacts tumour growth independent of protein translation. .....235
Figure 6-16. Significant reduction of protein translation was observed in another cohort of mice fed a HRD. .....237
Figure 6-17. The HRD significantly alters amino acid profiles in the serum, MGT, and liver. .....240
Figure 6-18. Glutamine metabolism is rewired in MGTs from mice fed a HRD. ...242
Figure 6-19. GOT1 and GOT2 are upregulated in MGTs from mice fed a HRD...245
Figure 6-20. The HRD does not alter cell proliferation or induce apoptosis in MGTs. .....246
Figure 6-21. Mammary tumours from mice fed a HRD have increased immune infiltration. .....247
Figure 6-22. The HRD increases IFNy and reduces IL-4 levels in the MGT. .....249
Figure 6-23. MGTs from mice fed a HRD have increased TAMs.....251
Figure 6-24. The immune system contributes to the anti-tumour efficacy of the HRD. .....253
Figure 7-1.Proposed model of the role of histidine in Myc-independent and dependent cancer cells. .....278
Appendix 1. Characterization of cell lines used. .....305
Appendix 2. RNA-sequencing of HCC and BC cell lines.....306
Appendix 3. Histidine-mediated exchange for specific amino acids blocked by LAT1 inhibition. .....307
Appendix 4. Histidine is a more efficient exchange factor for EAAs than glutamine. .....308
Appendix 5. Histidine is a more efficient LAT1 exchange substrate than asparagine or glutamine. .....309
Appendix 6. Differential activation of RPS6 and inhibition of 4E-BP1 is mediated through mTORC1. .....310
Appendix 7. MYC regulates ribosome biogenesis. .....311
Appendix 8. Histidine preload does not significantly affect cell size.....312
Appendix 9. LAT1 inhibition by JPH203 significantly retards cell proliferation. .....312
Appendix 10. Mice fed a 50% histidine diet have impaired glucose clearance. ....313
Appendix 11. Mice fed a HRD do not have significantly altered food consumption. .....313

Appendix 12. A HRD significantly reduces Myc-driven tumour growth. .....314

# List of tables

Table 1-1. Key characteristics of metabolic subtypes in TNBC.....27
Table 1-2. Characteristics of SLC subfamilies that transport amino acids.....48
Table 1-3. Classification of LAT transporters. .....51
Table 2-1. Stable Isotopes.....59
Table 2-2. qPCR primers.....59
Table 2-3. Recombinant DNA.....60
Table 2-4. Antibodies used for WB, IF, and IHC analysis. .....60
Table 2-5. Chemicals and Reagents. .....62
Table 2-6. Commercial Assays and Kits.....64
Table 2-7. sgRNA oligonucloetides .....64
Table 2-8. Components of reaction to anneal oligonucleotides .....65
Table 2-9. Restriction enzyme digest of FgH1tUTG.....65
Table 2-10. GLUL targeting primers with attB flanks for Gateway™ cloning. .....66
Table 2-11.Thermocycling conditions for GLUL primers. .....67
Table 2-12. MMEC media composition. .....69
Table 2-13. Medium I Composition.....82

# Abbreviations

| | |
|---|---|
| 4E-BP1 | eukarytoic Initiation Factor **4E**-**B**inding **P**rotein **1** |
| a-KG | **alpha K**eto**g**lutarate |
| ACC | **A**cetyl-**C**oA **c**arboxylase |
| ACLY | **A**TP **C**itrate **Ly**ase |
| AFMID | Arylformamidase |
| ALL | **A**cute **L**ymphoblastic **L**eukemia |
| ASCT2 | **A**lanine-**S**erine-**C**ysteine **T**ransporter **2** |
| ASNS | **A**sparagine **S**ynthetase |
| ATF4 | **A**ctivating **T**ranscription **F**actor **4** |
| BBB | **B**lood-**B**rain **B**arrier |
| BC | **B**reast **C**ancer |
| BCAA(s) | **B**ranched-**C**hain **A**mino **A**cid(s) |
| BCKA(s) | **B**ranched-**C**hain **K**eto**a**cid(s) |
| bHLH | **B**asic **H**elix **L**oop **h**elix |
| BrdU | Bromodeoxyuridine |
| bZIP | **B**asic Leucine **Zip**per |
| CAT | **C**ationic **A**mino Acid **T**ransporter |
| CD | **C**ontrol **D**iet |
| CNV | **C**opy **N**umber **V**ariation |
| CS | **C**arnosine **S**ynthase |
| EAA(s) | **E**ssential **A**mino **A**cid(s) |
| EGFR | **E**pidermal **G**rowth **F**actor **R**eceptor |
| eIF2a | **e**ukaryotic **I**nitiation **F**acto**r 2 alpha** |
| eIF4E | **e**ukaryotic **I**nitiation **F**actor **4E** |
| ER | **E**strogen **R**eceptor |
| FASN | **F**atty **A**cid **S**ynthase |
| FE | **F**ractional **E**nrichment |
| FIGLU | **F**orm**i**mino**glu**tamate |
| FTCD | **F**ormimino**t**ransferase **C**yclo**d**eaminase |
| G-6-P | **G**lucose-**6**-**P**hosphate |
| G6PD | **G**-**6**-**P D**ehydrogenase |
| GAP | **G**TPase **A**ctivating **P**rotein |
| GCN2 | **G**eneral **C**ontrol **N**onderepressible **2** |
| GLS | Glutaminase |
| GLUT | **Glu**cose **t**ransporter |
| GS | **G**lutamine **S**ynthetase |
| HAL | **H**istidine **A**mmonia **L**yase |
| HCC | **H**epato**c**ellular **C**arcinoma |
| Hcy | Homocysteine |
| HDC | **H**istidine **D**e**c**arboxylase |

| | |
|---|---|
| HER2 | **H**uman **E**pidermal Growth Factor **R**eceptor-2 |
| HRD | **H**istidine **R**educed **D**iet |
| IDO | **I**ndoleamine-Pyrrole 2,3-**D**i**o**xygenase |
| iMMECs | **I**mmortalized **M**ouse **M**ammary **E**pithelial **C**ells |
| IP | **I**ntra**p**eritoneal |
| ISR | **I**ntegrated **S**tress **R**esponse |
| IV | Intravenous |
| KD | **K**nock**d**own |
| KO | **K**nock**o**ut |
| LAPTM4B | **L**ysosomal Protein Transmembrane 4 beta |
| LAT | **L**-type **A**mino Acid **T**ransporter |
| LDH | **L**actate **D**e**h**ydrogenase |
| LeuT | **Leu**cine **t**ransporter |
| LRS | **L**eucyl-t**R**NA **S**ynthetase |
| MAX | **M**yc-**a**ssociated Factor **X** |
| MFP | **M**ammary **F**at **P**ad |
| MFS | **M**ajor **F**acilitator **S**uperfamily |
| MGT(s) | **M**ammary **G**land **T**umours(s) |
| MMTV | **M**ouse **M**ammary **T**umour **Vi**rus |
| mORF | **M**ain **O**pen **R**eading **F**rame |
| MS | **M**ethionine **S**ynthase |
| mTORC1 | **m**ammalian **T**arget **o**f **R**apamycin **C**omplex **1** |
| NEAA(s) | **N**on-**E**ssential **A**mino **A**cid(s) |
| NMG | **N**ormal **M**ammary **G**land |
| OAA | **O**xalo**a**cetic **A**cid |
| OE | **O**ver**e**xpressing |
| OG | **O**ral **G**avage |
| OS | **O**verall **S**urvival |
| PARP | **P**oly (**A**DP-**R**ibosome)-**P**olymerase |
| PC | **P**yruvate **C**arboxylase |
| PERK | **P**KR-like **ER K**inase |
| PHGDH | **Ph**ospho**g**lycerate **D**e**h**ydrogenase |
| PI | **P**ropidium **I**odide |
| PI3K | **P**hospho**i**nositide **3**-**K**inase |
| PPP | **P**entose **P**hosphate **P**athway |
| PR | **P**rogesterone **R**eceptor |
| PSAT | **P**hospho**s**erine **A**mino**t**ransferase |
| PSPH | **P**hospho**s**erine **P**hosp**h**atase |
| QDD | Glutamine (**Q**) **D**eficient **D**iet |
| RPS6 | **R**ibosomal **P**rotein **S6** |
| RTK | **R**eceptor **T**yrosine **K**inase |

| | |
|---|---|
| S6K1 | **R**ibosomal **P**rotein **S6 K**inase beta-1 |
| SAH | **S**'**a**denosyl**h**omocysteine |
| SAM | **S**'**a**denosyl**m**ethionine |
| SCD | **S**tearoyl-CoA **De****s**aturase |
| SHMT | **S**erine **H**ydroxy**m**ethyl**t**ransferase |
| SLC | **S**o**l**ute **C**arrier |
| SNAT | **S**odium-Dependent **N**eutral **A**mino Acid **T**ransporter |
| SQ | Subcutaneous |
| SUnSET | **Su**rface **Sen**sing of **T**ranslation |
| TAD | **T**rans**a**ctivation **D**omain |
| TAMs | **T**umour **A**ssociated **M**acrophages |
| TCGA | **T**he **C**ancer **G**enome **A**tlas |
| THF | **T**etra**h**ydro**f**olate |
| TIF | **T**umour **I**nterstitial **F**luid |
| TME | **T**umour **M**icro**e**nvironment |
| TN | **T**riple **N**egative |
| uORF | **u**pstream **O**pen **R**eading **F**rame |
| UPR | **U**nfolded **P**rotein **R**esponse |
| UPS | **U**biquitin **P**roteasome **S**ystem |
| UROC1 | Urocanase |

# Chapter 1. Introduction

## 1.1 Breast Cancer

At the outset of this PhD project, breast cancer became recognised as the most commonly diagnosed cancer among women in 159 countries[1]. Surpassing lung cancer as the dominant cause of cancer death in women in 110 countries. Indeed, in 2020, there were 2.3 million cases of BC diagnosed globally, making it responsible for 1 in 6 cancer-related deaths among women[2]. In the United Kingdom, BC is the most commonly diagnosed cancer, accounting for 15% of all cancers diagnosed[3]. Much of this is due to increased detection through organised mammographic screenings, which are associated with increased BC incidence rate[2,4]. Indeed, the majority of cases are diagnosed at earlier stages as a result of routine mammographic screenings[4,5]. Therefore, this early detection gives BC patients a better prognosis than other aggressive cancers. Breast cancer that is detected when it is localised (stage I to II) has a 99% 5-year survival rate, which drops to 86% for regional disease (stage II to III) and 27% for metastatic disease (stage IV)[6]. Significantly, although high-resource countries observe the highest incidence rates of BC, low-resource countries experience disproportionately higher mortality rates[2]. Even within high-resource countries, women of African descent demonstrate an increased mortality rate compared to other demographics, which is not fully explained by socioeconomic status or access to healthcare[2,7,8]. If these trends continue, and without accounting for the effect of the COVID-19 pandemic on breast cancer screening[9,10], the global burden of BC is projected to rise to 3 million new cases and 1 million deaths per year by 2040, solely due to population growth and ageing[2]. This underscores the critical need to enhance treatment strategies and improve our understanding of the risk factors to effectively manage the burden of BC on the population and public healthcare system.

The most significant risk for breast cancer is age, with greater than 70% of BC cases observed in women over 50 years old[2]. However, there are many risk factors associated with BC, which vary depending on the subtype. These include genetic, reproductive (menopause status, age at first birth, breastfeeding, parity), and lifestyle-related factors (diet, metabolic syndrome, exercise)[11–13]. Significantly,

these risk factors unequally impact each subtype of BC. While molecular subtypes of breast cancer can share some similarities, they are often regarded as distinct diseases due to their unique biological behaviours, responses to treatments, and clinical outcomes. Therefore, understanding the biological differences between subtypes is crucial for developing targeted therapies.

### 1.1.1 Overview of Subtypes

Classical classification of BC subtypes relies on immunohistochemical scoring of the expression of hormone receptors for estrogen (ER), progesterone (PR), and human epidermal growth factor (HER2, encoded by *ErbB2*)[14]. Therefore, the four widely recognised breast cancer subtypes fall into their respective groups depending on the expression of these receptors. These subtypes include luminal A, luminal B, HER2-positive, and triple-negative (TN). Loosely, these subtypes are grouped based on ER expression. Luminal A/B tumours are characterised as primarily HER2-negative ER+/ PR+/-, whereas HER2-positive express HER2 and are ER-negative[14]. In contrast, the TN subtype is characterised by the absence of these hormone receptors and can be further classified into basal-like or claudin-low, among others[14]. Classification into these subtypes is required to tailor treatment strategies, which have successfully treated hormone-receptor positive and HER2-positive tumours.

Incorporating molecular subtyping of BC samples alongside traditional immunohistochemical classification can improve patient stratification[15]. This ensures the best treatment strategies are implemented while elucidating other potential therapeutic targets. Global gene expression profiling has identified four subtypes: ER-positive Luminal-like (ErbB2-low, further classified into Luminal-A and B[15,16]), basal-like (ER-negative), ErbB2-positive (ER-low), and normal-like[16]. Notably, while these subtypes were broadly characterised as ER-high and ER-low, significant variation and overlap exist within these categories (Figure 1-1). Subsequent research from van ’t Veer *et al.* (2002) demonstrated that gene expression profiling of BC can reveal differences in disease outcomes among these subtypes[17]. In addition to improved identification of patients that would benefit from adjuvant chemotherapy and hormone- or HER2- targeted therapies, this can also

identify specific genes associated with tumours with worse prognoses. Gene expression assays, such as Oncotype DX, are now frequently used in breast cancer treatment[18]. This highlights the substantial genetic variation within each subtype and underscores the importance of identifying these subtypes for tailored treatment strategies and improved patient outcomes.

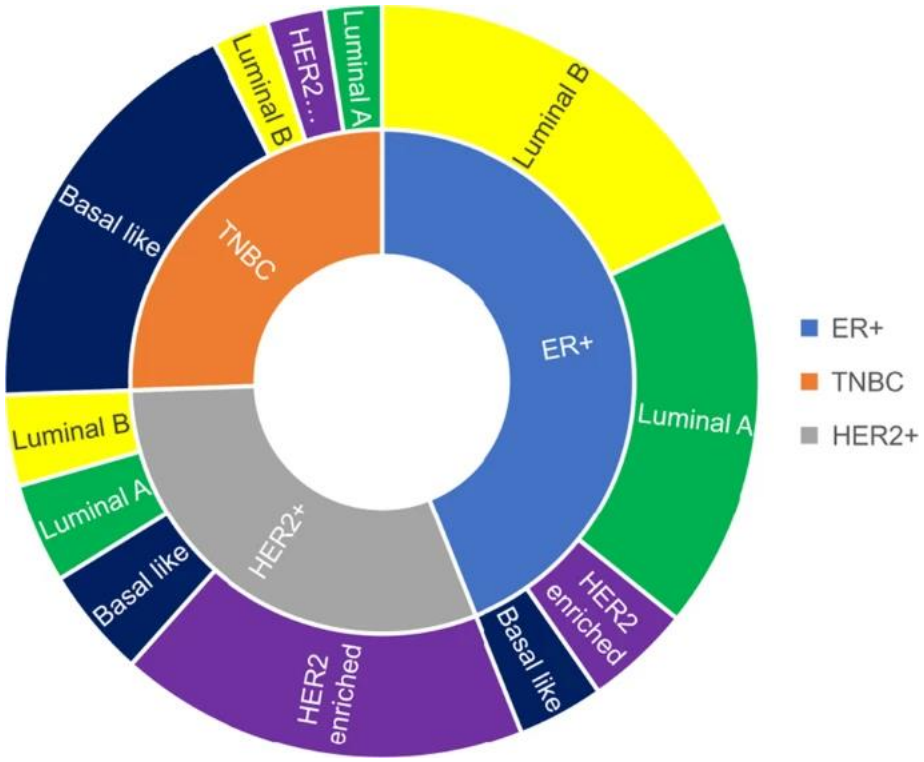



**Figure 1-1. Molecular subtypes within clinical subtypes of breast cancer.** Reproduced Fig.1 from Zagami & Carey (2022), *Triple negative breast cancer: Pitfalls and progress*, *npj Breast Cancer*[19]. Licensed under a Creative Commons Attribution 4.0 International License. No changes were made to this image.

#### *1.1.1.1 Prognosis*

Classification of tumours provides valuable prognostic information and guides treatment decisions. Luminal-A tumours account for 50-60% of breast cancers. As mentioned above, luminal-A tumours are ER+, PR≥20%, HER2 negative, and Ki67 (marker for proliferation index)-low[20]. Luminal-A BC has a favourable prognosis, with low relapse rates[15,21–23]. Luminal-B tumours account for 15-20% of BCs and can be HER2-positive or negative[15,20]. They are associated with high Ki67 scores and have a similar prognosis to non-luminal subtypes if left untreated[24]. These are typically associated with an aggressive phenotype, with worse overall survival

(OS)[15,21,25]. As a standard, tumours in which more than >1% of cells express ER by immunohistochemistry are considered ER-positive and are typically treated with adjuvant endocrine therapy, such as tamoxifen or aromatase inhibitors[26,27].Gene expression assays can aid in determining whether an ER+ tumour patient would benefit from chemotherapy in addition to endocrine therapy[26,28]. Recently, there has been increased interest in treating HER2-low tumours, which are more common in ER-positive than ER-negative BC, with HER2-targetting treatments such as trastuzumab antibody-drug conjugate, which improved outcomes for this tumour type[29,30]. HER2-positive tumours account for 15-20% of BCs, display over-expressed or amplified HER2/ErbB2, and lack ER and PR[15,20]. These tumours are highly proliferative and aggressive, and without treatment they have poor prognosis and OS[27]. HER2-positive breast cancers have greatly benefited from HER2-targeted therapy, trastuzumab being one of the first treatments approved in combination with chemotherapy as an adjuvant therapy for HER2-positive BC[27]. Triple-negative breast cancer accounts for 15-20% of BCs and is common in women younger than 40[31], women of African descent[8], and BRCA1 mutation carriers[32]. TNBC is heterogeneous and displays several subtypes. However, the basal-like subtype accounts for 70-80% of TNBC cases[19,20]. Due to the lack of hormone receptors and HER2 expression in TNBC, it has limited response to adjuvant endocrine or HER2-targetted therapy. Therefore, management often requires a combination of chemotherapy, surgery, and radiation[33]. Basal-like tumours have a poor prognosis, decreased time to relapse, and an increased likelihood of metastasis to the brain and visceral organs compared to the other subtypes[19,33,34]. Underscoring the unmet requirement for alternative therapeutic targets for this BC subtype.

### 1.1.2 Triple Negative Breast Cancer

Triple-negative BC is an aggressive subtype of breast cancer characterised by poor prognosis, shorter disease-free survival (8% to 16%), and a high risk of relapse. Furthermore, TNBC is more likely to be detected as an interval cancer, emerging between routine screenings rather than during scheduled screenings[35]. This contributes to later-stage detection, increasing the likelihood of metastatic disease

and significantly reducing survival rates from 91% in localised BC to just 12% in metastatic cases[36] Furthermore, women diagnosed with stage IV TNBC have an average OS of 12 months, compared to 36 months for those with ER+ /HER2- negative tumours[37]. This highlights the challenge of treating TNBC. Besides surgery, the mainstay treatment is chemotherapy, used in both neoadjuvant and adjuvant settings. However, Poly (ADP-ribose) polymerase (PARP) inhibitors, immune checkpoint inhibitors (ICIs), and antibody-drug conjugates (ADCs) have been approved for the treatment of advanced-stage TNBC in the United States and Europe[36]. In addition, gene expression profiling of tumours has revealed numerous potential targets in TNBC, some of which are in phase I/II clinical trials for TNBC. For example, the RAS/MAPK and PI3K/AKT/mTOR pathways downstream of receptor tyrosine kinases, such as epidermal growth factor receptor (EGFR), are dysregulated in TNBC. However, EGFR inhibitors such as gefitinib and afetinib have shown limited efficacy in phase II trials in TNBC[38,39]. Indeed, gefitinib as a neoadjuvant therapy with chemotherapy did not significantly improve complete response or overall objective response compared to the placebo-treated group[38]. Furthermore, gefitinib led to increased toxicity, with many patients discontinuing treatment due to adverse events. While afatinib had limited efficacy in a phase II trial as a standalone neoadjuvant therapy, a subsequent phase I study demonstrated more promise when combined with chemotherapy[40]. However, recent results suggest that many TNBC patients were resistant to afatinib targeted-EGFR inhibition due to compensation from PI3K (Phosphoinositide 3-kinase) and JAK2 (Janus kinase 2) pathways[41]. Similarly, inhibitors targeting the PI3K pathway, such as Buparlisib showed limited efficacy in TNBC in a phase II trial[42]. These results highlight the challenges in developing treatments that effectively target TNBC and underscore the value of identifying novel targets. Notably, the role of metabolic reprogramming in TNBC has been increasingly recognised, revealing ample metabolic targets that could offer effective treatment options for this challenging BC subtype.

#### *1.1.2.1 Metabolic reprogramming in TNBC*

Metabolic reprogramming has been considered a hallmark of cancer since 1924, when Otto von Warburg discovered the uncoupling of glycolysis from oxygen in

proliferating cancer cells – termed the Warburg effect[43]. Just over a century past this pivotal discovery, cancer is understood to be a complex metabolic disease. While the metabolic reprogramming of cancer presents powerful therapeutic potential, the metabolic flexibility inherent to these cells calls for careful consideration. Proto-oncogenes often control metabolic activities; however, not all metabolic activities are essential for the survival of cancer cells. Therefore, determining which enables survival is necessary to identify exploitable targets[44]. Gong *et al.* (2021) utilised multiomic data from a TNBC cohort and identified that TNBCs could be stratified into three metabolic subtypes (Table 1-1)[45]. Metabolic-Pathway-Stratification (MPS)-1 correlated with the luminal androgen receptor subtype and was characterised by a lipogenic phenotype. Indeed, tumours of this subtype had increased mRNA expression of metabolic genes involved in lipid synthesis, which correlated with a significant accumulation of lipids. MPS2 was characterised by glycolytic, with increased pathways enriched for glycolysis, Krebs cycle, and purine and pyrimidine metabolism. These tumours were identified as comprising the basal-like subtype and were associated with worse relapse-free survival. A specific metabolic phenotype or molecular subtype did not characterise the MPS3 subtype. Notably, TNBC cell lines and patient-derived organoids that recapitulate MPS-1 and MPS-2 subtypes were sensitive to inhibitors that target de novo lipid synthesis and glycolysis, respectively. Importantly, MPS1 tumours had a higher frequency of PI3K (PIK3CA, PIK3R1, PTEN) and receptor tyrosine kinase (RTK)-Ras (HRAS) mutations than MPS2 and MPS3 subtypes. Notably, this could suggest that targeting metabolic pathways in combination with growth factor signalling inhibitors (such as those currently in phase I/II trials) may be a potential therapeutic strategy.

**Table 1-1. Key characteristics of metabolic subtypes in TNBC.**
Based on metabolic pathway subtypes described in Gong et al., (2021)[45]. *RFS: relapse free survival.*

| Subtype | TNBC Subtype | Metabolic Phenotype | Metabolic Pathways | Therapeutic Sensitivity | Prognostic Implications |
|---|---|---|---|---|---|
| **MPS1** | Luminal Androgen Receptor | Lipogenic | Lipid metabolism: fatty acid, cholesterol, and steroid biosynthesis | Sensitive to lipid synthesis inhibitors | Favourable (3-year RFS, 91%) |
| **MPS2** | Basal-like | Glycolytic | Carbohydrate and nucleotide metabolism: Krebs cycle, purine/pyrimidine | Sensitive to glycolysis inhibitors | Poor (3-year RFS, 81%), high tumour grade |
| **MPS3** | Mixed | Mixed | Partial dysregulation of metabolic pathways | No specific drug sensitivity profile identified | Favourable (3-year RFS, 91%) |

*MYC* (encoding c-MYC, and henceforth MYC) is a proto-oncogene that orchestrates cell metabolism, including genes involved in glycolysis, glutaminolysis, and biosynthesis (which will be discussed in greater detail in the next section)[46]. Although MYC was not identified as uniquely enriched in any metabolic subtypes, it was amplified in 29.1% of the MPS-1, 40.0% of MPS-2, and 38.8% of MPS-3, highlighting the broad impact MYC has on cellular metabolism and metabolic reprogramming. Importantly, in a multi-platform genomic and transcriptomic analysis of 825 BCs, MYC hyperactivation was identified as a critical oncogenic driver in basal-like subtypes of TNBC and amplified in 40% of TNBC[45,47]. Although amplification of chromosome 8q24, where MYC is located, occurs across all BC subtypes, it is amplified MYC that uniquely characterises the basal-like molecular subtype[47]. Chandriani *et al.* (2009) identified a “Core MYC Signature”, a set of 398 genes responsive to MYC activation[48]. Compared to microarray data from 146 breast tumour samples, hierarchical clustering revealed that basal-like tumours exhibited the highest levels of MYC expression and a significant overlap with the Core MYC Signature. Suggesting that MYC has a prominent role in this breast cancer subtype[48]. Therefore, identifying metabolic vulnerabilities associated with MYC-driven metabolic rewiring of TNBC is warranted and necessary.

Understanding the metabolic adaptation of this challenging breast cancer subtype and how these adaptations contribute to metastasis and drug resistance will be imperative to inform treatment strategies that can work in combination with established TNBC therapies, such as immunotherapy.

## 1.2 MYC

Cancer has historically been studied as a proliferative disorder driven by oncogenes. However, producing the biomass necessary to sustain the proliferation of cancer cells requires a coordinated network driven by MYC. The primary function of MYC is to transcriptionally regulate cell mass through an extensive and varied repertoire of transcriptional targets[49]. Cellular biomass constitutes proteins, lipids, and nucleic acids, the biosynthesis of which is dependent on metabolic pathways that acquire, utilise, and produce various nutrient sources. The role of MYC as a metabolic regulator was first noted in 1997 when lactate dehydrogenase (LDH) was discovered as a MYC target gene that cooperates with MYC-mediated transformation of fibroblast cells[50,51]. Subsequently, MYC was shown to regulate the transcription of most glycolytic enzymes[52]. Fast forward three decades, MYC is considered a master regulator of metabolism, coordinating the uptake of nutrients, their catabolism, and their use as building blocks for macromolecule biosynthesis. Given the widespread dysregulation of *MYC* across many cancer types, identifying effective therapeutic strategies has been a significant research priority in the field. However, challenges in directly targeting MYC have led to the exploration of alternative strategies. One promising avenue is MYC-driven metabolic rewiring, which supports the aberrant cellular growth caused by MYC hyperactivation but also presents an Achilles' heel. Consequently, significant research efforts have sought to identify metabolic dependencies and vulnerabilities in MYC-amplified tumours. The role of MYC in cancer and emerging therapeutic strategies targeting metabolism in these tumours will be discussed in detail below.

### 1.2.1 MYC in cancer

The oncogenic potential of MYC was recognised during a period when viral infections were established as the cause of animal tumours; a time that saw significant discoveries in oncogenes[53]. Before MYC was identified as a proto-oncogene, researchers had isolated a retrovirus, MC29, from avian tumours[54]. This virus was shown to have the ability to transform cells *in* vitro. Subsequent studies revealed that the retroviruses contained a specific 1500 bp nucleotide sequence; this sequence was named v-Myc, reflecting its role in **my**elo**c**ytomatosis, a type of tumour that affects chickens[54]. Subsequently, the sequence encoding v-MYC was found in the genomes of uninfected vertebrates beyond just birds. This led to the hypothesis the MC29 virus had acquired this sequence from the host genome[54]. This sequence was confirmed to be a critical transforming element of these retroviruses[55,56], leading to significant research efforts to understand its function and role in oncogenesis. Indeed, MYC was quickly recognised as a human oncogene after it was found to be involved in chromosomal translocations in Burkitt lymphoma[57,58].

MYC is a basic-helix-loop-helix (bHLH) protein that binds with preference to the canonical E-box[59], 5'-CACGTG-3', dependent on dimerization with another bHLH protein, MYC-associated factor-X (MAX)[60]. Three paralogs, c-MYC, N-MYC, and L-MYC, comprise the MYC family of proteins. c-MYC is ubiquitously expressed, whereas N-MYC and L-MYC are found in specific tissues[61]. In normal healthy cells, MYC expression correlates with periods of cellular growth and is a critical regulator of genes involved in cell cycle, growth, and proliferation[62]. Indeed, MYC regulates the expression of many genes that positively regulate the cell cycle while simultaneously inhibiting those that act as negative regulators[63]. However, beyond its role in cell cycle regulation, MYC regulates apoptosis through the intrinsic apoptosis pathway, effectively balancing pro-survival and pro-apoptotic signals. This duality in MYC-targeted transcription prevents unchecked cellular growth and proliferation. However, dysregulation of MYC disrupts this balance, highlighting its potential to drive oncogenesis. As a result, MYC is under tight control in normal healthy cells at transcriptional and post-translational levels. Concordantly, MYC is a short-lived protein that is degraded within 20 minutes[64]. MYC levels are primarily

regulated by the ubiquitin-proteasome system (UPS), where MYC is polyubiquitinated and degraded by the 26S proteasome[65,66,62]. This process involves three key enzymes: E1 activates ubiquitin in an ATP-dependent manner, E2 transfers the activated ubiquitin to the target protein, and E3 ligases facilitate the transfer of ubiquitin to the target, with E3s determining substrate specificity[65]. Polyubiquitin chains, primarily at lysine 48 (K48), are formed and recognized by the 26S proteosome for degradation. The selectivity of the UPS is influenced by degron elements within MYC's transactivation domain (TAD), which interact with E3 ligases to regulate MYC stability[67]. A number of E3 ligases regulate MYC stability, but the best-studied is Fbw7, which requires phosphorylation MYC at T58 and S62 within its TAD[68,69]. Phosphorylation of S62, driven by signalling pathways such as ERK, stabilizes MYC but also primes phosphorylation of T58 by GSK3-β[70]. This results in the dephosphorylation of S62 and recognition of phosphorylated T58 by Fbw7, leading to MYC degradation. MYC is activated downstream of multiple signalling pathways, requiring the integration of signals from growth factors and nutrients[71]. Not surprisingly, tumours induced by MYC often acquire additional genetic alterations that uncouple MYC input from growth factor signalling pathways or checkpoints[71]. This is evidenced by a transgenic model with tetracycline-inducible MYC under an MMTV (mouse mammary tumour virus) promoter, which develops mutations in potent oncogenes such as Kras[72]. Notably, MYC-driven tumours lacking concurrent Kras mutations regressed upon de-induction of MYC. This highlights that while MYC can initiate tumourigenesis, its oncogenic potential is enhanced through the acquisition of additional mutations, highlighting its role in both the initiation and progression of tumours.

Genetic alterations of *MYC* are observed across myriad tumours. Indeed, some of the estimations suggest that MYC is dysregulated in up to 70% of all cancers[46]. Significantly, elevated *MYC* expression in cancers can occur without direct genetic alterations in *MYC.* This elevation is often driven by oncogenic signalling pathways, such as aberrant PI3K/AKT signalling resulting from PIK3CA mutations[73]. While protein stabilising mutations in *MYC* have been described in Burkitt's lymphoma[64,74], these are relatively rare compared to *MYC* copy number gains. Indeed, recurrent mutations in MYC occur in only about 0.7% of cancers in The Cancer Genome Atlas (TCGA) database, a pan-cancer atlas of genome

sequencing across 33 cancers. At the same time, amplification of at least one of the *MYC* paralogs is detected across all cancers[73]. Indeed, analysis of *MYC* alterations across this database revealed amplification of *c-MYC* across 21% of all cancers[73]. Notably, MYC amplification appears to be more frequent in some cancer types than others. A meta-analysis of MYC amplification across 26 distinct studies of human BC revealed that, on average, 1 in 6 breast cancers have amplification of *MYC*, with a 95% confidence interval of 12.5 - 18.8%[75]. Furthermore, the authors suggested that MYC amplification could be an independent prognostic factor for BC. Using 6 of the 26 studies revealed that patients with *MYC*-amplified tumours had decreased disease-free survival and OS. These patients were approximately twice as likely to experience relapse or death compared to those without MYC amplification[75]. Furthermore, the frequency of MYC amplification was increased in the high-grade tumours, from 12.5% for grade I tumours to 31.4% for grade 3[75]. However, other studies suggest this may be observed in up to 70% of high-grade BCs[76].These results indicate a role for MYC in aggressive tumour types and underscore the importance of understanding how MYC induces and enables BC.

### 1.2.2 MYC in TNBC

The association of MYC in BC was recognised in 1986, shortly after the discovery of v-Myc. Escot *et al.* (1986) observed frequent amplification of MYC in 38% of a small cohort of 121 human primary BCs[77]. Within the next decade, significant research emerged on the frequency of MYC alterations in breast cancer, observing amplification of MYC in 1 to 50% of BCs[75]. An association between MYC and basal-like BC was demonstrated by seminal research from Perou *et al.* (2000)[78]. Gene expression profiling of breast cancer revealed that certain genes were associated with specific subtypes, as mentioned above. Among these genes, they observed an increased frequency of enhanced MYC expression in basal-like tumours (50%) compared to luminal (11%) and ErbB2-overexpressing (9%) tumours[78]. More recently, analysis of MYC expression across subtypes in two different breast cancer databases (TCGA and METABRIC) revealed significant bias for MYC amplification in the basal-like subtype[79]. Indeed, 34.05% (TCGA) and 44.02% (METABRIC) of basal-like tumours had MYC amplification, compared to

7.22% (TCGA) and 12.99% (METABRIC) in Luminal A tumours (Figure 1-2)[79]. Notably, nearly ¾ of BRCA1-mutated breast cancers are of the TNBC subtype. However, significant variability from 42-100% was noted across studies[32]. MYC amplification is a common feature of BRCA1-dysregulated breast tumours. Indeed, MYC amplification was observed in up to 53% of BRCA1-mutated tumours and 23% of tumours without BRCA1 mutations. However, more than half of these tumours lacking mutations in BRCA1 exhibited promoter hypermethylation, highlighting the association between MYC amplification and dysregulated BRCA1[80–82]. BRCA1 has been demonstrated to bind MYC and form complexes that modulate the transcriptional activity of MYC[81,82]. Therefore, loss of BRCA1 function could drive amplification of MYC or aberrant MYC regulation[81,82]. Currently, an alternative treatment for TNBC is neoadjuvant therapy with PARP1 inhibitors, such as olaparib[19,33]. Cells with BRCA1/2 mutations cannot repair DNA through homologous recombination. Therefore, they rely more on PARP1 to repair single-stranded DNA breaks, sensitising them to PARP1 inhibition[83]. However, PARP1 inhibitors such as Olaparib have shown limited efficacy in patients with germline BRCA mutations and TNBC at both early- and late-stage due to resistance mechanisms[19,36,84]. Strikingly, combining CDK inhibition with PARP inhibition suppresses MYC, thereby preventing MYC-induced restoration of homologous recombination in TNBC xenografts[83,85]. Indeed, MYC amplification has been linked to drug resistance across various tumour types, highlighting the critical need to identify and target MYC-driven dependencies in TNBC. Given the limited treatment options available for TNBC, addressing these dependencies could significantly enhance therapeutic strategies. These synthetic lethal interactions targeting MYC-dependencies in TNBC have emerged over the last decade and include metabolic targets such as glutamate and fatty acid biosynthesis[86]. However, significant work remains to fully understand these mechanisms and translate these findings into effective clinical treatments.

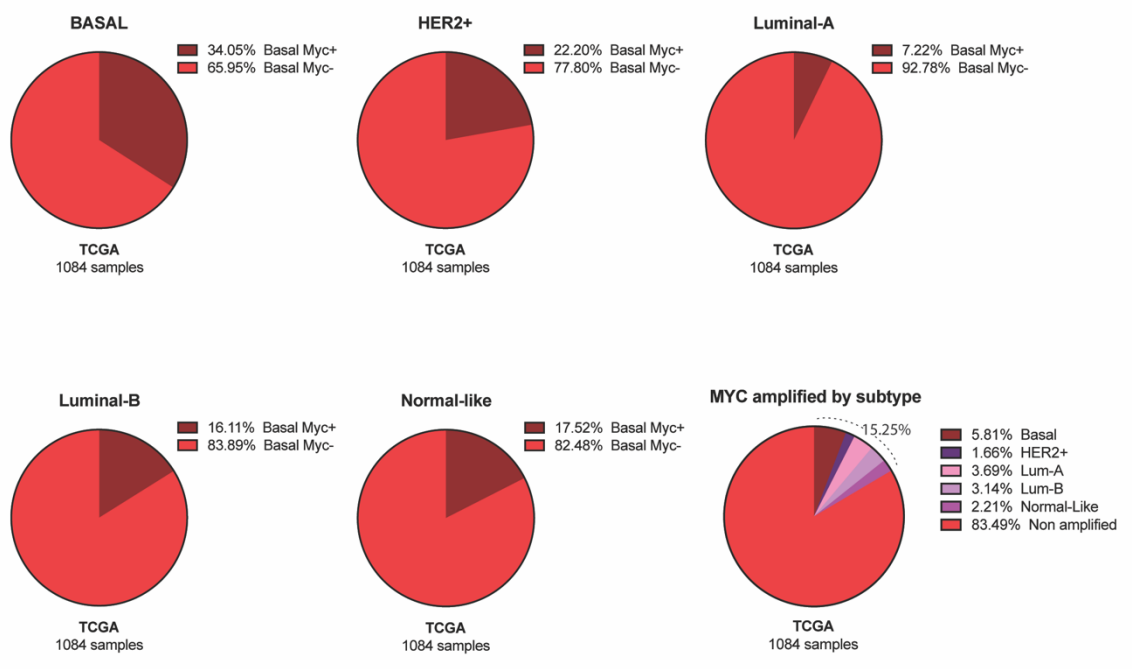



**Figure 1-2 The percentage of MYC amplified tumours within each subtype.** Data from the TCGA database (n=1084). Data adapted for visual presentation from Table 1 from AlSultan et al. (2020), Investigational New Drugs, © 2020 Springer Nature[79]. Reproduced with permission. License ID: 5877841268828.

### 1.2.3 Targeting MYC Therapeutically

In preclinical tumour models, ablating MYC inhibits or retards tumour growth, underscoring its therapeutic potential[72,87]. However, significant barriers have hindered the development of MYC-targeted inhibitors. MYC is often considered "undruggable" due to its structure, which is not conducive to small molecule enzymatic or allosteric inhibitors[88]. Additionally, its nuclear localisation makes it inaccessible to larger monoclonal antibodies[88]. However, several strategies show potential in targeting MYC[88,89]. These include (i) inhibition of MYC-MAX dimerization (see review on OmoMYC[90]), (ii) prevention of MYC expression, and (iii) exploiting synthetic lethal interactions, a strategy particularly relevant to this thesis, which aims to target vulnerabilities specific to MYC-dependent cancers.

Metabolic rewiring driven by MYC-hyperactivation is a double-edged sword. While increased nutrient uptake and catabolism give MYC-driven cancer cells a fitness advantage over other cells in the tumour microenvironment (TME), it also leads to metabolic dependencies. As the tumour grows, the ever-changing TME, characterised by poor vascularization, hypoxia, and limited nutrient availability, can

disproportionately affect MYC-driven cancer cells that have been rewired to rely on specific nutrients to meet their biosynthetic demands. As a result, identifying metabolic genes that are synthetic lethal with MYC overexpression has become a key area of interest. However, few enzymes in metabolic pathways have been identified as synthetic lethal with MYC in screens[91,92]. It is important to note that metabolic rewiring is influenced not only by oncogenes like *MYC* but also by the tissue of origin[93]. Thus, synthetic lethal interactions identified in cell lines with ectopic MYC expression[91,92,94,95] may not accurately reflect the tissue-specific metabolic vulnerabilities driven by MYC. Another challenge is that MYC hijacks metabolic pathways essential for normal proliferating cells, which may limit the potential of synthetic lethal interactions that selectively target MYC-overexpressing cells. Therefore, the impact on normal cells must be considered when identifying metabolic vulnerabilities in MYC-dependent tumours. Despite these challenges, targeting various aspects of MYC-driven metabolic rewiring in preclinical cancer models has shown promising efficacy[46,71].

### 1.2.4 Myc-driven metabolic rewiring

Over the past 30 years, research into MYC's role in cancer has expanded dramatically from the initial discoveries of LDHA and ornithine decarboxylase as its first target genes[50,71,96]. MYC has since been implicated in nearly every aspect of cellular metabolism, influencing processes like carbohydrate metabolism, oxidative phosphorylation, fatty acid metabolism, nucleotide biosynthesis, and amino acid metabolism (Figure 1-3)[46,71,87]. Initially, cancer metabolism research was dominated by the "Warburg Effect", which centred on glucose as the primary fuel for cancer cells. However, a pivotal study by Yuneva *et al.* (2007) shifted the focus towards glutamine as a critical nutrient for cancer cell survival and proliferation[97], laying the groundwork for the last decade and a half of research into oncogene-induced metabolic rewiring. While this study coined the term glutamine "addiction" from glutamine deprivation studies in MYC-transformed cells, it expanded beyond glutamine by highlighting the potential role of other amino acids in tumourigenesis, often driven by MYC and other oncogenes[98]. Despite these advances, much of the research has concentrated on a handful of nutrients, while other vital nutrients and

amino acids remain less understood. Identifying the role of these overlooked nutrients, alongside advancing therapeutic strategies against existing metabolic targets, is necessary.

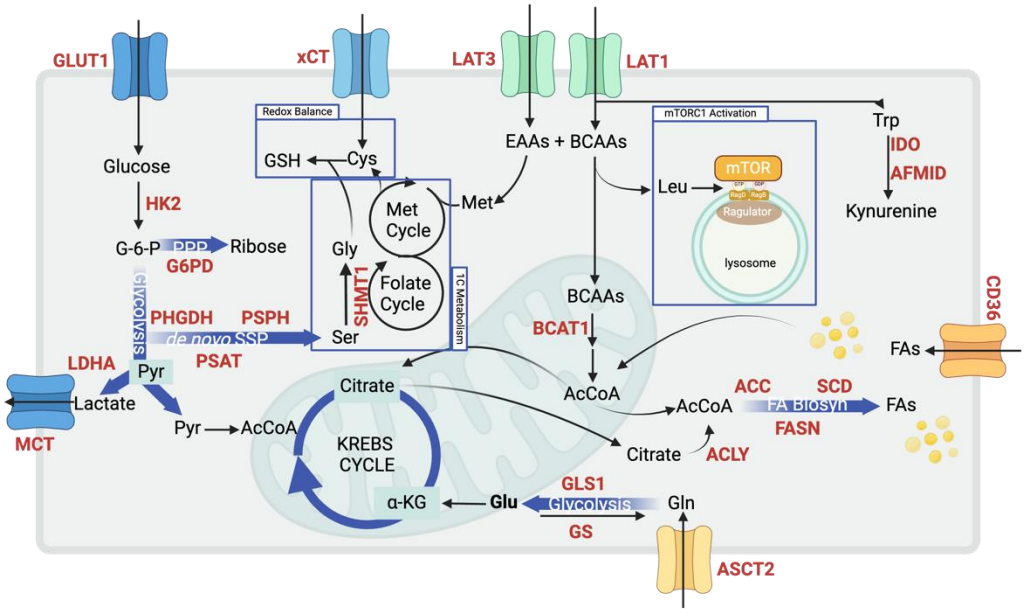



**Figure 1-3. MYC-regulated metabolic pathways in cancer[46].**
Enzymes highlighted in red are known direct or indirect targets of MYC activation. Glucose enters the cell through the glucose transporter (GLUT)[52] and is phosphorylated by hexokinase (HK) to form glucose-6-phosphate (G-6-P). G-6-P can proceed through glycolysis or the pentose phosphate pathway (PPP). The PPP, facilitated by G-6-P-dehydrogenase (G6PD), generates 2 NADPH and 1 ribose per glucose molecule, contributing to nucleotide synthesis. In parallel, G-6-P can also feed into the *de novo* serine biosynthesis pathway. This pathway, branching off from 3-phosphoglyceric acid, is driven by phosphoglycerate dehydrogenase (PHGDH), phosphoserine aminotransferase (PSAT), and phosphoserine phosphatase (PSPH)[99]. Serine (Ser) is subsequently converted to glycine (Gly) by serine hydroxymethyltransferase 1 (SHMT1, cytoplasmic isoform), a key enzyme in the folate cycle and one carbon (1C) metabolism, which is crucial for nucleotide biosynthesis, antioxidant production, and methylation processes[100]. The methionine cycle regenerates methionine (Met) and produces cysteine (Cys) from homocysteine and serine. Cys, along with Gly and glutamate (Glu), is a crucial component of glutathione (GSH), essential for neutralising reactive oxygen species (ROS). The xCT transporter also facilitates cysteine import into cells[101]. Lactate is generated from pyruvate (Pyr) by LDHA[52]. Alternatively, Pyr can enter the Krebs cycle, be converted to acetyl-CoA (AcCoA), and subsequently be used to generate citrate from oxaloacetate. Citrate can either continue through the Krebs cycle or be exported into the cytoplasm, where it is then converted into AcCoA by ATP Citrate Lyase (ACLY). This cytoplasmic AcCoA is utilised for fatty acid (FA) synthesis involving Acetyl-CoA carboxylase (ACC), fatty acid synthase (FASN), and stearoyl-CoA desaturase (SCD)[102]. Free FAs can also be imported via the FA transporter, CD36. Glutamine (Gln) is transported into cells by alanine-serine-cysteine transporter 2 (ASCT2), serving as an anaplerotic substrate for the Krebs cycle. It is converted into Glu via glutaminase (GLS1) or vice versa via glutamine synthetase (GS). Glu can then be converted into alpha-ketoglutarate (α-KG). EAA transporters, LAT1/3 mediate branched-chain amino acids (BCAAs, leucine, valine, isoleucine), which are then converted to branched-chain keto

acids (BCKAs) via branched-chain amino acid transaminase 1 (BCAT1)[103]. BCKAs produce AcCoA, which fuels the Krebs cycle and FA synthesis. Leucine (Leu) is also critical for activating the mammalian target of rapamycin complex 1 (mTORC1), a key regulator of cellular growth and translation. Tryptophan (Trp) plays. A significant role in cancer metabolism is converted into kynurenine through the action of indoleamine-pyrrole 2,3-dioxygenase (IDO) and arylformamidase (AFMID). This image was created with biorender.com.

#### *1.2.4.1 Glutamine Metabolism*

Glutamine is a primary biosynthetic resource for cancer cells, providing both carbon and nitrogen for the production of nucleotides, amino acids, and lipids[46]. Additionally, glutamine catabolism (glutaminolysis) fuels the Krebs cycle, supporting the bioenergetic demands of cancer cells[104]. Glutamine can be synthesised from glutamate and ammonia via glutamine synthetase (GS), which is highly expressed in tissues such as the liver, kidney, skeletal muscle, and brain[105]. The skeletal muscle and liver are major amino acid reservoirs, allowing cells to maintain glutamine levels through *de novo* synthesis and uptake under normal physiology[106,107]. Notably, GS expression can predict glutamine dependence. Luminal BC cells, which express high levels of GS, are insensitive to exogenous glutamine[108]. In contrast, basal BC cells have low GS expression, rendering them glutamine-auxotrophic[108,109]. High GS expression is also linked with slower-growing, less aggressive luminal A BCs, whereas basal BCs with low GS expression are more proliferative and aggressive[110]. In agreement, tissues with high self-renewal capacity, such as the intestine, rely on exogenous glutamine to fuel the Krebs cycle[106]. Similarly, MYC-driven transformation increases glutamine demand Krebs cycle anaplerosis[97,111]. Indeed, MYC-overexpressing cells divert glucose from the Krebs cycle, secreting glucose-derived metabolites as lactate while using glutamine to fuel the Krebs cycle[111]. As a result, MYC-driven cancer cells are susceptible to glutamine depletion, which can be rescued by supplementing cells with intermediates of the Krebs cycle, such as membrane soluble, dimethyl α-ketoglutarate (α-KG)[111]. This regulation of both glycolysis and glutamine metabolism by MYC provides cancer cells with the metabolic intermediates necessary for nucleotide, non-essential amino acids (NEAAs), and FA synthesis, as well as a rapid supply of ATP generation, all of which are necessary for biosynthesis[112]. Glutamine metabolism is further regulated by the enzyme glutaminase (GLS), which converts glutamine to glutamate (Figure 1-3)[111].

MYC indirectly upregulates GLS by repressing microRNAs, mir-23a/b, which generally suppress GLS expression[113]. There are two GLS isoforms: GLS1, the predominant form in most tissues, and GLS2, primarily expressed in the liver, brain, and pancreas[114]. High GLS1 expression is associated with poor outcomes in BC patients, particularly in basal-like BCs, which exhibit high GLS1 and low GS levels, correlating with decreased survival. Conversely, luminal BCs have low GLS1 but high GS expression, contributing to a more favourable prognosis.

The heightened expression of GLS1 in TNBC has positioned it as a promising therapeutic target. The GLS1 inhibitor CB-839 has shown effectiveness in preclinical models of TNBC[109,115]. However, due to tumour heterogeneity, GLS1 inhibition alone is often insufficient, prompting the exploration of additional therapeutic targets that sensitise cells to GLS inhibition[116]. These targets, which vary across tumour types, include glycolysis[117–120], FA oxidation[121,122], and cystine import via xCT[123–125]. The combination of GLS1 inhibitors with inhibitors of these pathways has shown promise. Understanding the compensatory mechanisms of tumours is crucial as it can guide the development of more effective therapies. For instance, the potential synthetic lethality with GLS1 inhibition is its paralog, GLS2. GLS2 can compensate for GLS1 inhibition in cells that express both paralogs[116,126]. Luminal BCs have high expression of GLS2, whereas TN or basal-like subtypes of BC do not express GLS2 expression[127]. Coincidentally, luminal breast cancer cells are relatively resistant to GLS inhibition compared to TNBC due to compensation from GLS2[127]. Targeting both GLS1 and GLS2, therefore, is a better strategy for this breast cancer subtype. This highlights how even tumours originating from the same origin can have different compensatory mechanisms determining their treatment response.

In addition to being a carbon doner, glutamine donates amino and amido groups for various biosynthetic processes. Glutamate derived from glutamine can be converted to α-KG through glutamate dehydrogenase (GLUD1/2), producing ammonia as a byproduct. Alternatively, aminotransferases can transfer the glutamine-derived amino group from glutamate to produce NEAAs such as alanine, aspartate, serine, and α-KG for the Krebs cycle (Figure 1-4)[128]. Many cancers upregulate aminotransferases to support NEAA production, redox balance,

nucleotide biosynthesis, and Krebs cycle anaplerosis[129–132]. Indeed, ectopic overexpression of GLUD1 was sufficient to reduce cellular proliferation due to reduced aminotransferase activity in mammary epithelial cells, highlighting the importance of these pathways to normal cellular function and tumourigenesis[128,133]. Targeting aminotransferase activity, for example, with aminooxy acetic acid, has shown potential in preclinical models[117,129,132]. Glutamine also supports *de novo* nucleotide synthesis as a nitrogen donor, donating its amido group for *de novo* pyrimidine and purine synthesis (Figure 1-4)[128,134]. This metabolic flexibility allows cancer cells to exploit glutamine in a tumour and oncogene-specific manner[124,135–141]. Beyond its role as a metabolic precursor, glutamine also regulates the mammalian target of rapamycin complex 1 (mTORC1) by mediating the uptake of EAAs[142], indicating a significant role for glutamine in cellular growth.

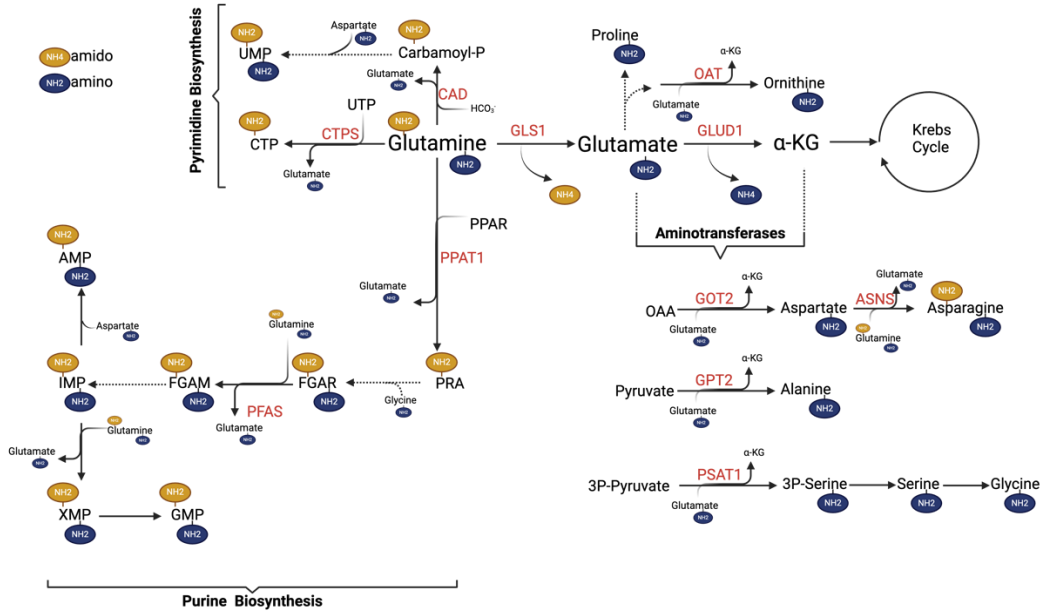



**Figure 1-4. Glutamine as a nitrogen donor[128].**
GLS1 converts glutamine to glutamate, donating its carbon skeleton and amino group. Glutamate can be converted to α-KG through GLUD1 and release ammonia or through aminotransferases, which produce α-KG and NEAAs. Glutamine can also directly contribute its amido group to pyrimidine and purine synthesis. *GLS1*: Glutaminase. *GLUD1*: Glutamate dehydrogenase 1. *OAT*: Ornithine aminotransferase. *GOT2*: glutamic-oxaloacetic transaminase 2. *GPT2*: glutamic-pyruvic transaminase 2. *PSAT1*: phosphoserine aminotransferase 1. *CAD*: Carbamoyl-phosphate synthetase 2, aspartate transcarbamylase, and dihydroorotase. *CTPS*: Cytidine triphosphate synthetase. *PPAT1*: palmitoyl protein thioesterase 1. *PFAS*: phosphoribosylformylglycinamidine synthase.

The increased demand for glutamine in cancer cells is met by amino acid transporters from the solute carrier (SLC) family, including high-affinity glutamine

transporters, sodium-dependent neutral amino acid transporter 1/2 (SNAT1/2), and alanine-serine-cysteine transporter 2 (ASCT2)[143,144]. These transporters are often upregulated during tumourigenesis and can be regulated by MYC and cellular stress[113,145]. The potential of targeting glutamine uptake, either through transporter inhibition or dietary restriction, offers a promising therapeutic strategy. However, the redundancy of SLC transporters and their overlapping substrate specificities complicate targeted approaches[144,146]. Indeed, while ASCT2 knockout (KO) initially slowed tumour growth in a TNBC xenograft, upregulation of SNAT1 and SNAT2 compensated for the loss of ASCT2, resulting in minimal impact on overall tumour burden[146]. ASCT2 is of particular interest due to its upregulation in MYC-driven cancers[147]. Inhibition of ASCT2 activity, through gene interference or inhibition, has been shown to impair tumourigenesis[147–151]. Although ASCT2 inhibitors such as GPNA and V-9032 have demonstrated promising results, issues in selectivity have hindered their clinical translation[152–155]. Furthermore, while ASCT2 is considered the primary glutamine transporter in cancer, it also transports other neutral amino acids such as serine, asparagine, or threonine, all of which have essential roles. Recently, ASCT2 has been identified as a critical transporter for serine uptake in cancer cells[156]. Therefore, inhibiting amino acid transporters could have serious off-target effects if the metabolic dependencies of specific tumour types are not well understood.

An alternative strategy is to starve cells of glutamine, exploiting the fact that tumours often have lower glutamine levels compared to circulation and in normal tissues[141]. However, several challenges arise: (i) the skeletal muscle and liver can provide glutamine through *de novo* glutamine synthesis or proteolysis[157], (ii) immune cells rely on glutamine for anti-tumour functions[158], (iii) NEAAs can protect cells from glutamine depletion[141]. Different NEAAs have been demonstrated to protect cells from glutamine limitation across cancer models[135,137,141,159,160]. Determining which metabolites become critical for cellular adaptation to glutamine limitation will likely depend on the TME, location, and oncogenic lesion. Identifying the processes that glutamine supports and the compensatory mechanisms active within a given context (i.e., MYC-driven TNBC) will be necessary to target glutamine metabolism effectively.

#### *1.2.4.2 Essential Amino Acid Metabolism*

There are nine essential amino acids: phenylalanine, valine, threonine, tryptophan, isoleucine, leucine, histidine, methionine, and lysine. Apart from methionine, these amino acids cannot be synthesised *de novo*, meaning that cells must acquire them from their environment through amino acid transporters. While the role of EAAs in cancer metabolism is less well studied than glutamine and other NEAAs, recent findings suggest they play important roles beyond their traditional function in protein synthesis. Notably, the MYC oncogene has been shown to promote the uptake and metabolism of EAAs.

MYC drives increased demand for EAAs by activating the transcription of genes involved in ribosome biogenesis and protein synthesis, which are essential for cellular growth and proliferation[161]. It not only upregulates components of the translation machinery but also enhances the expression of amino acid transporters on the cell surface to facilitate EAA uptake[162]. This increased availability of EAAs stimulates mTORC1 signalling, a key regulator of global translation. Specifically, MYC directly binds to the promoters of the **L**-type **a**mino acid **t**ransporters, LAT1 and LAT3, encoded by *SLC7A5* and *SLC43A1*, respectively[163]. LAT1 and LAT3 mediate the uptake of EAAs and are crucial for the uptake of BCAAs like leucine. A feed-forward loop exists in which MYC upregulates LAT1 and LAT3 expression, leading to increased EAA uptake, which sustains MYC translation and its metabolic activities[163]. However, when LAT1 and LAT3 are ablated, EAA uptake is reduced, resulting in decreased MYC translation and its downstream targets, including genes involved in glucose and glutamine metabolism[163]. This reduction is partly mediated by the integrated stress response (ISR) activation, which responds to amino acid deprivation by inhibiting global protein synthesis[164]. This highlights the important role of EAAs in maintaining mTORC1 signalling, protein translation, and, therefore, MYC-dependent transformation. Significantly, this also links LAT1/3-mediated uptake of EAAs to MYC-dependent glutamine addiction.

While all EAAs are required for protein synthesis, they do not equally regulate mTORC1. mTOR is a growth-factor-responsive serine/threonine kinase that forms two distinct complexes, mTORC1 and mTORC2, each involved in different cellular

processes[165]. mTORC2 regulates cell movement and cytoskeletal organisation through kinases such as PKCα and AKT and is primarily influenced by growth factor signalling via the PI3K pathway. In contrast, mTORC1 integrates signals from nutrient availability and growth factors to regulate anabolic and catabolic cellular processes[165].

mTORC1 promotes cell growth by inducing protein translation through the regulation of crucial downstream targets such as 4E-BP1 (eukaryotic translation initiation factor **4E**-**b**inding **p**rotein **1**) and S6K1 (ribosomal protein **S6 k**inase beta-**1**)[166]. These targets increase the synthesis of key translation machinery components and promote translation[166,167]. Additionally, mTORC1 suppresses autophagy when nutrients and growth factors are available. mTORC1 activation thus involves a complex signalling cascade that starts with nutrient sensing at the lysosomal surface.

mTORC1 activation integrates signals from nutrient availability and growth factors, depending on Rag GTPases and Rheb, respectively. Rag GTPases exist as obligate heterodimers, Rag A or B bound to Rag C or D. These Rags are tethered to the lysosome by the Ragulator complex, where mTORC1 is activated. Nutrient availability, particularly amino acids, plays a significant role in mTORC1 activation. When amino acids are abundant, RagA/B is bound to GTP, and RagC/D is bound to GDP, promoting the recruitment of mTORC1 to the lysosome[165,168–170]. This process is further modulated by regulatory proteins such as GTPase-activating proteins (GAPs). GATOR1, a GAP, negatively regulates mTORC1 by converting RagA/B to an inactive GDP-bound state[171,172]. In contrast, GATOR2, an upstream negative regulator of GATOR1, enables the GTP-bound active state of RagA/B, thereby promoting mTORC1 recruitment, where it is activated by Rheb.

The mechanisms by which amino acids and nutrients are sensed by mTORC1 are continuously emerging. However, it is widely acknowledged that mTORC1 is particularly sensitive to leucine and arginine levels (Figure 1-5)[173–175]. However, it can also indirectly sense methionine levels through S'adenosylmethionine (SAM; Figure 1-5)[176], a product of the methionine regeneration pathway. Leucine and arginine are sensed by SESTRIN2 and CASTOR1, respectively (Figure 1-5)[174,175],

which mediate their mTORC1 modulating capabilities through GATOR2. When leucine levels are low, SESTRIN2 binds GATOR2, leading to the release of GATOR1 and inhibition of mTORC1. SESTRIN2 can also sense isoleucine and methionine; however, it is significantly less sensitive to the levels of these amino acids[175]. Another mechanism of leucine sensing is through leucyl-tRNA synthetase (LRS)[173]. Leucine binds LRS, which subsequently translocate to the lysosomal membrane and mediates GTP hydrolysis of Rag D, promoting the GDP-bound active state of Rag D, thereby activating mTORC1[173]. Like SESTRIN2, LRS can bind isoleucine and methionine with lower affinity. The exact reasons why LRS acts as a GAP towards Rag D specifically, despite its similarity to Rag C, are not fully understood. However, RagD has been shown to recruit mTORC1 to the lysosome more effectively than Rag C[177]. mTORC1 also exhibits differential substrate specificity depending on whether RagC or RagD is present. For instance, RagA/B-RagC heterodimers promote canonical mTORC1 signalling through S6K1 and 4E-BP1, whereas RagA/B-RagD dimers inhibit the transcription factor EB[177], which regulates autophagy and lysosome biogenesis[178]. Thus, leucine sensing by LRS may help promote cellular anabolism by inhibiting catabolic processes to avoid premature protein degradation. However, the GAP activity of LRS remains controversial, as other groups have failed to demonstrate the GAP activity of isolated LRS[179]. Therefore, the exact mechanisms that underlie how leucine availability is relayed to mTORC1 remain to be determined, and additional mechanisms of leucine sensing are still being explored[180–182].

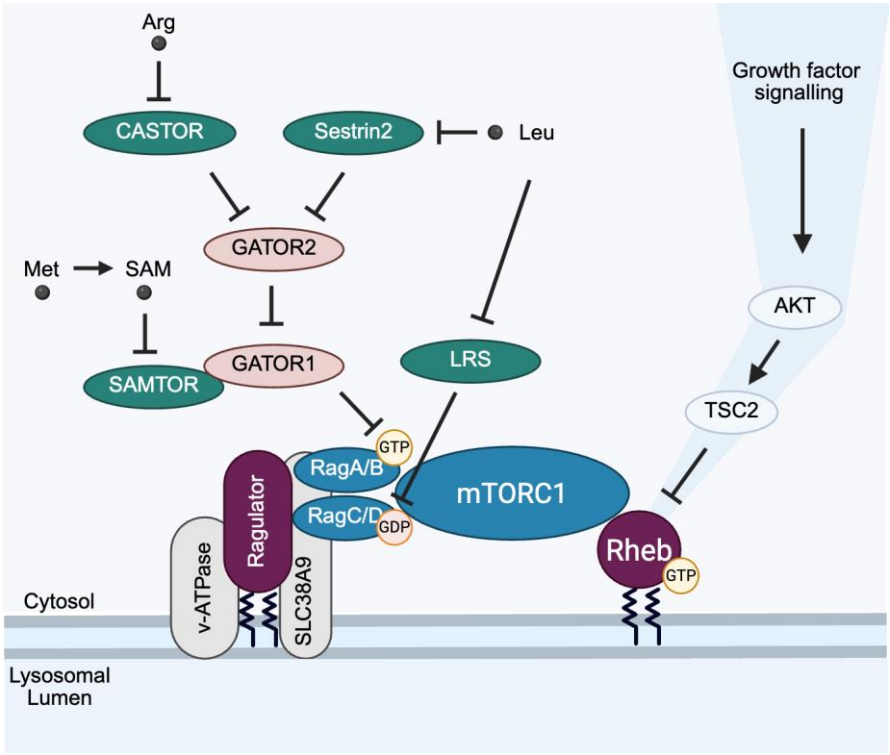



**Figure 1-5. Mechanisms of mTORC1 activation via amino acids.**
Leucine, Arginine and SAM are detected by sensors in the cytosol (Sestrin2, LRS, CASTOR1, and SAMTOR). These signals activate Rag GTPases (RagA/B and RagC/D), which help recruit mTORC1 to the lysosome where it is activated by Rheb downstream of growth factor signalling pathways. Data adapted for visual presentation from Figure 2 from Takahara et al. (2020), *Journal of Biomedical Science*[183]. under a Creative Commons Attribution 4.0 International License. Image created with biorender.com.

MYC-driven metabolic reprogramming also facilitates the degradation of EAAs by upregulating critical enzymes in these pathways (Figure 1-3). For example, MYC enhances tryptophan uptake through LAT1 and promotes its conversion into kynurenine via the enzyme arylformamidase (AFMID)[164]. Inhibiting the kynurenine pathway or downstream interactions has shown therapeutic potential in certain MYC-dependent cancers[184]. Additionally, MYC-induced tryptophan uptake supports liver cancer cell growth by producing the oncometabolite indole-3-pyruvate [185]. MYC also upregulates BCAT1, an aminotransferase involved in BCAA catabolism, which has been linked to increased cancer cell migration and invasion[103]. Methionine has been well studied due to its role in one-carbon metabolism. The methionine regeneration pathway produces SAM, a global methyl donor, through MAT-2A, which catalyses the transfer of a methyl group from methionine onto ATP,

producing SAM[186]. Oncogenic MYC has been associated with methionine addiction[187] and can regulate MAT-2A activity through a mTORC1-dependent signalling axis, which supports histone methylation and tumour growth[188]. Importantly, dietary methionine restriction has demonstrated efficacy in numerous preclinical models and shows significant promise as a treatment strategy in clinical trials[188–190]. This supports the idea that targeting EAA metabolism, or availability, is a feasible treatment strategy for cancer. While significant progress has been made in understanding the role of EAAs in MYC-driven tumourigenesis, further research is needed to explore the functions of other lesser-known EAAs fully.

## 1.3 SLC7A5/LAT1

### 1.3.1 SLC transporters

The SLC superfamily is an ever-expanding group of transporters responsible for moving a wide range of solutes into and out of cells. Over 450 SLC genes have been identified in the human genome, organised into 65 subfamilies based on sequence similarity[191,192]. These transporters facilitate the transport of amino acids, nucleotides, metal and inorganic ions, fatty acids, co-factors, vitamins, and other organic ions and compounds into cells[193]. Although subfamilies are primarily grouped by their substrate specificity, this can vary within subfamilies. SLC transporters are highly specialised, with tissue-specific and temporal expression patterns[194,195]. Some are only expressed in specific cell types; for example, the lysosomal transporter, SLC11A1, is required for phagocyte function but not for lymphocytes[196]. In contrast, others like SLC2A1, which encodes GLUT1, are ubiquitously expressed to support basic cellular processes, such as maintaining glucose transport[197]. Furthermore, the expression of SLC transporters changes over time, with some predominantly present during periods of rapid proliferation and growth, such as during embryonic development or cancer[195,198]. The temporal dynamics of SLC transporter expression are regulated by a network of proteins that control their transcription, post-translational modifications, localization, and function[192].

Unlike other transporter superfamilies, SLC transporters do not share a common evolutionary origin, resulting in significant structural diversity across subfamilies[191].

However, SLC transporters are typically characterised as 12-pass or 10-pass transmembrane proteins. The two prominent structural folds in this family are: (i) the major facilitator superfamily (MFS) fold, with 12 transmembrane helices arranged in two mirrored groups of six, and (ii) the leucine transporter (LeuT)-like fold, with 10 transmembrane helices in two mirrored groups of five[191] (Figure 1-6).These structural features influence how SLC transporters change conformation to transport substrates. For example, MFS transporters primarily use a “rocker-switch” mechanism oscillating between outward and inward states. LeuT-like transporters primarily use a “gated-pore” mechanism where the gate opens to reveal the binding site, allowing for substrate binding and release[191]. Some transporters with distinct structural folds utilise different transport mechanisms, such as an “elevator” mechanism, where the substrate-binding domain moves across the cell membrane like an elevator[191]. Different energy coupling mechanisms are also used to support transport across the SLC family. Importantly, SLC transporters from different subfamilies can have different folds but transport similar substrates, while those with similar structures can have different substrate specificities and mechanisms of transport. This diversity allows for significant redundancy and overlap of substrates, which is integral for cell survival, given their importance in nutrient uptake.

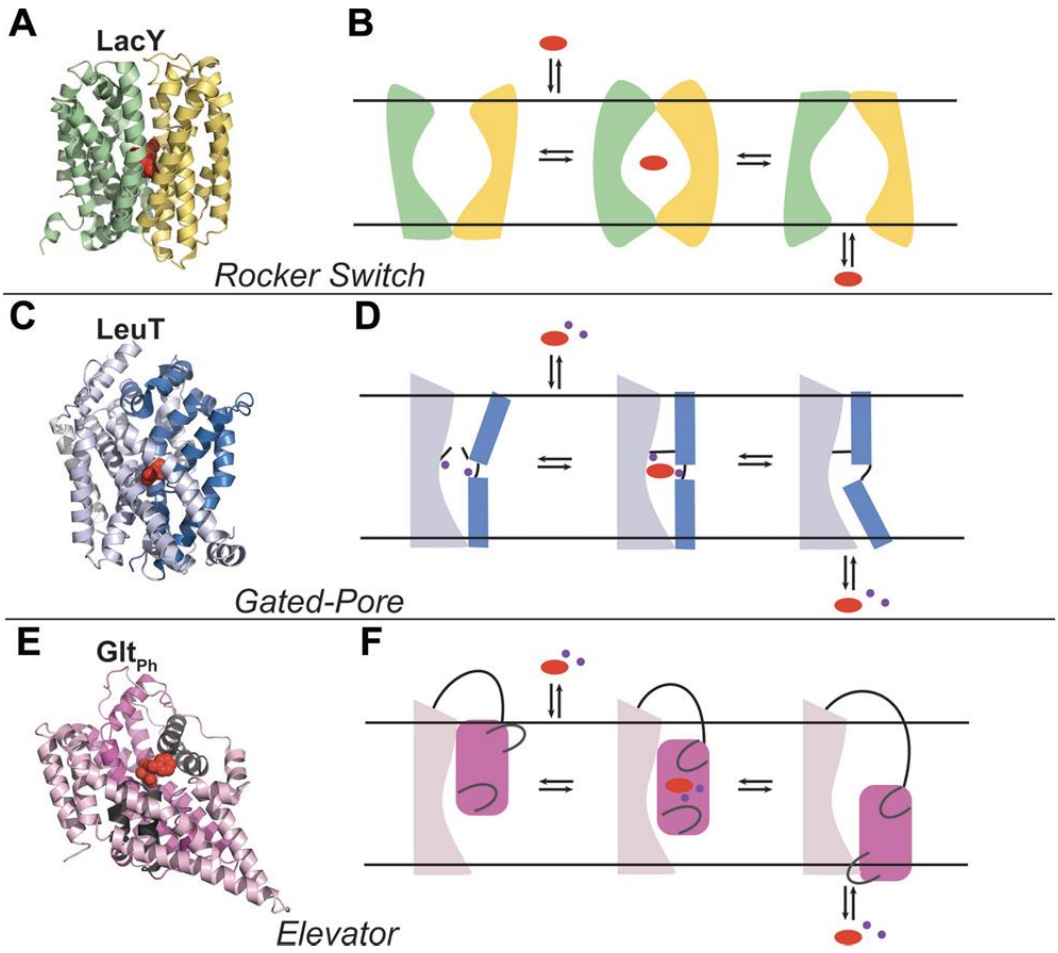



**Figure 1-6. Prominent structures associated with members of the SLC transporter superfamily.**
These include the rocker-switch, gated-pore, and elevator models, associated with the MFS fold and LeuT-like structural folds. The red spheres indicate the substrate. Reproduced from Figure 1 from *SLC Transporters: Structure, Function, and Drug Discovery*, *MedChemComm*, © Royal Society of Chemistry, with permission[199]. License ID: 1608526-1. No changes were made to the image.

As mentioned above, members of the SLC superfamily mediate transport across membranes using various energy-coupling mechanisms, including secondary active transport (via symporters and antiporters) and facilitated diffusion (Figure 1-7)[199–201]. Both mechanisms rely on electrochemical gradients of ions or substrates. Facilitated diffusion is typically carried out by uniporters, which transport substrates along their concentration gradient. For example, SLC2A1 (encoding GLUT1), enables passive glucose uptake when intracellular glucose levels are low[202]. In contrast, secondary active transporters harness the energy from the movement of an ion or molecule down its concentration gradient to drive the transport of another molecule against its gradient. When both substrates move

in the same direction, the transporter is termed a symporter; when they move in opposite directions, it is classified as an antiporter. The net charge resulting from transport can vary; it is classified as electronegative if negative charge accumulates intracellularly, electropositive if positive charge accumulates, and electroneutral if there is no net change in charge. Well-characterized symporters include SLC38A1/2 (encoding SNAT1/2, respectively), which co-transport $Na^+$ along its gradient with amino acid substrates into the cell[201]. In contrast, LAT1 (encoded by SLC7A5) is an antiporter that exchanges intracellular amino acid substrates for extracellular ones and does not contribute to net amino acid uptake in the way symporters do. Ion and substrate gradients critically influence the capacity of secondary active transports to accumulate substrates. For example, SLC38A3/5 (encoding SNAT3/5, respectively) mediate electroneutral $Na^+$- amino acid symport coupled with $H^+$, antiport, limiting net amino acid uptake to the prevailing Na+ and $H^+$ gradients[201]. In contrast, SNAT1 and SNAT2, which do not exchange $H^+$, are better equipped to drive intracellular amino acid accumulation.

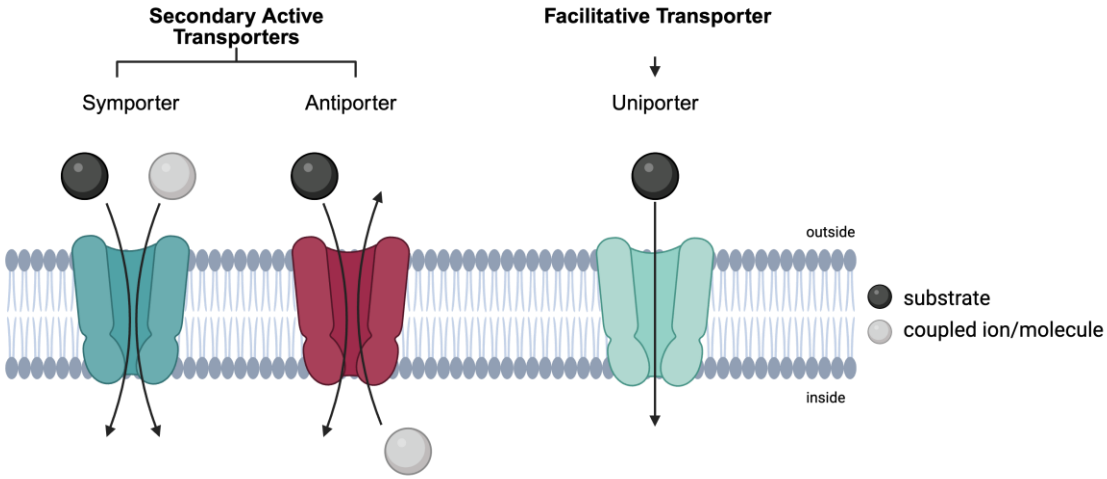



**Figure 1-7. Overview of SLC transporter amino acid exchange mechanisms.**

Amino acid uptake is mediated by members of the SLC1, SLC6, SLC7, SLC38, and SLC43 families (Table 1-2)[191]. There are significant differences in substrate specificity and transport mechanisms within these families. For example, the SLC7 family partially includes cationic amino acid transporters (CATs, SLC7A1-4) and large neutral amino acid transporters (LATs, SLC7A5-11)[203]. LATs form heterodimers with SLC3 family subunits, such as SLC3A2 (4f2hc), while CATs function as monomeric N-glycosylated transporters[203]. Both transporters have LeuT

folds, but CATs facilitate diffusion of cationic amino acids like arginine, while LATs function as exchangers for a broader range of amino acids[203]. Transport substrates also have significant redundancy, both within and across SLC subfamilies. For instance, SLC7 and SLC43 subfamilies transport neutral amino acids (Table 1-2)[204]. SLC43 transporters, such as SLC43A1/2 (LAT3/4), are facilitative diffusers, whereas SLC7 transporters, such as SLC7A5/8 (LAT1/2), are exchangers[204]. Facilitative diffusion of amino acids may help maintain baseline levels of amino acids by responding to changes in their availability and transporting them along their concentration gradient[201]. In contrast, an exchanger can modulate the composition of amino acids available to the cell. Therefore, both allow cells to precisely regulate amino acid concentrations in response to their environments.

**Table 1-2. Characteristics of SLC subfamilies that transport amino acids.**
LeuT: leucine transporter-type fold. MFS: Major facilitator superfamily.

| SLC Subfamily | Members | Key members | Fold | Mechanism | Function |
|---|---|---|---|---|---|
| SLC1 | 7 | ASCT1/2 EAAT1/2 | Other | Na+/K+ H+ dependent | glutamate (excitatory AA transporters) and neutral amino acid transporters (alanine-serine-cysteine transporters)[205] |
| SLC6 | 20 | DAT, SERT,NET | LeuT | Na+/Cl- dependent | neurotransmitter and amino acid transport[206] |
| SLC7 | 15 | CAT1 LAT1 xCT | Other/LeuT | Na+ independent/ dependent | cationic amino acid and large neutral amino acid transport[203] |
| SLC38 | 11 | SNAT1-3 | Other | Na+ dependent | neutral amino acid transport/ glutamine, asparagine and histidine transport[207] |
| SLC43 | 3 | LAT3 | MFS | Na+/Cl- independent | neutral amino acid transport[204] |

SLC-mediated transport of essential nutrients is crucial for maintaining cellular homeostasis. At the cellular level, SLC transporters regulate the overall metabolic state by providing essential nutrients for biosynthesis. At the whole-body level, SLC transporters play critical roles in nutrient absorption in the intestine and kidney,

neurotransmitter signalling, and energy homeostasis by regulating glucose and amino acid levels[208]. The importance of SLC transporters in these processes is underscored by the pathological consequences of inborn errors or dysregulation[209–211]. For example, lysinuric protein intolerance is caused by mutations in SLC7A7, leading to defective cationic amino acid absorption and resulting in a multisystemic disorder[212]. Moreover, several SLC transporters are embryonically lethal when deleted in animal models, emphasising their critical role in development[213,214]. Notably, SLC transporters are key targets of activating transcription factor 4 (ATF4), which regulates genes that reestablish cellular homeostasis in response to stress[215]. Therefore, SLC transporters are also often dysregulated in cancer and metabolic disease, highlighting the crucial role of SLC transporters in sustaining metabolic demands.

Cancer cells exhibit an increased demand for certain nutrients due to abnormal growth and proliferation, often in an oncogene-, tissue-, and microenvironment-specific manner. The repertoire of solute transporters expressed determines the availability of these nutrients[201]. As a result, many SLC transporters are implicated in tumourigenesis. Among plasma membrane SLC transporters mediating amino acid uptake, several are involved in tumourigenesis: *SLC1A5*, *SLC7A5*, *SLC7A11*, *SLC6A14*, *SLC38A1*, *SLC38A2*, *SLC43A1*, and *SLC7A1*[216]. Furthermore, *SLC1A5*[147,150,156,217], *SLC7A11*[123,218], *SLC7A5*[219–221], *SLC38A1*[222], and *SLC38A2*[223] are critical amino acid transporters in TNBC. Importantly, MYC directly binds the promoters of several of these transporters[224], highlighting their role in sustaining MYC-driven metabolic rewiring. Notably, *SLC1A5*/ASCT2 and *SLC7A5*/LAT1 are particularly important in cancer[151]. These transporters have been demonstrated to work together to maintain amino acid homeostasis, and their co-regulation by MYC supports the coupling of these transporters[142]. However, there are discrepancies regarding the requirement of ASCT2 for LAT1 function that remain to be addressed.

### 1.3.2 LAT1 Structure and Function

LAT1 is a high-affinity Na+-independent transporter of large neutral amino acids with branched or aromatic side chains (leucine, isoleucine, phenylalanine,

methionine, tyrosine, histidine, tryptophan, and valine). However, it can also transport glutamine and asparagine with lower affinity[225,226]. In addition to its amino acid substrates, LAT1 has been demonstrated to transport amino acid derivatives, such as L-DOPA[227]. LAT1 acts in an obligatory heterodimer with SLC3A2, 4f2/CD98, to facilitate amino acid transport[225,226,228]. Importantly, LAT1 is the transport-competent unit of this heterodimer and 4f2 acts to stabilise LAT1 and support LAT1 transporter activity at the plasma membrane[229,230]. LAT1 contains 12 transmembrane domains and utilises a “rocking bundle” mechanism that exposes the substrate binding site and enables LAT1 transition between inward or outward-facing states, thereby facilitating the movement of substrates across the membrane in both directions[228]. LAT1 mediates the uptake of its substrates with varying affinities, with the highest affinity for histidine and the lowest affinity for glutamine and asparagine (Table 1-3)[225,226]. However, these affinities can differ across tissues, indicative of tissue-specific requirements[231]. LAT1 mediates amino acid uptake by exchanging intracellular amino acids for extracellular amino acids with a 1:1 stoichiometry[231,232]. Notably, only specific substrates can be transported bidirectionally; these include glutamine, histidine, and tyrosine[229]. Therefore, LAT1 transport is dependent on the intracellular availability of these amino acids.

The importance of LAT1 in tumours was evident from the earliest study, spurring the last two decades of research into this integral amino acid transporter[225]. While LAT1 has overlapping substrates with other LAT proteins (Table 1-3), its expression is limited to specific tissues and found to be selectively upregulated in tumours[151,225]. LAT1 expression is primarily restricted to the blood-brain barrier (BBB), lymphocytes, and placenta, whereas other LAT transporters, such as LAT2 are ubiquitously expressed in the epithelial cell tissues (Table 1-3)[231]. LAT1 has a higher affinity for its substrates than LAT2, supporting rapid proliferation and specialised functions within tissues and cancer[233]. For instance, LAT1 expression in the blood-brain barrier is required to uptake BCAAs, high-affinity LAT1 substrates[234]. Deletion of LAT1 at the BBB of mice had severe neurological abnormalities and has been associated with intrinsic mutations in SLC7A5 in patients with autism[234].

**Table 1-3. Classification of LAT transporters.**
The table shows a list of Km values taken from a curated list by Gauthier-Coles et al. (2021)[201]. These Km values represent values published from a single study of each transporter. Gauthier-Coles et al. (2021) estimated some of the Km values.

| SLC | Acronym | Transport | Tissue | Substrates | Affinity (μM) |
|---|---|---|---|---|---|
| SLC7A5 | LAT1 | Antiporter | Brain, spleen, placenta, testis[203] | Leu | 20 |
| | | | | Ile | 25 |
| | | | | Val | 47 |
| | | | | Met | 20 |
| | | | | Phe | 14 |
| | | | | Tyr | 28 |
| | | | | Trp | 21 |
| | | | | **His** | **12** |
| | | | | Gln | 1640 |
| | | | | Asn | 2150 |
| SLC7A6 | y+LAT2 | Antiporter | Brain, small intestine, testis, heart, kidney , lung, thymus[203] | Arg | 138 |
| | | | | Lys | 138 |
| | | | | His | 138 |
| | | | | Leu | 236 |
| | | | | Tyr | 500 |
| | | | | Trp | 236 |
| | | | | Phe | 236 |
| | | | | Gln | 295 |
| | | | | Met | 236 |
| | | | | Cys | 500 |
| | | | | Ile | 500 |
| | | | | Ala | 1000 |
| SLC7A7 | y+LAT1 | Antiporter | Small intestine, kidney, spleen, placenta, lung[203] | Arg | 340 |
| | | | | Lys | 68 |
| | | | | His | 44 |
| | | | | Leu | 44 |
| | | | | Tyr | 200 |
| | | | | Phe | 300 |
| | | | | Gln | 60 |
| | | | | Met | 60 |
| | | | | Ile | 60 |

| SLC | Acronym | Transport | Tissue | Substrates | Affinity (uM) |
|---|---|---|---|---|---|
| SLC7A8 | LAT2 | Antiporter | Small intestine, kidney, lung, heart, spleen, liver, brain, placenta, prostate, ovary, fetal liver, testis, skeletal muscle[203] | His | 181 |
| | | | | Trp | 58 |
| | | | | Tyr | 46 |
| | | | | Phe | 45 |
| | | | | Val | 124 |
| | | | | Ile | 97 |
| | | | | Leu | 119 |
| | | | | Met | 204 |
| | | | | Gln | 151 |
| | | | | Asn | 81 |
| | | | | Cys | 109 |
| | | | | Thr | 69 |
| | | | | Ser | 116 |
| | | | | Ala | 187 |
| | | | | Gly | 265 |
| SLC43A1 | LAT3 | Uniporter | Liver, skeletal muscle, pancreas, kidney, testis, ovary[192,204,235], | Leu | 1024 |
| | | | | Ile | 1418 |
| | | | | Val | 1885 |
| | | | | Phe | 1206 |
| | | | | Met | 2000 |
| SLC43A2 | LAT4 | Uniporter | Placenta, kidney, small intestine, brain, testis, heart, spleen[192,204,235] | Leu | 3733 |
| | | | | Ile | 4000 |
| | | | | Val | 4000 |
| | | | | Phe | 4694 |
| | | | | Met | 4000 |

One of the mechanisms by which LAT1 supports rapidly proliferating cells is through the uptake of leucine. Indeed, LAT1 KO results in a significant reduction in leucine uptake[163,234,236]. mTORC1 integrates signals from leucine availability and growth factors to regulate protein translation and cellular growth[165,175]. Therefore, LAT1 has been implicated in the regulation of mTORC1[142,236–238]. Additionally, while LAT1 is primarily localised in the plasma membrane, it is also recruited to the lysosome membrane by lysosomal protein transmembrane 4 beta (LAPTM4B), where it is necessary for mTORC1 activation[239]. In addition to its role in mediating mTORC1 signalling, LAT1 is critical for the activation of general control nonderepressible 2 (GCN2), a serine/threonine kinase that is activated when amino acids are low, regulating cell response to amino acid starvation through the ISR.

Indeed, LAT1 ablation has been demonstrated to be sufficient for the induction of ATF4, a key downstream effector of the ISR[236]. Therefore, LAT1 is essential in the regulation of two key signalling pathways during cellular growth, both of which are essential for MYC-driven tumourigenesis[224,240–242]

### 1.3.3 Glutamine in LAT1 Function

LAT1 is an obligatory antiporter, therefore the uptake of one of its substrates is dependent on the efflux of another. LAT1 can use histidine, glutamine, or tyrosine as efflux substrates. LAT1 and ASCT2 are targets of MYC-driven metabolic reprogramming and are often concordantly upregulated in cancer[151,163,243,244]. ASCT2 is a Na+ dependent antiporter, responsible for maintaining glutamine levels in cancer cells[147], although it also transports small neutral amino acids, such as asparagine and serine[156]. Aside from providing cancer cells with glutamine for biosynthesis, ASCT2 is critical in facilitating LAT1-activity. Glutamine uptake through ASCT2 was shown to be exported by LAT1 and coupled to leucine uptake, activating mTORC1 signalling[142]. This was essential for leucine-mediated activation of mTORC1/S6K1 signalling. However, subsequent studies demonstrated that ASCT2 KO did not affect LAT1 transporter activity and was dispensable for mTORC1 activation in multiple cancer cell lines[148]. SNAT1/2 have been demonstrated to compensate for ASCT2 KO in other cancer models[144]. Therefore, these compensatory pathways could maintain glutamine-facilitated LAT1 transport. However, other studies suggest that asparagine, rather than glutamine, is the preferred exchange substrate facilitating amino acid uptake[245]. The discrepancies between these findings may arise from several factors, notably the low affinity of LAT1 for glutamine (Table 1-3). Because LAT1 binds glutamine poorly, high intracellular glutamine concentrations are necessary for it to function effectively as an exchange substrate. These concentrations can vary significantly depending on the cell type and experimental conditions. Importantly, standard cell culture media contain glutamine at concentrations 2- to 5- fold higher than physiological levels, and tumours often experience even more restricted glutamine availability[246]. Moreover, media typically provide glutamine at 5- to 20- fold higher concentrations than other amino acids[141], potentially skewing LAT1 activity, which is sensitive to substrate availability. The mismatch between experimental and physiological

conditions helps explain observed differences in cellular responses to ASCT2 ablation *in vitro* versus *in vivo*[148,247]. While glutamine likely contributes to LAT1-mediated uptake of EAAs, its effectiveness may be context-dependent, influenced both by its availability in the TME and by the competing demands from other metabolic pathways driven by specific oncogenic lesions.

### 1.3.4 Histidine in LAT1 Function

LAT1 has been identified as the “high-affinity histidine transporter” due to its exceptionally high affinity for histidine (Table 1-3)[226,232,229,248,249]. Significantly, unlike the other EAAs, which are preferentially transported inward, histidine can be transported bidirectionally[229]. To facilitate the transport of extracellular amino acids, the extracellular affinity of LAT for its substrates is in the μM range, while the intracellular affinity is in the mM range[248]. Notably, concentrations of amino acids are higher in the cytosol compared to the extracellular environment[201,250]. This asymmetry enables LAT1 to transport substrates even when present at low extracellular concentrations by utilizing substrates available at higher concentrations within the cytosol[248,251]. Notably, many factors determine the concentration of amino acids in the cytosol, including the expression of cell surface amino acid transporters, cellular metabolism, and proliferation. Furthermore, the higher concentration of glutamine in the medium compared to histidine may bias LAT1 towards the use of glutamine as an exchange substrate, which may not accurately reflect the role of LAT1 under physiological conditions or during MYC-driven metabolic reprogramming when the demand for glutamine catabolism is enhanced.

Despite the high affinity of LAT1 for histidine as a bidirectional substrate, the contribution of histidine to LAT1-activity in cancer has not received significant attention. The sole study demonstrating the requirement for histidine as a bidirectional substrate *in vivo* was in the BBB[234]. Indeed, a conditional deletion of *Slc7a5* in the endothelial cells of blood vessels and BBB in mice resulted in a significant accumulation of histidine with a concurrent decrease in BCAAs[234]. This demonstrated that histidine was the primary bidirectional LAT1 substrate in the

BBB and may also highlight that under physiological settings, histidine is preferred over glutamine.

Unlike glutamine, histidine catabolism is restricted to specific tissues[252], making histidine a metabolic dead end in some cell types. Therefore, histidine may be preferred over glutamine as a LAT1 exchange substrate. This switch from glutamine to histidine for LAT1 activity could facilitate cancer cells, allowing them to continue catabolising glutamine for biosynthetic processes while maintaining EAA uptake via histidine-facilitated LAT1 antiport. Investigating the role of histidine in these contexts could unveil its essential role in mTORC1 signalling and amino acid homeostasis.

## 1.4 Histidine and its role in cancer

### 1.4.1 Histidine Metabolism

Histidine is primarily metabolised through 3 distinct pathways: (i) decarboxylated by histidine decarboxylase (HDC) to produce histamine in the mast cells, the stomach, and brain, (ii) combined with β-alanine to produce the dipeptide, carnosine, in the brain and skeletal muscle, and (iii) degraded to produce glutamate and one-carbon intermediates in the liver and skin (Figure 1-8)[252]. The histidine degradation pathway appears to occur primarily in the liver and skin due to the high expression of key rate-limiting enzymes in these tissues. The first step of histidine degradation is conversion into trans-urocanate by histidine ammonia lyase (HAL), which is highly expressed in the liver and skin[252,253] and binds histidine with a $K_m$ of 1-4 mM. This concentration is significantly greater than the physiological concentration of histidine in the blood, at 70-120 μM[252]. This may act to balance histidine degradation with its availability, as cells cannot synthesize histidine *de novo*, and suggest that histidine degradation only proceeds when histidine concentrations are high. Trans-urocanate is then hydrolysed into 4-imidozolone-5-proprionate by the liver-enriched protein urocanase (UROC1). This product is then converted into formiminoglutamate (FIGLU). Glutamate formiminotransferase cyclodeaminase (FTCD) transfers one-carbon unit from FIGLU onto tetrahydrofolate (THF) to produce glutamate and 5'-10'-methenyl-THF. This step implicates histidine in central and one-carbon metabolism in the liver. 5'-10'-methenyl-THF can be

converted into several different intermediates of the folate cycle, such as 5',10'-methylene THF for nucleotide synthesis, or 5'-methyl-THF for regeneration of methionine in the methionine regeneration cycle[252]. Indeed, the histidine degradation pathway contributes to one-carbon metabolism in cancer cells[254,255]. Despite histidine's capacity to contribute carbon and nitrogen to glutamate production and one-carbon metabolism, intrinsic errors in genes encoding enzymes in this pathway do not result in severe pathophysiology. The most significant of these is histidinemia, which is characterised by impaired HAL function and an increase in plasma histidine levels, with the disease manifesting as asymptomatic in most patients or mental retardation in the minority[252]. Therefore, it is unclear how essential histidine degradation is to physiological metabolism.

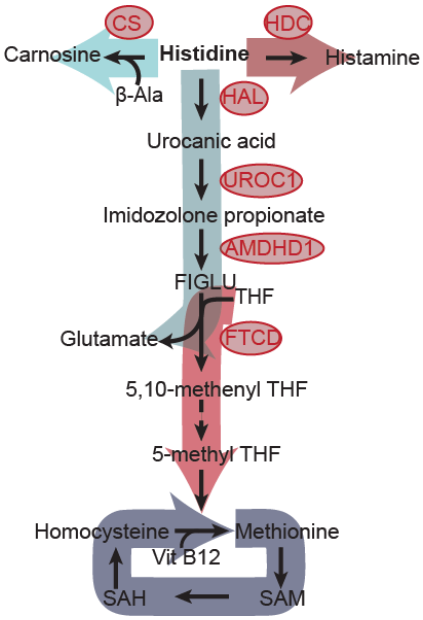



**Figure 1-8. Simplified schematic of histidine metabolism.**
Dashed lines indicate multiple enzymatic steps that have not been shown here. Key enzymes and products in His catabolism are depicted. *CS: Carnosine Synthetase; HDC: Histidine Decarboxylase; HAL: Histidine Ammonia lyase; UROC1: Urocanase; AMDHD1: Amidohydrolase Domain Containing 1; FTCD: formimidoyltransferase cyclodeaminase*.

### 1.4.2 Histidine Metabolism in Cancer

The role of histidine in cancer has emerged in recent years. Some studies have identified altered histidine levels in patients with cancer[256–258], leading to an increased interest in the potential role of histidine metabolism in cancer. The possible use of histidine supplementation has been of particular interest for limiting

drug resistance. This phenomenon was first observed in a CRISPR-Cas9-based screen in cancer cells treated with the anti-folate drug, methotrexate, which is widely used in the treatment of several cancers such as acute lymphoblastic leukaemia (ALL)[255]. These authors found that depletion of FTCD, the enzyme that converts FIGLU into glutamate and consumes THF to produce 5',10'-methenyl THF, confers resistance to methotrexate treatment[255]. Indeed, KO of FTCD or HAL increased THF pools and decreased levels of downstream intermediates of the folate cycle, suggesting that histidine catabolism drains cellular THF[255]. Therefore, histidine supplementation sensitised cells and tumour xenografts to methotrexate treatment by enhancing histidine catabolism and depleting THF levels[255]. Subsequently, others have used histidine supplementation combined RTK inhibitors (Sorafenib) in HCC cells[259] or with a chemotherapeutic drug, gemcitabine, in pancreatic cancer cells and xenografts[260]. In both studies, histidine supplementation enhanced the anti-tumour efficacy of the drug. However, it is unclear whether this was mediated through histidine metabolism. Indeed, in pancreatic cancer cells, histidine supplementation increased the accumulation of histidine but did not contribute to downstream intermediates of its metabolism assessed with stable isotope tracing of histidine[260]. However, in both experiments, histidine supplementation resulted in significant but varied metabolic alterations, suggesting histidine may have important roles in cellular metabolism in a tissue-dependent manner.

In a *Drosophila* neural tumour model, using Myc/eiF4E (eukaryotic initiation factor 4E) dependent neural mutant clones, *nerfin-1* and *Notch*$^{activated}$, or a Myc-independent/S6K-dependent neural mutant clone, *Prospero*, Froldi *et al.* (2018) demonstrated that Myc-dependency sensitised clones to histidine restriction[261]. How histidine supports Myc/eiF4E-dependent cellular growth and dedifferentiation in *nerfin-1* or *Notch*$^{activated}$ clones was not determined. However, the authors found that HDC activity may be necessary for this process, as genetic knockdown (KD) of CG3454 (a predicted HDC) reduced *nerfin-1* clonal volume. However, this appeared to be independent of histamine-mediated signalling[261]. Furthermore, MYC and eIF4E phenocopied the effect of histidine on clonal growth. However, histidine sensitivity could be overcome by Myc overexpression[261]. These results suggest an essential interaction between histidine and MYC/eIF4E, by which

histidine supports Myc/eIF4E-driven cellular growth, which is inhibited under histidine restriction but can be “rescued” by increased Myc or histamine. Considering the role of Myc in cellular metabolism, this could suggest that histidine is a critical amino acid for Myc-driven tumourigenesis. Furthermore, given the essential role of LAT1 in regulating mTORC1 signalling, and the potential implication of histidine in LAT1 function, understanding the interplay between MYC, LAT1, and histidine may reveal potential metabolic vulnerabilities.

## 1.5 Thesis Aims

A significant body of research has demonstrated “glutamine addiction”, characteristic of MYC-dependent tumourigenesis[97,111,111,141]. Much of this work has focused on the biosynthetic roles of glutamine in supporting tumour growth. However, glutamine has been demonstrated to have essential roles in EAA uptake and mTORC1 signalling, mediated through the LAT1 transporter, although this has been faced with contention[142,148]. Significantly, LAT1 relies on high intracellular levels of glutamine to facilitate its exchange[226]. This prompts us to consider how MYC-driven cancer cells balance an increased demand for glutamine catabolism with an increased demand for EAAs in an environment often limited in glutamine.

Our hypothesis proposes a novel perspective on the use of histidine as a LAT1 exchange factor for EAA uptake in MYC-driven cancer cells with extensive glutamine catabolism. Given the crucial role of LAT1 in MYC-translation and metabolic reprogramming[163], histidine could be a key vulnerability in these tumours, opening up new avenues for targeted therapies.

To investigate this hypothesis, this thesis will focus on three primary objectives:

(1) To evaluate the relationship between glutamine availability and histidine requirement in Myc-driven tumourigenesis.
(2) To investigate the role of histidine in LAT1-mediated transport and mTORC1 signalling.
(3) To target the role of histidine to impede Myc-driven mammary tumourigenesis.

# Chapter 2. Materials & Methods

## 2.1 Reagents and Chemicals

**Table 2-1. Stable Isotopes.**
All isotopes were ordered from Cambridge Isotope Laboratories

| Stable Isotope | Catalogue Number |
|---|---|
| L-Histidine ($^{13}C_6$) | CLM-2264-PK |
| L-Glutamine (amide-$^{15}N$) | NLM-557-PK |
| L-Glutamine ($^{13}C_5$) | CLM-1822-H-PK |
| L-Leucine ($^{13}C_6$) | CLM-2262-H-PK |
| D-Glucose ($^{13}C_6$) | CLM-1396-PK |
| L-Valine ($^{13}C_5$, $^{15}N$) | CNLM-442-H |

**Table 2-2. qPCR primers.**
Primers with references were sourced, while those without were designed using Primer-BLAST (https://www.ncbi.nlm.nih.gov/tools/primer-blast/).

| Gene | Forward Primer (5'- to-3') | Reverse Primer (5'- to-3') |
|---|---|---|
| *cMyc* | TTGGAAACCCCGCAGACA | CGGAGTCGTAGTCGAGGTCA |
| *cMYC*[262] | CCTTCTCTCCGTCCTCGGAT | TCTTGTTCCTCCTCAGAGTCG |
| *Slc7a5*[263] | CTGGTCTTCGCCACCTACTT | GCCTTTACGCTGTAGCAGTTC |
| *Slc7a6*[264] | TCTACCTTCGCTGGAAAGAGCC | GCCACCAGAAACAAGGAGCAGA |
| *Slc7a7*[264] | AAGGTGTTGGCGCTGATTGCAG | AGAGTGCCAGAGCAATGTCACC |
| *Slc7a8*[264] | GCATACGTCACTGCAATGTCCC | GGAGCCATTGACTCCACCAAAC |
| *Slc38a1*[264] | TACCAGAGCACAGGCGACATTC | ATGGCGGCACAGGTGGAACTTT |
| *Slc38a2*[264] | GCGTTGGCATTCAATAGCACCG | TCGTAGATGGGAAGAACAGCGG |
| *Slc38a3* | CTACGAGCAGTTGGGCTACC | TGCCATCCATGTACCACACC |
| *Slc38a5* | TGAATGGAACCCTCTCTGCG | CCCCATGATAGCGTTGCTGA |
| *Slc38a8* | ATCCTCTTGAAGTCCGCTCTG | GCATGCCTCCTGCCTTGTAG |
| *Slc43a1*[264] | TTCCTGTGGAGCCTTGTCACCA | CTCCACCTTCTGTCTCTGCTCA |
| *Slc43a2*[264] | CAGCATCCTTGAGTTCCTGGTC | TGATGTAGCCGATGACAGGAGC |
| *Slc1a5*[262] | GCCTTCCGCTCTTTTGCTAC | GACGATAGCGAAGACCACCA |
| *Slc7a1* | GCAAAAACCTGCTCGGTCTG | TCATAGGTGTTGAGGCAGCG |
| *Slc36a1* | GGTCGGGAGAGGTAGAGGTT | AAAGAGCAGACACTGACGGG |
| *Hal*[255] | GGTGGCCTT AGAGGACAATG | GCTCCCGGTATTTGCTGTAT |
| *Amdhd1*[255] | TCCACGAGTTTGCAATGAAG | CTCCACCGTGAAGTTGATCC |
| *Ftcd*[255] | AACCTGCTAAGCACCAAGGA | GGACC TTTTTCAGACGTCCA |
| *Atf4* | TCCCTTTCCTCTTCCCCTCC | GGATTTCGTGAAGAGCGCCA |
| *Polr1a*[265] | CGTTCATCGAGGACTACCAGT | TCTTCATCAGTGGGAGCTTCA |

| | | |
|---|---|---|
| *Polr1b*[265] | ATGGCGACCCTTACTACAGC | GTTGTCCACAACACAGTTTTCTTTA |
| *Polr1c*[265] | CGGTAACTACGCCGGTTATG | ATTTGCACCACGTCCACAC |
| *Polr1d*[265] | AGCGCCACCTGAGGATTT | TTGAGGTCTTCAATCCTGATATTTT |
| *Polr1e*[265] | GAAAGGTCACATCGGAAGACA | GGGCAGAGACTTCAGCATTT |
| *Ubtf*[265] | TCACTAGCACCCACTTGCTC | GCTTCTCCGTTCATTCTCCA |
| *Sirt7*[265] | TGTCATGCAACTCCTCATGAAT | GGTCGCCAAGGAGAAGATT |
| *Rrn3*[265] | GCCTCCTGCCATGTACAGTT | CAAAAATGCTTCTGCAAATCC |
| *Fbl*[265] | AGGAGGATGCCCTTGTCAC | GGTTCCAGGCTCTGTACTCAA |
| *Got1* | CCATCAGTCTTTGCCCAGGT | TCATCTGTGCGGTACGCTCC |
| *Got2* | GCCTAAAGCCAGAGCAGGTAG | TCTGTTCCTTTGCACCTGGG |
| *Gls1* | AGTCTGGAGGGAAGGTTGC | GTTCCCAGGTCATTAACAGCA |
| *β-Actin* | GGCTGTATTCCCCTCCATCG | CCAGTTGGTAACAATGCCATGT |
| *HPRT* | TGAC ACTGGCAAAACAATGCA | GGTCCTTTTCACCAGCAAGCT |

**Table 2-3. Recombinant DNA.**

| Plasmid | Source | Item No. |
|---|---|---|
| pMDLg/pRRE | Didier Trono (Addgene) | 12251 |
| pRSV-Rev | Didier Trono (Addgene) | 12253 |
| pMD2.g | Didier Trono (Addgene) | 12259 |
| psPAX2 | Didier Trono (Addgene) | 12260 |
| pLenti PGK V5-LUC Neo | Eric Campeau (Addgene) | 21471 |
| pBabepuro-Gateway | Matthew Meyerson (Addgene) | 51070 |
| FUCas9Cherry | Marco Herald (Addgene) | 70182 |
| FgH1tUTG | Marco Herald (Addgene) | 70183 |
| pVSV-G | Akitsu Hotta (Addgene) | 138479 |
| pDONR™221 | ThermoFisher Sci Inc. | 12536017 |
| pBabepuro-GLUL | This project | N/A |

**Table 2-4. Antibodies used for WB, IF, and IHC analysis.**
CST: Cell Signalling Technology, SCBT: Santa-Cruz Biotechnology.

| Antibody | Supplier | Item No. |
|---|---|---|
| 4E-BP1 | CST | 9644 |
| Active Caspase-3 | Bio-Techne | AF835 |
| Akt | CST | 9272 |
| ASCT2 (H-52) | SCBT | sc-99002 |
| Asns | Proteintech | 14681-1-AP |
| ATF4 (SD20-92) | ThermoFisher | MA532364 |
| BrdU B44 | BD Biosciences | 347580 |
| c-Myc [Y69] | Abcam | ab32072 |
| CD11b | Abcam | ab133357 |
| CD11c (D1V9Y) | CST | 97585 |

| Antibody | Supplier | Item No. |
|---|---|---|
| CD163 [EPR19518] | Abcam | ab182422 |
| CD3G [EPR4517] | Abcam | ab134096 |
| CD45 (D3F8Q) | CST | 70257 |
| CD68 [EPR23917-164] | Abcam | ab283654 |
| CD8 [EPR21769] | Abcam | ab217344 |
| Cyclin B1 | CST | 4138 |
| E-cadherin (24E10) | CST | 3195 |
| eIF2α (D7D3) | CST | 5324 |
| Gls1 [EP7212] | Abcam | ab93434 |
| Gls2 | ProSci Inc. | 6217 |
| Glutamine Synthetase | BD Biosciences | 610518 |
| GOT1 | Proteintech | 14886-1-AP |
| GOT2 | Proteintech | 14800-1-AP |
| GSK-3α (D80E6) | CST | 4337 |
| H3K4me | Abcam | ab8995 |
| H3K4me3 [14-10C-E4] | Merck | 05-745R |
| HER2/ErbB2 [EP1045Y] | Abcam | ab16901 |
| K48-liknked Poly-Ub [EP8589] | Abcam | ab140601 |
| Ki67 | Abcam | ab15580 |
| LAT1 (human) | CST | 5347 |
| LAT1 (mouse) | 2BScientific | KAL-KE026 |
| LC3B (E7X4S) | CST | 43566 |
| mTOR | CST | 2972 |
| P-4E-BP1 (Ser65) | CST | 9451 |
| P-eIF2α (Ser51) (D9G8) | CST | 3398 |
| P-GSK3α (Ser21) (36E9) | CST | 9316 |
| P-p44/42 MAPK (Thr202/Tyr204) | CST | 9101 |
| P-RPS6 (Ser240/244) (D57.2.2E) | CST | 4858 |
| p21 Waf1/Cip1 | CST | 2947 |
| p44/42 MAPK | CST | 9102 |
| p53 | SCBT | sc-126 |
| Phospho-AKT (Ser473) | CST | 9271 |
| Puromycin [12D10] | Merck | MABE343 |
| RPS6 (54D2) | CST | 2317 |
| SQSTM1/p62 | Abcam | ab91526 |
| Ubiquitin (E412J) | CST | 43124 |
| Vimentin (R28) | CST | 3932 |
| Vinculin [EPR8185] | Abcam | ab129002 |
| β-actin-Peroxidase | Merck | A3854 |

**Table 2-5. Chemicals and Reagents.**

| Chemicals/Reagents | Source | Item No. |
|---|---|---|
| 10X T4 PNK Buffer | New England Biolabs | B0201 |
| 10X Tango | ThermoFisher Inc | BY5 |
| 2-Hydoxypropyl beta-cyclodextrin | Merck Life Sci Ltd. | H107 |
| 2-Mercaptoethanol | Bio-Rad Laboratories | 1610710 |
| 4x Laemmli Sample Buffer | Bio-Rad Laboratories | 1610747 |
| Adenine | Cambridge Bioscience | HY-B0152 |
| Bafilomycin A1 | ThermoFisher Inc | J61835.MCR |
| Bovine Serum Albumin (BSA) | Merck Life Sci Ltd. | A9647 |
| BP Clonase™ II | ThermoFisher Inc | 11789020 |
| BRD-0705 | Gift from Alejandro Gutierrez[266] | |
| BrdU | Cambridge Bioscience | 40024-BT |
| Cholera Toxin | Merck Life Sci Ltd. | C8052 |
| Concanamycin A | Merck Life Sci Ltd. | C9705 |
| Corning™Matrigel™ | Fisher Scientific | 11553620 |
| D-Histidine | ThermoFisher Inc | B21027.06 |
| DH5α competent cells | ThermoFisher Inc | 18265017 |
| dithiothreitol (DTT) | ThermoFisher Inc | R0862 |
| DMEM, high glucose, no glutamine | Gibco | 11960044 |
| DNase I | ThermoFisher Inc | 18068015 |
| dNTP Mix (10 mM) | ThermoFisher Inc | R0192 |
| Doxycycline | Merck Life Sci Ltd. | D9891 |
| ECL Select WB Detection Reagent | Cytiva | RPN2235 |
| EGF Recombinant Mouse Protein | ThermoFisher Inc | 10144983 |
| Ethidium Bromide 10 mg/mL | Bio-Rad Laboratories | 1610433 |
| Fast Digest Esp31 (BsmBI) | ThermoFisher Inc | ER0451 |
| FBS | Gibco | A5256701 |
| Glutamine | Gibco | 25030081 |
| GPNA | Selleck Chem | S6670 |
| HALT™ Protease Inhibitor Cocktail | ThermoFisher Inc | 78429 |
| HBSS | ThermoFisher Inc | 14170070 |
| HEPES (1M) | Gibco | 115630056 |
| Homocysteine | Merck Life Sci Ltd. | 69453 |
| Hydrocortisone | Merck Life Sci Ltd. | H0888 |
| Insulin | Merck Life Sci Ltd. | I1882 |
| L-Histidine | Merck Life Sci Ltd. | H6034 |
| L-Isoleucine | ThermoFisher Inc | J63045.14 |
| L-Leucine | Merck Life Sci Ltd. | L8912 |
| L-Methionine | Merck Life Sci Ltd. | M5308 |

| Chemicals/Reagents | Source | Item No. |
|---|---|---|
| LR Clonase™II | ThermoFisher Inc | 11791020 |
| Methylcobalamin (Vit B12) | Merck Life Sci Ltd. | M9756 |
| MG-132 | Selleck Chem | S2619 |
| Nanvuranlat (JPH203) Batch 03 | Selleck Chem | S8667-03 |
| Nanvuranlat (JPH203) Batch 05 | Selleck Chem | S8667-05 |
| Nitrocellulose Membrane | Bio-Rad Laboratories | 1620112 |
| NP-40 (10% in H2O) | Cambridge Bioscience | 2111-100 |
| One Shot™ OmniMAX™ 2T1R | ThermoFisher Inc | C854003 |
| PEI MAX | Generon | 24765-100 |
| Pen/Strep (5,000 U/mL) | Gibco | 15070063 |
| Pictilisib (GDC-0941) | Selleck Chem | S1065 |
| Pierce 660 Protein Assay Reagent | Fisher Scientific | 10177723 |
| Pierce BCA Protein Assay Reagent A | ThermoFisher Inc | 23223 |
| Pierce BCA Protein Assay Reagent B | ThermoFisher Inc | 23224 |
| Polybrene | Merck Life Sci Ltd. | H9268 |
| Ponceau S | Fisher Scientific | 17435103 |
| Precellys ceramic kit 1.4 mm | Bertin Instruments | 432-3751 |
| ProLong Gold Anitfade Mountant | ThermoFisher Inc | P10144 |
| Propidium Iodide | Cambridge Bioscience | 14289 |
| Puromycin Dihydrochloride | ThermoFisher Inc | 11417620 |
| Q5 High Fidelity | New England Biolabs | M0491 |
| Quick CIP | New England Biolabs | M0525 |
| Random Hexamers | 2B Scientific | PM-301S |
| Rapamycin | Selleck Chem | S1039 |
| RNase A | ThermoFisher Inc | R1253 |
| RNaseOUT™ | ThermoFisher Inc | 10777019 |
| S.O.C. Medium | ThermoFisher Inc | 15544034 |
| Sapanisertib (INK 128) | Selleck Chem | S2811 |
| SuperScript™III Reverse Transcriptase | ThermoFisher Inc | 18080044 |
| T4 PNK | New England Biolabs | M0201 |
| T7 DNA Ligase | New England Biolabs | M0318 |
| Telaglenastat (CB-839) | Selleck Chem | S7655 |
| Trametinib (GSK1120212) | Selleck Chem | S2673 |
| Transferrin | Merck Life Sci Ltd. | 90190 |
| Triiodothyronine | Generon | AOB9374 |
| Triton X-100 | Merck Life Sci Ltd. | T8787 |
| TRIzol | ThermoFisher Inc | 15596026 |
| Tween-20 | Merck Life Sci Ltd. | P9416 |
| VivoGlo Luciferin | Promega | P1043 |

**Table 2-6. Commercial Assays and Kits**

| Kit | Source | Item No. |
|---|---|---|
| Nucleospin Gel and PCR Clean-up | Fisher Scientific | 12303368 |
| QIAprep Spin Miniprep | Qiagen | 27104 |
| QIAGEN Plasmid Midi | Qiagen | 12143 |
| Proteome Profiler Mouse Cytokine Array Kit, Panel A | Bio-Techne | ARY006 |
| Mouse IFNgamma ELISA | Abcam | ab282874 |

## 2.2 Cloning

### 2.2.1 CRISPR-Cas9

#### *2.2.1.1 sgRNA Design*

CRISPR/Cas9 target sites for SLC7A5 in humans and mice, as well as c-Myc in mice, were identified using the CHOPCHOP web tool (https://chopchop.cbu.uib.no/) and 24 bp oligonucleotides were synthesised with a 4-bp overhang, where the forward oligo included a TCCC overhang and the reverse complement oligo included an AAAC overhang to clone into the BsmBI site of FgH1tUTG (gift from Marco Herold (Addgene plasmid # 70183; http://n2t.net/addgene:70183; RRID: Addgene_70183) as previously described(Table 2-7)[267].

**Table 2-7. sgRNA oligonucloetides**

| | Sense (5'-TCCC…) | Anti-Sense (5'-AAAC…) |
|---|---|---|
| sgSLC7A5 | TGTCTCCACAGTGCTGCTCA | TGAGCAGCACTGTGGAGACA |
| sgSlc7A5 | CGCGGGCGCCAAGAGGCGCG | GCCGAGAGCATGGCGGTCGC |
| sgMyc | TCGGGCTCATCTCCATCCCG | CGGGATGGAGATGAGCCCGA |

#### *2.2.1.2 Cloning sgRNA into FgH1tUTG*

The oligos were annealed in a total volume of 10 µL (Table 2-8) in a 96-well Bio-Rad T100 Thermal Cycler PCR (Bio-Rad Laboratories, Inc) under the following conditions: 30 minutes at 37°C, 2 minutes at 95°C, a 45-minute temperature

decline from 95°C to 25°C, and a final hold at 12°C. This mixture was then diluted at 1:200 for further use.

**Table 2-8. Components of reaction to anneal oligonucleotides**

| Reagent | Volume |
|---|---|
| 10X T4 PNK Buffer | 1 µL |
| T4 PNK | 1 µL |
| ddH2O | 6 µL |
| Forward (100 µM) | 1 µL |
| Reverse Complement (100 µM) | 1 µL |
| Total Volume | 10 µL |

The FgH1tUTG vector was digested for 1 hour in a total volume of 20 µL at 37°C (Table 2-9). After the restriction digestion, 1 µL of quick CIP (Calf-intestinal alkaline phosphatase) was added to prevent re-ligation. The entire volume was run on a 1% agarose gel (1x TAE buffer (2 M Tris, 1M glacial acetic acid, 50 mM EDTA, pH 8.5) and stained with 0.5 µg/mL ethidium bromide (Bio-Rad Laboratories, Inc)). The linearized vector was excised from the agarose gel, and the plasmid DNA was extracted using the NucleoSpin® Gel and PCR Clean-up commercial kit (MACHEREY-NAGEL GmbH & Co.).

**Table 2-9. Restriction enzyme digest of FgH1tUTG.**

| Reagent | Volume |
|---|---|
| FgH1tUTG vector | 1 µg |
| 10X Tango Buffer | 2 µL |
| FastDigest BsmBI | 1 µL |
| DTT (10 mM) | 1 µL |
| ddH2O | X µL |
| Total Volume | 20 µL |

The linearised vector and annealed oligos were ligated at a 1:3 ratio with T7 DNA Ligase (New England Biolabs) according to manufacturer instructions and ligated for 1 hour at room temperature. Subsequently, 5 µL of the ligation mixture was used to transform chemically competent DH5α *Escherichia coli* (*E. coli*) (ThermoFisher Scientific Inc.), which were incubated overnight at 37°C.

#### *2.2.1.3 Validation*

Colonies were selected and cultured overnight in 2 mL of LB medium supplemented with 100 µg/mL ampicillin. Plasmid DNA was extracted using the QIAprep Spin Miniprep Kit (QIAGEN) according to the manufacturer's instructions. The plasmid DNA was sequenced by Source Bioscience Sanger DNA sequencing with the *5'- CAGACATACAAACTAAAGAAT-3'* sequencing primer.

### 2.2.2 Plasmid Construction for Protein Overexpression

To generate a plasmid expressing the GLUL gene encoding GS, the gene was amplified from cDNA extracted from T47D cells. Primers were designed to target the GLUL coding sequence, and four 5' G residues and 25-bp attB flanking regions were added to the primer to insert the PCR product into the pDONR™221 Gateway plasmid (Table 2-10).

GLUL was amplified from 0.5 µg of cDNA using the Q5 High-Fidelity DNA Polymerase (New England Biolabs) following the manufacturer's instructions in a final volume of 50 µL. Gene amplification was done using a 96-well Bio-Rad T100 Thermal Cycler PCR (Bio-Rad Laboratories, Inc) (Table 2-11). The entire volume of the PCR reaction was run on a 1% agarose gel (1x TAE buffer and stained with 0.5 µg/mL ethidium bromide (Bio-Rad Laboratories, Inc)). The 1145-bp gene was excised from the agarose gel and extracted using the NucleoSpin® Gel and PCR Clean-up commercial kit (MACHEREY-NAGEL GmbH & Co.).

**Table 2-10. GLUL targeting primers with attB flanks for Gateway™ cloning.**

| | Primer Sequence (5') |
|---|---|
| attB1 GLUL F | GGGGACAAGTTTGTACAAAAAAGCAGGCTCGATGACCACCTC AGCAAGTTC |
| attB2 GLUL R | GGGGACCACTTTGTACAAGAAAGCTGGGTGTTAATTTTTGTAC TGGAAGG |

**Table 2-11.Thermocycling conditions for GLUL primers.**

| Temp (°C) | Time | Cycles |
|---|---|---|
| 98 | 1 min | 1X |
| 98 | 10 s | x40 |
| 60 | 60 s | |
| 72 | 30 s | |
| 72 | 2 min | 1X |
| 12 | ∞ | N/A |

The attB-PCR was inserted into pDONR™221(ThermoFisher Scientific Inc.) with BP Clonase™ II (ThermoFisher Scientific Inc.) following the manufacturer's instructions and 1 µL of the reaction was transformed into competent One Shot® OmniMAX™ 2 T1 Phage-Resistant cells (ThermoFisher Scientific Inc) and incubated overnight at 37°C.

#### *2.2.2.1 Validation*

Colonies were selected and cultured overnight in 2 mL of LB medium supplemented with 50 µg/mL kanamycin. Plasmid DNA was extracted using the QIAprep Spin Miniprep Kit (QIAGEN) according to the manufacturer's instructions. Positive clones were sequenced using the M13 universal sequencing primer (Fwd 5'- GTAAAACGACGGCCAGT) by Source Bioscience Sanger DNA sequencing. Sequences were carefully checked to ensure no mutations were within the coding sequence of GLUL.

#### *2.2.2.2 Cloning into Lentiviral Expression Vector*

GLUL from pDONR™221-GLUL was inserted into pBabepuro-gateway (a gift from Matthew Meyerson (Addgene plasmid # 51070; http://n2t.net/addgene:51070; RRID: Addgene_51070)) using LR Clonase™ II (ThermoFisher Scientific Inc.) as instructed by the manufacturer, and 1 µL of the reaction was transformed into competent One Shot® OmniMAX™ 2 T1 Phage-Resistant cells (ThermoFisher Scientific Inc) and incubated overnight at 37°C. Colonies were similarly amplified and extracted as above, and successful insertion of GLUL into pBabepuro-gateway was validated using restriction enzyme digestions.

### 2.2.3 Transformation and Amplification of Plasmids

Each cloning reaction (ligation/ LR Clonase/BP Clonase) was transformed into 50 µL of indicated competent bacteria and incubated on ice for 30 minutes. After this, they were heat shocked at 42°C for 30 seconds and transferred onto ice for 2 minutes. Recovery was done by adding 250 µL of S.O.C. Medium (ThermoFisher Scientific Inc) to each sample and incubating at 37°C for 1 hour with rotation at 220 rpm. Each transformation (50-100 µL) was plated on LB agar plates containing relevant antibiotic for positive selection and incubated overnight at 37°C.

For amplification of the plasmid DNA, positive clones were cultured overnight in 2 mL of LB medium at 37°C with 220 rpm rotation. For midi-preps, 500 µL of the 2-mL culture was spiked into 50 mL of LB medium and cultured overnight at 37°C with 220 rpm rotation. Plasmid DNA was isolated from cells using the QIAGEN® Plasmid Midi Kit (QIAGEN) according to manufacturer instructions.

## 2.3 Cells and *in vitro* experimental procedures

### 2.3.1 Cells

The MYC310, MYAZ16.1e, MYAZ6.6g, and MYAZ12.3i MMTV-Myc mammary tumour cell lines were generated by previous PhD students, Dr Benedict McIntyre and Dr Emma Still. Briefly, MMTV-Myc mammary tumours were collected and minced on ice with sterile razor blades. The chunks were then dissociated in 10 mL/gram of tissue of Digestion Buffer (MMEC media supplemented with 1% BSA, 1 mg/mL Collagenase (Type L)) for 30 minutes at 37°C, at 200 rpm. The mixture was filtered through a 70 µm mesh filter and pelleted by centrifugation at 530 *xg* for 5 minutes. The supernatant was discarded, and the pellet was washed with 5 mL of RBC lysis solution (170 mM Tris, 150 mM ammonium chloride, pH 7.4) and centrifuged as before. The cell pellet was resuspended in MMEC media and propagated to generate a tumour cell line (Table 2-12).

**Table 2-12. MMEC media composition.**

| Component | Final Concentration |
|---|---|
| DMEM | N/A |
| iFBS | 10% |
| HEPES | 10 mM |
| Glutamine | 2 mM |
| Insulin | 5 µg/mL |
| Hydrocortisone | 1 µg/mL |
| EGF | 10 ng/mL |
| Pen/Strep | 100 µg/mL |

The other cell lines used in this project, 67NR, BT-549, MDA-MB-231, Hs578T, T47D, AU565, MCF7, HCC202, SKBR3, MDA-MB-453, and MDA-MB-157, HEK293T, and Phoenix-AMPHO were obtained from the Francis Crick cell lines repository from Cell Services. Cell Services authenticated all human cell lines by STR (short tandem repeat) profiling. Furthermore, all cell lines used in this project (mouse and human) were tested for mycoplasma contamination by Cell Services and confirmed negative. The primary mouse cell lines were cultured in MMEC media, and the remaining cell lines were cultured in DMEM (Gibco) supplemented with 10% heat-inactivated FBS, 2 mM glutamine (Gibco), and 1% Penicillin-Streptomycin (Pen-Strep). Cells were maintained in standard cell culture conditions in a humidified incubator at 37°C and 5% $CO_2$ and at atmospheric oxygen levels.

Experimental DMEM including (i) amino acid-free DMEM, (ii) histidine, isoleucine, methionine, leucine, and glutamine-free DMEM, (iii) histidine and glutamine-free DMEM, and (iv) glutamine and glucose-free DMEM were all prepared by the Media Preparation service at the Francis Crick based on the composition of DMEM. L-histidine, L-isoleucine, L-methionine, L- leucine, L-glutamine and D-glucose were supplemented at the indicated concentrations. Where mentioned, homocysteine, vitamin B12, D-histidine, and doxycycline were supplemented into DMEM. In experiments with stable isotope labelling, the unlabelled amino acid was replaced by the stable isotope in the medium; these included [U-$^{13}$C]-histidine, [U-$^{13}$C]-glutamine, [amide-$^{15}$N]-glutamine, and [U-$^{13}$C]-glucose (all Cambridge Isotope Laboratories, Inc.) at the indicated concentrations. Experimental media was supplemented with heat-inactivated, dialysed FBS, which was prepared by dialyzing 50 mL of FBS against 2 L of calcium-and-magnesium-free PBS (137 mM

NaCl, 2.7 mM KCl, 10 mM $Na_2HPO_4$, 1.8 mM $KH_2PO_4$, pH 7) using dialysis tubing with a 3,500 Da molecular weight cut-off (Cat No. 68035, ThermoFisher Scientific Inc.). The PBS was changed daily for 5 days.

### 2.3.2 Generating Stable Knockdown Cell Lines

MYAZ16.1e and 67NR cells with stable knockdown of Atf4 were generated via lentiviral transduction. Lentiviral particles were produced by transiently transfecting HEK293T cells grown in 60-mm cell culture dishes with 2 µg of the shRNA containing vectors, pLKO-puro shAtf4 and shLuc plasmids were a gift from Dr Andrés Méndez Lucas (Universitat de Barcelona), along with 750 ng of the psPAX2 packaging plasmid and 250 ng of the pMD2.g envelope plasmid. Transient transfection was achieved using standard chemical transfection with 10 µg/mL polyethylenimine (PEI) transfection at a 3:1 ratio of PEI to DNA. Media was changed 16 hours after transfection, and virus-containing supernatants were collected after an additional 48 hours, spun at 1000 *xg* for 5 minutes, and filtered through a 0.45 µm PES filter. For infection, MYAZ16.1e and 67NR cells were plated in 6-well plates at an optimised density to reach ~60-80% confluency at infection and incubated with 1 mL of virus-containing supernatant and 1 mL of standard medium with 8 µg/mL polybrene for 48 hours. Cells were then selected with 5 µg/mL (MYAZ16.1e) and 1 µg/mL (67NR) puromycin until all the cells on the respective control plates were killed. Multi-clonal cultures were propagated and used for experiments, and knockdowns were confirmed by RT-qPCR.

### 2.3.3 Generating Stable Knockout Cell Lines

BT-549 and MYAZ16.1e cells were used to knockout *SLC7A5*/*Slc7a5* or *Myc* using a two-vector system. Cells were first transduced with lentiviral particles containing only Cas9 with a fluorescent cherry promoter (FUCas9Cherry (a gift from Marco Herold (Addgene plasmid # 70182; http://n2t.net/addgene:70182; RRID: Addgene_70182)). These cells were then selected for a pure population and subsequently transduced with lentiviral particles containing (i) an empty FgH1tUTG vector or (ii) FgH1tUTG containing the desired sgRNA. Notably, the FgH1tUTG is

an inducible sgRNA with a constitutive fluorescent GFP reporter. After which, double-positive cells were selected.

Lentiviral particles were produced in HEK293T cells as described above; however, a third-generation lentiviral packaging system was used with 2 µg of the vector: pMDL (1 µg), pRSV-rev (500 ng), and p-VSV-G (600 ng).

For BT-549 sg*SLC7A5* cells, a bulk population of double-positive cells expressing FuCas9Cherry and FgH1tUTG were selected via flow-assisted cell sorting for mCherry and GFP using an Avalon cell sorter. For MYAZ16.1e cells, a bulk population of mCherry positive FUCas9Cherry expressing cells were sorted. After the transduction with FgH1tUTG with sg*Slc7a5* and sg*Myc*, the cells were sorted as double-positive single cells into a single well of a 96-well cell culture plate to generate clonal populations using the MoFlo XDP cell sorter (Beckman Coulter Life Sciences), assisted by the Flow Cytometry service at the Francis Crick. Knockouts were confirmed by immunoblotting.

### 2.3.4 Generating Stable Overexpression Cell Lines

Phoenix-AMPHO cells were plated in a 60-mm cell culture dish and transfected with 5 µg pBabepuro-GLUL at a 1:3 ratio with PEI. The media was changed after 16 hours and the virus-containing supernatant was collected after another 48 hours. MYAZ16.1e cells were transduced in a 6-well plate with 1 mL of the virus-containing supernatant, 1 mL of MMEC media, and 8 µg/mL polybrene and cultured for 48 hours. Positive cells were selected with 5 µg/mL puromycin until all cells on the control plate were killed. The culture was propagated, and successful overexpression of GS was confirmed via immunoblotting.

HEK293T cells were plated in a 60-mm cell culture dish and transfected with 2 µg pLenti PGK V5-LUC Neo (was a gift from Eric Campeau (Addgene plasmid # 21471; http://n2t.net/addgene:21471; RRID: Addgene_21471)) and 750 ng psPAX2 and 250 ng pMD2.g using standard chemical transfection of PEI at a 3:1 ratio PEI to DNA. MYAZ16.1e cells were transduced as described above and selected with 500 µg/mL Geneticin™ (Thermo Fisher Scientific Inc.).

### 2.3.5 Small Molecule Inhibitors

A range of inhibitors, including CB-839, JPH203, GDC0941, Trametinib, Rapamycin, Ink128, Concanamycin A (ConA), Bafilomycin A1 (BafA1), MG-132, GPNA, BRD-0705 were used to modulate pathway activity as required for each experiment. The specific inhibitors, their concentrations, and treatment conditions are provided in the corresponding figure legends.

### 2.3.6 Proliferation Assays

For proliferation assays, the indicated cells were washed with PBS prior to changing to the indicated experimental conditions. If the proliferation assays lasted for >3 days, the experimental media was refreshed. Cell proliferation was quantified using the IncuCyte® imaging system (Sartorius) which tracks living cells and quantifies the confluency of cells over time.

### 2.3.7 SUnSET

To measure nascent global protein synthesis, the SUnSET(**su**rface **sen**sing of **t**ranslation)[268] assay was used; prior to the collection of cells for the preparation of lysates, they were administered 10 µg/mL of puromycin for 10 minutes. To confirm the efficacy of puromycin incorporation into proteins, cells were treated with 100 nM of cycloheximide (CHX) 20 minutes before the addition of puromycin, for a total time of 30 minutes. After which cells were washed with ice-cold PBS on ice and lysed as described below for western blot (WB) analysis.

### 2.3.8 BrdU-PI Cell Cycle Analysis

MYAZ16.1e, MYAZ6.6g and MYAZ12.3i cells were seeded in 5 x150-mm plates at 8.0 x $10^6$ cells/plate and cultured overnight. These plates correlated to a control (pre-starved), starved (-AA), histidine preloaded (-AA+H), starved replenished (-AA/DMEM) and histidine preloaded replenished (-AA+H/DMEM). Besides the control plate, the media was changed to amino acid free medium (DMEM without amino acids supplemented with 2% dFBS and 1% Pen-Strep) with or without 200

μM of histidine for 48 hours. After which the medium was changed to amino acid replete MMEC media on the indicated plates for 15 hours. One hour prior to collection, 10 μM bromodeoxyuridine (BrdU) was added to each plate, and cells were detached with Trypsin (Gibco) for collection and neutralised with MMEC media, cells were pelleted via centrifugation at 300 *xg* for 5 minutes and the pellet was washed with PBS. The supernatant was discarded, and for every 2.0 x $10^6$ cells, the cell pellet was resuspended in 50 μL of HBSS with 2% FBS, followed by the dropwise addition of 1 mL ice-cold 70% ethanol while gently vortexing. Cells were then incubated on ice for 60 minutes to allow fixation before proceeding with BrdU and PI (propidium iodide) staining.

The following protocol is for 2.0 × $10^6$ cells. The cells were pelleted at 500 *xg* for 5 minutes, the supernatant was carefully removed, and cells were washed twice with HBSS containing 2% FBS. The pellet was resuspended in 1 mL of 2N HCl with 0.5% Triton X-100 and incubated at room temperature for 30 minutes. Following another centrifugation, cells were resuspended in 1 mL of 0.1 M sodium borate ($NaB_4O_7$, pH 8.5) and incubated for at least 30 minutes at room temperature.

Cells were then pelleted and resuspended in 0.5 mL of antibody solution (PBS, 1% BSA, 0.2% Tween-20) containing mouse anti-BrdU antibody (1:100, BD Biosciences). After incubation at room temperature for 30 minutes, cells were washed with 1 mL PBS, pelleted, and resuspended in 500 μL antibody solution containing Alexa Fluor™ 488 goat anti-mouse secondary antibody (1:200, ThermoFisher Scientific Inc.). The mixture was incubated in the dark for 30 minutes at room temperature.

Following a PBS wash, cells were pelleted again and resuspended in 0.5 mL propidium iodide (PI) solution (0.1 mg/mL in HBSS with 0.6% NP-40), vortexed gently, and 0.5 mL RNase A solution (0.2 mg/mL in HBSS) was added. The cells were incubated for 30 minutes at 37°C in the dark. Finally, cells were filtered through a 40 μm mesh filter and stored at 4°C in the dark until analysis.

The samples were analysed for FITC- (i.e., BrdU) and PI-positive cell detection using a BD FACSAria™ III Cell Sorter (BD Biosciences), assisted by a postdoctoral

fellow in our lab, Dr Sharavan Venkateswaran. Single cells were identified by gating based on forward and side scatter. Compensation and gating were done using unstained and single-stained controls. The FITC-positive cells were detected using the 530/30 band-pass filter, and PI was detected in the 695/40 band-pass filter. Between 5,000 to 10,000 events were collected for each sample. Data was analysed by Dr. Sharavan Venkateswaran using FlowJo software (BD Biosciences). Both parameters were plotted against each other, and the populations were identified as G0/G1, S, and G2/M based on PI (DNA-content) and FITC (BrdU)-Positive cells. FITC(BrdU)-negative cells were denoted as G0/G1 and G2/M and separated by their DNA content. BrdU positive cells were denoted as S-phase.

### 2.3.9 Immunofluorescence

For indicated experiments, cells on glass coverslips were washed three times with ice-cold PBS, then fixed in 4% paraformaldehyde (PFA) in PBS for 12 minutes at room temperature. After fixation, cells were washed five times with PBS. Blocking and permeabilisation were performed using 3% BSA and 0.2% Triton-X in PBS for 12 minutes at RT. Cells were washed three times with PBS, followed by incubation with the indicated primary antibody solution (3% BSA in PBS) at the appropriate dilution overnight at 4°C. The primary antibodies used were ASCT2 (Santa Cruz Biotechnology) and BrdU (BD Biosciences).

After incubation with the primary antibody, cells were washed five times with PBS and incubated with the required secondary antibody solution (3% BSA in PBS), for 1 hour at room temperature in the dark. Cells were washed five times with PBS before nuclear staining by incubating cells with DAPI (1:10,000) for 5 minutes. Cells were washed another 5 times before mounting onto slides with ProLong™ Gold Antifade Mountant (ThermoFisher Scientific Inc.).

The staining was imaged with an Axio-Imager M2 upright microscope (ZEISS) and images were prepared with the opensource image analysis software, FIJI (https://github.com/fiji).

## 2.4 Mouse models and *in vivo* experimental procedures

### 2.4.1 Mouse Models

All mouse procedures and husbandry complied with United Kingdom Home Office under the Animals (Scientific Procedures) Act 1986 regulations and received approval from the Animal Welfare and Ethical Review Panel under the project license number PP3464389 at the Francis Crick Institute. The mouse models utilised in this project included wildtype FVB/NJ and NOD-SCID (Nod-Pkrdc$^{scid}$) females (from in-house colonies at the Francis Crick Institute), and transgenic MMTV-MYC (Tg(MMTV-MYC)141-3Led, MGI ID: 2447500), and MMTV-ErbB2 (Tg(MMTV-ErbB2)NK1Mul, MGI ID: 3050871), originally obtained from The Jackson Laboratory, but crossed onto the FVB/N mouse strain for >10 generations. Mice were genotyped to confirm expression of MYC and ErbB2. Mice were bred and housed under specific-pathogen-free conditions at the Francis Crick Institute.

### 2.4.2 Tumour initiation by Mammary Fat Pad Injection

*In vivo* experiments were either done directly on transgenic MMTV-Myc and MMTV-ErbB2 mice, or on orthotopic allografts generated through mammary fat pad injection of MYAZ16.1e cells or tumour cells that were dissociated and isolated from MMTV-Myc or MMTV-ErbB2 tumours, as described above, and prepared, without passaging (P0), in FBS with 10% DMSO and stored in liquid nitrogen.

MYAZ16.1e mammary tumour cells and derivative cell lines cultured overnight were detached with Trypsin (Gibco), neutralised with MMEC media, and washed two times with PBS. Cells were counted and resuspended to 10.0 x $10^6$ cells/mL. Individual aliquots per mouse were prepared by combining 12 µL of the cell suspension with 48 µL of Matrigel (Corning) to make a total volume of 60 µL. The resulting mixture consists of a 1:4 ratio of cell suspension to Matrigel™, and 1.2 x $10^5$ cells. From these aliquots, 50 µL of the suspension was injected into the fourth inguinal mammary fat pad of 8- to 10- week-old virgin FVB/NJ or NOD-SCID mice, as indicated. MMTV-Myc and MMTV-Erbb2 P0 cells were prepared via a similar method. However, they were thawed at 37°C and centrifuged at 300 *xg* for 5

minutes before being washed two times with PBS. Furthermore, the cell suspension was modified to inject a 2.5 x $10^5$ cells/mouse. Tumours were detected within two weeks of injection and were carefully monitored for signs of distress, poor health, or weight loss. Weight loss of 20% from the initial measurement or 15% in the last 72 hours was used as a criterion for humane euthanasia. Calipers were used to measure the length and width of tumours, and the tumour volume was calculated by determining the ellipsoid volume[269]:

$$\frac{length \times width^2}{2}$$

Tumours were measured by the Biological Research Facility at the Francis Crick Institute.

### 2.4.3 Diets

For amino acid restriction diets, the following TestDiet® Baker AA synthetic diets (IPS Product Supplies Ltd.) were used:

- 5WTU: no added histidine
- 5GFQ: 0.1% added histidine (20% histidine diet)
- 5WA1: histidine control diet
- 5BYB: no added glutamine or non-essential amino acids (5BYB)
- 5BYA: glutamine control, which includes glutamine but no NEAAs.

Other amino acids were proportionally increased in these diets to maintain overall amino acid intake.

Mice were placed on the histidine diets at 5-6 weeks of age and for 3 weeks prior to tumour initiation via mammary fat pad injection. During the first week, mice were weaned onto their respective diets through a stepwise increased in the amount of the experimental diet relative to their regular diet. This included 2 days at 25%, 2 days at 50%, and 2 days at 75% before being placed on 100% experimental diet for the remainder of the experiment. Mice remained on the same diet until the experimental endpoint. For the glutamine diets, mice were started on the diet from 4-5 weeks of age and continued for 6 weeks until tumour initiation by mammary fat pad injection. To assess the efficacy of the diets, approximately 50-200 µL of blood

was routinely collected from tail vein bleeds. This was allowed to clot on ice for 10 minutes before centrifugation at 1,600 *xg* for 10 minutes at 4°. The serum was transferred to a new Eppendorf, flash frozen in liquid nitrogen, and moved to long-term storage at -80°C.

The other experimental diets used in this project were Teklad custom rodent diets (Envigo):

- TD.08541: 0.625 g/Kg Doxycycline hyclate on a standard diet base
- T.2918Mi.12: standard diet

For the doxycycline diet treatments, mice were placed on the standard or doxycycline diet when tumours reached 100 $mm^3$ and maintained on the diet throughout the experiment.

The Biological Research Facility at the Francis Crick Institute weighed mice daily for the first week of experimental diets and then once a week for the duration of the experiment.

### 2.4.4 JPH203 Preparation and Administration

JPH203 (Selleck Chem) was prepared for intraperitoneal injections by first dissolving 1.25 or 2.0 mg of JPH203 in DMSO. This solution was then diluted with a mixture of 25% w/v (2-Hydroxypropyl)-β-cyclodextrin (Merck) in 0.9% saline, resulting in a final solution where the drug and diluent were mixed in a 1:4 ratio. The final preparation has a concentration of 1.25 mg/mL or 2 mg/mL JPH203, respectively, with 20% DMSO/20% β-cyclodextrin in 0.9% saline. The vehicle was 20% DMSO/20% β-cyclodextrin in 0.9% saline.

Mice received a daily intraperitoneal (IP) injection of JPH203 at the indicated experimental concentrations and duration. Daily administration of JPH203 was done by the Biological Research Facility at the Francis Crick Institute

### 2.4.5 Stable-isotope Labelling

Stable-isotope labelling was achieved either through a bolus injection (one injection of histidine or leucine for 5 minutes or 2x injections of glutamine for 15 minutes each) or a 3-hour infusion of histidine. The short-term histidine and leucine boluses were used to assess uptake and transporter function into tissues, whereas the long-term infusion assessed $^{13}C$ incorporation from histidine into various metabolites. The glutamine was used to assess whether the tumour's capacity to take up and catabolize glutamine was affected.

[U-$^{13}C$]-histidine (Cambridge Isotope Laboratories) was diluted to 25 mg/mL in 0.9% saline and administered through intravenous (IV) injection into the tail vein at 0.107 mg/gBW (body weight). [U-$^{13}C$]-leucine (Cambridge Isotope Laboratories) was diluted to 20 mg/mL in 0.9% saline and administered through the tail vein at 0.086 mg/gBW. [U-$^{13}C$]-glutamine (Cambridge Isotope Laboratories) boluses were separated into two consecutive 15-minute boluses due to the poor solubility of glutamine. [U-$^{13}C$]-glutamine was diluted to 40 mg/mL in 0.9% saline and administered through the tail vein for a combined total of 0.34 mg/ gBW.

Infusions of [U-$^{13C}$]-histidine were provided through a tail vein catheter, using an Aladdin AL-1000 pump (World Precision Instruments) in mice under general anaesthesia with isofluorane. [U-$^{13C}$]-histidine was dissolved to 40 mg/mL in 0.9% saline. A 0.12 mg/gBW bolus was first administered, followed by a 3.45 µg/gBW/min infusion for 3 hours.

At the end of the bolus or infusions, the blood was collected via cardiac puncture, incubated on ice to clot for 10-30 minutes, and centrifuged at 1,600 *xg* for 10 minutes at 4°C. The serum was transferred to a new Eppendorf and flash-frozen in liquid nitrogen before storage at -80°C until further use.

### 2.4.6 IVIS Bioluminescence Imaging

Bioluminescence images were captured using the IVIS Spectrum (PerkinElmer Inc), and the bioluminescence signal within the region of interest (ROI) was quantified with the Living Image® software (Revvity). Mice bearing orthotopic

allografts of MYAZ16.1e V5-Luc-expressing cells received an IP injection of 150 mg/kg D-Luciferin (30 mg/mL in 0.9% saline, Promega Corporation). Approximately 10 minutes post-injection, the mice were placed in an induction chamber under general anaesthesia with isoflurane and then transferred to the IVIS Spectrum imaging chamber, where anaesthesia was maintained. Bioluminescence images were captured 15 minutes post-injection. The ROI was drawn around the tumour area, and the total flux (photons/second) was calculated.

### 2.4.7 Tumour Interstitial Fluid Collection

To collect tumour interstitial fluid (TIF), tumours collected from mice were first washed in 0.9% saline and blotted on Whatman filter paper to remove any residual blood. The tumours were placed into chilled 0.22 µm filter centrifuge tubes (Costar, Product No.8160) and centrifuged 500 *xg* for 10 minutes at 4°C. The resulting TIF volume was measured, flash-frozen in liquid nitrogen, and stored at -80°C for future use.

### 2.4.8 In vivo SUnSET

For *in vivo* measurement of nascent global protein translation, mice were administered an IP injection of 0.02 mg/gBW puromycin (5 mg/mL in 0.9% saline). After 30 minutes, tissues were dissected and flash-frozen in liquid nitrogen before storage at -80°C for future WB analysis.

### 2.4.9 Immunohistochemistry and Analysis

Dissected tissues were placed in 10% neutral buffered formalin and incubated for 48 hours at 4°C with rotation. Tissues were then stored in 70% EtOH and dehydrated for up to one week before embedding in paraffin blocks. Haematoxylin and Eosin (H&E) staining, along with immunohistochemistry (IHC), was performed by the Experimental Histopathology (EHP) service at the Francis Crick Institute. IHC markers used include Ki67, Cleaved Caspase 3 (CC3), Lat1, Myc, CD45, CD3, CD8, CD11b, CD68, CD163, CD11c. Images were acquired using an Axioscan 7 brightfield microscope slide scanner (Zeiss) at 20x magnification.

#### *2.4.9.1 Cell Positive Detections*

Cell detection for IHC staining was performed using the open-source image analysis software, QuPath (version 0.5.1) (https://qupath.github.io/) with the positive cell detection tool (*Analyze → Cell Analysis → Positive cell detection)*. Key parameters were defined based on stain intensity and localization. For quantification of Ki67, CC3, CD45, CD8, and CD3 a Nucleus:DAB OD mean was applied, as the nucleus was obscured by staining, and a cell expansion of 5 was used. The minimum and maximum areas were set to 10 µm and 400 µm, respectively, and the staining threshold was set to 0.05. Staining intensity was not scored, and the total number of positive cells was quantified as a percentage of the total cells within the tumour.

#### *2.4.9.2 Membrane Staining Scoring*

A previously published method was employed to score LAT1 IHC staining intensity at the cell membrane[270]. Briefly, this method used a custom Groovy script to detect cells, and thresholds were applied to score staining as high (> 1.0), medium (> 0.6 and ≤ 1.0), or low (> 0.3 and ≤ 0.6) based on the mean DAB signal intensity in the membrane compartment, following image deconvolution and cell segmentation. The resulting quantification provides the total number of cells and the number of cells classified as high, medium, or low.

### 2.4.10 Cytokine Array

The Proteome Profiler Mouse Cytokine Array Kit (Bio-Techne Ltd.) was used to assess changes in the cytokine profile within mammary tumours on control or histidine diets according to manufacturer protocol. Protein lysates were prepared as described previously for tumour tissue, and 250 µg of each sample was loaded onto each membrane. Membranes were imaged using an Amersham ImageQuant™ 800 (Cytiva Life Sciences). Images were taken consecutively every 1 minute for up to 10 minutes. To quantify pixel intensity for each cytokine/chemokine the Protein Array Analyzer for ImageJ macro was used in FIJI (https://github.com/fiji )[271].

### 2.4.11 IFNγ Assay

To quantify IFNγ in tumours from mice fed either a control diet or histidine-reduced diet, a Mouse IFN gamma ELISA kit (Abcam Ltd.) was used according to the manufacturer's instructions. For each reaction, 50 µg of tumour protein lysate was prepared as previously described. IFNγ concentration for each sample was determined by interpolation from a standard curve.

## 2.5 Tumour Slice Culture

An *Ex vivo* tumour slice culture system was carried out as previously published[272]. A brief overview is provided below.

### 2.5.1 Tissue Processing

Large (> 500 $mm^3$) MMTV-Myc mammary tumours were dissected from mice, cut in half using a sterile razor blade for easier handling and stored in ice-cold PBS for processing. Automated slicing was carried out using a Leica VT1200 S Semi-Automatic Vibrating Blade Microtome (Leica Biosystems). Tumour slices were cut to a thickness of 300 µm and transferred to a cell-culture dish with sterile ice-cold PBS. Tumour slices were all prepared within 2 hours of tumour collection.

### 2.5.2 Culture Conditions

Medium I, as detailed in Naipal et al. (2016)[272], was used as the culture medium (Table 2-13). The Media Preparation service at the Francis Crick Institute was used to prepare DMEM and HAM's F12 and amino acid-free versions. Tissue slices were cultured in 2 mL of media in a 12-well tissue culture plate and cultured at 5% $CO_2$ at 37°C and atmospheric oxygen levels and were subjected to rotation with an orbital microplate shaker. After 24 hours, the media was changed to experimental conditions, where DMEM and HAM's F12 were replaced with the amino acid free version, and tumour slices were either starved in the presence or absence of 1.6 mM histidine for 48 hours. After 48 hours, the respective tissue slices were replenished with the complete Medium I for indicated times. For WB analysis, the tumour slices were provided with 10 µg/mL of puromycin for 10 minutes prior to

collection. At collection, the slices were washed in PBS, flash frozen in liquid nitrogen, and stored at -80°C until further use.

**Table 2-13. Medium I Composition.**
For *ex vivo* tumour slice cultures[272]

| Component | Final Concentration |
|---|---|
| DMEM | 66.60% |
| HAM's F12 | 33.30% |
| iFBS | 2% |
| Glutamine | 2 mM |
| Hydrocortisone | 0.3 µg/mL |
| Insulin | 4 µg/mL |
| Transferrin | 4 µg/mL |
| Triiodothyronine | 1 ng/mL |
| EGF | 8 ng/mL |
| Cholera toxin | 7 ng/mL |
| Adenine | 0.2 mg/mL |
| Pen/Strep | 1% |

## 2.6 Metabolomics for LC-MS

All polar extracts were analysed by Liquid-Chromatography Mass-Spectrometry (LC-MS) using a Q Exactive Plus (Orbitrap) Mass Spectrometer coupled to a Vanquish UHPLC system (ThermoFisher Scientific Inc.), conducted by Dr. Paul Driscoll of the Metabolomics Science Technology Platform at the Francis Crick Institute as previously described[273]. Chromotographic separation was performed on a SeQuant Zic pHILIC (150 mm x 4.6 mm, 5-µm particle) column (Merck). The LC parameters were set to a flow rate of 300 µL/min, and 5 µL of each sample was injected. MS was operated to alternate between positive negative polarity modes, scanning across a mass range of 70-1050 m/z with a resolution of 70,000. Quality control samples were regularly analysed to monitor system stability and performance.

### 2.6.1 Tissue

Tissues were ground in liquid nitrogen using a mortar and pestle, then lyophilised overnight in a FreeZone 4.5 Freeze Dry System (Labconco). Notably, the normal

mammary gland was not lyophilised; therefore, the dry weight of this tissue was not determined. Polar metabolites were extracted using a biphasic extraction method. For each sample, 3-5 mg of lyophilised tissue was extracted with 1.2 mL of chloroform and 0.6 mL of methanol (2:1) containing the internal standard, 5 $\mu M_{[final]}$ [U-$^{13}C^{15}N$]-valine. Samples were vortexed at maximum speed for 30 seconds each, sonicated for three rounds of 8 minutes and incubated for 1 hour at 4°C. Following this, samples were centrifuged at 21,000 *xg* for 20 minutes at 4°C, and the supernatant (SN1) was collected and vacuum-dried using a rotational-vacuum-concentrator RVC 2-33 CD (Christ). The remaining pellet was re-extracted with 500 µL methanol and 250 µL water (Optima™LC/MS Grade, fisher scientific, 10095164) (2:1). After vortexing for 30 seconds and sonication for three 8-minute rounds at 4°C, the samples were centrifuged at 21,000 *xg* for 20 minutes at 4°C. The resulting supernatant (SN2) was combined with SN1 and vacuum dried. The final pellet was retained for protein quantification.

Once the samples were thoroughly dried, biphasic partitioning was performed to separate the polar phase. A 1:3:3 ratio of chloroform:methanol:water was added to each sample, followed by vortexing for 30 seconds. Samples were then centrifuged at 21,000 *xg* for 5 minutes at 4°C, resulting in three distinct phases: a top polar phase, an interphase of insoluble proteins and debris, and a bottom apolar phase. The polar phase was either vacuum-dried for storage at -80°C or 100 µL was submitted to the facility at the Francis Crick Institute for analysis.

### 2.6.2 Cells

Cells were seeded in triplicate in a 6-well cell culture plate for all metabolomics experiments with the indicated experimental conditions. At collection, cells were rinsed with ice-cold PBS before submerging the plate in liquid nitrogen and maintaining it on dry ice until metabolite extraction. Cells were scraped with 750 µL of ice-cold MeOH, 250 µL water with 5 $\mu M_{[final]}$ [U-$^{13}C^{15}N$]-valine and 250 µL chloroform (3:1:1). Samples were vortexed at maximum speed for 30 seconds each and sonicated for 3 rounds of 8 minutes and incubated overnight at 4°C. Then, samples were centrifuged at 21,000 *xg* for 10 minutes at 4°C. The supernatant was collected and 500 µL of water was added, adjusting the methanol:water: chloroform

ratio to 3:3:1 and enabling biphasic partitioning. The samples were vortexed and centrifuged at 21,000 *xg* for 5 minutes at 4°C. The polar phase was vacuum-dried using a rotational-vacuum-concentrator RVC 2-33 CD (Christ). The vacuum-dried polar phase was either stored at -80°C until submission or resuspended in 100-200 µL of a 1:1 mixture of methanol: water, and 100 µL was submitted to the Metabolomics facility for LC-MS analysis. The pellet was retained for protein quantification.

### 2.6.3 Protein Quantification from MeOH:Chloroform Lysates

The cell pellets following methanol chloroform extraction were used for protein extraction for LC-MS data analysis normalization. For experimental subsets where the mammary fat pad was not included in the analysis, the dry weight was used for normalization. Pellets were resuspended in 100 µL of freshly prepared Urea lysis buffer (6M Urea, 15 mM DTT, 2% CHAPS). Samples were vortexed for 30 seconds each and sonicated for 8 minutes and incubated at room temperature on an orbital shaker at 100 rpm for 30 minutes. Samples were then centrifuged at 10,000 *xg* for 5 minutes at room temperature. BSA standards were prepared in the urea lysis buffer and the Pierce™ 660nm protein assay kit (ThermoFisher Scientific Inc.), which is compatible with high concentrations of urea, was used to quantify protein. Briefly, 10 µL of each sample was loaded into a well of a 96-well plate and 150 µL of the assay reagent was added to each sample. The samples were then incubated for 5 minutes in the dark at RT. Absorbance was then measured on an Infinite M1000 Pro Multimode Microplate Reader (Tecan Group) at a wavelength of 660 nm. Total protein content for each sample was quantified by interpolating from a standard curve of known concentrations that was prepared.

### 2.6.4 Media/Serum

Media from *in vitro* experiments and serum collected from blood were extracted following the same protocol. For each sample, 10-15 µL was first precipitated with 3:1 ratio of ice-cold methanol with the serum or media. Samples were vortexed and incubated on ice for five minutes for precipitation and then centrifuged at 21,000 *xg* for 10 minutes at 4°C. A 1:1 mixture of methanol and water was prepared with 5

$\mu M_{[final]}$ [U-$^{13}C^{15}N$]-valine. The supernatant was then collected for biphasic partitioning with a 3:3:1 ratio of methanol: water: chloroform. The samples were vortexed and then centrifuged at 21,000 *xg* for 5 minutes at 4°C, revealing three phases. The top polar phase was isolated and submitted to the Metabolomics facility at the Francis Crick Institute for LC-MS analysis.

### 2.6.5 LC-MS Data Analysis

The LC-MS data analysis was performed using either the TraceFinder software (version 5.1, ThermoFisher Scientific Inc.) or Xcalibur™ software (ThermoFisher Scientific Inc). Compound identification across both platforms was based on accurate mass measurements (± 5 ppm), retention time (± 0.5 min), and matching isotope patterns.

TraceFinder was used for the method development, data processing, semi-automated peak detection, and report generation, providing quantified peak areas. A compound database containing accurate masses was employed for method development, and retention times were verified using standard mixes containing relevant compounds. Peak areas were normalized against the internal standard area and either the total protein content (µg) or dry weight (mg). To quantify fractional enrichment and apply natural isotope abundance correction, a custom script (IDLE, Python version 3.12) developed by the Metabolomics facility at the Francis Crick Institute was used. Fractional enrichment is presented as the percentage of all labelled isotopologues (> m+0) relative to the total amount of the metabolite.

XCalibur was used for most of this project but was later discontinued due to software issues. Compound identification and retention times were determined using FreeStyle™ (version 1.7, ThermoFisher Scientific Inc.) by comparing to standard mixes of relevant compounds. A method for peak detection was developed in XCalibur using the Processing Setup function, which incorporated relevant compounds and their retention times. Samples were processed using the Sequence Setup function, and peak areas were quantified in Quan Browser through semi-automated peak detection, which generated the final reports. For

normalization and natural isotope abundance correction, an in-house LC-MS data analysis script, developed by Dr. Avinash Ghanate (https://avi-crick.shinyapps.io/MS-Wizard/), was applied.

Normalized relative abundance indicates peak area (arbitrary units) normalized to the peak area of the internal standard ([U-$^{13}C^{15}N$]-valine) and either the dry weight (milligram, tissue), protein (microgram, cells and tissues with the NMG), or volume (microlitre, media and blood).

Percent labelling or fractional enrichment was quantified as the proportion of a specific metabolite that contains any labelled atom (m+1 and above) relative to the total amount of that metabolite (m+0 to m+n). This reflects the percentage of molecules with any incorporation of the stable isotope tracer.

## 2.7 Quantitative Real-Time PCR

### 2.7.1 RNA Extraction

Cells were washed with ice-cold PBS and scraped with 0.5- 1.0 mL of TRIzol™ (ThermoFisher Scientific Inc.). For tissues, 1 mL of TRIzol™ was added to approximately 3-5 mg of tissue. RNA was extracted according to the manufacturer's instructions. Then, 1 µg of RNA was treated with 1U of DNase (1 U/µL ThermoFisher Scientific Inc.) before reverse transcription. The RNA quality and concentration were measured using a NanoDrop™ 2000 spectrophotometer (ThermoFIsher Scientific Inc.). RNA was stored at -80°C until future use.

### 2.7.2 Reverse Transcription

1 µg of DNase-treated RNA was incubated with 0.5 µM random hexamers (0.5µM/µL, Jena Bioscience GmbH) and 10 nmol dNTP mix (10 mM, ThermoFisher Scientific Inc.) and heated to 65°C for 5 minutes and incubated on ice for up to 5 minutes. This was then used for reverse transcription reactions with Superscript™III Reverse Transcriptase and treatment with RNase OUT (both ThermoFisher Scientific Inc.) according to the manufacturer's instructions. The cDNA was then stored at -20°C until further use.

### 2.7.3 qPCR

Quantitative PCR was performed on the ViiA 7 Real-Time PCR system (Applied Biosystems) using Power SYBR™ Green PCR Master Mix (ThermoFisher Scientific Inc.), following the manufacturer's instructions. In brief, 100 ng of cDNA and 5 pmol of forward and reverse primers were used in each 10 µL reaction, loaded onto a MicroAmp Optical 384-Well Reaction Plate (ThermoFisher Scientific Inc.). Primer sequences are listed in (Table 2-2). Thermal cycling conditions included an initial enzyme activation step at 10 minutes at 95°C, followed by 40 cycles of denaturation at 95°C for 15 seconds and annealing at 60°C for 60 seconds. A melting-curve analysis was performed at the end of amplification to verify primer specificity.

Relative gene expression was calculated from *Ct* values using the $2^{-\Delta\Delta Ct}$ method, normalized to β-actin or HPRT. Primer binding efficiencies were not calculated. Each sample was run in triplicate, with a standard deviation below 0.2; a single technical replicate was discarded if it markedly shifted the standard deviation away from 0.2. No-template controls were included to check for contamination.

## 2.8 Immunoblotting

### 2.8.1 Cell and tissue lysis

Prior to lysis, cells were scraped on ice in ice-cold PBS and centrifuged at 300 *xg* for 5 minutes at 4°C, the supernatant was discarded and the cell pellet was resuspended in 100-200 µL of Triton-X lysis buffer (1% Triton X-100, 150 mM NaCl, 50 mM Tris (pH 8.0)) supplemented with Halt™ Protease Inhibitor Cocktail (100X, ThermoFisher Scientific Inc.) and phosphatase inhibitors 10 mM sodium fluoride (NaF) and 1mM sodium orthovanadate ($Na_3VO_4$) and samples were vortexed for 15 seconds at maximum speed. Tissue samples and tumour slices were lysed in Triton-X lysis buffer supplemented with protease and phosphatase inhibitors using the Precellys Cryolys Evolution tissue homogenizer with ten 1.4 mm ceramic beads per sample (both Bertin Technologies). Cell and tissue samples were subsequently processed the same. Samples were incubated on ice for 15 minutes, then centrifuged at 21,000 *xg* for 15 minutes at 4°C to pellet cell debris.

The supernatant was collected, and protein was quantified using the Pierce™ BCA Protein Assay kit (ThermoFisher Scientific Inc.) according to manufacturer's protocols. Briefly, 2 µL of each sample was loaded in duplicate in a 96-well plate, along with protein standards prepared from a known concentration of BCA, and 200 µL of a 50:1 mixture of Reagent A and Reagent B was added to each well. The samples were incubated at 37°C in the dark for up to 30 minutes. Absorbance was measured on an Infinite M1000 Pro Multimode Microplate Reader (Tecan Group) at 562 nm. The concentration of each sample was interpolated from a standard curve. Samples were prepared to 1-2 µg/µL using 4x Laemmli Sample Buffer supplemented with 10% 2-mercaptoethanol (both Bio-Rad Laboratories, Inc.) and directly loaded onto SDS-polyacrylamide gel or stored at -20°C for future use.

#### *2.8.1.1 Histone Extraction*

Cells were harvested by scraping in ice-cold PBS and centrifuged at 300 *xg* for 5 minutes at 4°C to pellet cells. The supernatant was discarded, and the cell pellet was resuspended in Triton X-100 lysis buffer supplemented with protease and phosphatase inhibitors at a concentration $10^7$ cells/mL. The suspension was gently vortexed for 10-15 seconds and incubated on ice for 15 minutes, followed by centrifugation at 6,500 *xg* for 10 minutes at 4°C to pellet the nuclei. The nuclei were washed with half the volume of Triton X-100 lysis buffer used in the first extraction, gently resuspended by vortexing, and centrifuged as above. The supernatant was discarded, and the pellet was resuspended in 100 µL of 0.2 N HCl (in Triton X-100 lysis buffer) and sonicated for 8 minutes to free histones. This suspension was rotated overnight at 4°C, then centrifuged again at 21,000 *xg* for 10 minutes at 4°C. The supernatant containing the histones was collected and neutralised with 2M NaOH (approx. 10 µL). The protein concentration was measured using the Pierce™ BCA Protein Assay Kit as described above, and samples were prepared in 1x Laemmli sample buffer at 1 µg/µL.

### 2.8.2 SDS-PAGE

Samples were incubated at 37°C for 20 minutes, and 10-20 µg were loaded onto 10-12% SDS-polyacrylamide gels and electrophoresed at 100-120V for 1-1.5

hours. Proteins were transferred onto a nitrocellulose membrane (Bio-Rad Laboratories, Inc.) via wet transfer at 400 mA (approx 160 V) for 1 hour at 4°C.

The membranes were then probed for successful transfer with Ponceau S staining solution (ThermoFisher Scientific Inc.) before being blocked in 1% BSA (phospho blots, in Tris-buffered saline, 0.1% Tween-20 (TBST)) or 5% non-fat dry milk (0.1% TBST) for 1 hour at room-temperature or overnight at 4°C. Membranes were washed 5x with TBST prior to incubation with primary antibodies (Table 2-4). Primary antibodies were diluted in 3% BSA in TBST and membranes were incubated at room temperature for 1 hour or overnight at 4°C. Membranes were washed for 3 rounds of 10 minutes with TBST and subsequently incubated with HRP-conjugated secondary antibodies for up to 1 hour at room temperature. Membranes were incubated in ECL WB detection reagent (Cytiva Life Sciences) and proteins were visualised using an Amersham ImageQuant™ 800 (Cytiva Life Sciences). For total levels of phosphorylated proteins and actin or vinculin, proteins were stripped from blots using a stripping buffer (0.2 M Glycine, 1% SDS, 0.1% Tween-20, pH 2.2) for 5 to15 minutes. Blots were re-blocked for 1 hour and re-probed with relevant primary antibodies.

For protein quantification, densitometric analysis was performed using FIJI (https://github.com/fiji). Protein levels were normalized to the loading control and subsequently to unphosphorylated protein levels (where relevant). The values were presented as minimum-maximum normalized values, where the minimum was set to no detection (0).

## 2.9 Computational Analysis

### 2.9.1 RNA-seq Data Analysis

#### *2.9.1.1 Lab-Generated RNA-seq Datasets*

The RNA-seq dataset generated by Dr. Chandan Seth-Nanda's was analysed by Dr. Deborah Schneider-Luftman from the Bioinformatics & Biostatistics Science Technology Platform at the Francis Crick Institute. Reads from RNA-sequencing were processed using the nf-core RNA-seq pipeline[274] (version 3.3), aligned to the

mouse genome assembly GRCm38 with Ensembl release 95 transcript annotations, using STAR[275] for alignment and RSEM[276] for transcript quantification. Gene-level abundance estimates from RSEM were used for downstream analysis with the DESeq2[277] package in R. Gene-expression was standardized with variance stabilising transformation across all samples in the dataset to ensure comparability, this was followed by principal component analysis of the transformed data. Hierarchical clustering based on Euclidean distances was used to generate heatmaps.

The RNA-seq dataset generated by Dr. Josep Tarrago-Celada was analysed using R (version 2024.04.2). Raw gene expression counts were filtered to include genes of interest. Gene annotations were retrieved from Ensembl using the biomaRt (version 2.58.2) package. The filtered data was normalized using Z-score normalization across all samples for each gene to ensure the expression values are comparable across samples. Hierarchical clustering was conducted, and a heatmap was generated with pheatmap (version 1.0.12) program to visualise the expression of the top 100 genes, identified based on average expression. Gene ontology (GO) analysis was performed using the clusterProfiler (version 4.10.1) package in R, on the top 100 highly expressed genes in each condition (iMMEC vs. iMMEC_MYC). Ensembl gene IDs were converted to Entrez IDs using the org.Mm.eg.db (version 3.18.0) database. GO enrichment analysis was conducted with the molecular function (MF) ontology, applying Benjamini-Hochberg correction for multiple testing. The results were visualised using a dot plot to display enriched GO terms for the iMMEC and iMMEC_Myc conditions.

#### *2.9.1.2 Publicly Available Datasets*

Gene expression data was obtained from the DepMap Expression Public 24Q2 dataset for cell-type specific expression patterns (https://depmap.org/portal/data_page/?tab=overview). This dataset provides RNA-seq-based log2 transformed gene expression levels (log(TPM+1)) for >2000 human cancer cell lines. The data was filtered for the indicated cell lines on the DepMap portal and the genes of interest were extracted with R (version 2024.04.2).

The gene expression was visualised with the pheatmap (version 1.0.12) program in R.

For comparative expression of genes involved in histidine metabolism in tissues of wild-type FVB/n females, gene expression data were obtained from the Gene Expression Omnibus database ((https://www.ncbi.nlm.nih.gov/geo/) under the accession number GSE75957[278]. The data was filtered in R (version 2024.04.2) to include indicated samples and genes. A heatmap was generated using the pheatmap program to visualise gene expression patterns, the reads per sample million (RPSM) values were Z-score normalized for each gene across all samples and hierarchical clustering was applied to genes and samples.

#### *2.9.1.3 Estimation of Usage Bias for Asparagine Codons*

Coding sequences from the GENCODE v24 annotation were used to investigate asparagine codon (AAT, AAC) usage bias in R (version 2024.04.2) as was adapted from Darnell *et al*. (2018)[279] (https://github.com/rasilab/adarnell_2018). Using the BSgenome.Hsapiens.UCSC.hg38 (version 1.4.5) reference genome coding sequences were extracted. Codon frequencies were computed for asparagine, and AAN (AAA, AAG) codons as controls. A binomial probability distribution was employed to calculate the expected frequency of asparagine codons for each gene using the average genome-wide frequency. The observed counts of asparagine were then compared to these expected values to derive Z-scores, indicating bias towards or against asparagine codon usage. GO enrichment analysis was conducted for the top 5% of genes exhibiting the highest bias in asparagine codon usage using the topGO library, focusing on MF and cellular component (CC) ontologies. Results were visualised through histograms and dot plots to highlight significant GO terms associated with asparagine-rich proteins.

## 2.10 Quantification and Statistical Analysis

Graph preparation and statistical analyses were conducted using GraphPad Prism (version 10.1.1). The specific statistical tests applied are described in the corresponding figure captions.

Some data presented in heatmaps, where metabolites of varying abundances were displayed together, were normalized using a min-max scaling. This method scales the values between 0 and 100%, with 0 representing the absence of a metabolite and 100% representing the highest abundance observed for that metabolite across samples. This normalization formula used is:

$$X_{norm} = \frac{X - X_{min}}{X_{max} - X_{min}} \times 100$$

$X_{norm}$ is the normalized value (as a percentage).
$X$ is the original value.
$X_{min}$ is the minimum value, set to 0% (metabolite not detected).
$X_{max}$ is the maximum value for that metabolite across all samples, set to100%.

Outliers were removed using the ROUT (Robust Regression and Outlier Removal) method as implemented by GraphPad Prism (version 10.1.1). The Q value was set to 5%.

# Chapter 3. MYC-driven mammary tumours have an increased demand for histidine

## 3.1 Introduction

Breast cancer is a highly heterogeneous disease; therefore, selecting a mouse cancer model that accurately reflects this heterogeneity improves our understanding of tumourigenesis to develop better therapeutic strategies targeting tumour progression. MMTV-Myc-driven mammary gland tumours (MGTs) exhibit significant genetic complexity and histological heterogeneity, representative of specific human breast cancer subtypes. This heterogeneity is reflected in diverse pathway activation in MMTV-Myc tumours[280–282]. Triple-negative BCs are often Myc-amplified and there is a lack of targeted therapeutic strategies for this subtype[81,280]. MYC is widely acknowledged as a master regulator of cellular metabolism. Thus, significant effort has been made to understand how the Myc oncogene reprograms cellular metabolism to support tumourigenesis. This strategy hopes to reveal metabolic vulnerabilities that underlie the progression of these difficult-to-treat tumours. While much of this research in cancer metabolism has concentrated on glutamine and glucose metabolism and certain non-essential amino acids (NEAAs) like serine, the role of other amino acids in Myc-driven tumour progression remains largely unexplored [46,99,283]. Essential amino acids serve as necessary building blocks for macromolecular biosynthesis but also have crucial roles in cellular signalling, such as, but not limited to, mTORC1 activation [173,175,176,284]. Breast cancers have an increased demand for EAAs to sustain proliferation [285]. However, EAAs cannot be synthesised *de novo;* thus, they must be taken up from the extracellular environment. SLC7 family transporters are essential mediators of EAA uptake. *SLC7A5* (LAT1) is particularly important because it is often overexpressed in various tumours and plays a crucial role in mTORC1 signalling [236,286]. In contrast, *SLC7A8* (LAT2) is predominantly expressed in normal breast epithelial cells. Recent research found that the SLC7A5/SLC7A8 ratio in breast cancer cells and patient samples positively correlated with EAA uptake[285]. A higher SLC7A5/SLC7A8 ratio was associated with poor prognosis and OS, regardless of tumour subtype or stage[285]. Additionally, MYC copy number

variations (CNVs) were linked to SLC7A5/SLC7A8 scores, with higher scores observed in breast cancers with Myc amplification[285]. Furthermore, as highlighted earlier, LAT1 and MYC participate in a feedforward loop. Where LAT1 mediated uptake of EAAs supports translation of MYC and MYC-driven metabolic reporgramming[163]. These findings indicate that Myc orchestrates enhanced demand and supply of EAAs in tumours, suggesting that targeting EAA uptake through LAT1 inhibition or EAA deprivation could be an effective anti-tumour strategy. However, further research is needed to elucidate the mechanisms by which EAAs support Myc-driven tumour growth and to identify which EAAs are most crucial for tumour development and progression. This will help determine metabolism of which EAA(s) is the most effective target for designing metabolism-based treatment strategies.

Given that *SLC7A5* is upregulated in various tumour types, we included a comparative mouse model in our study to evaluate the requirement for LAT1 in Myc-driven tumourigenesis. Like MYC, the oncogene *ERBB2* (encoding HER2) is amplified in 25-30% of breast cancers [287]. Therefore, we decided to use the MMTV-Neu/ErbB2 (henceforth MMTV-ErbB2) model, expressing an activated rat form of HER2 (NeuNT) [282]. Compared to MMTV-Myc MGTs, MMTV-ErbB2 tumours exhibit little molecular or histological heterogeneity [281]. MMTV-ErbB2 tumours are characterised by significant involvement of metabolic processes and nucleic-acid metabolism [282,288]. Therefore, these tumours could show a similar demand for EAAs, and thus LAT1 activity, as MMTV-Myc tumours. In agreement with this, high levels of *SLC7A5* mRNA and protein levels were observed in TNBC, HER2+, and luminal B subtypes. By comparing MMTV-Myc and MMTV-ErbB2 tumours, we can determine whether Myc-driven tumourigenesis relies more on *Slc7a5* and its associated metabolic and signalling pathways. Identifying this specificity is necessary for the development of targeted therapies, leading to improved treatments for Myc-driven breast cancers, which have proven challenging to target with conventional therapies[89].

In chapter 3 we will first investigate Slc7a5 transcript and protein levels in MMTV-Myc and MMTV-Erbb2-driven mammary gland tumours compared to

untransformed normal mammary glands (NMG). We will then assess the uptake of the high-affinity LAT1 substrate, histidine, using [U$^{13}$C]-histidine in these tumours.

**Aims**

To understand the importance of Slc7a5 in Myc-driven tumourigenesis, this chapter will:

1) Determine transcript and protein levels of *Slc7a5*/Lat1 in Myc- and ErbB2-driven MGTs.
2) Assess uptake of histidine in MMTV-Myc and MMTV-ErbB2 driven MGTs.
3) Interrogate the role of histidine metabolism in Myc-driven tumour cells.

## 3.2 Lat1 mRNA and protein levels are significantly upregulated in Myc-driven mammary gland tumours.

MYC binds the promoter of *SLC7A5*, thus regulating its expression [162,163]. To assess whether *Slc7a5* mRNA expression was affected during Myc-driven mammary gland tumourigenesis, unpublished bulk RNA-sequencing data provided by Dr Chandan Seth-Nanda, a previous post-doctoral fellow in our lab, were analysed. The samples analysed included NMGs from 6-week-old MMTV-Myc$^{-/-}$ mice and the progression from NMGs from 6 weeks MMTV-Myc$^{+/+}$ mice to hyperplastic 12-week-old mammary glands to small (<3 x 3 mm) and large (10 x 10 mm) tumours. The analysis revealed a subset of Slc transporters positively correlated with Myc-driven tumourigenesis. Most of these include those of the Slc7, *Slc43a2,* and *Slc38a2* families (Figure 3-1A), previously identified as Myc-target genes [162,163]. Furthermore, *Slc7a5* expression is observed as early as 12 weeks, during hyperplasia, and throughout tumourigenesis (Figure 3-1A). *Slc3a2*, encoding CD98, which anchors LAT1 to the plasma membrane, also correlates with Myc-driven cell transformation, tumour progression, and *Slc7a5* expression (Figure 3-1A).

Next, I compared *Slc* transcript expression via RT-qPCR in large MMTV-Myc and MMTV-ErbB2 tumours. Specific transporters were increased in Myc-driven MGTs

compared to ErbB2-driven tumours. These included *Slc1a5*, encoding Asct2, a recognised Myc-target gene[289], and *Slc7a5* (Figure 3-1B). This was confirmed at the protein level and compared to age-matched NMG controls (Figure 3-1C). Indeed, Myc-driven MGTs had increased Lat1 and Asct2 protein expression compared to the NMG and Erbb2-driven MGTs. In agreement with the RNA-seq data, the NMG had low Lat1 expression, suggesting that Lat1 expression is associated with Myc-driven mammary gland transformation. Furthermore, IHC images confirmed increased LAT1 expression in MMTV-Myc compared to MMTV-ErbB2 MGTs. Strong immunoreactivity was observed at the cell membrane of Myc-driven tumours (Figure 3-1D). The percentage of total cells scored high, medium, low or negative for Lat1 membrane staining was quantified. ErbB2-driven mammary gland tumours that were positive for Lat1 mostly had medium expression and significantly more negative cells (Figure 3-1E). In contrast, Myc-driven tumours had significantly increased high-expressing cells (Figure 3-1E). This is indicative of an important role for LAT1 in Myc-driven tumourigenesis. Considering LAT1 functions as an obligatory antiporter, identifying the specific substrates that mediate its activity could uncover a potential metabolic vulnerability in these tumours.

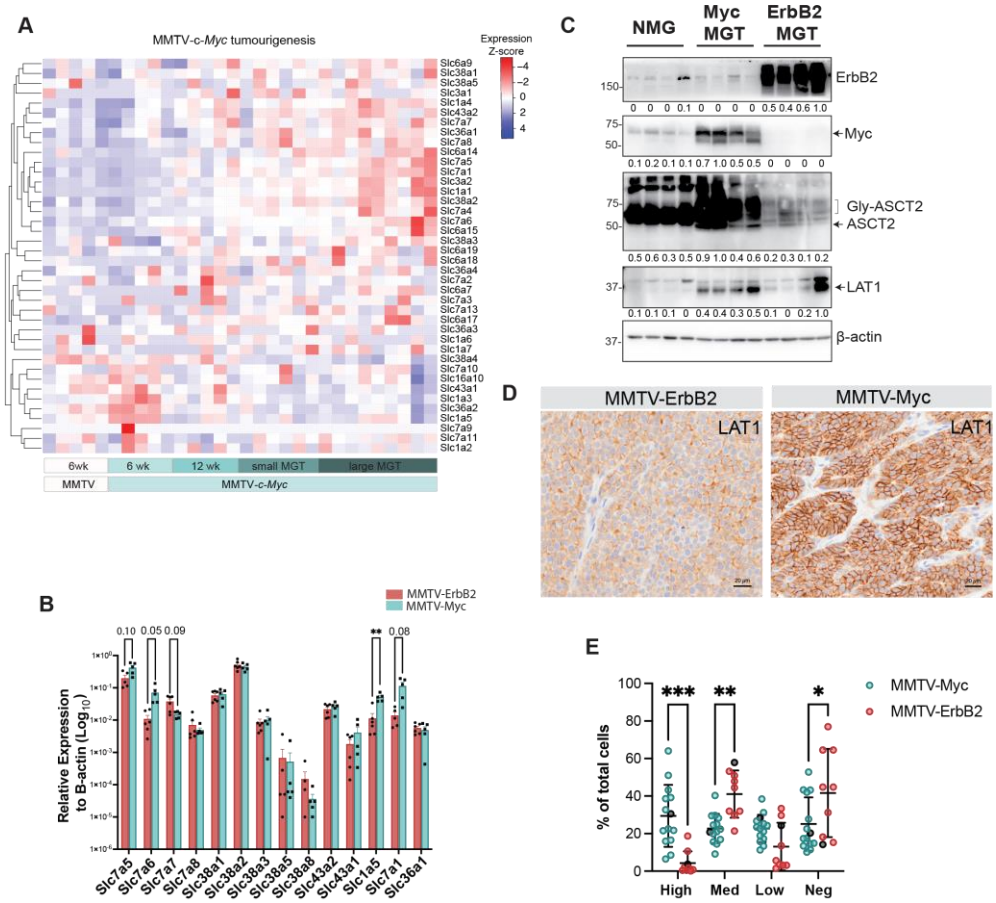



**Figure 3-1. Myc-driven MGTs have increased expression of Slc7a5/Lat1.**
**(A)** Heatmap displaying *Slc* gene expression patterns from RNA-sequencing data throughout MMTV-Myc mammary tumourigenesis. **(B)** RT-qPCR of MMTV-Myc (n=5) and MMTV-ErbB2 (n=6) MGTs (> 500mm$^3$), with relative expression normalized to *β-actin*. Data represent mean ± s.d.; two-tailed unpaired t-tests with FDR correction (Benjamini, Krieger, and Yekutieli method, q<0.05). **(C)** WB of MMTV-Myc and MMTV-Erbb2 tumours and the NMG, protein levels are normalized to β-actin and min-max normalized. **(D)** Representative IHC staining of LAT1 expression in MMTV-Myc and MMTV-ErbB2 tumours. **(E)** LAT1 IHC scoring of MMTV-Myc (n=14) and MMTV-ErbB2 (n=9) tumours, with black points indicating the representative tumours in panel D. Data represents mean± s.d. Two-way ANOVA with Šídák correction (*p≤0.05, **p≤0.01, ***p≤0.001).

## 3.3 Myc-driven mammary gland tumours have increased histidine uptake.

LAT1 is a high-affinity histidine transporter that can transport histidine bidirectionally, unlike other high-affinity EAA substrates preferentially transported inward. Therefore, histidine uptake was assessed in Myc-driven MGTs compared to the NMG and MMTV-ErbB2 tumours. MMTV-Myc$^{-/-}$ age-matched wild-type mice and MMTV-Myc$^{+/+}$ and MMTV-ErbB2$^{+/+}$ tumour-bearing mice were given an intravenous bolus of 0.107 mg/gBW [U-$^{13}$C]-histidine after 5 minutes the NMGs or MGTs and serum were collected for LC-MS analysis. The levels of histidine isotopologues were quantified in these tissues to assess histidine levels and uptake (Figure 3-2A). Corresponding with higher Lat1 expression, Myc-driven MGTs had a significantly higher total abundance of histidine than the NMG controls and the Erbb2-driven tumours (Figure 3-2A). Furthermore, Myc-driven tumours also had higher levels of m+6 histidine than the NMG controls and ErbB2 tumours, indicating higher histidine uptake (Figure 3-2B). The fractional enrichment of histidine in the serum was lower in MMTV-Myc mice than in WT or MMTV-ErbB2 mice; this could be due to the increased uptake of histidine in these tumours or due to suboptimal bolus administration (Figure 3-2C). The total abundance and m+6 histidine was not normalized to serum enrichment. Therefore, the m+6 histidine uptake in Myc-driven MGTs may be underestimated. This may suggest histidine has an important role in LAT1 function in Myc-driven tumours.

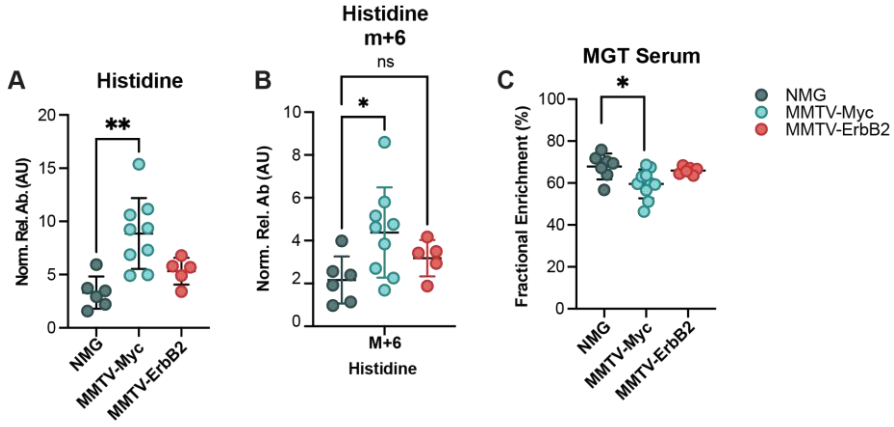



**Figure 3-2. Myc-driven MGTs have increased uptake of histidine.**
LC-MS analysis of MMTV-Myc (n=9), MMTV-ErbB2 (n=5), and NMG (n=7) following a bolus of 0.107 mg/gBW [U-$^{13}$C]-histidine. **(A)** Total abundance of histidine; **(B)** abundance of the m+6 isotopologue. Data are mean ± s.d. One-way ANOVA with Tukey correction. **(C)** $^{13}$C enrichment of histidine in the serum; data shown as mean ± s.d. One-way ANOVA with Tukey correction. *p≤0.05, **p≤0.01.

Several SLC transporters mediate histidine transport, including those of the SLC38 and SLC7 families. To assess whether histidine uptake in the MMTV-Myc tumours was dependent on Lat1, MMTV-Myc and MMTV-ErbB2 tumour bearing mice received an intraperitoneal (IP) injection of 12.5 mg/kg of a LAT1 inhibitor, JPH203, for 30 minutes before administration of an IV bolus of 0.107 mg/gBW histidine for 5 minutes. The serum, liver, and tumour were collected for LC-MS analysis (Figure 3-3A). Notably, the experiments with MMTV-ErbB2 and MMTV-Myc mice were carried out independently, which could result in some technical discrepancies. However, JPH203 was identified in MMTV-Erbb2 and MMTV-Myc tumours and livers (Figure 3-3B, F). Furthermore, similar serum fractional enrichment of histidine was observed among all groups (Figure 3-3C, G). Surprisingly, Lat1 inhibition was more effective at inhibiting uptake of the m+6 isotopologue of histidine in ErbB2-driven MGTs than Myc-driven MGTs (Figure 3-3D, H). The liver was selected as a control because it predominantly expresses *SLC43A1* (LAT3), whereas LAT1 is typically observed in fetal liver and hepatoma cells[290]. This makes the liver an appropriate negative control for evaluating Lat1-mediated histidine uptake. Indeed, JPH203 did not affect histidine uptake in the livers of both MMTV-ErbB2 and MMTV-Myc mice (Figure 3-3E, I). Therefore, this suggests that although Lat1 expression and histidine uptake are significantly increased in Myc-driven tumours, other transporters may contribute to the uptake of histidine levels in these tumours.

In contrast, ErbB2 tumours appear to depend on Lat1-mediated histidine uptake to a greater extent. These differences could be due to increased expression of other histidine transporters in Myc-driven tumours compared to ErbB2 tumours, such as *Slc7a6,* which is also upregulated in Myc-driven tumours (Figure 3-1A, B). Furthermore, while no significant difference was observed in MMTV-Myc tumours following JPH203 treatment, the high degree of heterogeneity in this model may have contributed to the variability in tracer uptake. With only six samples per group, the study may have been underpowered, and a larger cohort could be necessary to determine the extent of LAT1 contribution to histidine uptake in MMTV-Myc tumours, and whether this is different from MMTV-ErbB2 tumours.

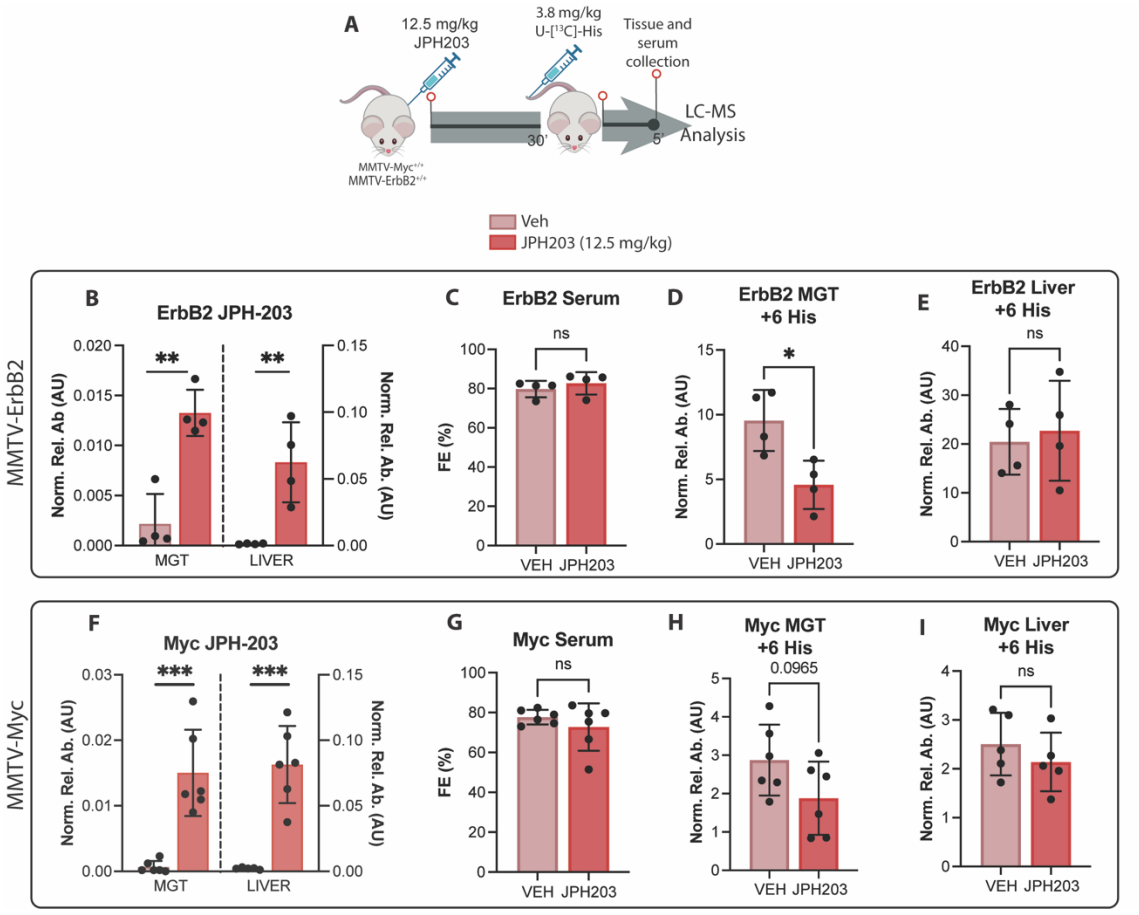



**Figure 3-3. Other transporters may compensate for LAT1 inhibition in Myc-driven MGTs.**
**(A)** Experimental schedule for LAT1 inhibition with JPH203 30 minutes before IV bolus of [U-$^{13}$C]-histidine for 5 minutes. **(B-I)** LC-MS analysis of tumours: **(B-E)** MMTV-ErbB2 and **(F-I)** MMTV-Myc, treated with vehicle or JPH203. **(B,F)** JPH203 abundance in the MGT and liver. (**d,h**) $^{13}$C enrichment of histidine in the serum, with normalized relative abundance of m+6 histidine in the **(d,e)** MGT and **(e,i)** liver. Sample sizes: ErbB2 vehicle (n=4), ErbB2 JPH203 (n=4), Myc vehicle (n=6), Myc JPH203 (n=6). Data are mean ± s.d. Unpaired two-tailed t-test (*p≤0.05, **p≤0.01, ***p≤0.001).

## 3.4 Histidine is primarily catabolised in the liver of healthy animals.

Increased histidine uptake was observed in Myc-driven MGTs, and several studies have highlighted the importance of histidine catabolism in cancer cells [254,255,259]. However, whether histidine catabolism is required for *in vivo* Myc-driven tumourigenesis is unknown. Histidine can participate in several pathways: it can be decarboxylated by HDC to produce histamine, combined with β-alanine to form the dipeptide carnosine, or degraded through a process initiated by HAL (Figure 3-4A). Histidine degradation is a multi-step process that produces glutamate and transfers a one-carbon unit onto THF, catalysed by FTCD (Figure 3-4A). This histidine-derived one-carbon unit can enter the folate cycle and contribute to methionine regeneration and methylation processes through SAM (Figure 3-4A). The contribution of histidine to these pathways was assessed in multiple tissues from healthy adult mice, including the brain, mammary gland, liver, quadriceps, lungs, and serum. Wildtype 12-15 wk female FVB/N mice were infused with [U-$^{13}$C]-histidine for 3 hours before collection of tissues and serum to trace $^{13}$C through metabolic pathways (Figure 3-4B). Serum samples were evaluated for histidine measurements to ensure $^{13}$C-histidine enrichment was similar across mice. Fractional $^{13}$C enrichment analysis showed 80.5% ± 5.5% enrichment in the serum of all infused animals (Figure 3-4C). Different levels of histidine enrichment were observed across the brain (63.3% ± 6.5%), quadriceps (64.6% ± 8.1%), NMG (68.7 % ± 7.9%), liver (74.1% ± 5.8%), and lungs (75.9% ± 6.6%) (Figure 3-4C). In the unlabelled samples, tissues and serum from the control mouse ranged from 1.1% (NMG) to 3.5% (lungs) enrichment (Figure 3-4C). Histamine was heterogeneously labelled in the NMG (14.6 ± 20.9%, p-value = 0.0436, n=4) and quadriceps (18.3% ± 29.2%, p-value = 0.0118, n=4) (Figure 3-4C). Carnosine labelling was observed the highest in the serum (33.9% ± 4.7%, p-value<0.0001, n=4), but also observed in the NMG (0.5 % ± 6.4%, p-value = 0.1839, n=4) and the lung (6.834 ± 8.1%, p-value = 0.339, n=4), with no labelling observed in the quadricep muscles (Figure 3-4C). Glutamate was significantly labelled in the liver (15.1 % ± 6.1%, p-value= 0.035, n=4) compared to the control mouse (Figure 3-4C). This also resulted in glutamine (8.2% ± 3.5%, p-value = 0.2526, n=4) labelling in the liver. No labelling

was observed in methionine or SAM across all tissues (Figure 3-4C). To better understand the contribution of histidine to these metabolite pools, the total abundance of metabolites across tissues was first quantified and normalized based on the internal standard and protein weight. Subsequently, the relative abundance of each metabolite was normalized to the minimum and maximum values across all tissues. This approach allows for the representation of the tissues with the highest metabolite levels. Despite histidine contributing to carnosine production, the relative carnosine pools in the NMG were low compared to the brain and quadriceps (Figure 3-4D), where carnosine is found at high concentrations [291]. Similarly, carnosine labelling in the lung, despite the low carnosine pools, could indicate contamination from blood. Surprisingly, histidine did not contribute to carnosine pools in brains and quadriceps despite large pools within these tissues (Figure 3-4C, D). This could indicate that carnosine has a slow turnover rate, meaning that synthesis from histidine might not be detectable within the 3-hour infusion period. Histamine levels were relatively high in the NMG and lung; however, labelling from histidine was only observed in the NMG and quadricep (Figure 3-4C, D). Given that the quadricep had low histamine levels, this could be sample contamination from the mammary gland during dissection or, more likely, due to histamine producing mast cells within the skeletal muscle[292]. Levels of glutamate and glutamine are relatively high in the brain and NMG, yet histidine did not contribute to maintaining these pools in these tissues (Figure 3-4C, D). Lastly, SAM is observed at similar levels across tissues, but histidine does not contribute a one-carbon unit to SAM in this experiment (Figure 3-4C, D). This could be due to high levels of methionine available within these tissues (Figure 3-4D). Together, these results suggest that the histidine degradation pathway is predominantly active in the liver, with no activity detected in the other tissues tested. While histidine does contribute to carnosine and histamine synthesis, labelling was inconsistent across the mammary glands of different mice, suggesting variable metabolic activity in these tissues. Additionally, some tissues with relatively large pools of these metabolites did not show labelling, suggesting these pools are stable and not actively turning over.

To correlate pathway utilisation to enzyme expression, I analysed publicly available RNA-seq data from normal tissues- including brain, muscle, lung, virgin mammary gland, and liver- of adult female FVB/n mice [278]. The data was normalized by tissue

of origin; thus, the relative expression of genes was compared within each sample rather than across different tissues. This approach allowed us to assess whether the expression of a gene of interest within a tissue deviates from the average expression of all genes within the sample. Notably, all the genes involved in histidine degradation are highly expressed exclusively within the liver, including *Hal*, *Amdhd1*, *Uroc1*, and *Ftcd* (Figure 3-4E). Whereas low expression of *Hdc,* which catalyses histamine synthesis, and *Carns* (encoding carnosine synthase (CS)), which produces the carnosine dipeptide, is observed (Figure 3-4E). This aligns with our data from the $^{13}$C-histidine infusions, where significant labelling was observed in glutamate and glutamine but not in histamine or carnosine (Figure 3-4C). The other tissues, where labelling in glutamate was not observed, show little to no expression of enzymes involved in the histidine degradation pathway (Figure 3-4E). Instead, the skeletal muscle and brain express higher levels of *Carns* (Figure 3-4E). Increased labelling of carnosine was observed in the NMG but not in the brain or the skeletal muscle; however, these tissues had relatively higher pools of carnosine (Figure 3-4C, D).Furthermore, the increased labelling of histamine in the NMG was corroborated by the higher relative expression of *Hdc* (Figure 3-4C, D). However, despite the relatively high levels of Hdc in the lungs, no labelling is observed in this tissue (Figure 3-4C-E). Overall, histidine utilisation across different tissues correlated with gene expression data and confirmed the tissue-specific nature of the histidine degradation pathway. In the next section, to assess the fate of histidine in transformed mammary epithelial cells, we used tumour cells isolated from a MMTV-Myc mammary tumour (MYAZ16.1e).

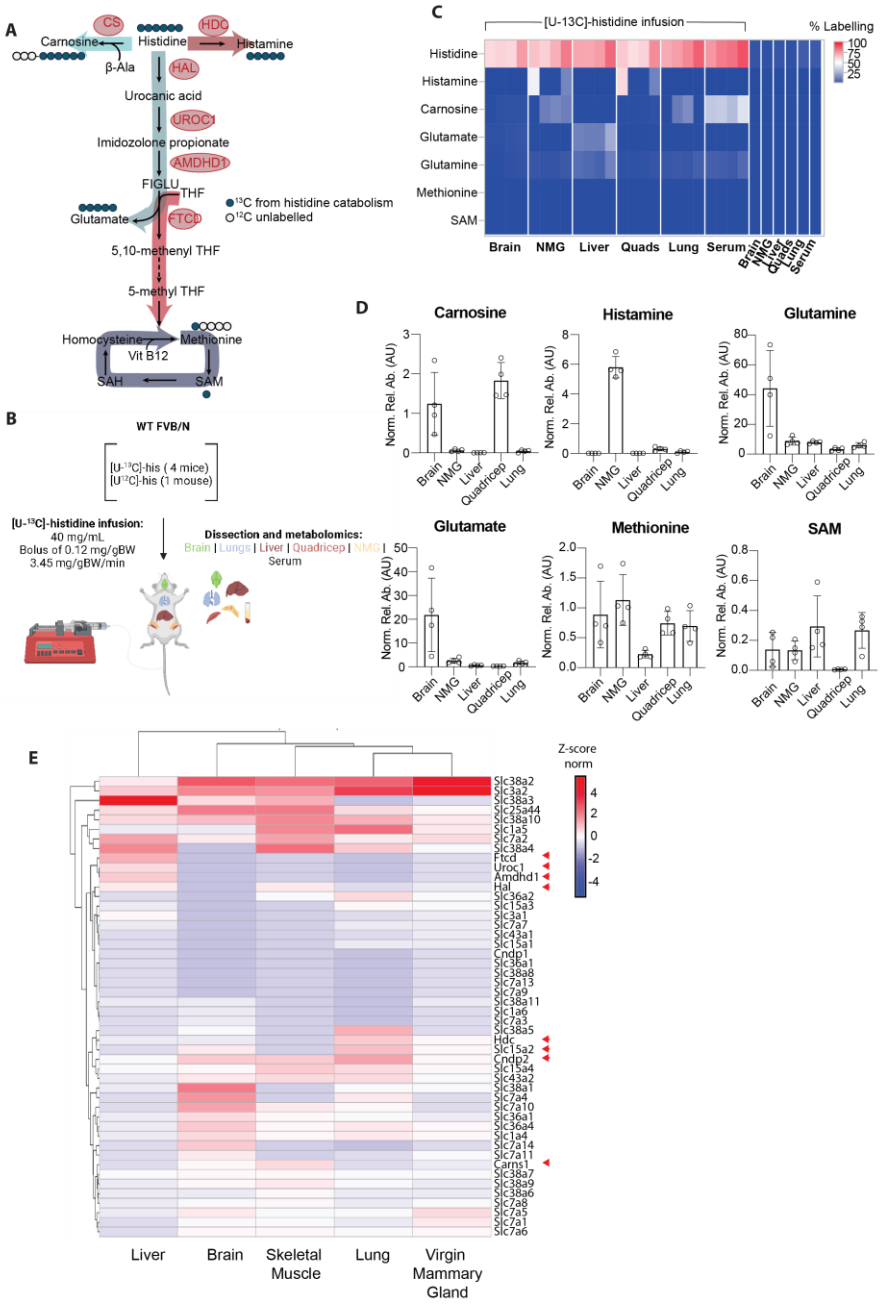



**Figure 3-4. Histidine metabolism is tissue-specific.**
**(A)** Schematic of histidine metabolism showing incorporation of $^{13}C$ from histidine tracer. **(B)** Experimental strategy for [U-$^{13}C$]-histidine infusions in WT FVB/N mice. **(C, D)** LC-MS analysis of intermediates of histidine metabolism: **(C)** heatmap showing $^{13}C$ enrichment in indicated tissues and serum; **(D)** Total abundance of indicated metabolites across tissues. **(E)** Heatmap showing relative gene expression of histidine metabolism enzymes and *Slc* transporters from GSE75957, displaying Z-scores scaled across tissues. Hierarchical clustering was applied to genes and samples. Red arrows indicate key genes involved in histidine metabolism.

## 3.5 Myc-driven tumour cells do not catabolise histidine.

To evaluate the contribution of histidine degradation to the Krebs cycle and methionine regeneration cycle, MYAZ16.1e cells were cultured in 200 μM of [U-$^{13}$C]-histidine for 24 hours under four different conditions: a) high/ctl (2.0 mM) glutamine, b) low (0.1 mM) glutamine, c) 10% methionine, and d) 10% methionine supplemented with homocysteine (Hcy) and vitamin B12 (Figure 3-5A). The low glutamine condition was used to assess incorporation into glutamate, as high glutamine levels in standard cell culture could mask histidine's contribution. To investigate histidine's role in methionine regeneration, cells were cultured in 10% methionine. Since homocysteine and vitamin B12 are required for methionine synthase (MS) activity and are not present in culture media, they were added to ensure the availability of essential metabolites. Importantly, all conditions had similar $^{13}$C-histidine enrichment (Figure 3-5B, C). Cells cultured in low glutamine had significantly decreased levels of glutamate, suggesting that glutamine is essential for glutamate production in these cells and that these cells are incapable of compensating for glutamate (Figure 3-5D). Furthermore, no labelling from histidine was observed in glutamate or glutamine under either low or high glutamine conditions (Figure 3-5E). Therefore, histidine does not appear to be degraded for glutamate production.

Regarding methionine regeneration, 10% methionine was sufficient to reduce intracellular methionine pools. Despite homocysteine and vitamin B12 supplementation, methionine levels were not rescued. However, the levels of SAM and SAH (S'adenosylhomocysteine) were (Figure 3-5F). This suggests that methionine is likely being consumed faster than it is being produced. However, despite the active flux into the methionine regeneration cycle in the presence of homocysteine and vitamin B12, no labelling from histidine was observed in methionine or SAM (Figure 3-5G). Levels of methylated histones, H3K4me and H3K4me3, further supported this. Indeed, histidine-deficient media did not appear to affect the methylation of these histones, whereas methionine limitation resulted in a significant decrease in methylation (Figure 3-5H). Supplementing methionine-depleted media with homocysteine and vitamin B12 ultimately rescued the reduction in methylation observed (Figure 3-5H). In contrast, supplementation into

histidine-depleted media attenuated histone methylation. This is likely due to SAH accumulation due to abundant homocysteine levels, which negatively regulates SAM activity[293]. RT-qPCR was used to assess expression levels of rate limiting enzymes involved in histidine catabolism. Myc-driven tumour cell lines (MYC310 and MYAZ16.1e) and immortalised mammary epithelial cells (iMMECS) were analysed for *Hal*, *Amdhd1*, and *Ftcd*. FTCD catalyses glutamate production downstream of histidine degradation, transferring a one-carbon unit onto THF, ultimately contributing to the cytoplasmic folate cycle (Figure 3-4A). Since histidine degradation was only observed in the liver, it is unsurprising that we do not see the expression of these enzymes in the iMMECS or the Myc-driven tumour cells (Figure 3-5I). In contrast, *Slc7a5* transcript expression significantly increased in MYC310 and MYAZ16.1e cells compared to iMMECS (Figure 3-5I). Overall, these results suggest that histidine degradation is not active in these cells, and histidine may have a role independent of catabolism in Myc-driven tumourigenesis.

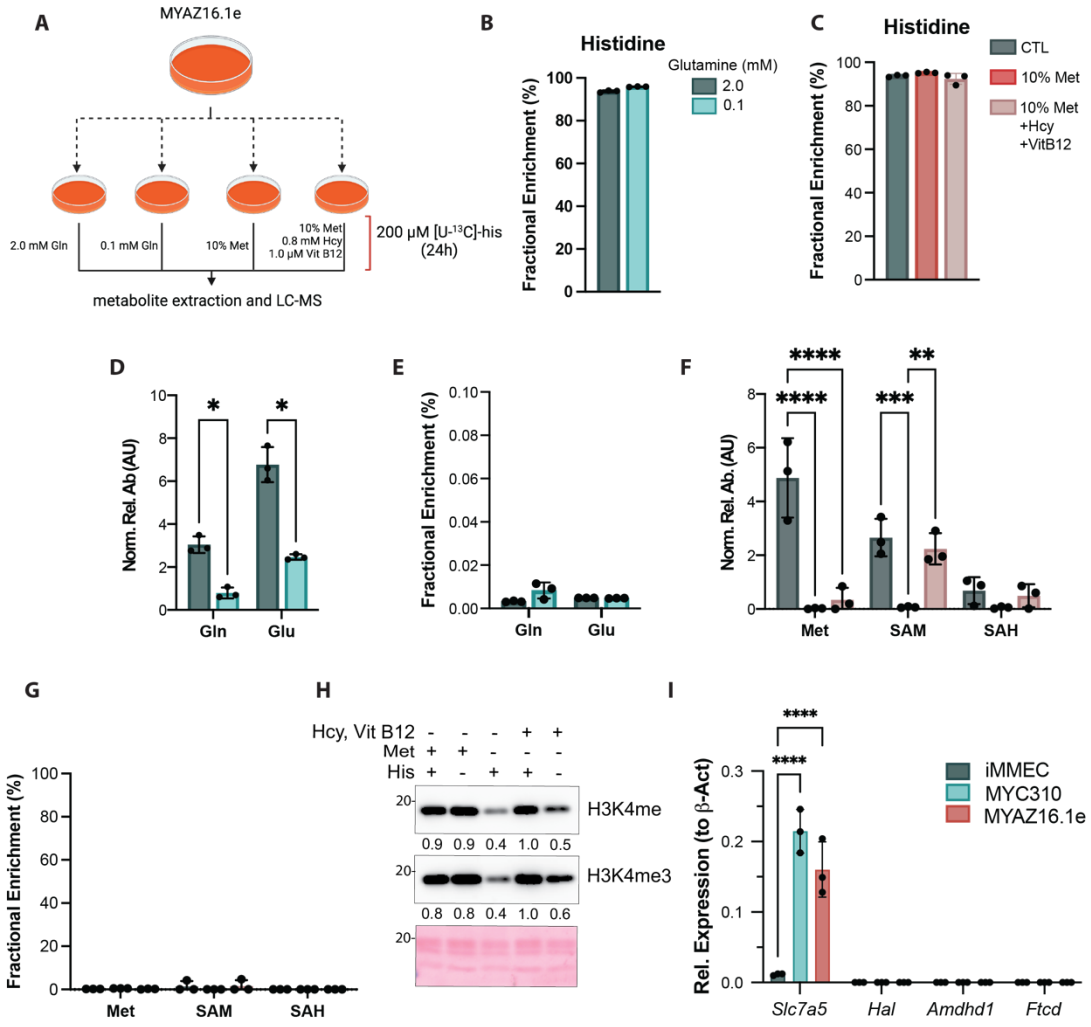



**Figure 3-5. Histidine is not catabolised in MYC-driven MYAZ tumour cells.**
**(A)** Experimental schedule and culturing conditions with 200 µM [U-$^{13}$C]-histidine for 24 hours. **(B-G)** LC-MS analysis: **(b,c)** $^{13}$C enrichment of intracellular histidine; **(D)** total abundance of glutamine (gln) and glutamate (glu) under 2.0 mM or 0.1 mM glutamine conditions; **(E)**$^{13}$C enrichment of glutamine and glutamate; **(F)** total abundance of methionine (Met), SAM, and SAH cultured in 10% Met conditions; **(G)** $^{13}$C enrichment of met, SAM, and SAH. **(H)** WB of histone extracts from cells cultured under indicated conditions, protein levels were normalized to ponceau and min-max normalized. (representative of three biological replicates). **(I)** RT-qPCR of mRNA expression of key enzymes in histidine degradation in iMMECs and Myc-driven tumour cells (MYC310 and MYAZ16.1e) Data shown as mean ± s.d. One-way ANOVA with Šídák correction, representative of 1 replicate (*p≤0.05, **p≤0.01, ***p≤0.001, ****p≤0.0001).

## 3.6 Discussion

MYC-overexpressing cancer cells depend on LAT1 to sustain MYC-dependent transcriptional amplification necessary for tumour cell growth and proliferation[163]. Of the LAT family of EAA transporters, LAT1 is the predominant form overexpressed in many cancers [294]. Here, we observed increased Lat1 mRNA and protein expression in Myc-driven MGTs compared to the NMG and ErbB2-driven MGTs. Coincidentally, Myc-driven tumours also had increased levels of EAAs and increased uptake of the high-affinity LAT1 substrate, histidine, independent of histidine catabolism. Unravelling the role of histidine in LAT1 transporter function could reveal therapeutic strategies to target Myc-driven tumourigenesis.

Myc-driven transcriptional regulation of *Slc7a5* is well understood. However, how LAT1 activity is maintained in Myc-driven mammary gland tumourigenesis is unknown. Myc upregulates protein synthesis, thereby increasing the demand for EAAs. This is supported by the increased levels of EAAs observed in Myc-driven MGTs. Histidine is among the least abundant amino acids in whole-body protein, second to tryptophan [295,296]. In Myc-driven MGTs, tryptophan levels were not significantly increased compared to the NMG or ErbB2-driven MGTs, consistent with its low demand for protein translation. In contrast, despite the similarly low requirement for histidine in protein translation, histidine levels were significantly elevated in Myc tumours. This suggests that the increased uptake of histidine may reflect a role for histidine beyond its function in protein synthesis in Myc-driven mammary tumourigenesis. Unlike some other amino acids, the role of histidine in cancer has only recently gained attention and remains comparatively understudied. However, histidine catabolism has emerged as an exploitable vulnerability in some cancers. In leukaemia cell lines, histidine degradation consumed THF pools, sensitising these cells to treatment with the anti-folate methotrexate [255]. Furthermore, in heterotopic leukaemia xenografts, combination treatment with histidine and methotrexate significantly decreased tumour size compared to methotrexate alone. In a similar study, extracellular histidine suppressed tumourigenesis in hepatocellular carcinoma (HCC) cells, making these cells more sensitive to treatment with the chemotherapeutic agent sorafenib. Histidine treatment induced metabolic changes in these cells, leading to the dysregulation of

genes involved in glycolysis and amino acid transport. However, how histidine supplementation exerts these metabolic changes was not determined. In this chapter, we employed stable isotope tracing of histidine to measure the contribution of histidine to key metabolites across different tissues. Importantly, evidence of histidine degradation into glutamate was exclusively observed in the liver. This was complementary to the increased expression of enzymes involved in histidine catabolism in this tissue. The production of glutamate from histidine requires that one-carbon unit be transferred onto THF. This produces 5-formimino THF, which is metabolised into 5,10-methenyl THF and can be metabolised into 5-formyl THF[252,255]. 5-formyl THF is a storage form of folate and can replenish folate pools, protecting against the toxic effects of anti-folate drugs like methotrexate. Alternatively, 5-formyl THF can be converted into other forms of folate, such as 5-methyl THF, which plays a role in the methionine regeneration cycle. Notably, histidine has been shown to contribute up to 6% of methyl groups to methionine under nutrient starvation conditions[254]. However, despite glutamate production, we observed no contribution from histidine to methionine in liver samples. This suggests that the one-carbon unit generated by histidine degradation is not used for methionine regeneration in the liver under normal circumstances. In contrast, other tissues had low expression of enzymes involved in histidine degradation. Rather, the brain and muscle have relatively high expression *Carns*, which agrees with our observation of high carnosine pools in the brain and skeletal muscle relative to other tissues, which aligns with previous studies[291]. However, no labelling was observed in these tissues, suggesting the carnosine pools are stable. Carnosine has many functions, particularly in the muscle, where it has a crucial role in buffering lactic acid, enhancing ion/proton exchange, and improving muscle contraction, relaxation, and endurance[297]. Furthermore, it can act as a neurotransmitter in the brain, with carnosine's antioxidative, anti-inflammatory, and anti-aggregate properties showing promise in treating neurodegenerative diseases such as Alzheimer's[298,299]. In contrast, the role of carnosine in the mammary gland is unexplored; however, the broad range of functions attributed to carnosine has shown promise in various diseases, including cancer. Indeed, carnosine supplementation inhibited the proliferation of breast cancer cells and tumours in breast cancer xenografts[300–302]. In this chapter, enrichment of $^{13}C$ from histidine was observed in carnosine pools in the NMG despite low *Carns* expression in this

tissue. However, the NMG has relatively less carnosine than the brain or muscle. Therefore, it is unclear whether this carnosine is produced in the NMG or if it is taken up. Interestingly, the adult mammary gland expresses relatively high levels of *Slc15a2*, encoding Pept2, an essential carnosine transporter in the kidneys[303]. Furthermore, the mammary gland expresses relatively high levels of *Cndp2*, a carnosine dipeptidase, suggesting that carnosine may be imported and hydrolysed to provide cells with β-alanine and histidine. Thus, these data suggest it is unlikely that histidine is utilised significantly for carnosine production in the mammary gland. In contrast, histamine levels are relatively higher in the NMG and the lung compared to the other tissues; this is corroborated by the high expression of *Hdc* in these tissues. Notably, high histamine levels have been observed in mammals' mammary glands[292]. Indeed, histamine concentration and HDC activity in the murine mammary gland peak during the proestrus and oestrous phases[304,305]. Therefore, the observed variability in histamine enrichment from histidine across our samples may be attributed to the mice being at different stages of their oestrous cycles. Given the importance of increased HDC and histamine levels during these phases of rapid cell proliferation and differentiation, it is not surprising that breast cancer cells have increased HDC and histamine levels as well. However, the role of histamine in breast cancer is not straightforward. Generally, breast cancer cells and tumours have increased expression of HDC, therefore histamine, compared to normal epithelial cells or normal tissue[306–308]. However, others have demonstrated downregulation of HDC in breast cancer compared to normal tissues [309]. Indeed, higher HDC expression has been linked to improved OS and disease-free survival in breast cancer, and aggressive breast cancer subtypes, such as TNBC, exhibit the lowest *HDC* expression levels[309]. However, mast cells are abundant within the mammary gland and tumours and are the predominant source of histamine[292,304]. Therefore, elevated levels of histidine observed in breast cancers could result from infiltration of inflammatory cells. In agreement with the pro-tumourigenic role of histamine, mast cell depletion was found to reduce tumour size and metastasis in the PyMT mouse model of breast cancer[310]. Histamine exerts its biological effect through binding to receptors (H1-4) on the cell surface. The receptor is thought to determine the differences in histamine response across breast cancer cell lines and tumours. Histamine binding to the H2 receptor promotes proliferation and tumour growth[311,312]. In contrast, binding to the H4

receptor elicits an anti-cancer effect and is associated with improved OS in breast cancer[307,309,313–315]. Indeed, histamine administration in a mouse model of TNBC was observed to significantly reduce tumour burden in immunocompromised and immunocompetent mice, indicative of a tumour cell-intrinsic mechanism[309,314]. Therefore, to better understand the contribution of histidine to histamine synthesis and tumourigenesis in this Myc-driven tumour model, stable isotope tracing of histidine into histamine should be done, with careful consideration of the immune system. However, given the extensive research on histamine's role in breast cancer, we chose to focus on the contribution of the histidine degradation pathway in Myc-driven cancer cells.

Myc-driven cancer cells are dependent on exogenous glutamine to meet bioenergetic demands[97,104]. Indeed, Myc-driven transformation is characterised by increased glutaminolysis[244]. Therefore, utilising histidine as a carbon source could provide an additional source of glutamate. However, we did not observe any contribution from histidine into glutamate or glutamine in Myc-driven tumour cells. Coupled with the lack of labelling in methionine or SAM, this suggests that the histidine degradation pathway is inactive in these cells. This was supported by the absence of enzymes involved in histidine degradation, *Hal*, *Amdhd1*, and *Ftcd*.

In line with previous studies, the data in this chapter highlight a relationship between Myc and *Slc7a5*/Lat1. Underscoring the importance of understanding the contribution of LAT1 in Myc-driven tumourigenesis. Intriguingly, histidine levels and uptake were significantly increased in Myc-driven MGTs compared to the NMG and ErbB2-driven MGTs. The abundance of other LAT1 substrates were also higher in Myc-driven tumours, such as phenylalanine and leucine. However, in contrast to histidine, phenylalanine and leucine are the most abundant amino acids in proteins. Therefore, there is an increased demand for these EAAs for protein synthesis[295]. While there is a possibility that the increase in histidine is simply a byproduct of increased LAT1 expression, other high-affinity LAT1 substrates, such as tryptophan or tyrosine, are not significantly increased in Myc-driven MGTs compared to the NMG or MMTV-ErbB2 tumours. Therefore, given that histidine is not catabolised in Myc-driven tumour cells and histidine is present at relatively low levels in proteins compared to other EAAs such as leucine, it remains to be determined whether this

increased demand for histidine plays a functionally relevant role in supporting Myc-driven tumourigenesis. Thus, in the following chapters, I sought to uncover the mechanisms that drive histidine requirement and identify the role of histidine in supporting Myc-driven tumours, aiming to reveal potential therapeutic strategies.

**Summary**

To summarise, this chapter has:

1) Confirmed increased *Slc7a5*/Lat1 mRNA and protein expression in the MMTV-Myc MGT model compared to the normal mammary gland and MMTV-ErbB2 MGTs.
2) Identified enhanced histidine uptake in MMTV-Myc MGTs.
3) Revealed the contribution of histidine metabolism to pathways that produce carnosine, histamine, glutamate, methionine, and SAM across healthy adult murine tissues.
4) Demonstrated that histidine is not catabolised through the histidine degradation pathway in Myc-driven tumour cells.

# Chapter 4. Glutamine availability influences histidine requirement

## 4.1 Introduction

Cells cannot synthesise EAAs; therefore, they must rely on uptake via amino acid transporters. Cancer cells have an increased demand for EAAs to sustain rapid cell growth and proliferation. Therefore, amino acid transporters are upregulated in myriad tumours. Indeed, several amino acid transporters are MYC target genes, some of which are essential for MYC-driven transcriptional amplification[163]. Previous work has shown that *SLC7A5* (encoding LAT1) is required for critical amino acid uptake in MYC-driven cancer cells. This supports the translation of MYC, thus maintaining MYC-driven metabolic rewiring, cellular proliferation, and tumourigenesis[163]. This links LAT1 to glutamine metabolism in MYC-driven tumourigenesis, suggesting that LAT1 promotes glutamine addiction. For example, *SLC7A5* knockdown in BE-2C cells with amplification of N-MYC displayed significant depletion of glutamine and Krebs-cycle intermediates, including glutamate[163]. Previous research has shown glutamine to be indispensable to LAT1-mediated uptake of EAAs, such as leucine[142]. This was demonstrated through coupling of the glutamine transporter, ASCT2, with LAT1. Whereby glutamine uptake via ASCT2 was followed by glutamine efflux through LAT1. However, others have found that ASCT2 knock-out did not affect LAT1 activity, as demonstrated by leucine uptake[148]. Therefore, this suggests that other substrates may be utilised for LAT1-mediated amino acid exchange in MYC-driven cancer cells and tumours. Interestingly, while glutamine has been proposed to be a critical LAT1 exchange substrate, LAT1 binds glutamine with low affinity with a Km= ~1.5 - ~2.0 mM [226]. Therefore, large amounts of free intracellular glutamine would be necessary to produce the concentration gradient necessary for exchange through LAT1. However, glutamine availability may be limited in the tumour microenvironment due to competition among different cell types, such as immune cells[158]. Furthermore, glutamine availability may vary within other regions of the tumour with inadequate vascular supply of nutrients [246]. In addition to these different variables that may affect exogenous glutamine availability, oncogenes such as MYC may compound

these effects due to increased demand for glutamine catabolism to meet biosynthetic and energetic demands[97,104,244]. Previous work by Dr Emma Still, a past PhD student in our lab, demonstrated that MMTV-Myc-induced tumours had significantly increased glutamine catabolism compared to MMTV-ErbB2 tumours [316]. Here, Dr. Still showed that not only was there increased contribution from glutamine catabolism into the Krebs cycle, but these Myc-induced tumours also utilised more glutamine into non-essential amino acids, aspartate, proline, and serine when compared to ErbB2-induced tumours [316]. Importantly, Myc-driven tumours expressed lower RNA and protein levels of glutamine synthetase (GS) than the NMG, demonstrating that these tumours could have reduced glutamine synthesis and may rely more heavily on exogenous glutamine to meet glutamine demands[316]. This was supported by increased RNA and protein expression of the glutamine transporter, *Slc1a5* (encoding Asct2)[316]. Thus, these data suggest that Myc-driven tumours from this MMTV-Myc model have an increased demand for exogenous glutamine, which is catabolised to support several biosynthetic pathways. Therefore, while glutamine levels may be sufficient in tumours such as Erbb2-driven tumours or tumours where glutamine levels are maintained to be transported by LAT1 with low affinity, it is likely that other LAT1 substrates may become critical for the uptake of EAAs via LAT1 when glutamine is limited. Interestingly, it is well documented that LAT1 has the highest affinity for histidine, with a Km between 5 - 50 μM[226,249]. Furthermore, experiments with reconstituted hCD98/hLAT1 complexes in liposomes preloaded with each individual amino acid and incubated in [$^3$H]-histidine demonstrated that histidine is the preferred bidirectional substrate for LAT1[229]. Tyrosine and glutamine were also used as substrates, but to a much lesser extent. In contrast, other high-affinity essential amino acids, such as isoleucine and leucine, did not promote the accumulation of [$^3$H]-histidine in the liposomes. Consequently, Chapter 4 will investigate whether glutamine availability and utilisation dictate the demand for histidine, another bidirectional LAT1 substrate, using tumour cell lines derived from MMTV-Myc tumours and other established human cancer cell lines. These experiments aim to reveal whether glutamine and histidine have potential overlapping roles in these tumours, setting the stage for further analysis of the role of histidine in Myc-driven cancer cells and tumours.

This chapter will first characterise the Myc-driven tumour cell lines to confirm that these cells are glutaminolytic, as demonstrated in the MMTV-Myc-driven tumours by Dr. Emma Still. Using these cells and the human cancer cell lines, a series of experiments will be conducted to assess the effect of exogenous glutamine availability, glutamine utilisation, and glutamine levels on histidine uptake. This will be achieved by employing several molecular biology techniques, assessing gene and protein expression of genes involved in glutamine catabolism and amino acid transporters, and liquid-chromatography mass spectrometry to trace glutamine, glucose, and histidine uptake and utilisation.

**Aims**

This chapter aims to address these aspects of my hypothesis:

1) Myc-driven cancer cells and tumours depend on exogenous glutamine for Krebs cycle anaplerosis.
2) Glutamine availability and utilisation underlie the requirement for histidine.
3) Glutamine and histidine have overlapping roles in Myc-driven tumour cells.

## 4.2 Myc-driven cancer cells depend on exogenous glutamine for central carbon metabolism and proliferation.

Initially, the aim was to use tumour cell lines derived from MMTV-Myc and MMTV-ErbB2-driven MGTs. ErbB2-driven tumours were less glutaminolytic than Myc-driven tumours, which could provide an excellent comparative model to assess the interplay between glutamine limitation and histidine requirement in two mammary tumour models driven by different oncogenes. Furthermore, given the increased *Slc7a5*/Lat1 gene and protein expression in Myc- compared to ErbB2-driven MGTs (Figure 3-1B-D) and the corresponding increased uptake of U-[$^{13}$C]-histidine in the Myc-driven tumours, ErbB2-driven tumour cell lines would be a helpful comparative *in vitro* model to assess the role of histidine. Therefore, we first compared Myc-driven tumour cell lines (MYC310, MYAZ6.6g and MYAZ16.1e) to an ErbB2-driven tumour cell line (MYDA2.1d). These cell lines were previously derived from individual MMTV-Myc or MMTV-Erbb2 tumours by past PhD students Dr. Emma Still and Dr. Benedict McIntyre and have been passaged multiple times.

Surprisingly, when protein expression of ErbB2 and Myc was assessed in these cell lines, none of the cell lines had amplified levels of ErbB2 in contrast to ErbB2-driven tumours, while all of them expressed high levels of Myc similar to MMTV-Myc tumours (Figure 4-1A). We next interrogated whether the culture medium could alter the expression of ErbB2. As outlined in the Materials and Methods Chapter, the tumour cell lines are cultured in MMEC medium that contains growth factors, EGF, and insulin (Table 2-12). The addition of EGF to the culture medium has been shown to accelerate ErbB2 internalisation, which could lead to its degradation [317]. Therefore, tumour cell lines were cultured in a medium without growth factors (GF), EGF and Insulin for 24 or 48 hours and ErbB2 protein expression was assessed. However, while ErbB2 expression stabilised with GF withdrawal in MYC310 cells compared to expression in cells cultured in GF-containing media, MYDA2.1d cells had decreased expression of ErbB2 (Figure 4-1B). Therefore, this loss of ErbB2 expression does not appear to result from being cultured in GF-containing media. However, these cells had been passaged 12 times since isolation at the point of this experiment. Therefore, I cannot negate the effects of repetitive exposure to EGF and Insulin. Given that Myc-expression was reduced when cultured in a GF-free medium within 24 hours (Figure 4-1B) and is required to maintain mammary epithelial cell growth, differentiation, and function, this condition is not ideal for our experiments. To determine how quickly ErbB2 expression was lost in cells isolated from ErbB2-driven MGTs, cells were freshly isolated from three ErbB2 tumours (1.1c, 2.2a, and 2.2b). The fresh tumour cells were collected along with subsequent early passages. Surprisingly, ErbB2 expression was lost as early as one passage (Figure 4-1C). However, these cells were passaged in complete MMEC medium with growth factors. Therefore, this effect could be due to the presence of EGF in the culture media. As a result, the experiments in this thesis only used Myc-driven tumour cell lines and various human cancer cell lines to avoid altering culture conditions significantly to maintain ErbB2 expression in MMTV-Erbb2 tumour-derived cell lines.

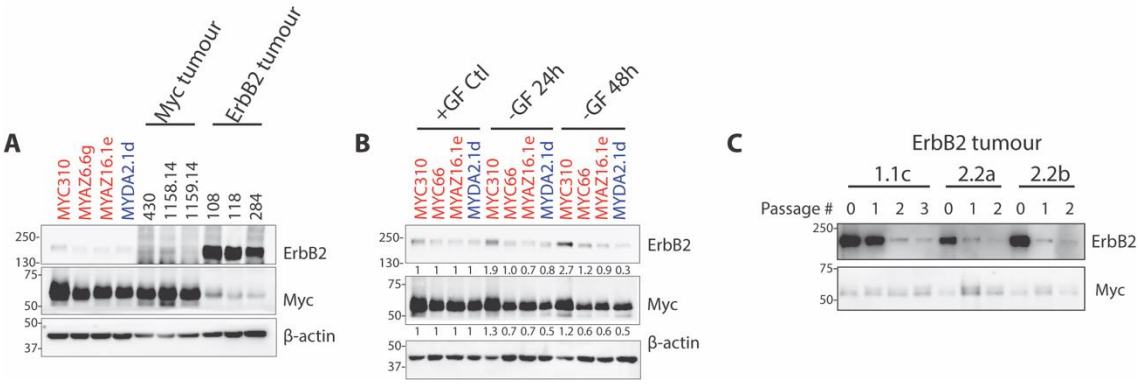



**Figure 4-1.ErbB2 is lost from MMTV-ErbB2 MGT-derived tumour cell lines.** (**A**) WB of lysates from Myc-driven (red) and ErbB2-driven (blue) tumour cell lines and representative MMTV-Myc and MMTV-ErbB2 tumours. (**B**) WB of Myc-driven and ErbB2-driven tumour cell lines cultured with or without growth factors (GF) for indicated times. (**C**) WB of three ErbB2 tumour cell lines derived from individual MMTV-ErbB2 MGTs at indicated passages. All western blots are representative of 1 replicate.

Using Myc-derived tumour cell lines (MYAZ16.1e, MYAZ6.6g, and MYAZ12.3i), we first sought to confirm the glutaminolytic phenotype observed by Dr Emma Still in the MMTV-Myc-driven MGTs. As expected, these cells maintain elevated levels of Myc compared to cultured mammary epithelial cells isolated from the MFP (Appendix 1A, B). Furthermore, when MYAZ16.1e cells were cultured in different concentrations of glutamine, a significant proliferative defect was observed in cells cultured with less than 1 mM of glutamine (Figure 4-2A, B). To determine whether glutamine is required for anaplerosis in the Krebs cycle in these cells, they were cultured in glutamine-deplete media with dimethyl α-ketoglutarate (DMKG), a membrane-permeable esterified α-ketoglutarate. Indeed, the addition of DMKG was able to rescue the proliferative defect observed in cells cultured in glutamine-depleted media (Figure 4-2C). BT-549 and MDA MB 231 TNBC cell lines were also used to assess glutamine requirement. BT-549 cells have endogenous amplification of Myc, but MDA MB 231 cells also display relatively high levels of Myc (Appendix 1A, C). Both cell lines depend on exogenous glutamine; however, while proliferation can be fully rescued upon adding DMKG in BT-549 cells, it is only partially rescued in MDA MB 231 cells (Appendix 1D, E). In MYAZ16.1e cells, the requirement for glutamine catabolism for the Krebs cycle was further supported by the low $IC_{50}$ value of the GLS1 inhibitor, CB-839, observed in these cells (Figure 4-2D).

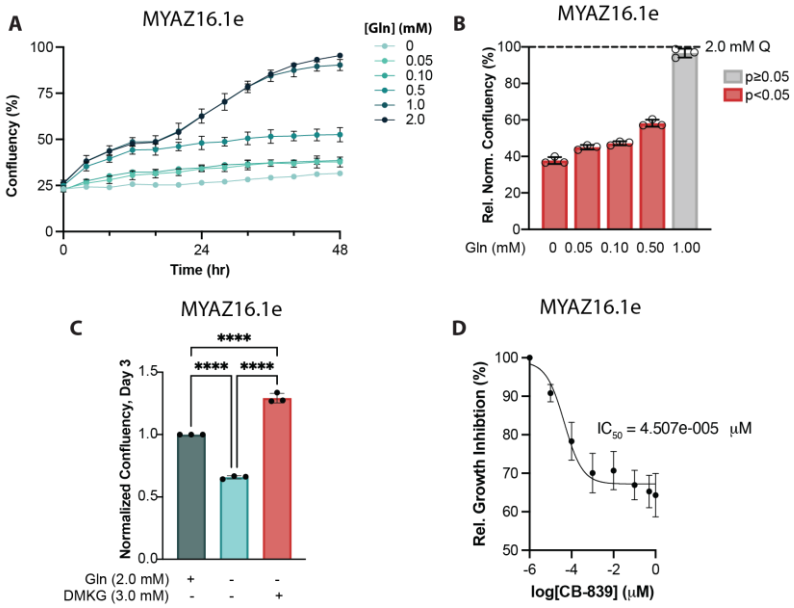



**Figure 4-2.Myc-driven tumour cells are glutamine auxotrophs.**
**(A)** Confluency of MYAZ16.1e cultured in different concentrations of glutamine (Gln) and imaged every 4 hours, representative of 1 independent replicate. **(B)** Quantification of panel A relative to the confluency at 2.0 mM glutamine after 48 hours. **(C)** Confluency of MYAZ16.1e cells cultured under indicated conditions relative to 2.0 mM glutamine after 72 hours, representative of 1 biological replicate. **(D)** $IC_{50}$ curve of CB-839 growth inhibition on MYAZ16.1e cells after 72 hours, representative of 1 biological replicate. All data are shown as mean ± s.d. One-way ANOVA with Šídák correction: ****p≤0.0001.

To further interrogate the contribution of glutamine to the Krebs cycle, the MYAZ cell lines were cultured with 2.0 mM or 0.1 mM U-[$^{13}$C]-glutamine for 24 hours. This will determine whether glutamine is required to maintain levels of Krebs cycle intermediates and assess the incorporation $^{13}$C from glutamine into these metabolites. Glutamine limitation significantly reduced glutamate abundance, Krebs cycle intermediates fumarate and malate, and oxaloacetate-derived aspartate (Figure 4-3A). Furthermore, glutamine is the primary carbon source for glutamate (80.62% ± 4.08% ), α-ketoglutarate (82.22% ± 4.48), succinate (56.76% ± 8.99), fumarate (72.64% ± 3.22%), malate (70.15% ± 3.18%), and aspartate (66.09% ± 4.41%), and a significant contributor to oxaloacetate (49.09 ± 5.58%) and citrate (47.48% ± 2.96%). Which was significantly suppressed by low glutamine conditions (Figure 4-3B). Therefore, glucose likely maintains oxaloacetate and citrate levels to compensate for glutamine limitation, but this is insufficient to support all Krebs-cycle intermediates' levels. Similarly, BT-549 and MDA-MB-231 cells also use glutamine as the primary carbon source for Krebs cycle intermediates (Appendix 1F). These results confirm that Myc-driven tumour cell lines and TNBC cells are

glutamine auxotrophic and depend on glutaminolysis for Krebs cycle anaplerosis. Therefore, these tumour cell lines were appropriate for further experiments.

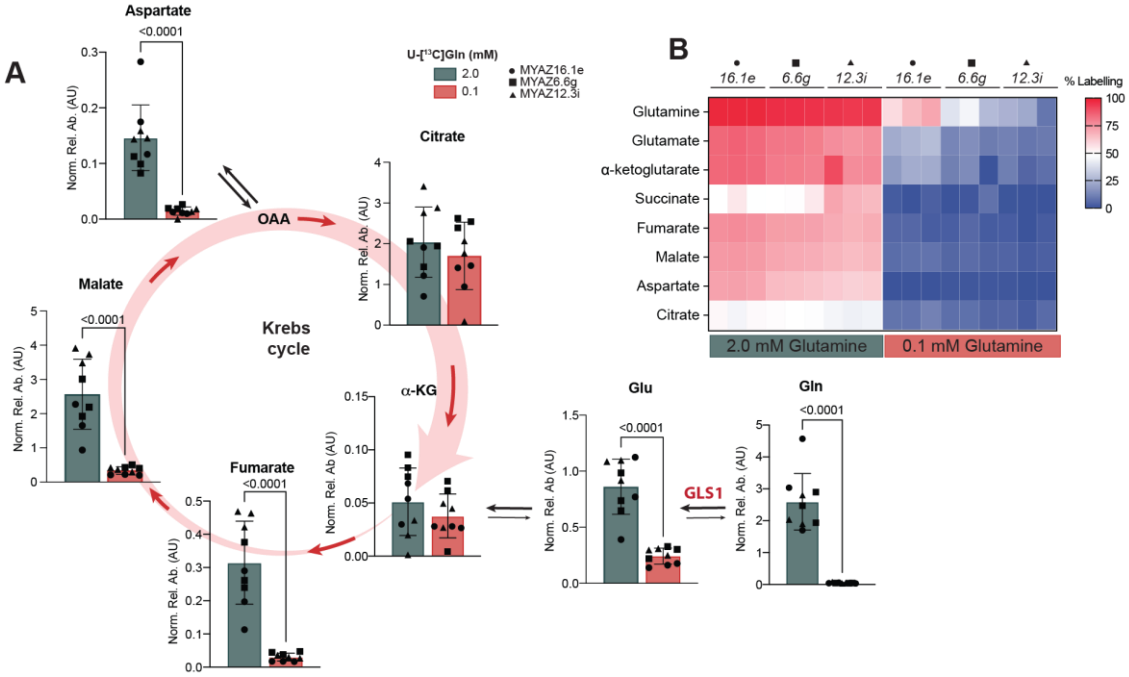



**Figure 4-3.Myc-driven tumour cells use glutamine as the primary fuel for the Krebs cycle.**
LC-MS analysis of Myc-driven tumour cells cultured in 0.1 or 2.0 mM [U-$^{13}$C]-glutamine for 24 hours: (**A**) Total abundance of Krebs cycle intermediates, data represented as mean ± s.d.; different shapes depicting each biological replicate (n=3). Unpaired two-tailed t.test (****p≤0.0001), and (**B**) heatmap showing $^{13}$C enrichment of Krebs cycle intermediates. OAA = oxaloacetic acid.

## 4.3 Exogenous glutamine limitation increases cellular requirement for histidine.

Glutamine was shown to be an essential exchange factor for LAT1-mediated EAA uptake [142]. However, glutamine is a low-affinity LAT1 substrate; therefore, high concentrations of free intracellular glutamine are necessary to provide the concentration gradient necessary for exchange through LAT1. Since glutamine is essential for central carbon metabolism in Myc-driven cancer cells, we hypothesised that there would be increased cellular demand for histidine in glutamine-limited conditions. Myc-driven tumour cell lines (MYAZ16.1e, MYAZ6.6g, MYAZ12.3i) cultured in high or low glutamine were subsequently incubated with 200 µM of U-[$^{13}$C]-histidine for 10 minutes, after which the cells were collected for

LC-MS analysis and the intracellular levels of the m+6 isotopologue of histidine were compared (Figure 4-4A). First, we assessed transcript and protein levels of Lat1 in high and low glutamine conditions. Cells cultured in low glutamine had significantly increased *Slc7a5* expression, as well as the glutamine transporter *Slc1a5*, whereas the EAA uniporter, *Slc43a1* (encoding Lat3), was unchanged with glutamine limitation (Figure 4-4B). Furthermore, an increase in *Atf4* transcription suggests activation of the ISR upon glutamine limitation may be driving these transcriptional changes (Figure 4-4B), which has been previously demonstrated[318]. This induction of Lat1 and Asct2 upon glutamine limitation was also observed at the protein level (Figure 4-4C). Therefore, we sought to determine whether histidine uptake was altered in cells cultured in low glutamine due to enhanced Lat1 expression. Indeed, cells cultured in low glutamine conditions took up significantly more of the m+6 isotopologue of histidine than those cultured in high glutamine (Figure 4-4D). If this increased histidine uptake indicates an overlapping role with glutamine, then increased histidine availability should result in a decreased requirement for glutamine. Therefore, cells were preloaded with different concentrations of histidine or asparagine, from 0 to 1 mM, without other amino acids (Figure 4-4F). Asparagine is an NEAA that was shown to be another important essential amino acid exchange factor, and LAT1 binds with a similar affinity as glutamine [226,245]. Subsequently, cells were replenished with AAs, including 2.0 mM glutamine, for 2.5 minutes and then collected for analysis via LC-MS (Figure 4-4F). Interestingly, increasing intracellular abundance of histidine correlated with decreased glutamine uptake, which was not observed in asparagine-preloaded cells (Figure 4-4G).

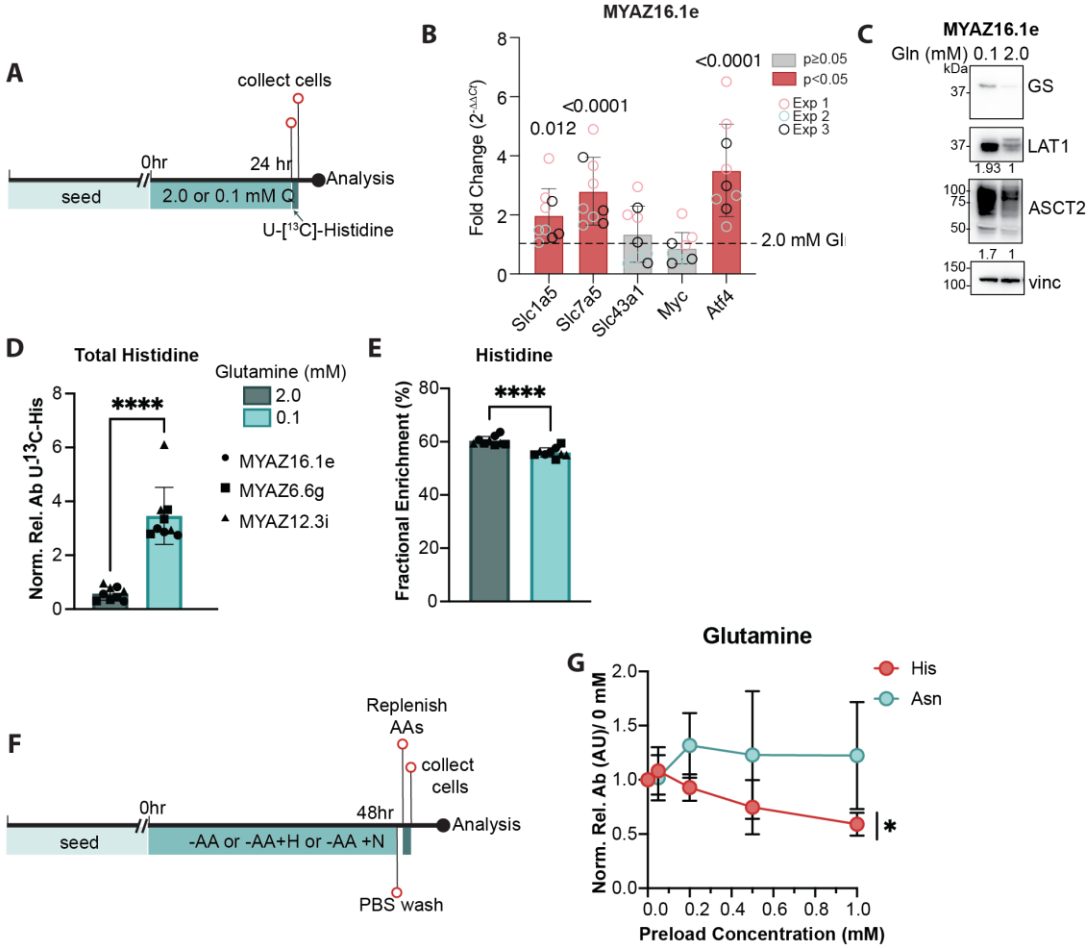



**Figure 4-4. Glutamine limitation increases histidine uptake in Myc-driven cancer cells.**
**(A)** Schematic of the experimental timeline of MYAZ16.1e culture conditions with 20 minutes [U-$^{13}$C]-histidine administration before collection. **(B)** RT-qPCR of fold change in gene expression normalized to *β-actin* in cells cultured in 0.1 mM glutamine relative to 2.0 mM glutamine conditions (one-way ANOVA with Šídák correction, representative of 3 independent replicates). **(C)** Representative WB of proteins in panel B. Protein levels are normalized to vinc and fold change relative 2.0 mM glutamine was determined. **(D-E)** LC-MS analysis: **(D)** total abundance of intracellular m+6 histidine levels and **(E)** intracellular$^{13}$C enrichment (unpaired two-tailed t-test, representative of 3 independent replicates). **(F)** Experimental strategy for histidine and asparagine preloading in MYAZ16.1e cells. **(G)** LC-MS analysis of intracellular glutamine levels relative to starved cells (two-way ANOVA with Dunnett correction, representative of 3 independent replicates). All Data are shown as mean ± s.d. *p≤0.05, ****p≤0.0001.

Next, we sought to determine the fate of histidine in cells cultured with low and high glutamine. If histidine is used as an exchange substrate, we expect to see the m+6 isotopologue of histidine in the media. To assess this, cells subjected to 200 μM of U-[$^{13}$C]-histidine for 20 minutes were washed and replenished with complete media for 10 minutes (Figure 4-5A), and the cells and media were then collected for

analysis. In both high and low glutamine conditions, cells rapidly depleted the m+6 isotopologue of histidine (Figure 4-5B). In agreement, significantly increased levels of m+6 histidine were observed in the media from cells cultured in low compared to high glutamine (Figure 4-5C). This suggests that cellular histidine is effluxed in high and low glutamine conditions, perhaps as an exchange substrate for amino acid antiporters, such as LAT1. Significantly, cells cultured in low glutamine have increased histidine uptake and can efflux more histidine, which may provide an advantage to glutamine-addicted Myc-driven cancer cells, providing the ability to maintain levels of EAAs even when glutamine is limited.

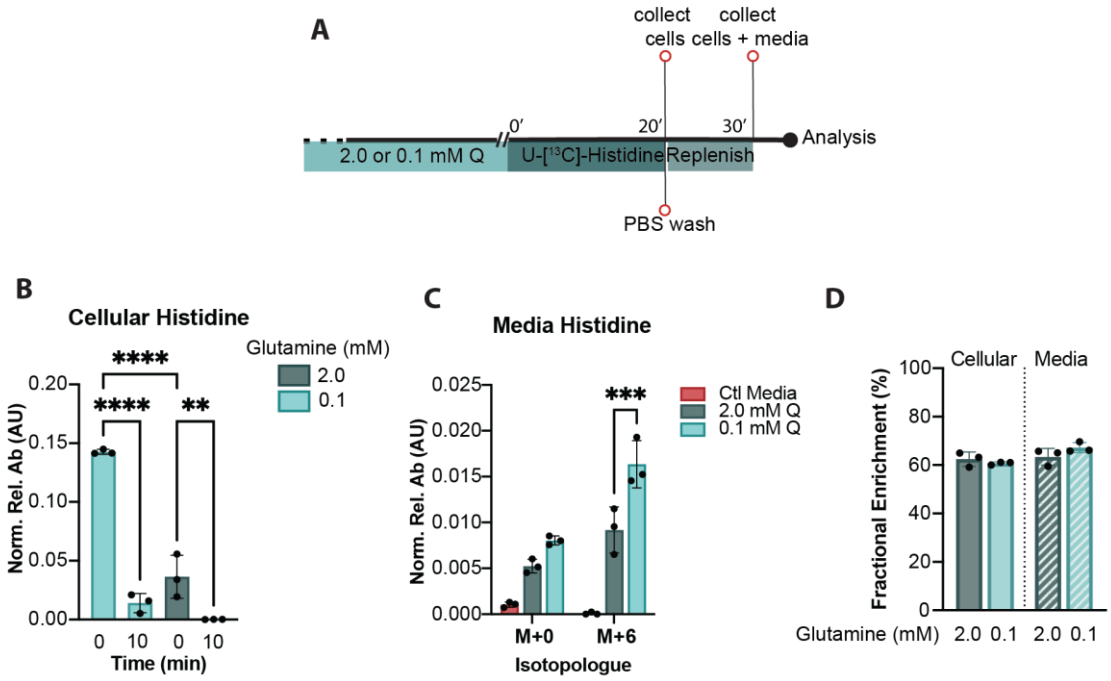



**Figure 4-5.Cells cultured in low glutamine have increased histidine efflux.** MYAZ16.1e cells cultured in 2.0 mM or 0.1 mM glutamine for 24 hours and administered 200 μM [U-$^{13}$C]-histidine for 20 minutes. **(A)** Schematic of experimental timeline for sample collection following [U-$^{13}$C]-histidine uptake. **(B-D)** LC-MS analysis of histidine: **(B)** total abundance of intracellular m+6 isotopologue before and after media change (one-way ANOVA with Šídák correction), **(C)** abundance of m+0 and m+6 histidine isotopologues in the medium (two-way ANOVA with Tukey correction), and **(D)** intracellular and extracellular $^{13}$C enrichment of histidine (one-way ANOVA with Šídák correction). Data are presented as mean ± s.d. Results are representative of one biological replicate. **p≤0.01, ***p≤0.001, ****p≤0.0001.

## 4.4 Glutamine Synthetase levels are negatively correlated with histidine requirement in BC cell lines.

GS levels are associated with glutamine independence in breast cancer cell lines [108]. Therefore, breast cancer cell lines with different GS levels were selected to assess whether the capacity to maintain intracellular glutamine pools reduces the requirement for histidine. These cell lines were selected by identifying those with low, mid, and high levels of GS expression by analysing previously published and publicly available single-cell RNA sequencing data[319]. Hs578t (low GS), T47D (mid GS), and AU565 (high GS) were selected. Protein expression of ErbB2, MYC, GS, GLS1, GLS2, LAT1 and ASCT2 were assessed (Figure 4-6A). AU565 is a HER2+ breast cancer with endogenous amplification of MYC; as expected, we observe higher levels in both ERBB2 and MYC (Figure 4-6A). In line with RNA-sequencing data, Hs578t cells had no GS protein expression, T47D cells expressed low levels, and AU565 cells expressed high levels of GS (Figure 4-6A). Furthermore, GS is induced further in T47D and AU565 cells when cultured in low glutamine conditions (Figure 4-6A). Furthermore, Hs578t cells have high levels of GLS1 when compared to T47D and AU565 cells (Figure 4-6A). This suggests that Hs578t cells are glutaminolytic and depend on glutamine for Krebs cycle anaplerosis, whereas T47D and AU565 cells can produce glutamine through GS activity. These protein expression patterns were supported by gene expression data from the DepMap 24q2 publicly available dataset (Appendix 2A). Given these results, we hypothesised that Hs578t cells would depend on exogenous glutamine for proliferation, whereas AU565 would not. Indeed, the $IC_{50}$ value of glutamine limitation for inhibiting cell proliferation in AU565 cells was 0.25 nM ($R^2 = 0.45$) compared to 12.23 µM (95% CI: 6.5 to 22.00 µM, $R^2 = 0.82$) in T47D cells, and 279.0 µM (95% CI: 234.7 to 328.3 µM, $R^2 = 0.86$) in Hs578t cells (Figure 4-6B). Each cell line was cultured in low or high U-[$^{13}$C]-glutamine for 24 hours and then 200 µM of U-[$^{13}$C]-histidine was added to the medium for 10 minutes. These human breast cancer cell lines lack *UROC1* (encoding urocanase), unlike liver cancer cell lines such as HepG2 and Huh7, an enzyme involved in histidine catabolism upstream of glutamate production (Appendix 2A). UROC1 is required to produce 4-imidazolone-5-propionate, which is the precursor to FIGLU[253]. Without FIGLU, glutamate cannot be produced from histidine. However, this must be confirmed with

longer incubations with U-[$^{13}$C]-histidine. We first assessed the contribution of glutamine into glutamate and Krebs cycle intermediates, α-KG, fumarate, malate, and citrate. Consistent with their elevated GLS1 expression, Hs578t cells rely on Gln to fuel the Krebs cycle (Figure 4-6C). Indeed, a reduction in the percent of labelled glutamine-derived glutamate (m+5), α-KG (m+5), fumarate (m+4), malate (m+4), citrate (m+4, m+5) was observed in T47D and AU565 cells (Figure 4-6C). In contrast, T47D and AU565 cells have increased contribution into glutamate and Krebs cycle intermediates from other carbon sources, as indicated by the increased abundance of unlabelled (m+0) metabolites compared to Hs578t cells (Figure 4-6C). However, despite the relatively high levels of GS in these cells, there was still a significant reduction in the total abundance of glutamine when cultured in low glutamine (Figure 4-6D). Given the high glutamine concentration in cell culture media these cells may take up significantly more glutamine than is needed to maintain biosynthetic processes, whereas Hs578t cells likely require more glutamine for glutaminolysis. Indeed, under glutamine replete conditions, Hs578t cells have lower glutamine levels than T47D and AU565 cells, which may be indicative of increased catabolism (Figure 4-6D). The relative abundance of Krebs cycle metabolites was measured under high and low glutamine conditions for all cell lines. While the abundance of all intermediates was reduced in glutamine low conditions, T47D and AU565 cells had increased abundance of these intermediates compared to Hs578t cells (Figure 4-6F-I). Furthermore, there was a significant increase in the amount of unlabelled (m+0) α-KG, malate, and citrate in AU565 cells when cultured in low glutamine compared to high glutamine, highlighting the ability of these cells to use alternate carbon sources when glutamine is not available (Figure 4-6F,H,I). Therefore, GS expression was a good predictor of glutamine independence in these cells.

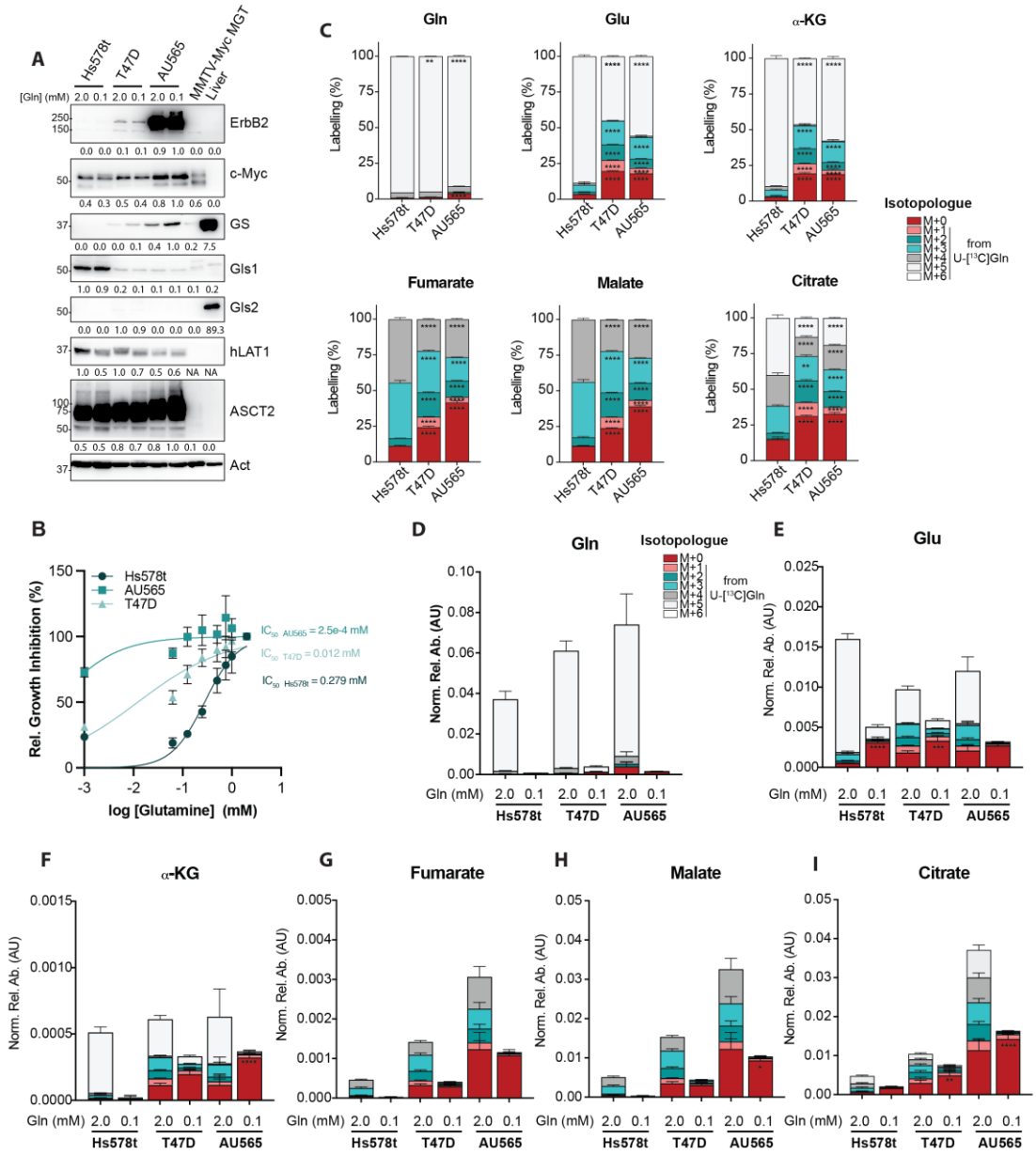



**Figure 4-6.GS expression positively correlates with glutamine independence.** **(A)** WB of Hs578t, T47D, and AU565 cells cultured in 2.0 mM and 0.1 mM glutamine. Myc-driven MGT and liver as positive/negative controls. Protein levels were normalized to β-actin and min-max normalized. Representative of 3 independent replicates. (**B**) Normalized relative confluency of cells cultured in 0-2.0 mM glutamine, relative to 2.0 mM glutamine. A non-linear fit of log(glutamine) vs. normalized response was applied to determine $IC_{50}$ values. Representative of 2 independent replicates. (**C**) % labelling of glutamine and Krebs cycle intermediates in cells cultured in 2.0 mM [U-$^{13}$C]-glutamine for 24h (two-way ANOVA with Šídák correction). (**D-I**) Isotopologue abundance of glutamine, glutamate, and Krebs cycle intermediates in cells cultured in 2.0 mM or 0.1 mM total abundance of glutamine with isotopologue abundance in cells cultured with 0.1 or 2.0 mM glutamine [U-$^{13}$C]-glutamine for 24h (two-way ANOVA with Šídák correction). Data represent mean ± s.d. (n=3) *p≤0.05, **p≤0.01, ***p≤0.001, ****p≤0.0001.

Similar to the previous sections, the intracellular abundance of U-[$^{13}$C]-histidine was assessed to determine whether the glutamine-dependence correlated with histidine requirement. The abundance of the m+6 isotopologue of histidine under high and low glutamine was measured, and its abundance under low glutamine was normalized to that of the high glutamine condition. Therefore, a value higher than '1' indicates that histidine uptake was increased under low glutamine conditions. Hs578t cells took up significantly more histidine when cultured in low glutamine relative to high glutamine (Figure 4-7A). Surprisingly, T47D cells did not take up more histidine, and AU565 cells took up significantly less in low glutamine than in high glutamine (Figure 4-7A). Importantly, all cell lines express LAT1, and there does not appear to be significant induction of LAT1 upon glutamine limitation (Figure 4-6A) as observed in the murine Myc-driven tumour cell lines (Figure 4-4C, D). Therefore, these differences in histidine uptake cannot simply be described by differences in LAT1 expression across cell lines. Consequently, glutamine-dependent, GS-low cells that cannot maintain sufficient glutamine pools to meet cellular demands may have an increased demand for histidine. This may result in these cells being more sensitive to deprivation of histidine. However, no significant differences were observed when comparing sensitivity to histidine limitation in these cell lines under glutamine-high conditions (Figure 4-7C). Furthermore, each cell line required very low concentrations of histidine to maintain proliferation (Figure 4-7C). Importantly, these cell lines have significantly different proliferative rates, confounding the conclusions that can be drawn from these results. Indeed, Hs578t cells proliferate significantly faster than T47D and AU565 cells (Appendix 2B). However, these cells also display significantly different cellular morphology and size (Appendix 2C). Unfortunately, confluency was used to measure proliferation. Given these differences in cellular morphology, cell number would have been preferable in this case. Nonetheless, we aimed to assess the correlation between GS levels and histidine requirement utilising an isogenic system to avoid these confounding factors.

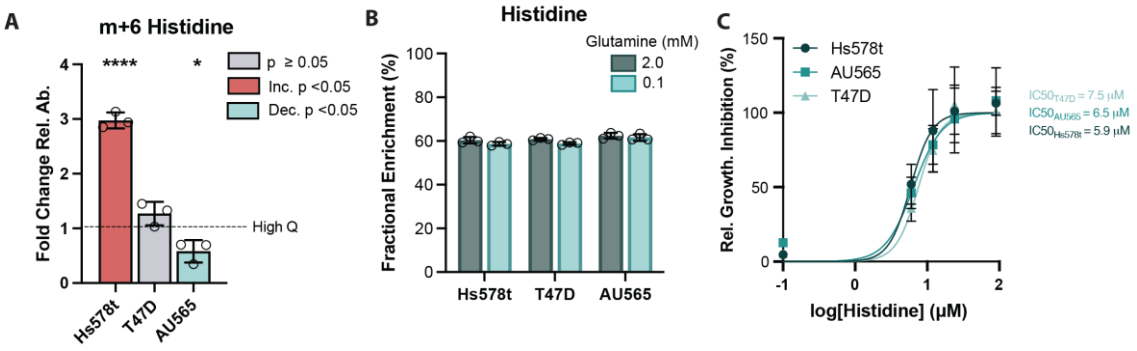



**Figure 4-7.Glutamine dependent BC cells have increased histidine uptake**.
**(A-B)** LC-MS analysis of Hs578t, T47D, and AU565 cells cultured in low (0.1) and high (2.0) glutamine and administered 200 μM [U-$^{13}$C]-histidine for 10 minutes: **(A)** fold change of abundance of intracellular m+6 histidine in cells cultured in low glutamine relative to high glutamine (one-way ANOVA with Šídák correction, representative of 1 replicate), and **(B)** $^{13}$C enrichment of histidine (representative of 1 replicate).**(C)** Normalized relative confluency of BC cells cultured in 0 to 120 μM of histidine relative to 120 μM histidine at 72 hours. A non-linear fit of log(histidine) vs. normalized response was applied to determine $IC_{50}$ values. Represents 2 independent replicates. All data presented as mean ± s.d. *p≤0.05, ****p≤0.0001

## 4.5 The ectopic overexpression of GS in Myc-driven tumour cell lines did not maintain glutamine pools.

Thus far, the data demonstrate that exogenous glutamine availability and utilisation for Krebs cycle anaplerosis influence histidine uptake. Furthermore, cells with greater GS expression, are less sensitive to decreased exogenous glutamine, which correlates to a reduced requirement for histidine when cultured in glutamine-limited conditions. To examine whether endogenous glutamine production is sufficient to dictate histidine requirement, we constructed a plasmid that overexpresses *GLUL* (Figure 4-8A), the gene encoding GS, as described in detail in the Materials & Methods Chapter. MYAZ6.6g cells were transduced with this plasmid to produce GLUL OE cells, which were compared to cells expressing the empty vector (EV) (Figure 4-8B). Surprisingly, GLUL OE cells were not less sensitive to glutamine limitation than EV cells (Figure 4-8C). The $IC_{50}$ value of glutamine that is insufficient for proliferation was 198.2 μM (95% CI: 176.3 to 223.0 μM, $R^2$=0.96) in EV cells and 179.8 μM (95% CI: 150.2 to 213.0 μM, $R^2$= 0.92) in GLUL OE cells. This implies that the glutamine levels produced by ectopic GS in these cells are insufficient to maintain proliferation.

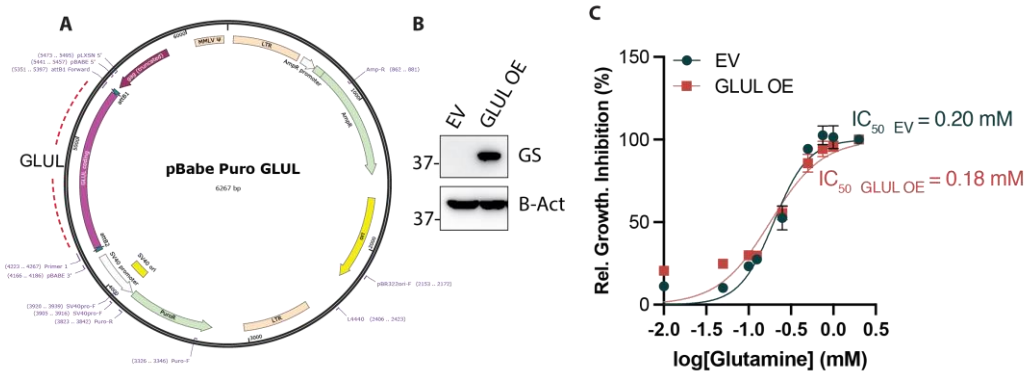



**Figure 4-8.Overexpression of GLUL did not confer glutamine independence in Myc-driven tumour cells**.
**(A)** Vector map of pBabepuro GLUL overexpressing vector generated by SnapGene. **(B)** WB of GS overexpression in EV and GLUL OE MYAZ6.6g cells. **(C)** Normalized relative confluency of MYAZ6.6g pBabe EV and pBabe-GLUL OE cells cultured in 0 to 2 mM of glutamine relative to 2 mM glutamine at 72 hours. A non-linear fit of log(glutamine) vs. normalized response was applied to determine $IC_{50}$ values. Represents 2 independent replicates.

EV and GLUL OE cells were cultured in either low or high-glutamine media to confirm whether GS was functional. Like wild-type cells (Figure 4-4C), when cultured in low glutamine, EV and GLUL OE cells had increased levels of GS, LAT1, and ASCT2 (Figure 4-9A). Therefore, aside from GS overexpression, no differences were observed in GLUL OE cells. To determine whether GLUL OE cells had increased GS activity, cells were cultured in high and low glutamine with U-[$^{13}$C]-glutamine or U-[$^{13}$C]-glucose. When both EV and GLUL OE cells were cultured in high glutamine conditions, there was no incorporation of $^{13}$C from glucose into glutamine (Figure 4-9B). However, upon glutamine limitation, GLUL OE cells (13.6% $\pm$ 0.4%) had significantly increased incorporation of glucose-derived $^{13}$C compared to EV cells (3.6% $\pm$ 2.8%; Figure 4-9B). However, GLUL OE cells could still not maintain glutamine levels (Figure 4-9C). Thus, like previous results in Myc-driven tumour cells (Figure 4-4D), when EV and GLUL OE cells were administered U-[$^{13}$C]-histidine, both cell lines had significantly increased abundance of the m+6 isotopologue of histidine when cultured in low glutamine media compared to high glutamine (Figure 4-9D). Furthermore, uptake of m+6 histidine was not significantly reduced in GLUL OE compared to EV cells cultured in low glutamine media ($p = 0.0530$, 2-way ANOVA).

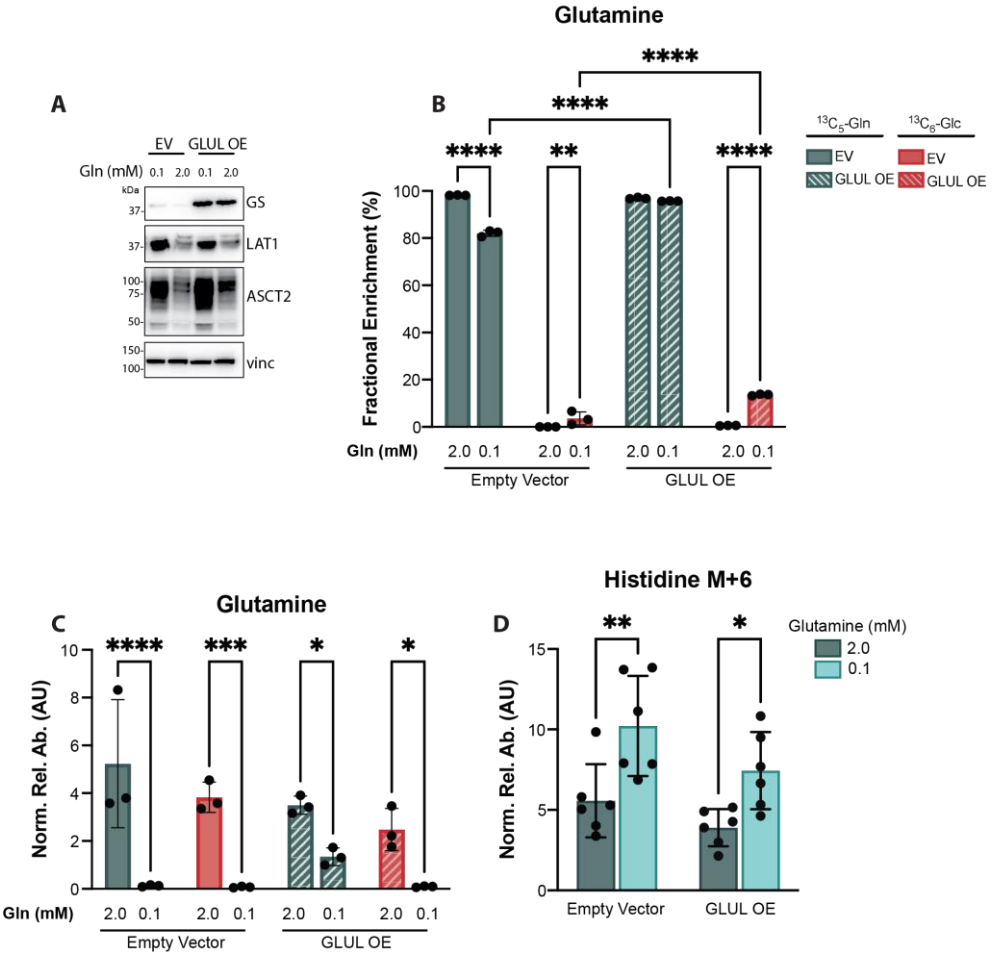



**Figure 4-9.GLUL/GS overexpression did not compensate for glutamine limitation.** **(A)** WB from lysates of empty vector (EV) control or GLUL OE MYAZ6.6g cells cultured in 0.1 or 2.0 mM glutamine (Gln), representative of 1 replicate. **(B-D)** LC-MS analysis of cells cultured in [U-$^{13}$C]-glutamine or [U-$^{13}$C]-glucose for 24 hours in 2.0 mM or 0.1 mM glutamine: **(B)** $^{13}$C enrichment in glutamine, **(C)** total abundance of glutamine, **(D)** abundance of m+6 histidine in cells administered 200 µM [U-$^{13}$C]-histidine for 20 minutes in cells cultured in 2.0 mM or 0.1 mM glutamine, representative of 2 replicates. All data represent mean ± s.d.; two-way ANOVA with Šídák correction. *p≤0.05, **p≤0.01, ***p≤0.001, ****p≤0.0001.

These experiments aimed to determine whether maintenance of glutamine pools due to increased GS activity would decrease cellular demand for histidine. While the generated GLUL OE cells overexpressed GS, the results suggest that ectopic GS was inefficient to produce sufficient amounts of glutamine and protect cells from glutamine limitation. Indeed, GLUL OE cells were glutamine auxotrophic and had no advantage in glutamine-limited conditions compared to EV controls. Furthermore, only a small percentage of glutamine was enriched with $^{13}$C from glucose in GLUL OE cells upon glutamine limitation, and glutamine abundance was

not maintained. Thus, this model could not provide the conditions necessary to assess the dependence of histidine requirement on intracellular glutamine levels and dependence on exogenous glutamine, therefore, further optimisation and characterisation are required to investigate this relationship further.

## 4.6 Glutamine compensates for histidine limitation.

Given that both glutamine and histidine can be used as LAT1 exchange substrates, mediating the uptake of EAAs, we hypothesised that increasing the availability of glutamine should compensate for histidine limitation if histidine is used as a LAT1 exchange factor in Myc-driven tumour cell lines. Myc-driven tumour cell lines were cultured in 100%, 25%, and 5% of the histidine in DMEM in 2 mM or 4 mM glutamine. Cells cultured in 5% histidine did not sustain proliferation in 2 mM or 4 mM glutamine (Figure 4-10A, B). However, the proliferative defect observed in cells cultured with 25% histidine in 2 mM glutamine was significantly rescued in 4 mM glutamine (Figure 4-10A, B). At the same time, cells cultured in 100% histidine with 4 mM glutamine did not grow faster than those cultured in 2 mM glutamine. Therefore, these results suggest that glutamine may compensate for histidine limitation. Importantly, SUnSET analysis at different concentrations of histidine shows that cells cultured in 5% of histidine are unable to maintain protein translation, display activation of the ISR as evidenced by induction of Atf4, and attenuate mTORC1 signalling as shown by decreased phosphorylation of Rps6 (ribosomal protein S6) (Figure 4-10C). Thus, as glutamine cannot compensate for the proteinogenic role of histidine, increasing glutamine availability is expected not to rescue the proliferative defect observed. However, cells cultured in 25% histidine do not have decreased protein translation, but Atf4 induction and mTORC1 attenuation are observed (Figure 4-10C). This indicates that histidine is essential in maintaining cellular amino acid homeostasis and mTORC1 signalling and that glutamine may compensate for this role when histidine is limited. These data suggest that increased glutamine abundance can protect cells from histidine limitation, alluding to the possibility that glutamine and histidine have overlapping roles. The next chapter aims to determine the role of histidine in Myc-driven cancer cells.

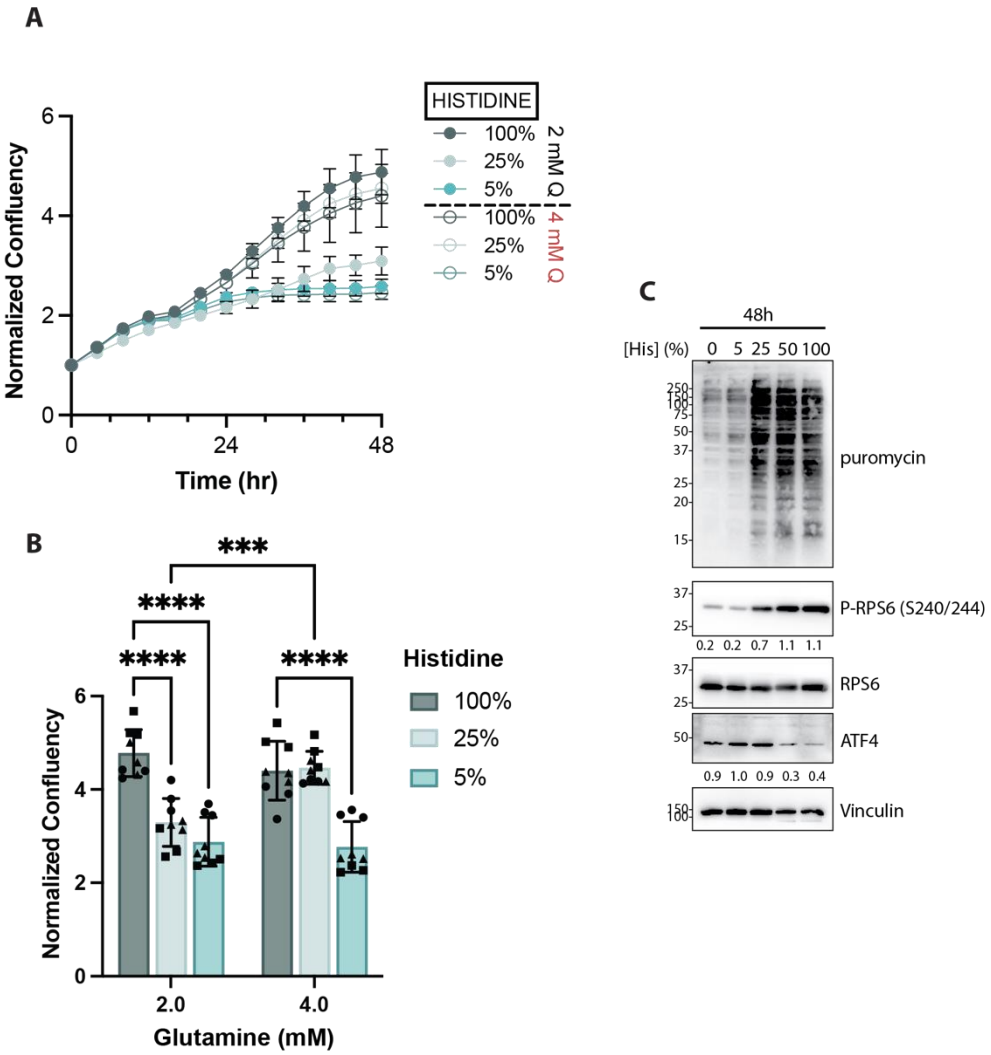



**Figure 4-10. Glutamine can rescue proliferation under histidine limitation.** **(A)** Normalized confluency of MYAZ16.1e cells cultured in 100%, 25%, or 5% histidine in the presence of 2.0 mM or 4.0 mM glutamine to starting confluency at 0hr. **(B)** Quantification of normalized confluency at 48 hours of panel A. Representative of 3 independent replicates (two-way ANOVA with Tukey correction; ***p≤0.001, ****p≤0.0001). **(C)** WB of MYAZ16.1e cells cultured in indicated levels of histidine for 48 hours. Representative of 1 replicate.

## 4.7 Myc-driven mammary gland tumours depend on exogenous glutamine for tumour growth.

To determine whether the limitation of exogenous glutamine affects the demand for histidine in Myc-driven MGTs, FVB/N mice were placed onto either a control diet (CD) or glutamine deficient diet (QDD) for six weeks (Figure 4-11A). After this, MYAZ16.1e tumour cells were orthotopically injected into the mammary fat pad (MFP; Figure 4-11A). In the end, mice were given an intravenous 5-minute bolus of

0.107 mg/gBW U-[$^{13}$C]-histidine and histidine uptake was assessed in the MGT via LC-MS (Figure 4-11A). As expected, based on *in vitro* results in Myc-driven tumour cells, mice fed a QDD had decreased tumour burden, demonstrating that exogenous glutamine is necessary for Myc-driven tumourigenesis (Figure 4-11B-D).

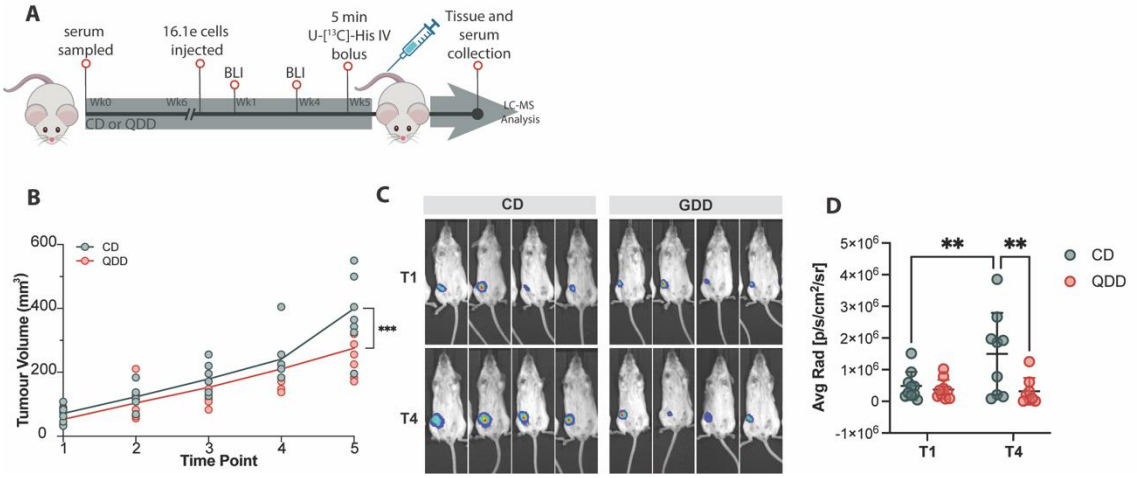



**Figure 4-11.Myc-driven MGTs rely on dietary glutamine.**
**(A)** Schematic of experimental timeline of monitoring Myc-driven tumourigenesis in mice fed a CD (control diet) or QDD (glutamine deficient diet. **(B)** Tumour volume of mice (n=9 mice per group; two-way ANOVA with Šídák correction). **(C)** Representative bioluminescence images of mice bearing luciferase-expressing MYAZ16.1e orthotopic allografts 1 (T1) and 4 (T4) weeks after tumour cell injection. **(D)** Quantification of bioluminescent signal (photons/second/cm$^2$/steradian) from panel C (n=9 mice per group). Data represent mean ± s.d. Two-way ANOVA with Tukey correction. **p≤0.01, ***p≤0.001.

Tumours and blood serum in CD and QDD mice were compared using LC-MS to assess glutamine levels and intermediates of glutamine metabolism. Paradoxically, serum glutamine levels were maintained on the QDD (Figure 4-12A). This may suggest that other tissues, such as the liver[320], might release glutamine when it is limited. This could provide the necessary exogenous glutamine stores to be utilised by the tumour. Indeed, glutamine is maintained in MYAZ16.1e tumours in mice fed a QDD (Figure 4-12B). Furthermore, tumours from mice on the QDD had increased protein expression of ASCT2, indicative of increased glutamine uptake in these tumours (Figure 4-12C, D). As reviewed in the Introduction Chapter, glutamine is deaminated by GLS1 to produce glutamate and ammonia (Figure 4-12E). Glutamate can then be fed into the Krebs cycle. To assess the impact of glutamine availability on the abundance of these intermediates, fold change was calculated by

dividing the abundance of each intermediate in tumours from mice on the CD by the corresponding abundance in the tumours from the QDD-fed mice. This approach enabled the determination of the relative increase or decrease in metabolite levels when glutamine was abundant compared to when it was withdrawn from the diet. Given that glutamine levels remain constant, it is not surprising that significant changes in the abundance of Krebs cycle intermediates were not observed in QDD compared to CD mice (Figure 4-12F). However, a slight decrease in glutamate levels was observed (Figure 4-12G). Previous work done by PhD student Amy Spicer has shown increased glucose incorporation into Krebs cycle intermediates upon glutamine starvation. Therefore, these results reflect the robust ability of tumours to compensate for glutamine deprivation through maintenance of systemic glutamine levels, upregulation of glutamine transporters, and utilisation of alternative carbon sources. However, despite this, there was insufficient glutamine to support tumour growth, suggesting glutamine may be a limiting nutrient in Myc-driven tumourigenesis.

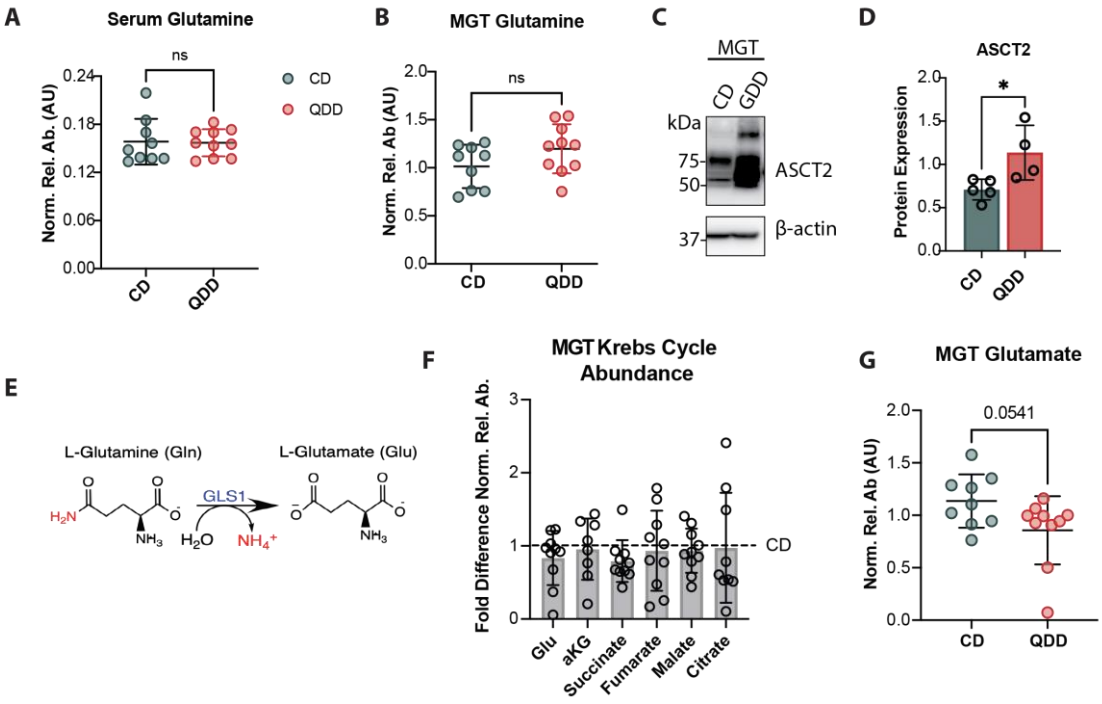



**Figure 4-12. MGTs from mice fed a QDD maintain glutamine levels and Krebs cycle intermediates.**
**(A-B)** LC-MS analysis of glutamine abundance in **(A)** serum and **(B)** MGTs of mice fed a CD and QDD (n=9 each group; unpaired two-tailed t-test). **(C)** Representative WB of ASCT2 levels in a CD and QDD MGT. **(D)** Quantification of protein levels from panel C (unpaired two-tailed t-test, CD (n=5), QDD (n=4)). **(E)** Mechanism of glutamine deamination catalysed by GLS1. **(F)** Fold-difference in the abundance of Krebs cycle intermediates in MGTs from mice on the QDD compared to the CD (two-way ANOVA with Šídák correction).**(G)** LC-MS analysis of glutamate levels (Unpaired two-tailed t-test). All data are presented as mean ±s.d. *p≤0.05.

The fractional enrichment and isotopologue abundance of histidine were quantified to determine whether histidine uptake is altered in MGTs from mice on the CD compared to QDD. The enrichment of $^{13}C$ histidine in the serum from the U-[$^{13}C$]-histidine bolus was not significantly different in mice fed the CD (83.62% ± 4.76%) compared to QDD (85.48% ± 5.55%) (Figure 4-13A). When the fractional enrichment was quantified in the MGTs, a trend towards a significant increase in U-[$^{13}C$]-histidine enrichment in tumours from mice on the QDD (78.27 ± 1.53%) compared to CD (74.80 ± 5.02%) was observed (Figure 4-13B). However, there was no difference observed in the abundance of the m+6 isotopologue of histidine in MGTs from mice fed the CD or QDD (Figure 4-13C). Together, these results suggest that although the depletion of dietary glutamine resulted in a significant reduction in tumour volume, it was not effective at reducing glutamine levels in the

tumour, therefore, histidine uptake was not affected as was observed with these tumour cells *in vitro*.

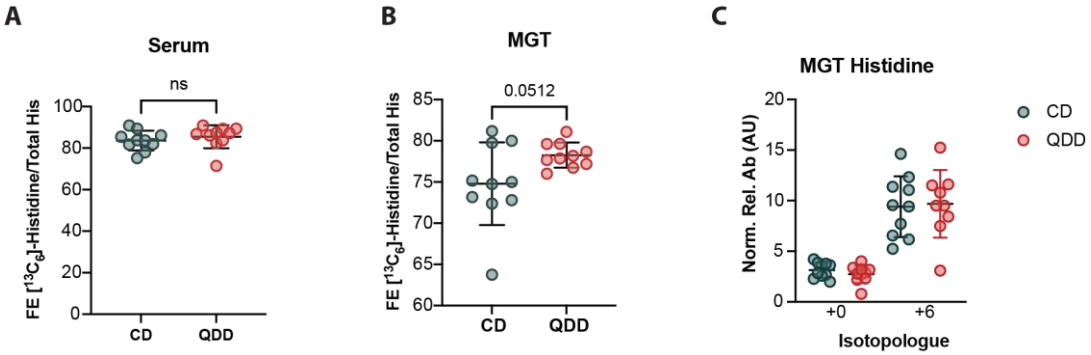



**Figure 4-13. MGTs from mice fed a QDD did not have increased histidine uptake.** LC-MS analysis of histidine in mice on a CD or QDD given a 5-minute IV bolus of 0.107 mg/gBW [U-$^{13}$C]-histidine (n=9 in each group): **(a-b)** $^{13}$C enrichment of histidine in the **(a)** serum and **(b)** MGT (Unpaired two-tailed t-test) and **(c)** abundance of m+0 and m+6 histidine isotopologues (two-way ANOVA with Šídák correction).

## 4.8 Discussion

Myc-driven cancer cells rewire cellular metabolism and heavily rely on glutamine to fuel the Krebs cycle. The results from this Chapter confirmed this phenotype in tumour cells derived from MMTV-Myc-driven MGTs. Indeed, these cells depend on high concentrations of exogenous glutamine (>1 mM) for proliferation, and the proliferative defect in the absence of glutamine could be rescued upon the addition of DMKG, which is in line with published research[97,244]. Furthermore, these data revealed that Myc-driven cell lines (MYAZ -16.1e, -6.6g, -12.3i) with an increased requirement for exogenous glutamine imported more histidine under glutamine limitation. Specifically, glutamine availability, dependence, and catabolism dictated histidine requirements. Importantly, this histidine was effluxed from the cell in Myc-driven tumour cell lines, indicating its use as a bidirectional LAT1 substrate. Furthermore, glutamine could compensate for histidine limitation independent of histidine catabolism.

Myc-driven murine tumour cell lines and Hs578t cells cultured in low glutamine had significantly increased histidine uptake compared to cells cultured in high glutamine. Previous work has suggested that histidine catabolism is required for

cytidine triphosphate synthase (CTPS) filament formation during glutamine deficiency [254]. Similar to these results, they observed increased histidine uptake in glutamine-free media. This histidine contributed to protein methylation required for CTPS filament formation, which was achieved by donating one carbon to methionine regeneration. The methionine was used to produce SAM, and the one-carbon unit was ultimately transferred from SAM to methylate proteins, such as CTPS. However, in the previous chapter, stable isotope tracing with histidine did not reveal any contribution from histidine into the methionine cycle, even when methionine was limited and histone methylation is attenuated. Instead, following histidine uptake, this histidine was found in the media. Furthermore, cells cultured in low glutamine, which imported significantly more histidine than those cultured in high glutamine, also effluxed significantly more histidine. Since glutamine is a bidirectional LAT1 substrate, an increased dependency on glutamine for Krebs cycle anaplerosis compounded with exogenous glutamine limitation could affect glutamine availability for LAT1 mediated exchange. Therefore, to maintain levels of EAAs, increased histidine uptake could compensate for glutamine by maintaining LAT1 activity. Thus, when glutamine is sparse, increasing histidine uptake could provide an advantage for tumour cells to better tolerate these adverse conditions and maintain levels of EAAs.

Glutamine is the second most rapidly consumed nutrient, after glucose, by most human cancer cell lines. However, as mentioned, the requirement for glutamine is heterogeneous across cancer cell lines. Although mammalian cells can produce glutamine from glutamate via GS activity, not all cancer cells express GS. Cancer cells that cannot synthesise glutamine depend more on exogenous glutamine to meet biosynthetic demands. In agreement with previous studies[108], in this Chapter, breast cancer cell lines that express high levels of GS are less sensitive to glutamine limitation. However, we also observed increased histidine uptake in low GS cells (Hs578t) cultured under low glutamine compared to high glutamine. In contrast, cells with high GS expression (T47D and AU565) did not increase histidine uptake under low glutamine. Furthermore, these cells were able to better maintain levels of TCA cycle intermediates compared to the low-GS cells. These results reveal a potential association between glutamine dependency and availability with histidine requirement. However, these tumours breast cancer cell

lines are derived from tumours of different subtypes and have distinct genetic signatures and phenotypic differences. To overcome some of these caveats and draw a more direct comparison, *GLUL* was overexpressed in Myc-driven tumour cell lines. However, this could not rescue proliferation or glutamine levels in cells cultured in low glutamine.

The increased import of histidine observed in cells cultured in low glutamine compared to high glutamine suggests a decreased requirement for histidine when there is sufficient exogenous glutamine. However, reducing histidine availability diminished cellular proliferation, suggesting that histidine is necessary for cellular proliferation independent of its proteinogenic role. Interestingly, this chapter revealed that increasing glutamine availability can rescue cells cultured in reduced histidine, restoring proliferation to normal levels. Histidine can contribute to glutamine pools by producing glutamate via histidine catabolism. If histidine catabolism significantly contributed to glutamate pools in Myc-driven cancer cells, then glutamine could compensate for histidine limitation through glutaminolysis. However, in the previous Chapter, using stable isotope tracing of histidine, there is no incorporation of $^{13}C$ from histidine into glutamate, even when glutamine levels were insufficient to maintain glutamate pools. Therefore, glutamine compensates for a role independent of histidine catabolism in Myc-driven tumour cells.

The role of LAT1 as a high affinity histidine transporter is well appreciated. In some tissues, such as at the BBB, histidine efflux through LAT1 is essential to maintain levels of BCAAs[321]. However, the question of how LAT1-mediated histidine exchange supports tumourigenesis has not received sufficient attention. The results in this chapter begin to unravel the metabolic basis of histidine requirement in Myc-driven and glutamine-addicted cancer cells and tumours. We reveal an association between two bidirectional LAT1 substrates, histidine and glutamine. Whereby glutamine dependency and availability determine histidine requirement. This data has alluded to a redundant role shared by glutamine and histidine. Interestingly, following the import of histidine, we observed efflux of this imported histidine shortly after, suggesting histidine may be used as an exchange substrate. The core of solid tumours has been observed to have significantly reduced glutamine levels compared to the periphery[246]. In comparison, histidine levels were

unchanged, if not slightly higher, in the core region compared to the periphery[246]. This observation suggests that glutamine availability may be a limiting factor for tumour growth, especially for tumour cells with an increased demand for glutamine catabolism, as discussed in this chapter. Conversely, histidine, due to its high affinity for LAT1 and availability within the tumour microenvironment, serves as a more reliable substrate for LAT1, thereby supporting the maintenance of essential amino acid pools necessary for tumourigenesis.

**Summary**

To summarise, this Chapter has:

1) Evaluated LAT1 gene and protein expression in Myc-driven MGTs.
2) Characterised glutamine dependency in MGTs and tumour cell lines.
3) Demonstrated elevated histidine import in glutaminolytic tumour cell lines.
4) Revealed a compensatory role for glutamine in sustaining proliferation under histidine limitation, suggesting a degree of functional redundancy between glutamine and histidine.

# Chapter 5. Histidine is the preferred LAT1 exchange factor in Myc-driven cancer cells

## 5.1 Introduction

Histidine is a high-affinity LAT1 substrate and has been shown to act as a bidirectional substrate, whereas the other EAA substrates are preferentially transported inwards. The role of histidine in mediating LAT1 function has been previously demonstrated as essential for the uptake of BCAAs across the BBB. Indeed, deletion of *Slc7a5* from the endothelial cells of the BBB resulted in elevated histidine levels in the brain and a significant reduction in leucine, isoleucine, and valine, which resulted in motor delay and autism-related phenotypes [321]. However, despite this high affinity for histidine as an exchange substrate, most research has focused on the glutamine in facilitating LAT1-mediated exchange for EAAs such as leucine [142]. In the previous chapter, we revealed an association between glutamine availability and dependency with histidine requirement. These data indicated histidine's use as an exchange substrate in glutamine-limited environments. This suggests that the tumour context in which LAT1 is expressed could play a critical role in its function. Understanding how LAT1 requirements vary across tumours expressing different oncogenes could uncover significant metabolic vulnerabilities, essential for developing effective strategies targeting LAT1.

LAT1 is overexpressed in a broad range of solid tumours, including prevalent cancers such as those of the breast[286,322], prostate[323], and lung[324–328]. In comparison, LAT1 is generally absent in normal, healthy tissue. This highlights the important role of LAT1 in tumourigenesis and underscores its potential as a specific target for cancer therapy. Indeed, deletion, knockout, or inhibition of LAT1 has successfully attenuated tumour growth in various tumour models, such as pancreatic, thyroid, and colon cancer[236,237,329–331]. However, other groups have challenged the view that LAT1 is vital to tumour growth, suggesting that due to the mechanism of LAT1-mediated amino acid uptake, this transporter acts as a 'harmoniser' rather than a 'loader'[201,247]. Therefore, cells are capable of compensating in the absence of LAT1. LAT1 functions as an amino acid

exchanger, facilitating the exchange of one amino acid for another without a net increase in the overall intracellular amino acid pool. However, this exchange allows the cell to adjust the composition of specific amino acid pools to meet metabolic and biosynthetic requirements, ensuring the most critical amino acids are available to meet cellular demands in developing tumours. LAT1 is particularly important for leucine uptake, which plays several key roles. Leucine is the most abundant amino acid in proteins[332] , given that cells cannot produce leucine *de novo*, so maintaining cellular pools of leucine is essential to maintaining unremitting cellular proliferation. This increased dependency on exogenous leucine for protein synthesis likely underlies its role as a key regulator for mTORC1 signalling, relaying information about nutrient status to initiate anabolic or catabolic responses. mTORC1 controls cellular growth in response to growth factors and amino acids. Free amino acids, such as leucine, can translocate mTORC1 to the lysosomal surface, where it is activated. Recruitment of mTORC1 to the lysosome is mediated by Rag GTPases, which are anchored to lysosomes in a nutrient-dependent manner[170]. These Rag GTPases function as heterodimers, consisting of Rag A/B paired with RagC/D. Cytoplasmic free leucine modulates Rag activation through various mechanisms [173,175,180–182]. SESTRIN1/2 are cytoplasmic leucine sensors that bind leucine when freely available in the cytoplasm[175,182]. In the absence of leucine, SESTRK 1/2 bind and inhibit GATOR2, an inhibitor of GATOR1. GATOR1 is a GTPase-activating protein (GAP) for RagA/B, resulting in an inactive state. In the inactive state, mTORC1 is not recruited to the lysosome, where it is activated by Rheb[333,334]. Therefore, mTORC1 activation requires dual activation from amino acids and growth factors. Given that leucine is a key effector of mTORC1 signalling, LAT1 is important in maintaining mTORC1 signalling. LAT1 can also be localised to the lysosome via the chaperone, LAPTM4b. LAPTM4b-mediated lysosomal localisation of LAT1 enhanced leucine uptake into lysosomes and was crucial for mTORC1 activation. Therefore, LAT1 regulates leucine levels in the cytoplasm and lysosome, two key sites for mTORC1 nutrient sensing. Therefore, LAT1 ablation and inhibition strongly inhibit mTORC1 activation *in vitro* and *in vivo*[236].

mTORC1 controls protein synthesis by phosphorylating 4E-BP1 and S6K1. In its unphosphorylated state, 4E-BP1 suppresses translation by binding and sequestering eIF4E, an essential component of the eIF4E cap-binding complex.

Phosphorylation of 4E-BP1 by mTORC1 causes it to release eIF4E, enhancing the 5' cap-dependent translation of mRNAs[335,336]. The regulation of protein translation by mTORC1 is primarily mediated through 4E-BP1, as mTOR inhibition did not impact protein translation in cells lacking 4E-BP1 and 4E-BP2[337]. In contrast, deletion of S6K1/2 in mice did not affect global protein synthesis, which remained sensitive to mTOR inhibition[338]. However, research suggests that phosphorylation of S6K1 by mTORC1 upregulates transcription of rRNA, the primary component of ribosomes, through increased activity of RNA Polymerase I (RNAPOL1) via regulation of upstream binding factor (UBF) and transcription initiation factor 1A (TIF-1A; also known as RRN3). S6K1subsequently phosphorylates RPS6, a component of the ribosomal 40S subunit[339]. The specific role of RPS6 in translation is unclear; some studies suggest RPS6 is essential for the translation of TOP mRNAs[340,341] involved in ribosome biogenesis, while others show that RPS6 deficient mice did not have impaired translation of TOP mRNAs[342]. Furthermore, substituting serine phosphorylation sites for alanine residues in Rps6 did not affect global protein translation [342]. Rather, these phosphorylation sites were determinants of cell size and substituting alanine residues resulted in a significant decrease in size. This is further supported by a study which showed that the translation of TOP mRNAs is carried out in a 4E-BP1-dependent manner [337]. This suggests that 4E-BP1 has a more prominent role in regulating global protein translation downstream of mTORC1 activation.

This chapter will first interrogate histidine's role as an amino acid exchange factor in Myc-driven tumour cell lines and in tumours *ex vivo* and *in vivo*. It will compare the requirement for histidine as a LAT1 substrate to other recognised amino acid exchange factors at physiological and supraphysiological concentrations. Furthermore, here, we assess the functional significance of histidine exchange in tumour cell lines. Molecular and biochemical approaches were employed to dissect metabolic pathways and histidine function in Myc-driven cancer cells. This was achieved by integrating techniques such as LC-MS and stable isotope tracing to garner detailed insights into histidine and interactions with other amino acids, as well as CRISPR-Cas9 mediated genetic knockout and pharmacological inhibition to assess the impact on histidine function. Using *ex vivo* and *in vivo* tumour model

systems, we aimed to evaluate the role of histidine in more representative physiological settings.

**Aims**

This chapter aims to address these aspects of my hypothesis:

1) Histidine is a bidirectional LAT1 exchange substrate.
2) Myc-dependent tumour cells preferentially utilise histidine over glutamine to uptake EAAs through LAT1.
3) Histidine is important for mTORC1 signalling in Myc-dependent cancer cells.

## 5.2 Histidine is exchange for amino acids through LAT1.

LAT1 can transport histidine bidirectionally; however, whether histidine is required for LAT1-mediated amino acid uptake in Myc-driven cancer cells is unknown. To test whether intracellular histidine is exchanged for other amino acids, MYAZ16.1e cells were cultured in amino acid-free DMEM (-AA) without or with 1.6 mM histidine (histidine preload) for 48 hours (Figure 5-1A). A control plate (Ctl) was collected before amino acid starvation to assess levels of amino acids before starvation (Figure 5-1A). The preloading concentration of histidine was determined empirically by treating cells with a range of concentration (0 – 6.4 mM) and selecting the highest concentration that did not induce significant cell death during nutrient starvation (this was only assessed visually). A final concentration of 1.6 mM was chosen, which is approximately tenfold higher than its reported physiological plasma concentration of histidine. This approach is consistent with previous studies investigating amino acid exchange substrates. For example, asparagine and glutamine have been used at concentrations of 2 mM and 10 mM, respectively, both approximately 20 times their physiological levels[142,245]. However, these studies employed significantly shorter incubation periods (1 hour); therefore, a less physiologically extreme approach was taken here to minimise cellular stress over the longer time course. This prolonged preloading period reduced experimental variability by allowing cells to reach steady-state intracellular concentrations of histidine. In addition, it can represent *in vivo*-like conditions, where the tumour core may be depleted of amino acids for prolonged periods. Therefore, in subsequent

experiments, this experimental design helped assess whether intracellular histidine accumulation was advantageous to cancer cells. Following the 48 hours of preloading, cells were either collected (-AA or -AA+H) or washed and replenished with histidine-free DMEM for 2.5 minutes (-AA/DMEM or -AA+H/DMEM) and the cells and media were collected and flash frozen in liquid nitrogen before metabolite extraction and LC-MS analysis (Figure 5-1A).

We first quantified the abundance of histidine intracellularly in these samples. As expected, histidine preloading (-AA+H) significantly increased cellular histidine pools compared to starved cells (-AA) (Figure 5-1B). Notably, upon replenishment with DMEM, intracellular histidine levels significantly decreased in histidine-preloaded cells (Figure 5-1B). This could suggest that upon nutrient availability, cells immediately utilise histidine for protein synthesis. Alternatively, it could be indicative of histidine efflux. To assess whether this is the case, cells and media were collected at regular intervals up to 30 minutes following amino acid replenishment. Intracellular histidine levels were compared to the abundance of histidine before DMEM replenishment (0 min), and the extracellular levels of histidine in the media were compared to the histidine-free DMEM that was used to replenish amino acid levels in cells. Supporting the hypothesis that histidine is used for exchange, the intracellular levels of histidine were depleted after 30 minutes of replenishment; in contrast, the levels of histidine in the media cumulatively increased over this time (Figure 5-1C). To assess if histidine exchange for other amino acids is a general tumour cell phenomenon, we also evaluated intracellular histidine levels following preincubation with 1.6 mM of histidine during amino acid starvation in TNBC cell lines, BT-549 and MDA MB 231. We observed a significant decrease in intracellular histidine levels upon reintroduction of amino acids in BT-549 cells but not MDA MB 231 cells (Figure 5-1D). This indicates that different cellular contexts mediate the requirement for histidine in amino acid exchange, as we expect. Overall, intracellular histidine is effluxed from the cell upon nutrient availability in MYAZ16.1e mammary tumour cells and BT-549 tumour and breast cancer cell lines, which indicates its role as an amino acid exchange factor.

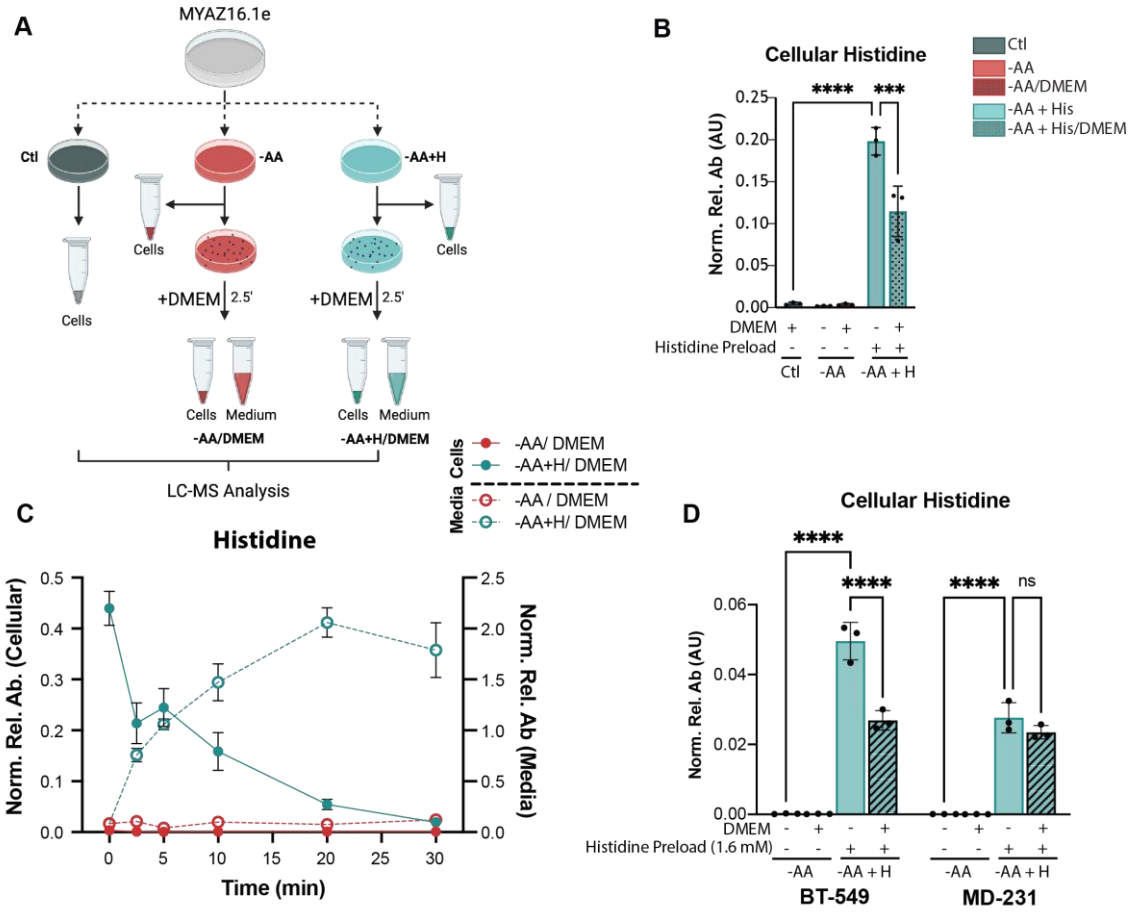



**Figure 5-1.Histidine is effluxed from the cell in Myc-dependent tumour cells.** **(A)** Schematic of experimental strategy for histidine preload in the absence of amino acids. Cells were starved of amino acids in the presence or absence of 1.6 mM histidine for 48 hours and replenished with DMEM for 2.5 minutes. **(B-D)** LC-MS analysis: **(B)** total abundance of intracellular histidine, **(C)** total abundance of histidine in the cell (left y-axis) and media (right y-axis) over 30 minutes of DMEM replenishment. Time 0' represents starved cells after 48 hours of histidine preload or starvation. **(D)** total abundance of intracellular histidine in amino acid starved or histidine preloaded TNBC cell lines, BT-549 and MDA-MB-231 (MD-231). All data are presented as mean ±s.d., and represent 1 replicate. Two-way ANOVA with Šídák correction. ***p≤0.001, ****p≤0.0001.

SLC transporters mediate the uptake of amino acids, with each transporter having varied substrate affinities. Therefore, we quantified the levels of amino acids present in DMEM to determine whether the uptake of specific amino acids was enhanced under histidine-preloaded conditions. MYAZ16.1e cells, along with TNBC cell lines, BT-549 and MDA MB 231, were cultured in amino acid-depleted DMEM with or without histidine preload and then replenished with amino acid-repleted

DMEM as described above. The net uptake of each amino acid was calculated by deducting the abundance after replenishment (-AA/DMEM or -AA+H/DMEM) from the abundance before replenishment (-AA or -AA+H). A positive value indicates amino acid influx, whereas a negative value indicates a net efflux from the cell. In MYAZ16.1e cells, intracellular levels of specific amino acids increased after 2.5 minutes of DMEM replenishment. Significant increases in EAAs such as leucine, isoleucine, methionine, phenylalanine, tryptophan and lysine were observed in histidine-preloaded cells (Figure 5-2A). An insignificant increase in valine was observed in histidine-preloaded cells (Figure 5-2A). In contrast, there was no effect on threonine uptake in histidine-preloaded cells (Figure 5-2A). The intracellular levels of NEAAs found in DMEM were also quantified; here, we observed increased uptake of tyrosine and arginine in histidine-preloaded cells (Figure 5-2B). While asparagine and proline are not observed in DMEM, the levels of these amino acids increased or were maintained following starvation in amino acid-starved cells. Interestingly, upon nutrient availability, the intracellular abundance of these metabolites is decreased, which could indicate amino acid exchange utilising asparagine or proline when histidine is unavailable (Figure 5-2B). In support of the previous chapter, histidine-preloaded cells have less glutamine uptake than starved cells (Figure 5-2B).

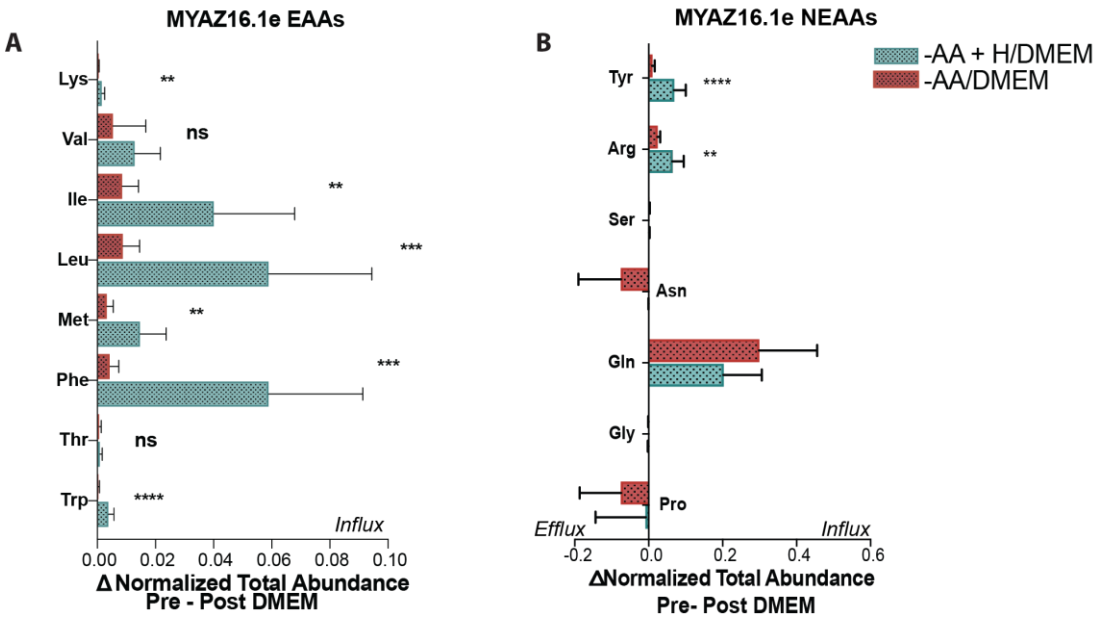



**Figure 5-2. Histidine preloaded cells have increased uptake of specific amino acids.**
LC-MS analysis of cells starved of amino acids or preloaded with 1.6 mM histidine and replenished with DMEM for 2.5 minutes. The x-axis represents the difference between the abundance of indicated amino acids after replenishment and before replenishment. A net positive value is indicative of influx and a net negative value is indicative of efflux. Change in intracellular abundance of **(A)** essential amino acids and **(B)** non-essential amino acids. Data are presented as mean ±s.d. representing 3 independent replicates. Multiple unpaired t-tests with Holm-Šídak correction. **p≤0.01, ***p≤0.001, ****p≤0.0001.

Similar results were observed in BT-549 and MDA MB 231 cells; however, differences in SLC transporter expression may dictate the uptake of specific amino acids across these cell lines. For example, the import of cationic amino acids, lysine and arginine, are not significantly increased in BT-549 cells under histidine preloaded conditions, whereas only arginine is observed in MDA MB 231 cells (Figure 5-3). Furthermore, methionine uptake is not significantly increased in BT-549 or MDA MB 231 cells (Figure 5-3A, C). Notably, in these TNBC cell lines, the uptake of certain NEAAs showed an opposite trend to EAAs. Indeed, serine and glutamine influx were increased in BT-549 and MDA MB 231 cells starved of amino acids compared to histidine-preloaded cells (Figure 5-3B, D). Furthermore, asparagine efflux in starved cells is significantly increased compared to preloaded cells (Figure 5-3B, D). Importantly, threonine levels do not increase significantly in cells preloaded with histidine in all cell lines tested. Indeed, the opposite trend is

observed in BT-549 cells, with a significant influx of threonine in starved cells (Figure 5-3A). Threonine is the only EAA that LAT1 does not transport; therefore, given that threonine import is not increased in histidine-preloaded cells, this indicates histidine is exchanged through LAT1. Increased uptake of LAT1 substrates in histidine preloaded MDA MB 231 cells was surprising, considering the lack of histidine efflux observed in these cells. Further experiments will be necessary to interrogate histidine exchange in these cells. Overall, these results suggest that histidine is used as an exchange substrate for a specific subset of EAAs, which is dependent on the cell line but appears to consistently include leucine, isoleucine, methionine, phenylalanine, tryptophan, and tyrosine.

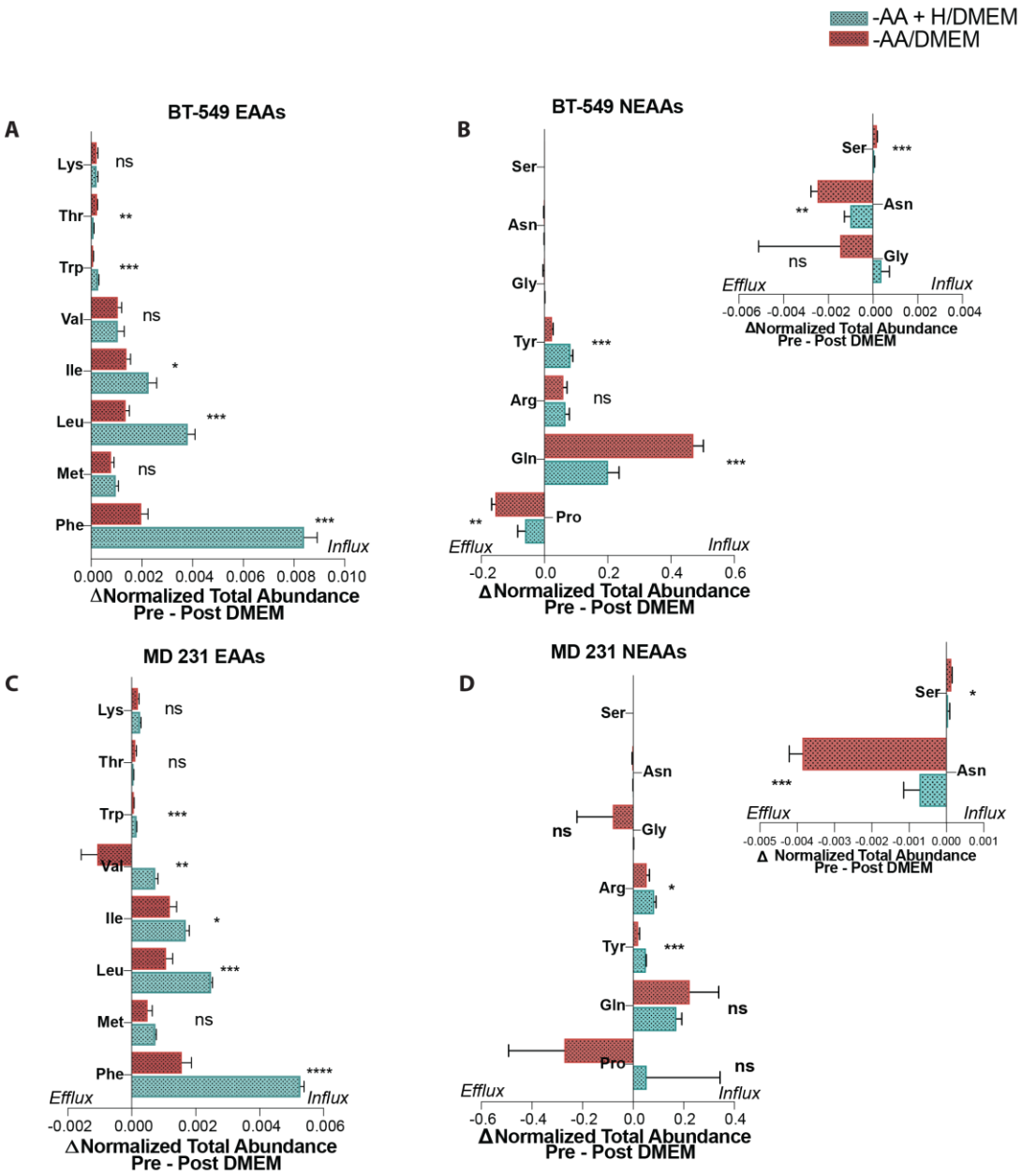



**Figure 5-3.Histidine preload increases uptake of specific amino acids in TNBC cells.**

LC-MS analysis of TNBC cells starved of amino acids or preloaded with 1.6 mM histidine for 48 hours and replenished with DMEM for 2.5 minutes. The x-axis depicts the difference in a bundance of indicated amino acids after replenishment and before replenishment. A net positive value indicates influx, and a net negative value indicates efflux. Change in intracellular abundance of **(A, C)** EAAs and **(B, D)** NEAAs are shown. Data are presented as mean ±s.d. representing 3 independent replicates. Multiple unpaired t-tests with Holm-Šídak correction. *p≤0.05, **p≤0.01, ***p≤0.001, ****p≤0.0001.

LAT1 is strongly stereoselective for L-histidine, although this level of stereoselectivity does not apply to all LAT1 substrates[226]. For example, D-isomers of leucine, phenylalanine, and methionine were able to competitively bind to LAT1 binding sites and inhibit uptake of L-leucine[226]. However, this level of stereoselectivity is not a universal feature among all SLC7 family members. For example, Asc1/CD98hc (SLC7A10), is capable of efficiently transporting both D- and L-serine[343]. LAT1's more restricted stereoselectivity provides a useful tool for experimental validation, therefore, we used D-histidine to confirm whether LAT1 mediates histidine efflux. BT-549 cells were cultured in amino acid-free DMEM(-AA) in the presence or absence of 1.6 mM of D-histidine or L-histidine for 48 hours before nutrient replenishment with histidine-free DMEM for 2.5 minutes. Cells could accumulate D-histidine and L-histidine; however, significantly decreased intracellular histidine was observed in cells cultured with D-histidine compared to L-histidine (Figure 5-4A). As was observed previously, intracellular levels of histidine are significantly reduced upon amino acid replenishment in L-histidine preloaded cells. In contrast, intracellular levels of histidine are unchanged upon nutrient replenishment in D-histidine preloaded cells (Figure 5-4A). Coincidentally, intracellular leucine uptake is not significantly increased in D-histidine preloaded cells compared to starved cells upon amino acid replenishment (Figure 5-4B). In contrast, as seen before, leucine levels were significantly increased in L-histidine preloaded cells (Figure 5-4B). The net intracellular levels of amino acids were compared across each condition, and uptake of phenylalanine, leucine, isoleucine, and tyrosine were significantly higher in L-histidine preloaded cells compared to D-histidine preloaded cells (Figure 5-4C). Furthermore, significant differences between amino acid starved and D-histidine preloaded cells were only observed for glutamine and phenylalanine (Figure 5-4C). Together, these results suggest that histidine exchange for EAAs is mediated through LAT1.

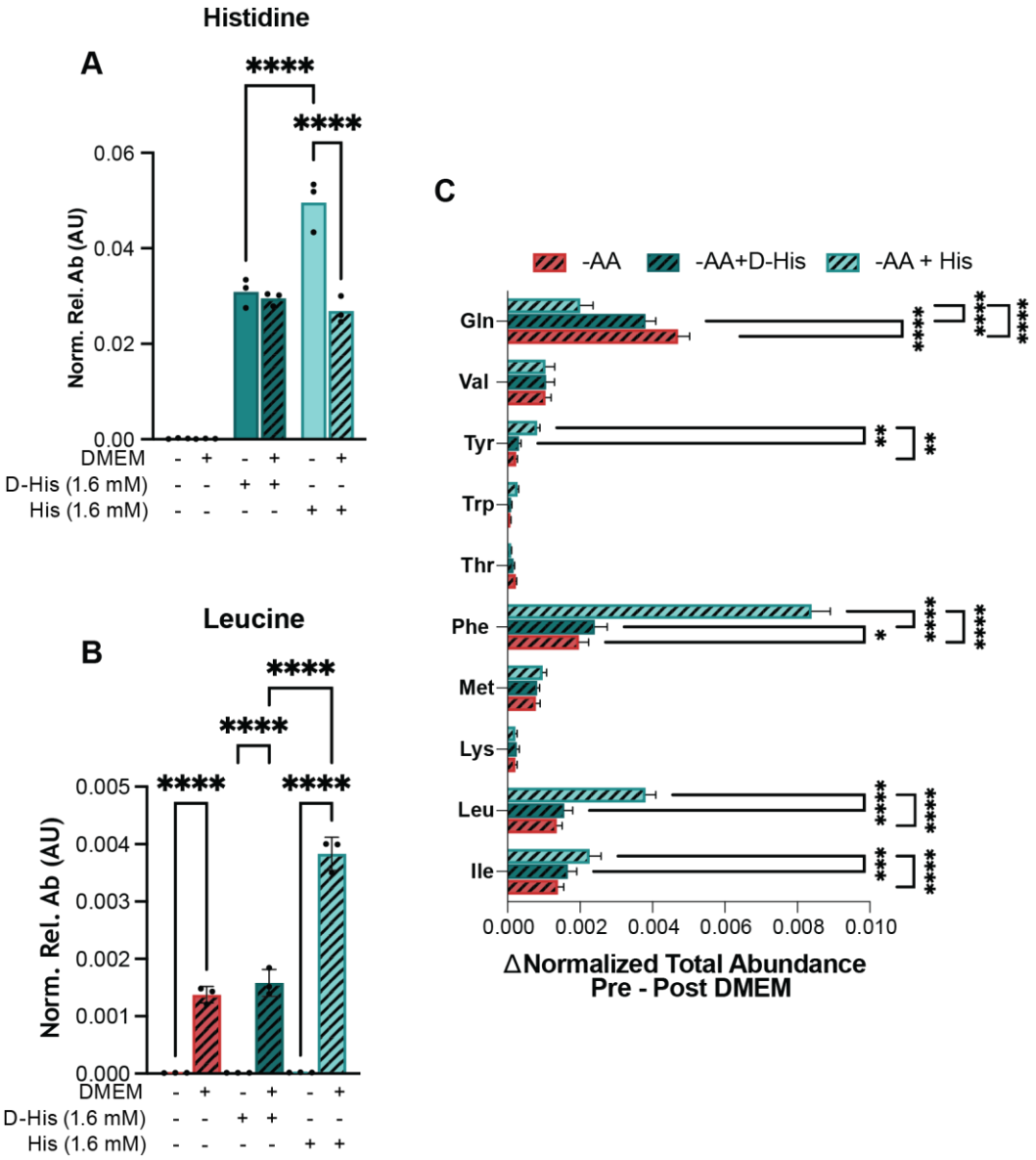



**Figure 5-4. Histidine exchange is mediated through a stereoselective transporter.** LC-MS analysis of MYAZ16.1e cells starved of amino acids or preloaded with 1.6 mM of D-Histidine or L-Histidine for 48 hours and replenished with DMEM for 2.5 minutes. Total intracellular abundance of **(A)** histidine and **(B)** leucine. **(C)** The relative influx of indicated amino acids. The x axis represents the net uptake calculated as the difference in total abundance after replenishment and before replenishment. All data are presented as mean ±s.d.; representative of 1 replicate. Two-way ANOVA with Tukey correction. **p≤0.01, ***p≤0.001, ****p≤0.0001.

To confirm LAT1-mediated histidine exchanges, CRISPR-Cas9 mediated knockout of *SLC7A5* was employed. To avoid any compensatory mechanisms resulting from LAT1 KO, BT-549 cells were transduced with two distinct vectors: (1) a constitutive expression vector for the Cas9 endonuclease linked to the mCherry fluorescent marker protein and (2) a doxycycline (dox)-inducible vector containing an *SLC7A5*

sgRNA cassette. This second vector is controlled by a ubiquitin promoter and regulated by a tetracycline repressor with the GFP protein for fluorescent tracking. Double-positive cells were selected via flow cytometry, and a mixed clone culture was used for these experiments. LAT1 protein expression was assessed in BT-549 sg*SLC7A5* cells upon adding doxycycline. LAT1 protein expression was observed in vehicle but not doxycycline-treated cells (Figure 5-5A). Therefore, these cells were used in histidine preloading experiments. Cells were cultured for 48 hours in the presence of 1 µg/mL doxycycline before the medium was changed to amino acid free DMEM with or without histidine as described above. Representative samples were collected to confirm LAT1 knockout before metabolite extraction and LC-MS analysis. Notably, this system became slightly leaky as the cell lines were passaged. Indeed, BT-549 cells expressing the dox-inducible sgSLC7A5 vector have decreased LAT1 expression compared to BT-549 cells expressing an empty sgRNA cassette without doxycycline (Figure 5-5B). However, the addition of doxycycline did ablate LAT1 protein expression (Figure 5-5B). Therefore, we compared intracellular histidine levels in the vehicle (dox-off) and doxycycline (dox-on) treated BT-549 sgSLC7A5 cells. Compared to dox-off cells, dox-on cells had significantly reduced histidine levels in histidine-preloaded cells (Figure 5-5C). Notably, while dox-off cells significantly reduced intracellular histidine levels upon amino acid replenishment, this was not observed in dox-on cells (Figure 5-5C). Therefore, intracellular histidine pools are partially maintained by LAT1, as was indicated in D-histidine preloading experiments. Furthermore, histidine efflux depends on LAT1 activity. Consistently, while leucine levels were significantly increased in dox-off cells in histidine-preloaded cells compared to starved cells upon nutrient replenishment, this was not observed in dox-on cells (Figure 5-5D). When comparing the net abundance of amino acids in dox-on and dox-off cells, significant changes are observed in high-affinity LAT1 substrates such as leucine, isoleucine, phenylalanine, and tyrosine (Figure 5-5E). Furthermore, upon LAT1 knockout, starved cells had significantly increased glutamine uptake compared to histidine-preloaded and dox-off cells (Figure 5-5E). Together, these results confirm that LAT1 mediates histidine amino acid exchange.

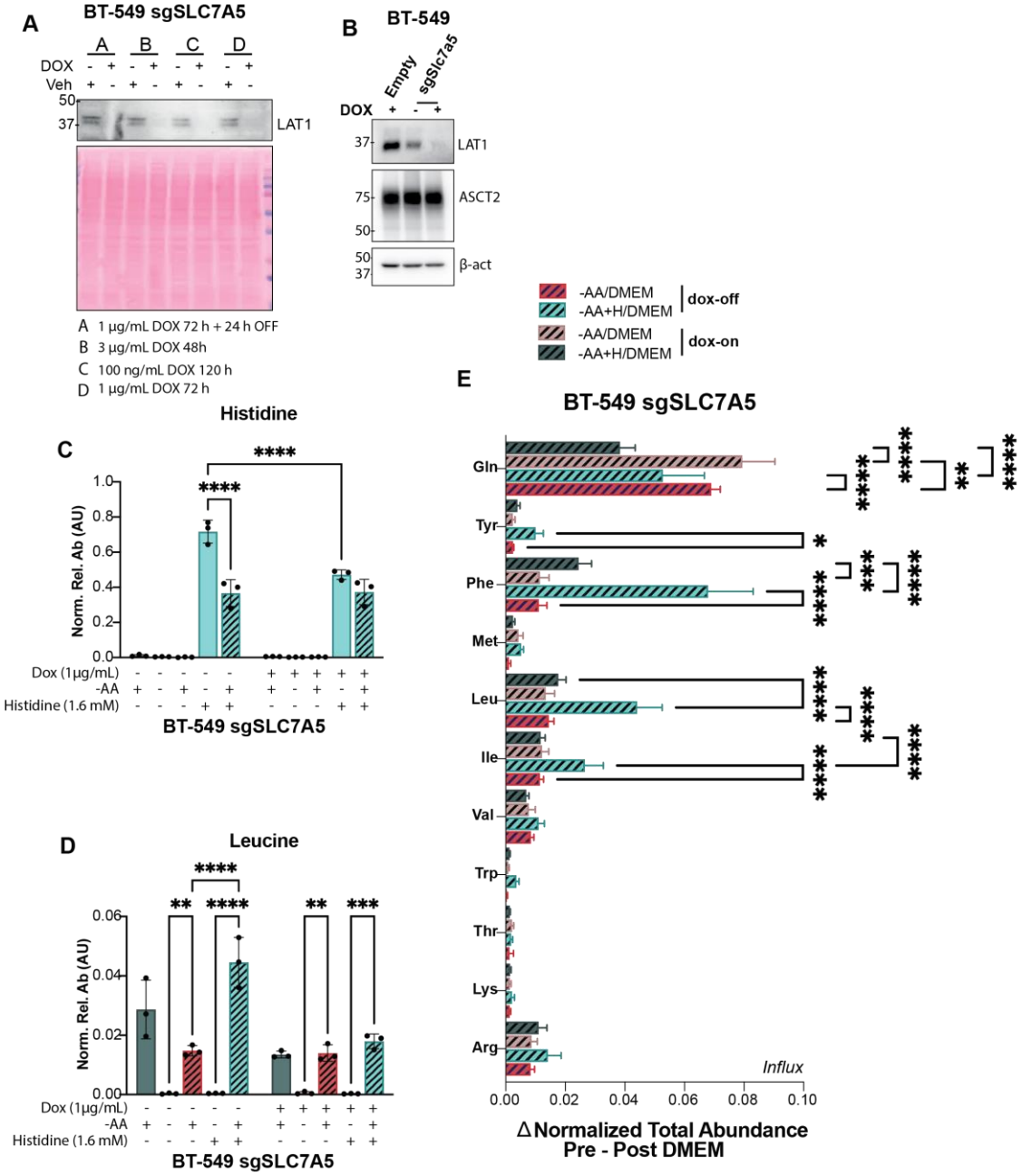



**Figure 5-5. Histidine is a bidirectional LAT1 substrate that facilitates uptake of EAAs.**
BT-549 cells with doxycycline-inducible KO of LAT1 were generated. **(A)** WB of LAT1 expression in BT-549 sgSLC7A5 cells subjected to different doxycycline conditions. **(B)** WB of LAT1 expression in cells used in panels C-E treated without or with 1 µg/mL doxycycline. **(C-E)** LC-MS analysis of BT-549 sgSLC7A5 cells subjected to 1 µg/mL doxycycline for 48 hours (dox-on) or vehicle (dox-off) before amino acid starvation or preload with 1.6 mM histidine for 48 hours and replenished with DMEM for 2.5 minutes. Total abundance of **(C)** histidine and **(D)** leucine. **(E)** The relative influx of indicated amino acids. The x-axis represents the net uptake calculated as the difference in total abundance after replenishment and before replenishment. All data are presented as mean ±s.d.; representative of 1 replicate. Two-way ANOVA with Tukey correction. *p≤0.05, **p≤0.01, ***p≤0.001, ****p≤0.0001.

Next, we employed a pharmacological approach using the LAT1 inhibitor, JPH203, to confirm the role of LAT1 in histidine-mediated exchange in MYAZ16.1e cells. Using the same histidine preloading experimental design described above, starved and preloaded MYAZ16.1e cells were replenished with histidine-free DMEM in the presence or absence of JPH203 or GPNA for 2.5 minutes. Cells and media were subsequently flash-frozen before metabolite extraction and LC-MS analysis. Given that LAT1-mediated amino acid exchange was previously described as a couple to ASCT2 activity, we utilised GPNA, an ASCT2 inhibitor, to compare the effect on LAT1 activity. However, GPNA is not a very selective ASCT2 inhibitor, and recent studies have demonstrated the ability of GPNA to inhibit members of the SNAT family (SNAT1,-2,-4,-5) and LAT family (LAT1/2) of transporters[153]. Therefore, the changes observed here upon GPNA inhibition may not wholly reflect the role of ASCT2. The results suggest that ASCT2 and LAT1 activity are not coupled in Myc-driven cancer cells. Histidine levels were first quantified intracellularly; here, we observed the expected increase in intracellular histidine levels in preloaded cells with a significant reduction in these levels upon amino acid replenishment in DMSO and GPNA-treated cells (Figure 5-6A). In contrast, we did not observe a significant decrease in histidine levels upon amino acid replenishment in JPH203-treated cells (Figure 5-6A). Consequently, while media levels of histidine are increased in DMSO and GPNA-treated cells, JPH203 treatment significantly reduces levels of histidine in the media following amino acid replenishment (Figure 5-6B). Therefore, histidine efflux appears primarily mediated through LAT1 in Myc-driven tumour cells, consistent with our observations in BT-549 cells. The abundance of amino acids was quantified across these conditions to assess the effect on amino acid uptake. As seen previously, histidine-preloaded cells had increased uptake of lysine, isoleucine, leucine, methionine, phenylalanine, tryptophan, tyrosine, and arginine upon amino acid replenishment compared to starved cells (Figure 5-6C). On the other hand, starved cells had increased uptake of threonine and glutamine compared to histidine-preloaded cells (Figure 5-6C). Furthermore, starved cells had increased levels of asparagine, which were subsequently reduced upon amino acid replenishment (Figure 5-6C). When starved or preloaded cells are replenished with amino acids in the presence of GPNA, decreased glutamine uptake is observed, indicative of successful ASCT2 inhibition (Figure 5-6C). Decreased threonine uptake is also observed upon GPNA inhibition (Figure 5-6C). Threonine can be

transported by ASCT2 or SNAT1, which GPNA could inhibit. Furthermore, GPNA exposure partially inhibits the decrease in asparagine levels upon amino acid replenishment (Figure 5-6C). Suggesting asparagine may be the bidirectional substrate that helps mediate the uptake of ASCT2 substrates, such as glutamine and threonine, during starvation. Therefore, these results indicate that uptake through these transporters may be more active without histidine availability. In comparison, the uptake of LAT1 substrates was slightly decreased under exposure to GPNA in histidine-preloaded cells (Figure 5-6C). However, this could be due to the off-target effects of GPNA on LAT1 or LAT2[344]. In contrast, inhibition of LAT1 using JPH203 strongly inhibited the uptake of tyrosine and EAAs, excluding threonine in amino acid-replenished histidine-preloaded cells (Figure 5-6C, Appendix 3). In MYAZ16.1e cells, histidine preloading significantly increased the uptake of cationic amino acids, lysine and arginine, which was not blocked by JPH203 (Figure 5-6C, Appendix 3). Therefore, histidine may be used as an exchange substrate for other transporters. For example, *Slc7a6* (encoding **γ**LAT2) has an affinity towards lysine and arginine and was positively correlated with Myc-driven tumourigenesis and mRNA expression was increased in Myc-driven MGTs compared to ErbB2-driven MGTs (Figure 3-1A, B). These data highlight histidine as a bidirectional LAT1 substrate in Myc-driven tumour cells and TNBC cell lines. Histidine accumulation primes cells for increased uptake of EAAs and other context-dependent substrates that may depend on the cellular expression of different amino acid transporters, such as **γ**LAT2. This increased EAA uptake in cells that can accumulate high levels of intracellular histidine could facilitate cell survival in nutrient adverse environments.

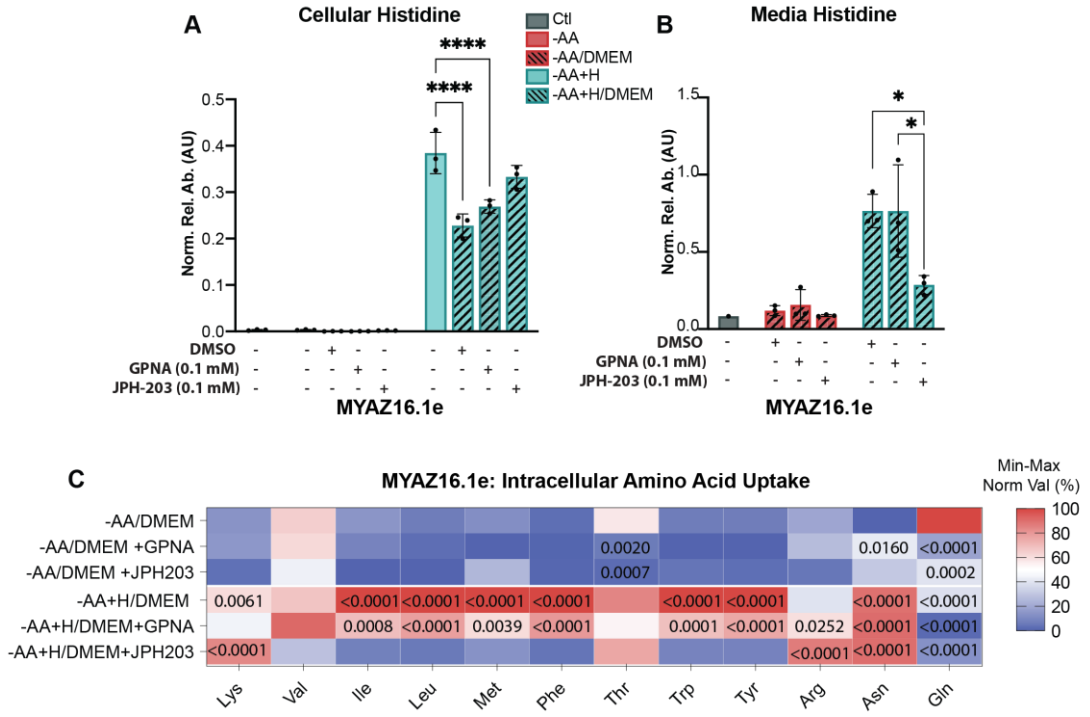



**Figure 5-6. Histidine exchange can be blocked by pharmacological inhibition of LAT1.**
LC-MS analysis of MYAZ16.1e cells amino acid starved or preloaded with 1.6 mM histidine for 48 hours and replenished with DMEM in the presence of indicated inhibitors for 2.5 minutes. Total abundance of **(A)** intracellular and **(B)** extracellular histidine. Data are presented as mean ± s.d. One-way ANOVA with Tukey correction, representative of 1 independent replicate. *p≤0.05, ****p≤0.0001. **(C)** Heatmap of intracellular amino acid abundance in cells preloaded with 1.6 mM His and replenished ± inhibitors (2.5 min), normalized to the maximum per amino acid, with *p*-values displayed relative to the -AA/DMEM condition.

## 5.3 Histidine is the preferred LAT1 exchange substrate in Myc-driven tumour cells.

LAT1-mediated amino acid exchange is dependent on substrate affinity and availability. The concentration of histidine used in the preloading experiments above was supraphysiological. Therefore, the utilisation of histidine as a LAT1 amino acid exchange substrate was compared to established amino acid exchangers, asparagine and glutamine, at a range of concentrations from 50 µM to 1 mM. Cells were starved of amino acids and preloaded with either histidine, asparagine, or glutamine at the indicated concentrations for 48 hours. After this, media was replenished with histidine, asparagine, or glutamine-free DMEM for 2.5 minutes, and cells were collected for metabolite extraction and LC-MS analysis.

Leucine uptake was significantly increased in histidine-preloaded cells with as little as 200 μM preloading and increased in a concentration-dependent manner (Figure 5-7A). In contrast, asparagine preloading up to 1 mM did not increase leucine uptake despite being significantly above physiological levels of asparagine in plasma from healthy adults (Figure 5-7A). Glutamine preloading at 1 mM resulted in a significant leucine uptake compared to starved cells. However, leucine uptake under these conditions was significantly less than in histidine-preloaded cells (Figure 5-7A). Similar trends were observed for other LAT1 substrates, such as phenylalanine, tryptophan, tyrosine, methionine, and isoleucine. In comparison, cells with glutamine and asparagine preload had increased uptake of threonine and serine compared to histidine-preloaded cells (Appendix 4).

We next assessed whether the uptake of these amino acids was mediated through Lat1. Therefore, cells were preloaded with 1 mM of histidine, asparagine, or glutamine and amino acids were subsequently replenished with or without JPH203. Intracellular amino acid levels were quantified across these conditions and normalized to the levels of the respective amino acid in starved cells (Figure 5-7B). Therefore, a fold change of >1 indicates increased uptake, whereas a fold change of <1 indicates reduced uptake. Interestingly, JPH203 treatment in DMEM replenished starved cells only significantly impacted histidine uptake (Figure 5-7B). In contrast, the uptake of other Lat1 substrates was not markedly reduced. This suggests that under starvation conditions, Lat1 is essential for histidine uptake. Comparing levels of amino acids in histidine-, asparagine-, or glutamine-preloaded cells replenished with DMEM, it is evident that histidine preload results in significantly increased levels of LAT1 substrates, particularly leucine, phenylalanine, tryptophan, and tyrosine (Figure 5-7B, Appendix 5). Furthermore, when histidine preloaded cells are replenished in the presence of JPH203, the uptake of these metabolites is significantly attenuated (Figure 5-7B, Appendix 5). In comparison, asparagine-preloaded cells do not appear to depend on Lat1 to transport amino acids, as the uptake of amino acids in asparagine preloaded cells are not reduced in the presence of JPH203 (Figure 5-7B, Appendix 5). Glutamine does appear to be exchanged for some amino acid substrates via Lat1, such as leucine, isoleucine, phenylalanine, tryptophan, and tyrosine (Figure 5-7B, Appendix 5). However, glutamine does not appear to be as efficient of a LAT1 exchange

substrate as histidine despite being available in the media at the same concentration, as indicated by the reduced abundance of Lat1 substrates in glutamine preloaded cells compared to histidine preloaded cells (Figure 5-7B, Appendix 5).

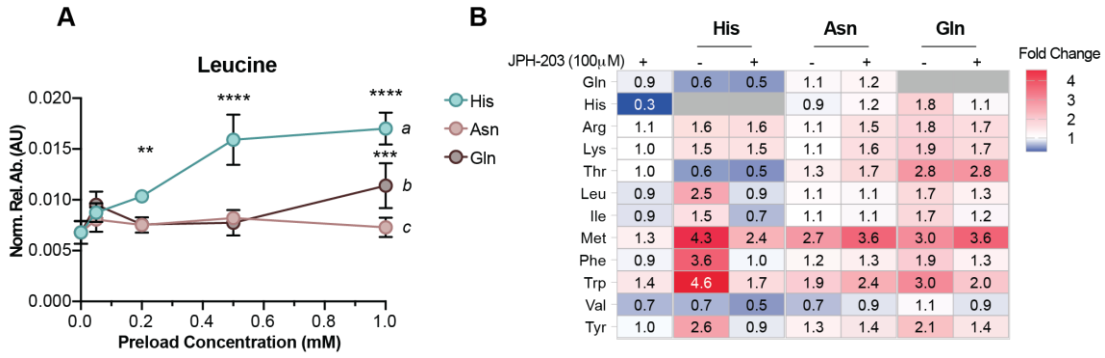



**Figure 5-7. Histidine is a more efficient LAT1 substrate than glutamine.** LC-MS analysis of intracellular amino acid levels. MYAZ16.1e cells were amino acid starved or preloaded with indicated concentrations of asparagine, glutamine, or histidine for 48 hours and subsequently replenished with DMEM for 2.5 minutes. **(A)** Total abundance of intracellular leucine, the 0.0 mM condition depicts amino acid starved cells replenished with DMEM. Data is presented as mean ± s.d. and is representative of 2 independent replicates. Stars denote statistical significance compared to amino acid starved cells (two-way ANOVA with Tukey correction) and letters denote statistical significance comparing preload conditions (two-way ANOVA with Dunnett correction: a vs. b ($p \leq 0.0001$), a vs. c ($p \leq 0.0001$), b vs. c ($p = 0.0014$). **(B)** Heatmap showing intracellular abundance of indicated amino acids in MYAZ16.1e cells starved or preloaded with 1.0 mM of histidine, asparagine, or glutamine, and replenished with DMEM with vehicle (0.1% DMSO) or JPH203 for 2.5 minutes. Colour scale represents mean fold change in abundance following replenishment relative to amino acid starved cells (=1). Values >1 indicate increased uptake and <1 indicate decreased uptake relative to starved cells.

Considering that glutamine preload could not facilitate the uptake of Lat1 substrates to the extent of histidine preload even when available at the same concentration, we hypothesised that this was due to its metabolic requirement. As demonstrated in previous chapters, histidine is a metabolic dead-end in these Myc-driven tumour cell lines, whereas glutamine catabolism is required to fuel the Krebs cycle. Therefore, we assessed the incorporation of glutamine into Krebs cycle intermediates in amino acid starved cells preloaded with glutamine at concentrations from 50 μM to 1 mM. Interestingly, even during amino acid starvation, cells utilise glutamine for anaplerosis in the Krebs cycle (Figure 5-8A). However, glutamine levels are significantly lower when preloaded in media containing 500 μM of glutamine and depleted when ≤200 μM (Figure 5-8A).

Coincidentally, pools of Krebs cycle intermediates are reduced, as observed previously. This agrees with previous data showing a proliferative defect in cells cultured in media containing ≤500 μM of glutamine (Figure 4-2A, B).

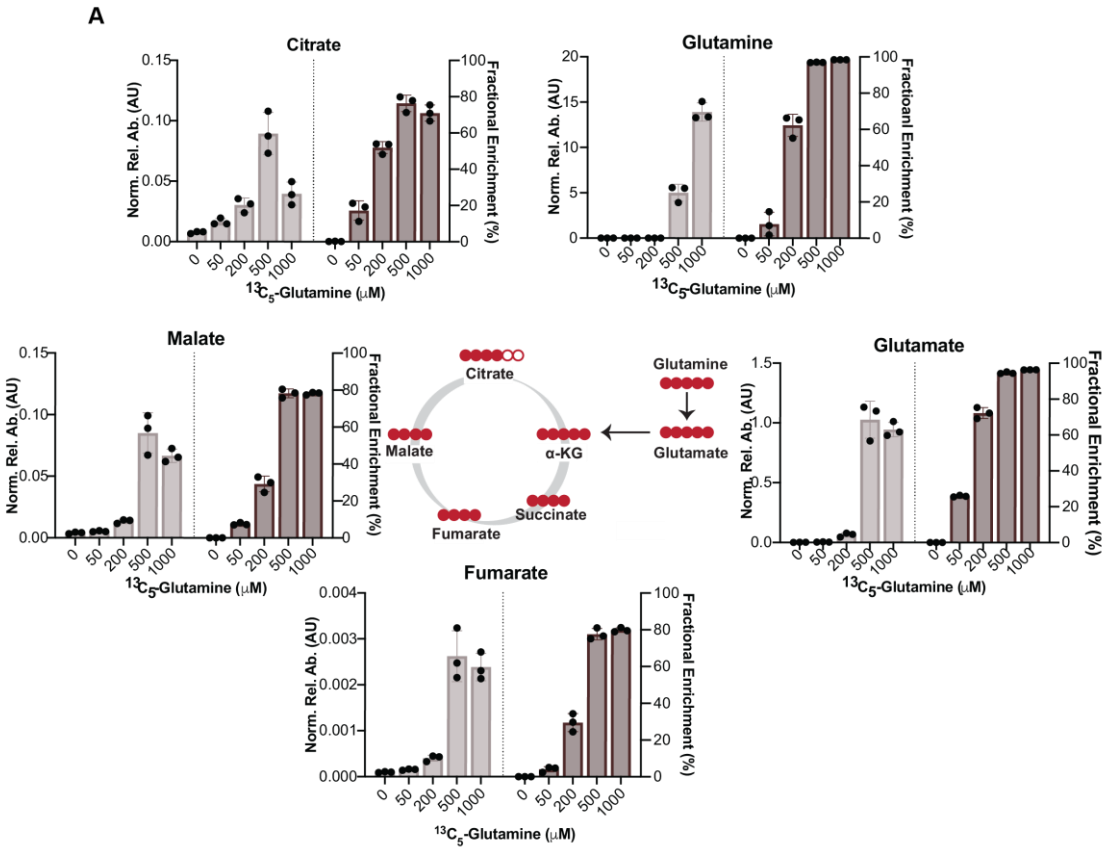



**Figure 5-8. Glutamine is used to fuel the Krebs cycle even during amino acid starvation.**
**(A)** LC-MS analysis of Krebs cycle intermediates in cells starved of amino acids and preloaded with indicated concentrations of [U-$^{13}$C]-glutamine for 48 hours. Total abundance (left Y-axis) and $^{13}$C enrichment (right Y-axis). Data are presented as mean ±s.d.; representative of 1 replicate.

In addition to Krebs cycle intermediates, glutamate is crucial for the biosynthesis of NEAAs such as proline, alanine, aspartate and serine. Indeed, glutamine contributes to the biosynthesis of these NEAAs through glutamate (Figure 1-4). Glutamine is also a direct nitrogen source for asparagine biosynthesis. Indeed, we observed a concentration-dependent increase in proline, alanine, aspartate, and asparagine levels in glutamine-preloaded cells (Figure 5-9). Increased serine levels

were also increased in glutamine preloaded cells in a concentration-dependent manner, but serine is available in DMEM (Appendix 4H). Therefore, we cannot disentangle serine production from serine uptake in glutamine preloaded cells. In summary, histidine is a more efficient bidirectional LAT1 substrate, leading to significantly increased uptake of EAAs. In contrast, glutamine is preferentially catabolised, which reduces the ability to facilitate EAA uptake when exogenous concentrations are ≤500 µM.

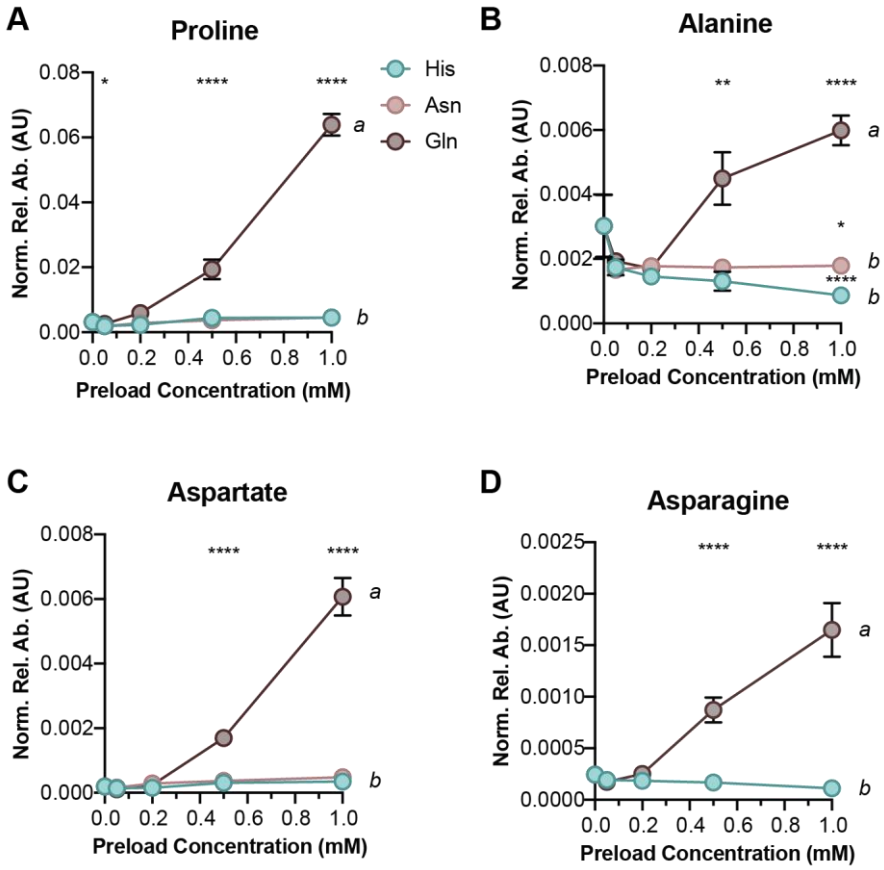



**Figure 5-9. Glutamine is used for NEAA biosynthesis during amino acid starvation.** **(A-D)** LC-MS analysis of NEAAs in MYAZ16.1e cells starved of amino acids and preloaded with indicated concentrations of glutamine for 48 hours and replenished with DMEM for 2.5 minutes. Total abundance of **(A)** proline, **(B)** alanine, **(C)** aspartate, and **(D)** asparagine. The 0.0 mM condition depicts amino acid-starved cells replenished with DMEM. Data is presented as mean ± s.d. and is representative of 2 independent replicates. Stars denote statistical significance compared to amino acid starved cells (two-way ANOVA with Tukey correction) and letters denote statistical significance comparing preload conditions (two-way ANOVA with Dunnett correction: a vs. b ($p<0.0001$))

The concentration of glutamine is higher than that of histidine in the serum of healthy adults. Indeed, glutamine concentrations range from 390 to 650 μM compared to 26 to 120 μM of histidine. Therefore, the preferred bidirectional LAT1 substrate could vary under physiological concentrations. Furthermore, the availability of these amino acids could differ in the serum compared to the tumour microenvironment. Therefore, we evaluated absolute concentrations of histidine and glutamine in the serum, tumour interstitial fluid (TIF), MGT, and livers of orthotopic allografts of MYAZ16.1e. Standard curves for histidine and glutamine were generated by running a series of standards of [U-$^{13}$C]-glutamine and [U-$^{13}$C]-histidine ranging from 7.5 nM to 75 μM through LC-MS alongside our experimental samples. The standard concentrations were correlated to the normalized relative abundances of these metabolites detected to generate the standard curve (Figure 5-10A). From there, the concentrations of glutamine and histidine in our samples were interpolated. As expected, the serum concentration of glutamine (294.3 ± 65.4 μM; n=10) was significantly higher than histidine (47.50 ± 10.9 μM; n=10) in tumour-bearing animals (Figure 5-10B). These were within the expected range of these metabolites. Notably, while the concentration of histidine in the TIF (133.7 ± 38.1 μM, n=9) was increased compared to serum levels, the concentration of glutamine in the TIF (165.7 ± 64.4 μM, n=8 (1 detected outlier)) was significantly reduced (Figure 5-10B). This could reflect the increased demand for exogenous glutamine for catabolism in Myc-driven MGTs. We then compared the fold change in glutamine to histidine levels across the serum, TIF, MGTs, and the livers of tumour-bearing mice. Notably, while the glutamine levels significantly exceeded histidine in the serum and liver, they were not significantly different in the TIF or MGT (Figure 5-10C). Therefore, glutamine is likely limiting in these Myc-driven MGTs, whereas histidine may be a readily available substrate to facilitate LAT1 activity. It is important to note that many amino acids were significantly increased in the TIF compared to the serum, including tyrosine, another bidirectional LAT1 substrate (Figure 5-10D).

In the previous experiments, glutamine and histidine were preloaded separately, and LAT1-mediated exchange was compared. To better mimic *in vivo* conditions, MYAZ16.1e cells were preloaded with concentrations of [U-$^{13}$C]-glutamine (300

μM) and [U-$^{13}$C]-histidine (50 μM) observed in the serum as previously described. They were then replenished with amino acids in the presence or absence of JPH203 for 2.5 minutes. As observed previously, histidine levels were depleted upon nutrient replenishment (Figure 5-10E). Notably, it took 30 minutes to deplete intracellular histidine in cells preloaded with 1.6 mM of histidine, compared to 2.5 minutes in cells preloaded with 50 μM. However, upon Lat1 inhibition, histidine efflux was impeded (Figure 5-10E, F). In comparison, while glutamine levels were significantly reduced upon amino acid replenishment, this was not dependent on Lat1 inhibition and likely not due to glutamine efflux (Figure 5-10G, H). Indeed, only labelled histidine was observed in the media following amino acid replenishment (Figure 5-10I, J). Furthermore, this was inhibited in the presence of JPH203 (Figure 5-10I). Therefore, given that at physiological serum concentrations, histidine is preferentially used as a bidirectional Lat1 substrate, despite being available at 1/6 the concentration of glutamine. Considering that the concentration of glutamine in the TIF and MGT are only 1.7x and 2x more than histidine, respectively, this supports an essential role for histidine in maintaining EAA pools in Myc-driven MGTs.

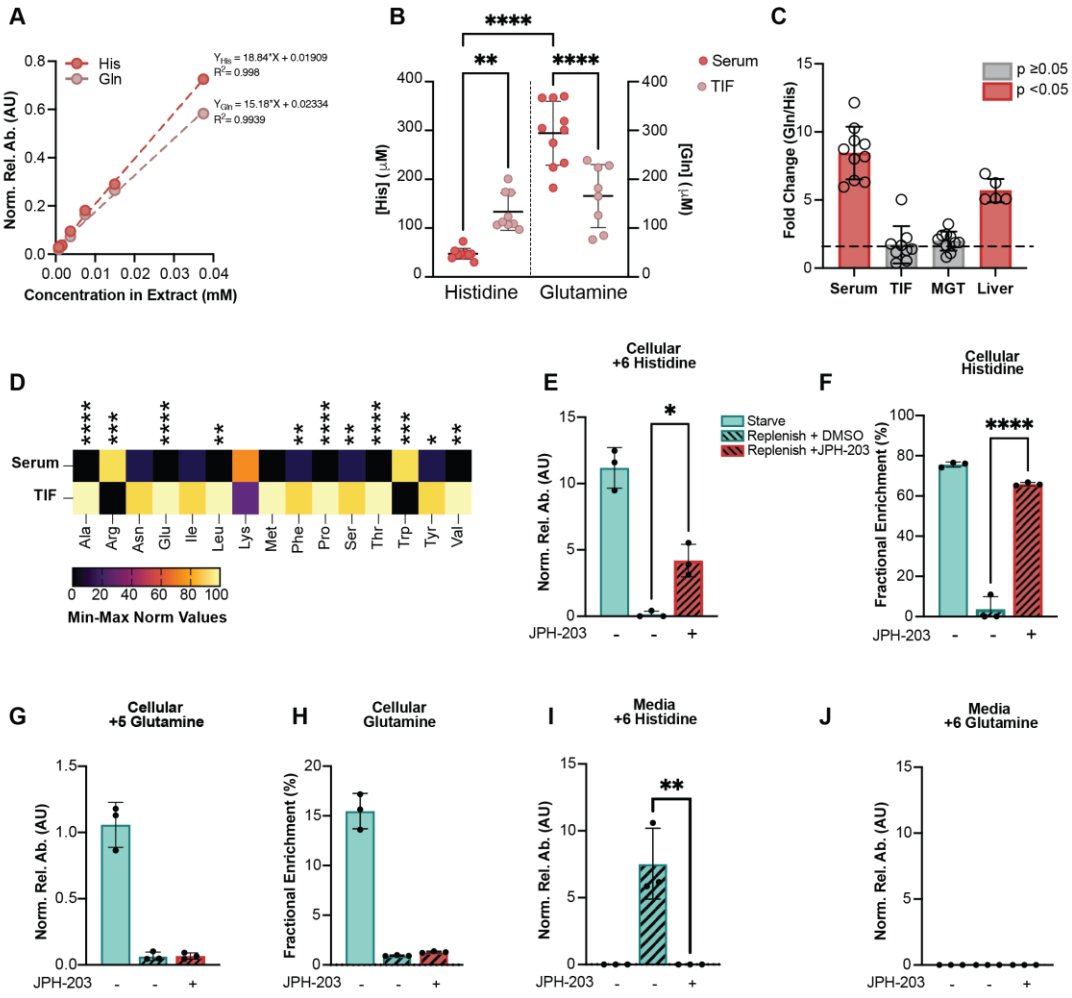



**Figure 5-10. Histidine is used as the preferential LAT1 exchange substrate at physiological levels.**

**(A)** Standard curves for histidine and glutamine, the abundance of m+6 isotopologues of glutamine and histidine are on the y-axis and the known concentrations are on the x-axis. **(B)** Concentration of histidine and glutamine in the serum (n=10) and TIF (n=9) of mice bearing MYAZ16.1e orthotopic MGTs interpolated from standard curves in panel A (one-way ANOVA with Šídák correction). **(C)** Fold difference in the concentration of glutamine relative to histidine in the serum (n=10), TIF (n=9), MGT (n=10), and liver (n=4). (one-way ANOVA with Šídák correction). **(D)** Heatmap showing mean total abundance of indicated amino acids in the serum and TIF. Colour scaling represents min-max normalized values (Multiple unpaired t-tests with Šídák-Bonferroni correction). **(E, F)** LC-MS analysis of cells preloaded with 300 μM [U-$^{13}$C]-glutamine and 50 μM [U-$^{13}$C]-histidine for 48 hours before replenishment with DMEM with vehicle (0.1% DMSO) or JPH203 (0.1 mM) for 2.5 minutes. Intracellular analysis: **(E)** abundance of m+6 histidine, **(F)** $^{13}$C enrichment of histidine, **(G)** abundance of m+5 glutamine, and **(H)** $^{13}$C enrichment of glutamine**. (I, J)** Extracellular (media) analysis **(I)** abundance of m+6 histidine and **(J)** abundance of m+5 glutamine. All data are presented as mean ± s.d.; representative of 1 replicate. One-way ANOVA with Šídák correction. *p<0.05, **p<0.01, ***p<0.001, ****p<0.0001.

## 5.4 Interrogating the role of asparagine during amino acid starvation

Asparagine was observed to promote cancer cell proliferation via exchange with extracellular amino acids, particularly serine, arginine, and histidine [245]. Indeed, it was reported that cells prefer to use asparagine rather than glutamine. Across all cell lines used, we observed a consistent increase in intracellular asparagine levels under amino acid starvation but not in cells preloaded with histidine. Furthermore, upon amino acid replenishment, asparagine levels were significantly reduced (Figure 5-11A). Quantifying the abundance of asparagine in the cell and media for up to 30 minutes after amino acid replenishment, we observe a decrease in cellular asparagine and an increase in extracellular asparagine in the media (Figure 5-11B). Therefore, this suggests that the asparagine produced during starvation may be used for amino acid exchange. Hence, we aimed to determine why increased asparagine levels were not observed in histidine-preloaded cells. Asparagine can be synthesised from glutamine via asparagine synthetase (ASNS) (Figure 5-11C). Therefore, we assessed whether glutamine was differentially catabolised in starved compared to histidine-preloaded cells. Before amino acid starvation, cells were cultured in 2.0 mM of [amide-$^{15}$N]-glutamine for 24 hours. Subsequently, cells were starved of amino acids in the presence or absence of 1.6 mM histidine. Cells were replenished with DMEM and collected as described previously. The incorporation of the amido group into asparagine was quantified. Interestingly, before amino acid starvation, 82.93% of asparagine was enriched with $^{15}$N from glutamine; however, upon amino acid starvation, only 30.37% enrichment was observed despite significantly increased intracellular abundance (Figure 5-11D, E). Indeed, significantly increased levels of unlabelled (m+0) asparagine were observed in amino acid-starved cells compared to the m+1 isotopologue of asparagine, which was not significantly increased in starved cells (Figure 5-11F). Furthermore, similar enrichment of asparagine was observed in starved and histidine-preloaded cells (Figure 5-11D). Therefore, increased *de novo* asparagine biosynthesis from glutamine cannot explain the increase observed during starvation. Notably, increased serine uptake was observed in amino acid-starved cells compared to histidine-preloaded cells (Figure 5-11G), previously observed in the TNBC cells. These data support the hypothesis that asparagine

may facilitate the uptake of necessary amino acids to support cellular proliferation in nutrient-adverse environments.

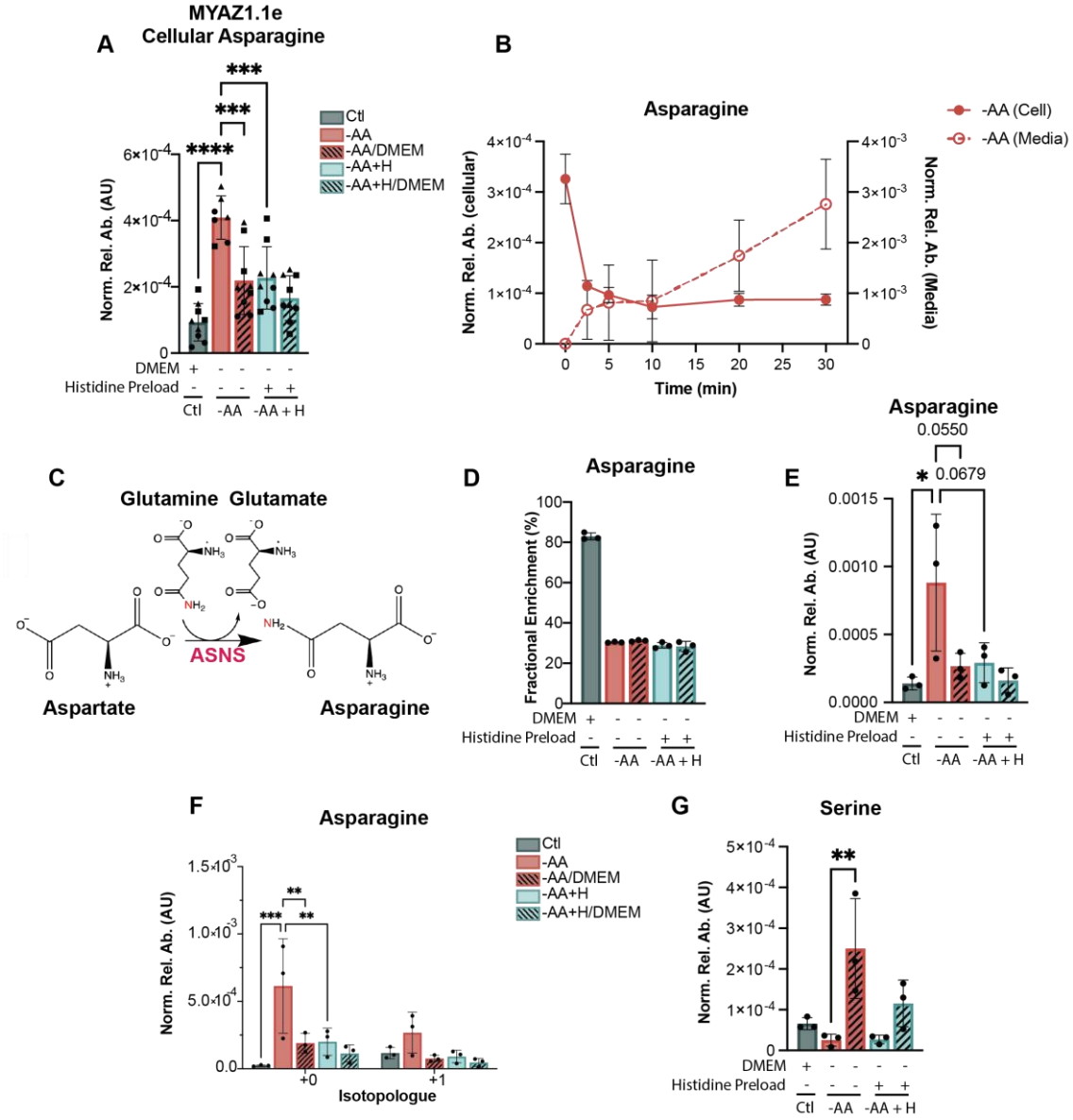



**Figure 5-11. Asparagine levels increase during amino acid starvation in a glutamine-independent manner.**
MYAZ16.1e cells were starved of amino acids or preloaded with 1.6 mM histidine for 48 hours followed by 2.5 minutes of DMEM replenishment. **(A)** Intracellular abundance of asparagine. **(B)** Intracellular (left y-axis) and extracellular (media, right y-axis) asparagine abundance over 30 minutes of DMEM replenishment. The 0-minute time point indicates the abundance of asparagine in starved cells prior to DMEM replenishment. **(C)** Mechanism of asparagine biosynthesis via ASNS. **(D-G)** MYAZ16.1e cells were cultured in 2.0 mM [amide-$^{15}$N]-glutamine before amino acid starvation or preloading with 1.6 mM histidine and then replenished with DMEM for 2.5 minutes: **(D)** intracellular $^{15}$N enrichment of asparagine and **(E)** intracellular asparagine abundance (one-way ANOVA with Šídák correction). **(F)** Asparagine isotopologue abundance (two-way ANOVA with Tukey correction). **(G)** Intracellular serine abundance (one-way

ANOVA with Šídák correction). All data presented as mean ± s.d.; representative of 1 replicate. *p≤0.05, **p≤0.01, ***p≤0.001.

Resistance to asparaginase, an enzyme widely used to treat leukaemia that depletes asparagine, has been linked to GSK3α-mediated protein degradation, which supplies leukaemia cells with asparagine[266]. This resistance can be overcome by activating the Wnt/STOP pathway, which inhibits GSK3α-dependent protein ubiquitination and subsequent protein degradation, thereby sensitising the cells to asparaginase treatment [266]. Therefore, we hypothesised that increased asparagine levels observed during starvation resulted from increased protein degradation. We assessed K48-linked protein ubiquitination in starved cells and histidine preloaded cells. Additionally, cells were starved of amino acids in the presence of MG-132, a proteasome inhibitor, and BRD0705, a GSK3α inhibitor. Cells subjected to 24 hours of amino acid starvation exhibited minimal K48-linked polyubiquitination as detected by western blot compared to cells preloaded with histidine (Figure 5-12A). This could suggest that the UPS is less active under histidine preload or more active under amino acid starvation. Similarly, increased K48-linked polyubiquitination was observed in cells preloaded with histidine compared to amino acid-starved cells for 48 hours (Figure 5-12A). MG-132 and BRD0705 treatment blocked the UPS system in amino acid-starved cells, as evidenced by increased K48-polyubiquitination (Figure 5-12A). Interestingly, although decreased proteasome activity was observed in histidine-preloaded cells, there was increased autophagy in these cells compared to amino acid-starved cells (Figure 5-12A). Furthermore, GSK3α phosphorylation was increased in histidine preloaded cells, which could underlie the increased autophagy observed in these cells. We next assessed whether MG-132 or BRD0705 treatment was sufficient to block asparagine production during starvation. As observed previously, amino acid-starved cells accumulated asparagine uptake, which was significantly reduced upon amino acid replenishment (Figure 5-12B). However, MG-132 or BRD0705 treatment in amino acid-starved cells completely blocked the observed increase in asparagine (Figure 5-12C). In comparison, proline, another amino acid whose levels were increased in amino acid starved cells compared to histidine-preloaded cells, was not impacted by MG132 or BRD0705 treatment (Figure 5-12C).

Therefore, these results suggest that asparagine is released due to increased protein degradation during amino acid starvation.

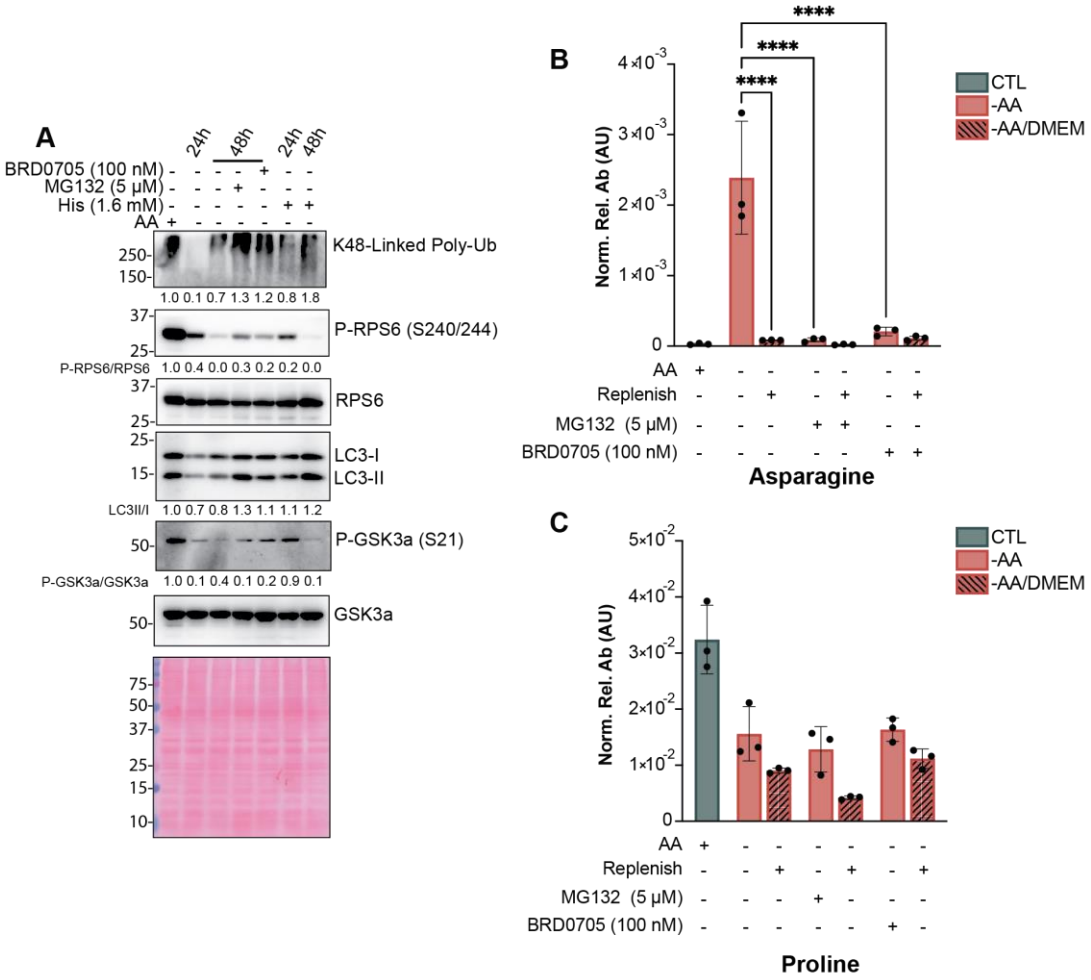



**Figure 5-12. Asparagine is released through proteolysis.**
**(A)** WB of MYAZ16.1e cells starved of amino acids or preloaded with 1.6 mM histidine for indicated times. Protein levels were normalized to ponceau and unstarved control cells (+ AA). Representative of 2 independent replicates. **(B-C)** LC-MS analysis of MYAZ16.1e cells starved of amino acids in the presence or absence of MG-132 or BRD0705 for 48 hours and replenished with DMEM for 2.5 minutes, intracellular abundance of **(B)** asparagine and **(C)** proline is shown. Data are presented as mean ± s.d.; one-way ANOVA with Šídák correction, representative of 1 replicate. ****p≤0.0001.

To identify the source of asparagine in starved cells, we calculated bias in the usage of asparagine codons AAT and AAC for 29,811 endogenous coding sequences based on the genome-wide average usage frequency of these codons to identify proteins enriched in asparagine codons. Intriguingly, coding sequences that showed an increased usage of asparagine codons were notably overrepresented in gene ontology (GO) terms related to the plasma membrane, cell adhesion, and transmembrane signalling (Figure 5-13A). Selective degradation of

plasma membrane proteins is essential in maintaining pools of amino acids for protein synthesis [345]. Furthermore, this study suggested that plasma membrane protein degradation occurred at the early stages of starvation. However, degradation of plasma membrane proteins was mediated by the multivesicular body (MVB) pathway, whereas the UPS system rapidly degraded cytoplasmic proteins to supply pools of amino acids. Given that many plasma membrane proteins are enriched in asparagine, this suggests that targeting the endosomal sorting complex required for transport (ESCRT) necessary for the MVB pathway may be a more selective way of targeting asparagine degradation.

**A**

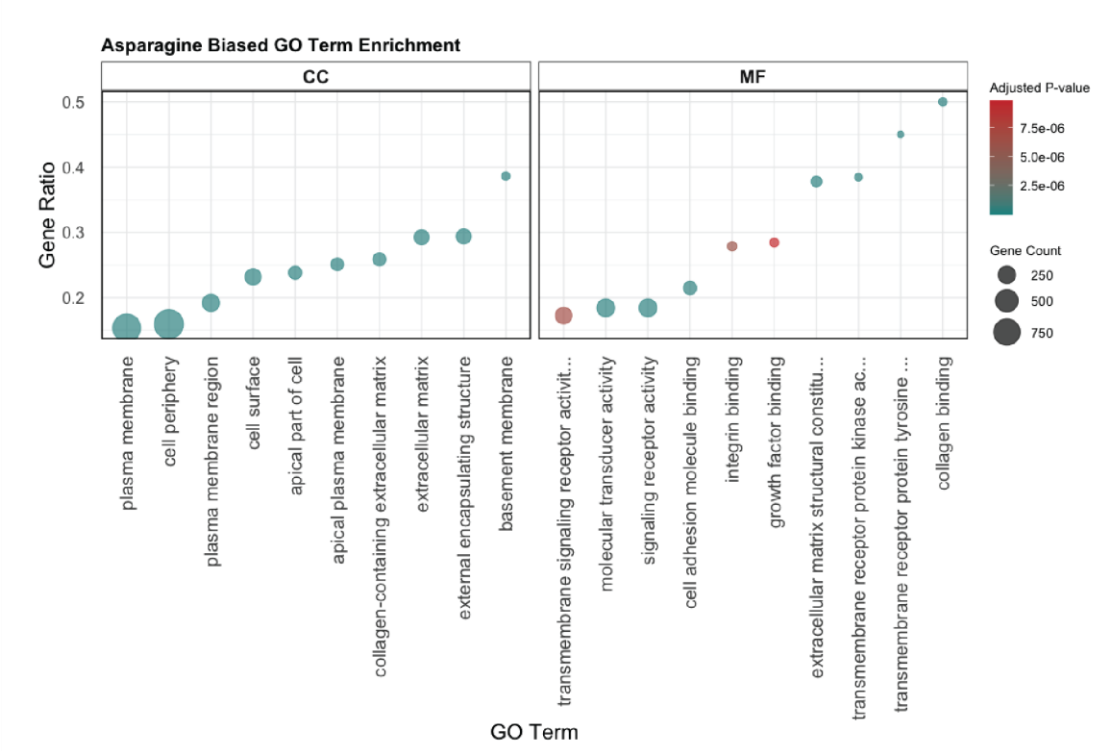



**Figure 5-13. Genes enriched in asparagine codons are associated with GO terms involving the plasma membrane.**
**(A)** Top 10 CC (cell compartment) and MF(molecular function) GO terms predicted to have the highest asparagine codon usage bias (AAT, AAC). Size of dot indicates the number of genes associated with each term and the colour scale indicates the adjusted p-values. P-values were adjusted for multiple testing using the Benjamini-Hochberg method. GO terms are displayed on the x-axis and their significance is reflected on the y-axis.

An MRes student in our lab, Wei Du, conducted further experiments interrogating asparagine's role during amino acid starvation. Importantly, Wei's research highlighted that asparagine release was not blocked explicitly in histidine-preloaded

cells. High availability of other amino acids, especially BCAAs, such as leucine and valine, completely abrogated asparagine release (unpublished data). Furthermore, cells preloaded with leucine and valine significantly reduced UPS activity, as K48-linked polyubiquitination suggested (unpublished data). Notably, Wei's results indicated that MG132-mediated inhibition of proteasome degradation during amino acid starvation resulted in decreased serine uptake, purine synthesis, and global methylation, which attenuated cellular proliferation when nutrients were made available (unpublished data). However, further work is necessary to understand these mechanisms to identify more specific targets and determine the implication of asparagine release in nutrient-adverse conditions *in vivo*.

## 5.5 Histidine preloading primes cells for increased mTORC1/4E-BP1 signalling.

LAT1 is a high-affinity leucine transporter. Importantly, leucine is one of the most abundant amino acids in proteins and is encoded by the highest number of codons (TTA, TTG, CTT, CTC, CTA, CTG). Therefore, sensing leucine availability is important in regulating mTORC1 activity. Indeed, leucine is sensed via multiple mechanisms, including LRS, SESTRIN2, and more recently demonstrated, SAR1B[173,175,181]. Therefore, given LAT1's important role in maintaining leucine levels, its activity is essential for mTORC1-dependent cellular growth. Due to increased leucine uptake in cells preloaded with histidine, we hypothesised that histidine availability would enhance mTORC1 pathway activation. To confirm our hypothesis, we collected BT-549 cells at different time points following DMEM replenishment after amino acid starvation in either the presence or absence of 1.6 mM histidine. Phosphorylation of RPS6 and 4E-BP1 were assessed as outputs of mTORC1 activation (Figure 5-14A). Histidine preloaded cells had significantly increased phosphorylation of 4E-BP1, indicating increased mTORC1 pathway activation in these cells (Figure 5-14B). However, unexpectedly, the opposite trend was observed for RPS6. Indeed, histidine-preloaded cells had decreased RPS6 phosphorylation compared to starved cells in the absence of histidine (Figure 5-14B). Furthermore, Myc protein levels were also reduced in histidine-preloaded cells. Notably, increased total RPS6 and 4E-BP1 levels was observed, thereby

modulating mTORC1 activity. While 4E-BP1 undergoes rapid phosphorylation in histidine-preloaded cells, the phosphorylation level stabilised due to increased 4E-BP1 protein levels (Figure 5-14B, C). In contrast, phosphorylation of RPS6 occurs steadily over time, with a near significant increase in phosphorylation relative to histidine-preloaded cells observed after 20 minutes (Figure 5-14B, D). We confirmed that this RPS6 and 4E-BP1 activation occurs downstream of mTORC1 and PI3K signalling as shown by ablated phosphorylation in the presence of the PI3K inhibitor, GDC0941, or the mTORC1 inhibitors, rapamycin and Ink128 (Appendix 6). However, inhibition of ERK did not affect the phosphorylation of RPS6 or 4E-BP1 (Appendix 6). This may be due to oncogenic PI3K signalling in BT-549 cells, which may be sufficient for TSC2 inhibition and, therefore, activation of RHEB and subsequent mTORC1 activation. mTORC1 activation was also assessed in MYAZ16.1e and MDA MB 231 cells. However, the Ras/ERK pathway can lead to mTOR-independent serine 235/236 phosphorylation on RPS6, sites where S6K1 can also phosphorylate. Therefore, the potential role of ERK in RPS6 activation cannot be discounted [346]. Similar trends were observed in MYAZ16.1e cells, with increased 4e-bp1 phosphorylation in histidine-preloaded cells, stabilising after 20 minutes (Figure 5-14E). However, despite increased leucine uptake in preloaded cells compared to starved cells, we did not observe any differences between mTORC1 pathway activation in MDA MB 231 cells preloaded with histidine (Figure 5-14F). Together, these results indicate a potential role for histidine-facilitated amino acid exchange in the mTORC1/4E-BP1, which appears to be cell type-dependent.

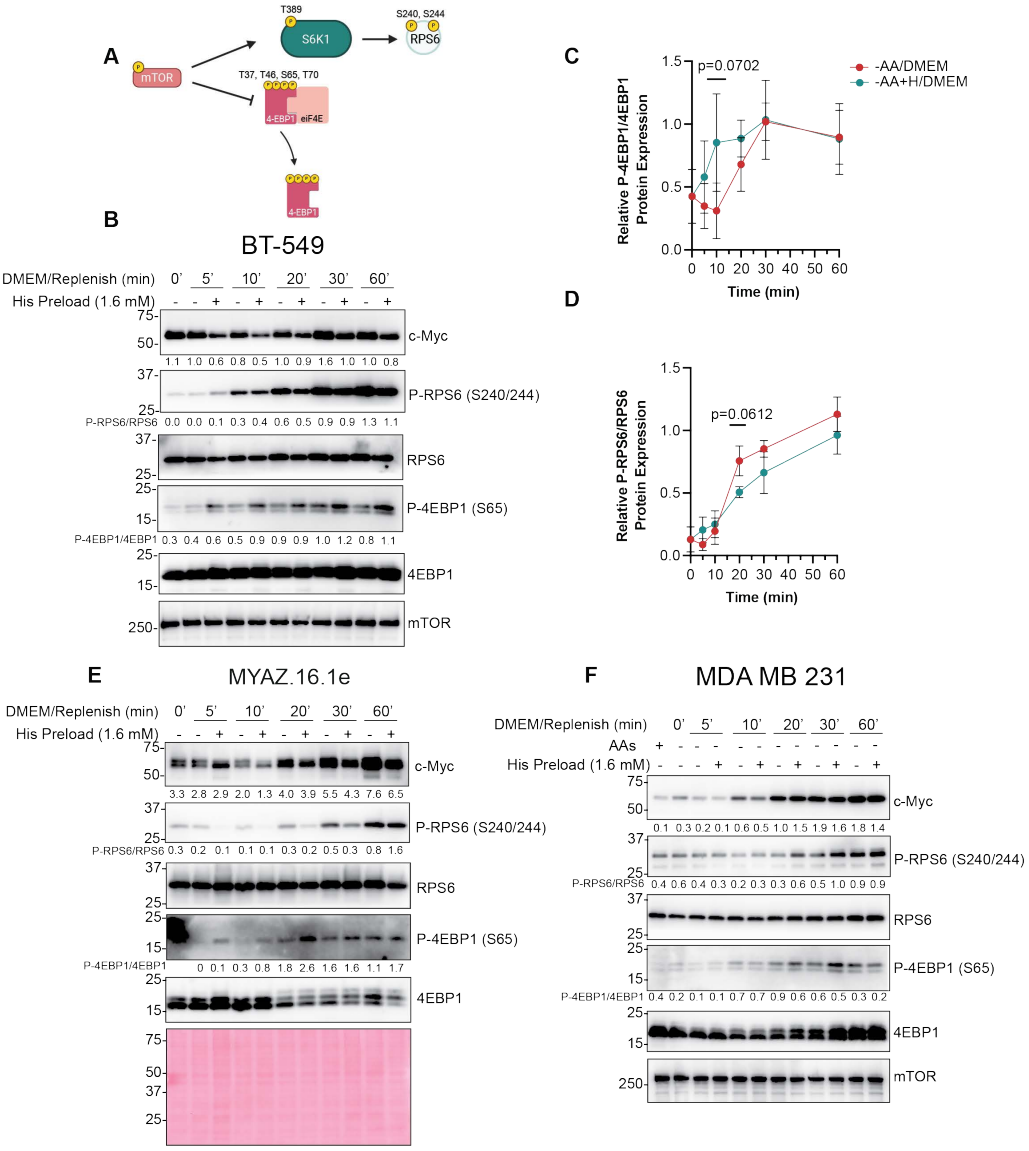



**Figure 5-14. Histidine availability enhances mTORC1/4E-BP1 signalling in Myc-dependent cancer cells.**
Cells were starved of amino acids or preloaded with 1.6 mM histidine for 48 hours and replenished with DMEM for indicated times. **(A)** Visual representation of canonical downstream mTORC1 targets. **(B)** WB of BT-549 cells, representative of 3 independent replicates. **(C-D)** quantification of relative **(C)** P-4E-BP1 and **(D)** P-RPS6 expression in replicates from panel A. Protein levels were normalized to vinculin or mTOR and then to the 0' time point (two-way ANOVA with Šídák correction). **(E)** WB of MYAZ16.1e cells, representative of 1 replicate. **(F)** WB of MDA MB 231 cells, representative of 1 replicate.

To determine whether this mTORC1 activation in replenished cells depended on LAT1 and histidine mediated uptake of EAAs, mTORC1 pathway activation was assessed in cells preloaded with D-histidine. Previously, we showed that D-histidine preloaded BT-549 cells could not exchange histidine for essential amino acids, including leucine. Therefore, we assessed the phosphorylation of 4E-BP1

and RPS6 following nutrient replenishment in these cells. As expected, no apparent differences were observed in either RPS6 or 4E-BP1 phosphorylation in histidine preloaded cells (Figure 5-15A). LAT1 KO in BT-549 cells similarly ablated histidine exchange for EAAs such as leucine. Therefore, we assessed mTORC1 pathway activation downstream of LAT1 activity in these cells. Like D-histidine preloaded cells, BT-549 sgSLC7A5 cells treated with doxycycline to induce LAT1 KO and preloaded with histidine did not have increased 4E-BP1 phosphorylation as was observed in dox-off cells (Figure 5-15B, C). Furthermore, dox-on cells starved of amino acids without histidine preload also did not have increased RPS6 phosphorylation as was observed in dox-off cells (Figure 5-15B, C). However, although these western blots show a trend consistent with our hypothesis, the P-4E-BP1 immunoblots exhibit reduced clarity and signal-to-noise ratio, impacting band intensity quantification. Therefore, these results are preliminary and must be rerun with optimised conditions for the 4E-BP1 antibody. Nonetheless, these results point to an important role for both LAT1 in mediating mTORC1 activity in starved cells through RPS6 phosphorylation, and both LAT1 and histidine in preloaded cells through 4E-BP1 phosphorylation.

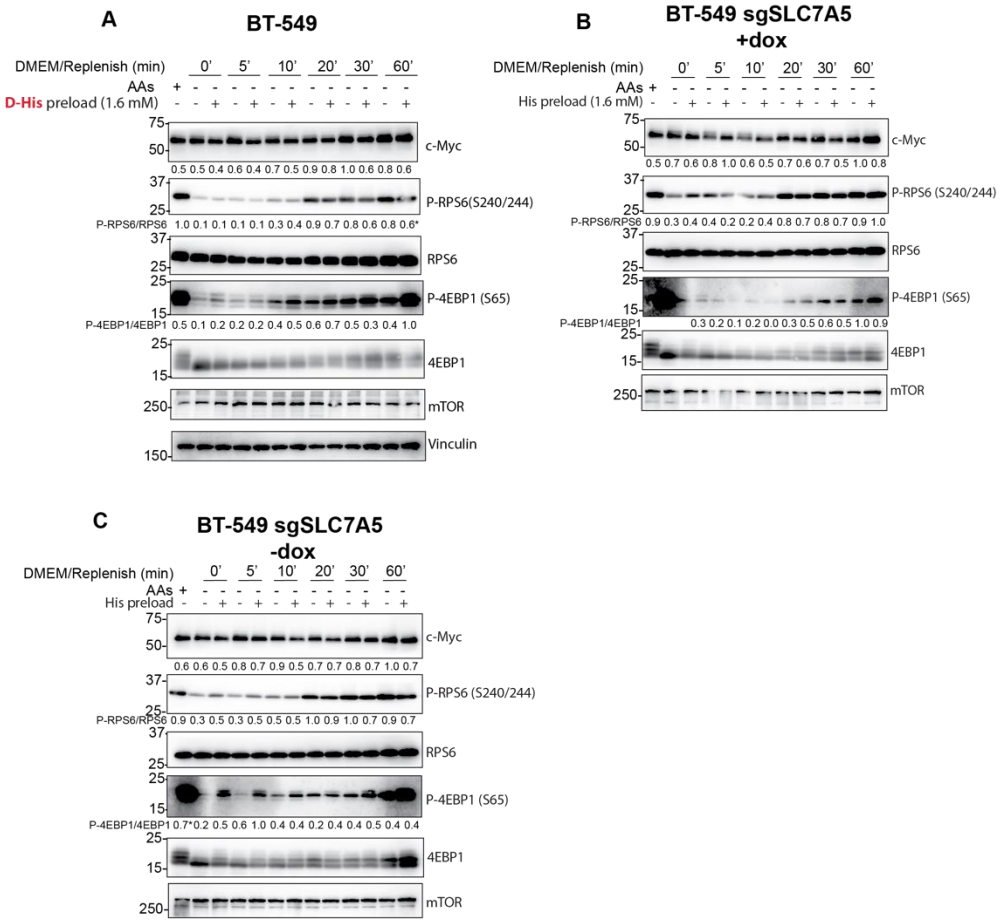



**Figure 5-15. mTORC1 activation is dependent on LAT1.**
**(A)** WB of BT-549 cells that were starved of amino acids or preloaded with 1.6 mM D-histidine for 48 hours and replenished with DMEM for indicated times. Representative of 2 independent replicates. **(B-C)** BT-549 sgSlc7a5 cells were cultured in 1 µg/µL doxycycline for 48 hours prior to amino acid starvation or preload with 1.6 mM histidine for 48 hours and replenished with DMEM for indicated times. WB of **(B)** dox-on and **(C)** dox-off conditions. Representative of 1 replicate.

Two complexes must form for translation initiation: the pre-initiation and cap-binding complexes. The protein 4E-BP1, when in its hypo-phosphorylated state, inhibits the formation of the cap-binding complex. It does this by binding the cap-binding protein, eIF4E, which generally interacts with eIF4G to assemble the complex. By sequestering eIF4E, 4E-BP1 prevents its association with eIF4G, thereby blocking the assembly of the cap-binding complex. Without forming this complex, the pre-initiation complex is not adequately recruited the mRNA, halting translation initiation. mTORC1 regulates the assembly of the cap-binding complex by modulating the activity of 4E-BP1. When mTORC1 phosphorylates 4E-BP1, it dissociates 4E-BP1 from eIF4E, allowing the cap-binding complex to assemble. This mechanism highlights the critical role of 4E-BP1 in regulating protein

translation in response to nutrient availability, as its activity is directly influenced by mTORC1 signalling. Therefore, we hypothesised that histidine preload would prime cells for increased protein translation due to rapid 4E-BP1 phosphorylation and amino acid uptake observed in histidine-preloaded cells. To assess the effect of histidine availability on protein translation the SUnSET technique was utilised to detect changes in protein synthesis by western blotting. MYAZ16.1e cells were starved of amino acids in the presence or absence of 120 μM histidine or 1.6 mM histidine for 48 hours. After this, cells were replenished for the indicated times with complete DMEM. Before cell collection for protein lysates, they were administered 10 μg/mL puromycin for 10 minutes. Western blots were probed for puromycin to assess nascent protein translation under these conditions. As expected, histidine-preloaded cells had increased puromycin incorporation and, therefore, protein translation compared to amino acid-starved cells (Figure 5-16A). Furthermore, protein translation occurred more quickly following amino acid starvation in histidine preloaded cells. Indeed, protein translation was observed as early as 30 minutes in cells preloaded with supraphysiological levels of histidine. In contrast, it was observed to a lesser extent after 2 hours of nutrient replenishment in starved cells (Figure 5-16A). Notably, cells that were starved in physiological concentrations of histidine at 120 μM had increased puromycin incorporation after 2 hours and compared to starved cells, but also greater levels at 24 hours compared to cells preloaded with 1.6 mM histidine (Figure 5-16A). In line with this observation, there is a concentration-dependent decrease in puromycin incorporation in cells preloaded with histidine (Figure 5-16B). As shown previously, increased 4E-BP1 protein expression was observed in cells preloaded with 1.6 mM of histidine (Figure 5-14A, B). Decreased protein translation after a prolonged period could be due to negative feedback driven by ER stress, activating the ISR and ATF4 upregulation and its target gene, 4E-BP1[347]. The expression of ISR proteins, such as PERK (PKR-like ER kinase), eIF2α, and ATF4, must be assessed to confirm this hypothesis. To assess whether the rapid protein translation observed in cells preloaded with 1.6 mM of histidine was due to increased availability of EAAs, intracellular levels of amino acids were quantified following amino acid replenishment for up to 30 minutes. We observed a consistently significant increase in intracellular EAA levels, such as leucine, methionine, isoleucine, and phenylalanine, for up to 10 minutes (Figure 5-16C-F). This was followed by a

decrease in intracellular levels. In comparison, without histidine preload, starved cells had significantly slower and reduced uptake of EAAs (Figure 5-16C-F). This suggests that histidine-preloaded cells can accumulate EAAs for protein translation significantly faster than starved cells. In comparison, the intracellular levels of other amino acids, such as threonine and glutamine, were not significantly altered in histidine-preloaded cells (Figure 5-16G, H). Intracellular glutamine levels were significantly higher in starved cells (Figure 5-16H). To summarise, the increased uptake of LAT1 substrates facilitated by histidine exchange leads to increased mTORC1/4E-BP1 activation, increasing 5'-cap-dependent mRNA translation.

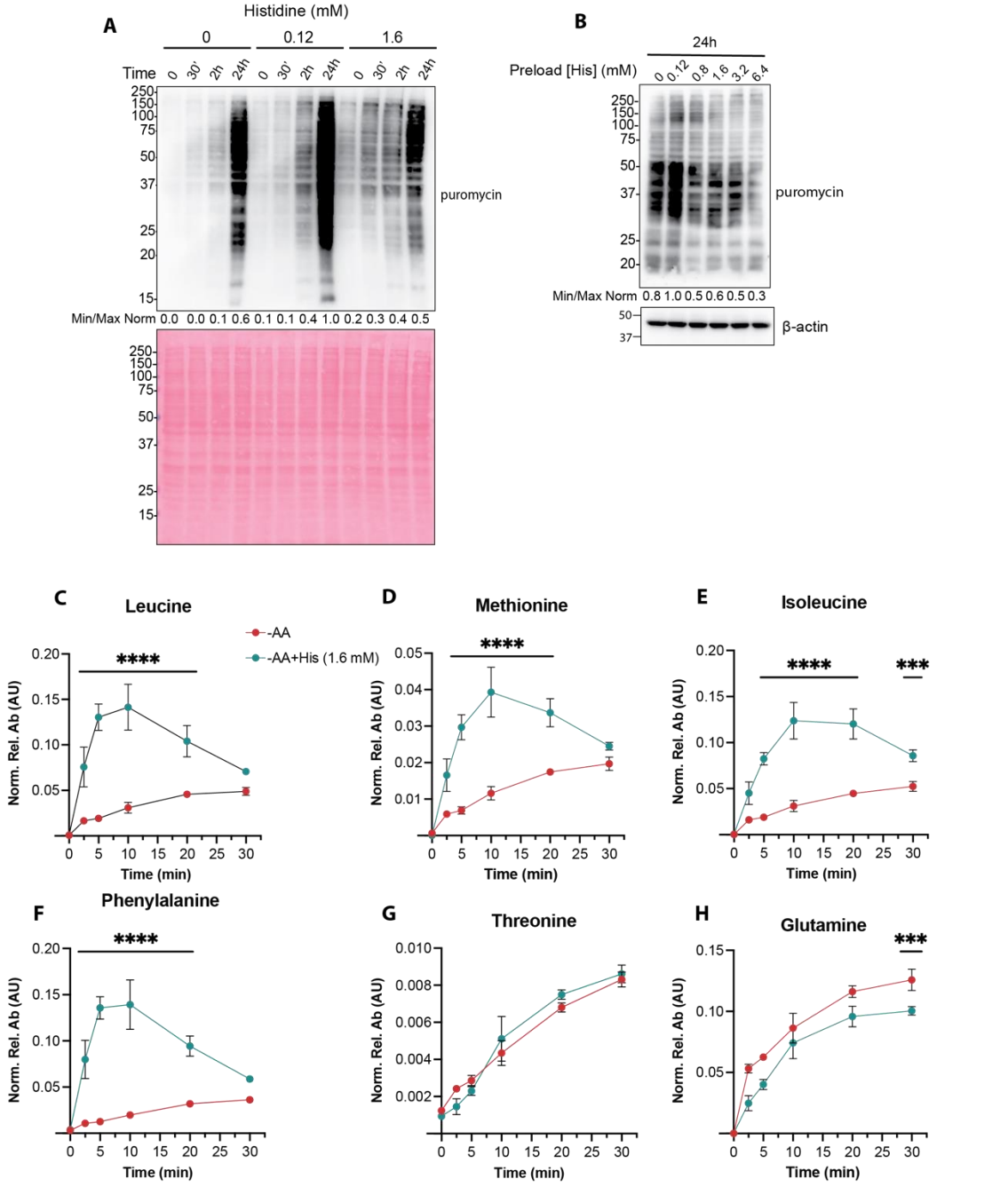



**Figure 5-16. Histidine preload enhances protein translation.**
**(A)** MYAZ16.1e cells were starved of amino acids or preloaded with 0.12- or 1.6-mM histidine for 48 hours and replenished with DMEM for indicated times. WB of puromycin incorporation. Puromycin levels were normalized to ponceau staining and min max normalized. Representative of 2 independent replicates. **(B)** WB of puromycin incorporation in MYAZ16.1e cells preloaded with histidine at indicated concentrations and replenished for 24 hours. Puromycin levels were normalized to β-actin and min-max normalized. Representative of 1 replicate. **(C)** LC-MS analysis of MYAZ16.1e cells starved of amino acids or preloaded with 1.6 mM of histidine for 48 hours and replenished with DMEM for up to 30 minutes. The 0-minute time point denotes the abundance prior to replenishment. Data are mean ± s.d.; two-way ANOVA with Šídák correction. Representative of 1 replicate. ***p≤0.001, ****p≤0.0001.

mTORC1 signalling is an important regulator of ribosome biogenesis, which is facilitated through phosphorylation of S6 kinases downstream of mTORC1 activation. Activated S6K1 can positively regulate Pol I transcription, which is essential for rRNA synthesis [348]. Furthermore, RPS6, which is phosphorylated downstream of S6K1, is a component of the 40S ribosomal subunit and is involved in the transcription of ribosomal biogenesis genes [341]. Given the increased phosphorylation of RPS6 observed in amino acid starved compared to histidine preloaded cells (Figure 5-14A, C), the mRNA expression of ribosomal biogenesis genes was quantified via RT-qPCR. Significant increases in mRNA expression between starved and histidine-preloaded cells were observed in *Polr1a*, *Polr1d*, *Rrn3*, and *Fbl*, indicative of an upregulation of rRNA transcription and processing machinery and an increased demand for ribosome biogenesis (Figure 5-17A). *Polr1a* and *Polr1d* encode subunits of RNA polymerase I (RNAPOLI1); however, no increase is observed in *Polr1b, Polr1c,* or *Polr1e*. Therefore, this does not necessarily suggest an increase in RNAPOL1 activity, which is responsible for the transcription of rRNA genes, including the 18S, 5.8S, and 28S subunits. For RNAPOL1-mediated transcription of RRN3, a pre-initiation complex must be formed. This requires the activity of RRN3 (also known as TIF-1A) and upstream binding transcription factor (UBF, encoded by *Ubtf*), which direct RNAPOL1 to rDNA promoters to start transcription. However, while we observe significant changes in *Rrn3* transcription in starved cells, this is not evident for *Ubtf* (Figure 5-17A). Furthermore, we do not observe any changes in *Sirt7* (encoding Sirtuin 7) transcription, which is important in stimulating the transcription of rDNA genes through deacetylation of the 1e subunit of RNAPOL1 and maturation of pre-rRNA. However, we observe upregulation in *Fbl* (encoding fibrillarin), a crucial regulator of pre-rRNA cleavages. Surprisingly, increased mRNA expression of *Polr1a*, *Polr1c*, *Polr1d*, *Rrn3* and *Fbl* are observed during amino acid starvation compared to control cells.

Ribosome biogenesis is the most costly process in the cell, accounting for greater than 70% of all transcription and 25% of all translation[349]. Therefore, regulation of ribosome biogenesis in nutrient-scarce environments is imperative. Therefore, pro-growth cellular processes such as protein synthesis and ribosome biogenesis are rapidly inhibited under these conditions. One of the ways this is achieved is through

the mTOR pathway, which can modulate protein synthesis and rRNA transcription. Indeed, mTOR-dependent modulation of TIF-1A/UBF activity is one mode that directly blocks RNAPOL1 transcription[348,350]. Therefore, given the inactivation of mTORC1 during amino acid starvation, it is likely that ribosome biogenesis is inhibited; however, perhaps transcription of genes necessary for ribosomal machinery is maintained in preparation for when nutrients become available to begin protein synthesis rapidly. Another possible explanation for this is abnormal ribosome biogenesis due to Myc-amplification. We observed increased Myc levels in amino acid-starved cells compared to histidine-preloaded cells (Figure 5-17B, C). Indeed, Myc regulates early ribosome biogenesis through RNA Pol I, II, and III-mediated processes. Indeed, Myc enhances rDNA transcription and rRNA processing through its interaction with transcription factors UBF and SL1[351]. This boosts ribosome production and is essential for the abnormal cellular growth in cells with Myc overexpression. Using RNA-sequencing data generated by a post-doctoral fellow in our lab, Josep Tarrago-Celado, on iMMECs expressing exogenous cMYC produced by a PhD student in our lab, Michael Kossifos, expression of genes involved in ribosome biogenesis was evaluated. We first computed the average of each gene across all samples. The top 100 genes with the highest average expression were mapped based on these averages. The variability of gene expression across different samples was then assessed by comparing individual sample expression to the calculated average expression of each gene. This data set revealed significant changes in ribosome biogenesis genes in iMMECs with ectopic Myc expression (iMMEC_Myc) compared to wild type iMMECs (Appendix 7A). Subsequently, Gene Ontology (GO) enrichment analysis was performed to examine molecular functions associated with the top genes in the WT iMMEC and iMMEC_Myc to determine whether molecular functions related to ribosome biogenesis were altered upon Myc overexpression. The top 500 genes were independently computed for iMMEC and iMMEC_Myc samples and mapped onto GO terms for molecular function. The GO terms were similar in iMMEC and iMMEC_Myc, with structural constituents and transcription coregulator activity being the top 2 hits (Appendix 7B, C). However, top GO terms in iMMEC_Myc cells included catalytic activity acting on RNA, mRNA binding, and rRNA binding (Appendix 7C). In contrast, iMMEC cell genes were enriched for GO terms in transcription coactivator activity, methyltransferase activity, and histone

modifying activity (Appendix 7B). Overall, these data support the role of Myc in regulating multiple aspects of ribosome biogenesis. When this data set was analysed for expression of genes encoding RNAPOL1 subunits and the genes involved in the early stages of ribosome biogenesis as quantified via qPCR, most of these genes were observed to be increased in iMMEC_Myc cells (Figure 5-17D). Notably, the genes upregulated in amino acid starved cells are similarly upregulated upon ectopic Myc expression (Figure 5-17A, D). This supports the hypothesis that this increase in ribosome biogenesis genes could be due to Myc activity in the absence of mTORC1 activation. Notably, a recent study demonstrated that Myc overexpression was sufficient to stimulate 47S pre-rRNA biogenesis independent of mTORC1 activation in skeletal muscle cells[352]. Therefore, given that rRNA is a limiting factor for ribosome production and protein synthesis, increased mRNA production of genes critical to these processes may act to reactivate ribosome biogenesis quickly when nutrients become available.

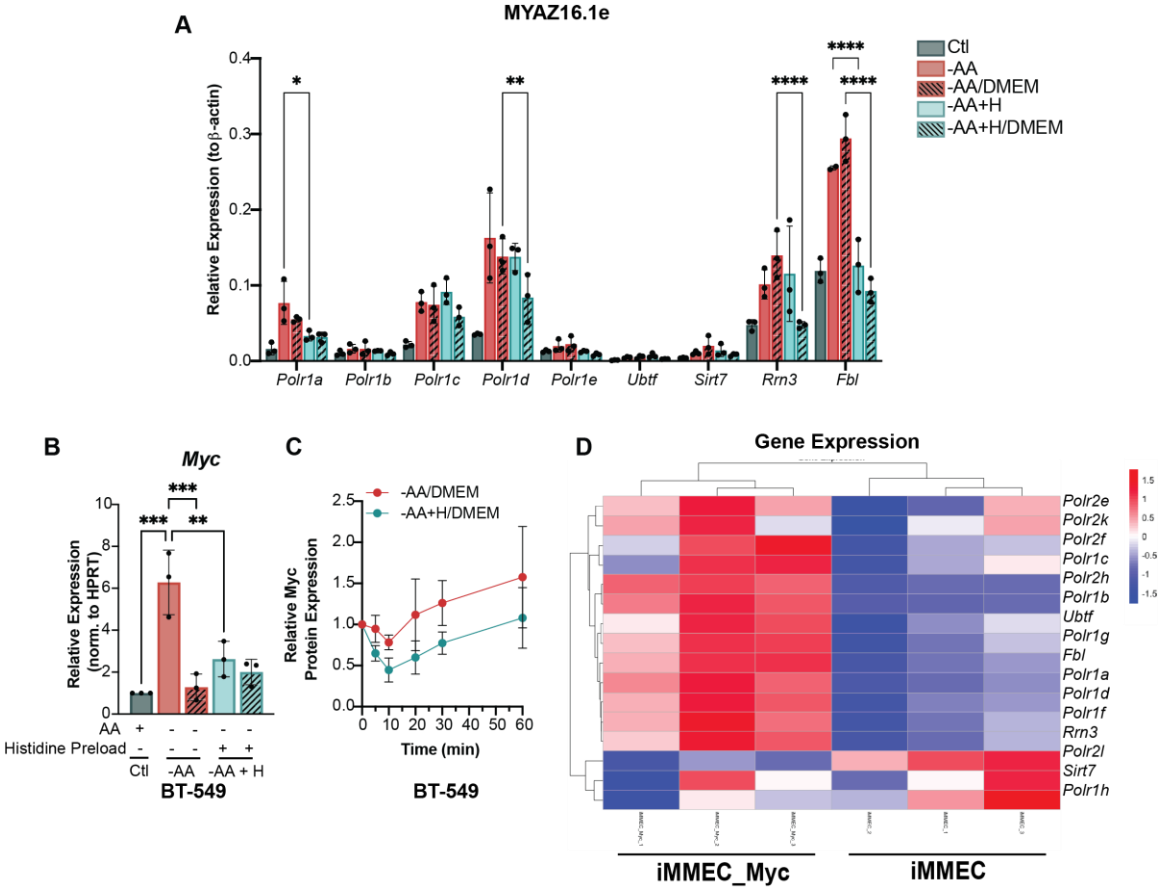



**Figure 5-17. Amino acid-starved cells have increased transcription of ribosomal biogenesis genes.**
**(A)** RT-qPCR of ribosome biogenesis genes relative to β-actin in MYAZ cells starved of amino acids or preloaded with 1.6 mM histidine for 48 hours and then replenished with DMEM for 30 minutes. Representative of 3 biological replicates (two-way ANOVA with Tukey correction). **(B)** RT-qPCR of Myc gene expression relative to HPRT in BT-549 cells starved of amino acids or preloaded with 1.6 mM histidine and replenished for 30 minutes. Representative of 1 independent replicate (one-way ANOVA with Šídák correction). **(C)** Quantification of Myc protein levels normalized to vinculin and relative to 0 minutes in BT-549 cells replenished for indicated times. Representative WB in Figure 5-14 panel A. (two-way ANOVA with Šídák correction on 3 independent replicates). Data are presented as mean ± s.d. *p≤0.05, **p≤0.01, ***p≤0.001, ****p≤0.0001. **(D)** Heatmap showing expression of ribosomal biogenesis genes in iMMEC and iMMEC_Myc cells, colour scaling depicts Z-scores scaled for each gene across samples. Hierarchical clustering was applied to genes and samples.

Given the rapid reactivation of protein translation observed in histidine-preloaded cells when amino acids were available, we hypothesised that these cells would have a proliferative advantage compared to starved cells. We first assessed whether a greater percentage of cells entered the cell cycle if preloaded with histidine. MYAZ16.1e cells were starved of amino acids in the presence or absence of 200 μM of histidine for 48 hours. Subsequently, they were replenished with

complete DMEM for 24 hours, and cells were administered 10 μM BrdU for 1 hour before collection. BrdU incorporation was measured with immunofluorescence, as described in the Materials & Methods chapter, to indicate the proportion of cells actively undergoing proliferation. As expected, there was no BrdU incorporation in starved or preloaded cells. However, no differences in BrdU incorporation were observed after 24 hours of amino acid replenishment (Figure 5-18A). When positive cells were quantified, a slight but insignificant increase in the percentage of BrdU+ cells was observed in histidine-preloaded cells (Figure 5-18B).

To gain a more detailed understanding, we performed flow cytometry using BrdU incorporation and PI staining as described in the Materials & Methods Chapter. This allowed us to simultaneously assess BrdU incorporation for proliferation, which is incorporated into DNA during the S phase. PI staining for cell cycle distribution to distinguish cells in G0/G1, S, and G2/M phases (Figure 5-18C). For this, MYAZ16.1e, MYAZ6.6g, and MYAZ12.3i tumour cell lines were treated as described above. Upon amino acid starvation, there is a significant increase in cells stuck in the G1 and G2 phases, which decrease upon amino acid replenishment (Figure 5-18C). Inversely, there was a total loss of cells in the S phase during amino acid starvation, as expected (Figure 5-18C). Upon amino acid replenishment, we saw a significant increase in the percentage of cells actively dividing. Notably, we observed an insignificant increase in the percentage of cells in the S phase in histidine-preloaded cells compared to starved cells (Figure 5-18C). Therefore, these data did not conclusively reveal whether histidine availability primes cells for cell division when nutrients become available.

For a more comprehensive view, overall cellular proliferation was assessed. RPS6 and Myc are essential cell growth regulators. Therefore, cell size was quantified given the increased expression of these proteins in amino acid-starved cells compared to histidine-preloaded cells. This was important in determining whether confluency could accurately be used as a measure of proliferation between these conditions. Following 24 hours of amino acid replenishment, cell diameter was measured. While histidine-preloaded cells tended to be slightly larger in diameter than starved cells, no significant differences were observed (Appendix 8). Therefore, MYAZ -16.1e, -6.6g, and -12.3i cells were starved of amino acids in the

presence or absence of 0.2 mM or 1.0 mM of histidine for 48 hours, after which media was changed to complete DMEM for up to 48 hours. In line with the increased mTORC1 signalling and protein translation, a slight but significant increase in proliferation was observed in cells preloaded with histidine compared to replenished amino acid starved cells (Figure 5-18D). Importantly, replenishing amino acid-starved cells with increasing concentrations of histidine did not result in a concentration-dependent increase in proliferation (Appendix 6C). This indicates that the proliferative advantage is not a result of increased histidine availability for protein synthesis or other functions but a result of its availability for bidirectional exchange. Together, these data indicate that the bidirectional exchange of histidine for LAT1-mediated uptake of EAAs can provide a proliferative advantage upon the reintroduction of amino acids. This could give the tumours an advantage in aiding survival in adverse nutrient conditions.

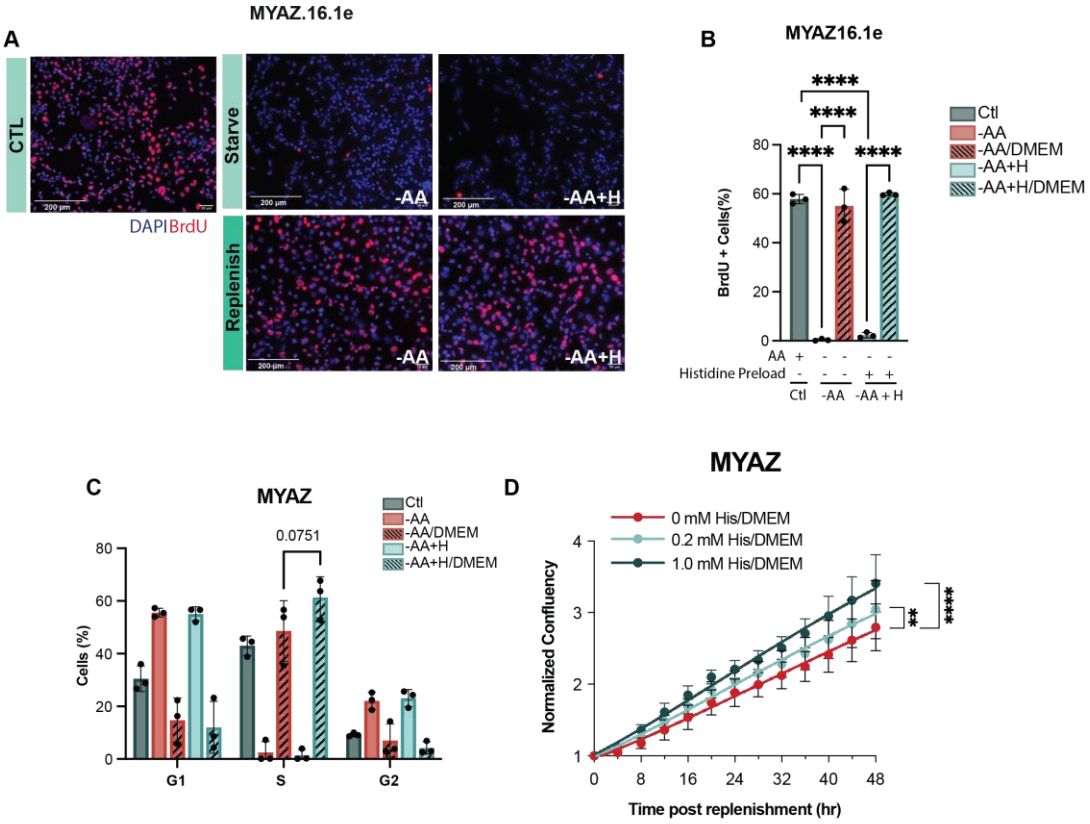



**Figure 5-18. Histidine preload does not significantly increase cell replication.** Cells were starved of amino acids or preloaded with 0.2 mM histidine for 48 hours and replenished with DMEM. **(A)** Representative IF images of nuclear BrdU in MYAZ16.1e cells were replenished with DMEM for 24 hours and cultured with 10 μM BrdU for 1 hour. Scale bar, 200 μm. **(B)** Quantification of panel A, 5 randomly selected regions were imaged and analysed by ImageJ for 3 independent replicates (one-way ANOVA with Tukey correction, ****p≤0.0001). **(C)** MYAZ6.6g, -12.3i, and -16.1e were replenished with DMEM for 15 hours and cultured with 10 μM BrdU for 1 hour. Cells were stained for BrdU and with PI and the percentage of cells in each phase of the cell cycle was quantified via flow cytometry as shown in panel C. two-way ANOVA with Tukey correction, representative of 3 biological replicate. **(D)** Confluency of DMEM replenished MYAZ cell lines preloaded with the indicated concentrations of histidine for 48 hours, normalized to confluency at the time of replenishment. Representative of 3 biological replicates. A non-linear Gompertz growth curve was applied. Statistical analysis was a two-way ANOVA with Dunnett correction. All data represented as mean ±s.d.

## 5.6 Assessing histidine exchange in tumours.

To confirm the role of histidine as the primary LAT1 exchange substrate in Myc-driven MGTs, I attempted to mimic preloading experiments *in vivo*. Since no previous studies have used labelled histidine to preload tumour cells *in vivo* we conducted a pilot study to determine whether we could effectively increase the total

abundance of histidine in tissues of wild-type fasted mice. In the pilot study, wild-type FVB/N mice were divided into control, oral gavage (OG), and IV groups (Figure 5-19A). All mice were fasted overnight for 12 hours and provided with drinking water supplemented with1.05 mg/mL [U-$^{13}$C]-histidine. The oral gavage and IV group also received a single bolus of 0.15 mg/gBW [U-$^{13}$C]-histidine at the start of the fasting period via oral gavage and IV injection, respectively (Figure 5-19A). Blood serum was collected before the bolus and intermittently throughout the 12-hour fasting period. After 12 hours, the lungs, liver, NMG, and serum were collected (Figure 5-19A). During this fasting period, we observed a significant decrease in serum methionine and threonine; however, after 8 hours of fasting, the levels of these metabolites began to increase (Figure 5-19B, C). Conversely, overnight fasting significantly increased serum BCAA levels (Figure 5-19D-F). These results agree with a study in humans, which observed increased concentrations of leucine and valine and decreased concentrations of methionine and threonine in serum from humans following 48 hours of fasting[353].

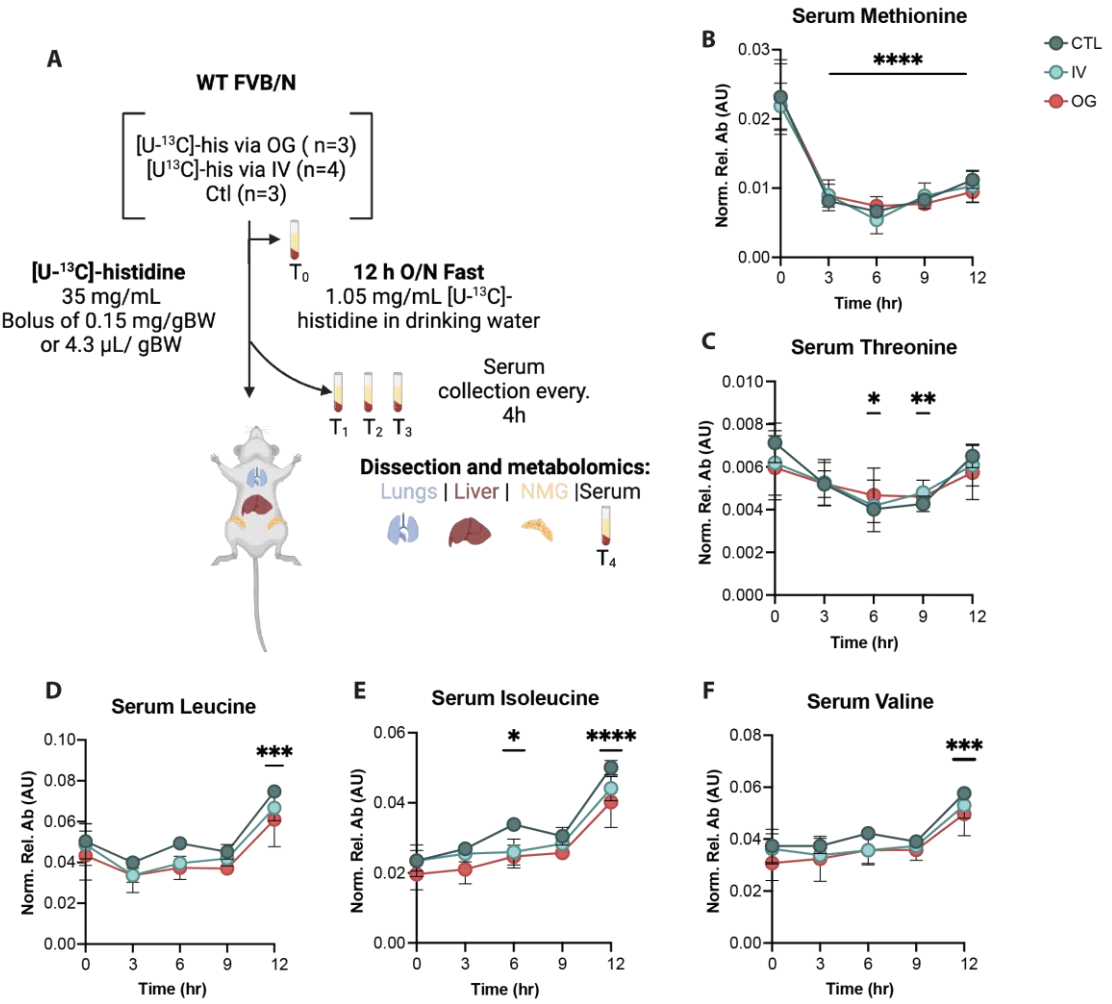



**Figure 5-19. Overnight fasting in mice results alters amino acid profiles in serum.** **(A)** Schematic of experimental strategy of [U-$^{13}$C]-histidine administration in mice fasted overnight. **(B-F)** LC-MS analysis of serum abundance of indicated amino acids every 3 hours in control (n=3), oral gavage (OG, n=3) and intravenously (IV, n=4) administered [U-$^{13}$C]-histidine. Data are presented as mean ± s.d.; two-way ANOVA with Dunnett correction. *p≤0.05,**p≤0.01, ***p≤0.001, ****p≤0.0001.

The abundance and enrichment of histidine were quantified in serum and tissues to determine whether there was a significant accumulation of histidine from either a bolus or drinking water during this period. Intravenous injection achieved a significantly increased concentration of histidine in the serum compared to the control and OG-treated mice at 3 hours, which subsequently declined (Figure 5-20A). Similarly, increased enrichment of $^{13}$C-histidine was observed in IV bolused mice at 3 hours (Figure 5-20C). In contrast, no differences in histidine levels were observed in any of the tissues, MFP, liver, or lung. However, OG and IV boluses resulted in slight but improved enrichment of histidine in tissues compared to

control mice who were only administered [U-$^{13}$C]-histidine in drinking water (Figure 5-20B D). These results suggest that a single histidine bolus cannot increase tissue histidine accumulation.

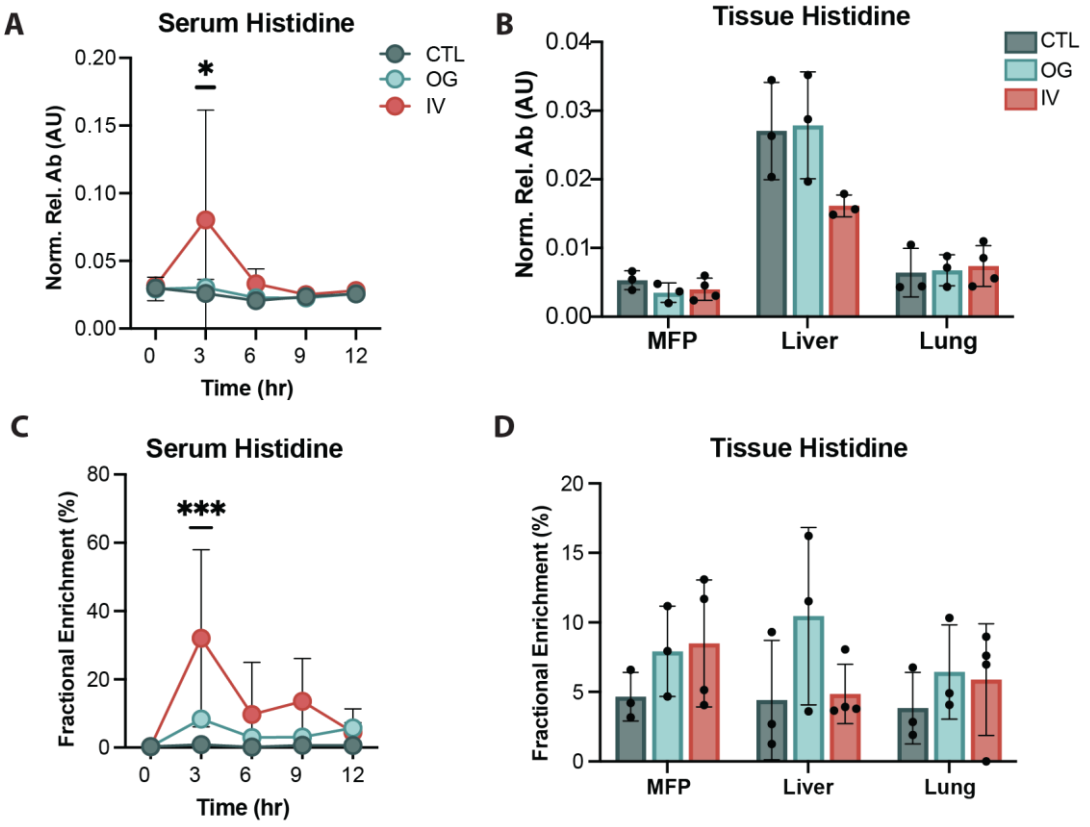



**Figure 5-20. A single bolus of histidine is unable to increase histidine levels in fasted mice.**
LC-MS analysis of serum and tissue from mice fasted overnight that received [U-$^{13}$C]-histidine through drinking water alone (ctl, n=3), OG (n=4), or IV (n=4) administration. **(A)** Serum abundance of histidine every 3 hours during overnight fasting period. **(B)** Total abundance of histidine in tissues collected at the end of the 12 hour fasting period. **(C)** $^{13}$C-enrichment of histidine in the serum every 3 hours during overnight fasting period.**(D)** $^{13}$C-enrichment of histidine n tissues collected at the end of the 12 hour fasting period. All data are presented as mean ± s.d.; two-way ANOVA with Dunnett correction. *p≤0.05, ***p≤0.001.

To evaluate whether we could improve histidine accumulation, we repeated this experimental design in tumour-bearing mice. We compared subcutaneous (SQ), intraperitoneal (IP), and IV histidine boluses, which were administered at regular intervals throughout the 12-hour fasting period, in line with maximum dosing volumes and frequencies outlined in our PPL (Figure 5-21A).

Furthermore, fasted mice were compared to mice fed *ad libitum*. Blood serum was

only collected at the beginning and end of the fasting period to avoid disturbing the mice frequently during their dark cycle. At the endpoint, muscle, liver, MGT, and serum were collected (Figure 5-21A). In line with previous research, the body weight of mice at the end of fasting was significantly lower than at the start, whereas mice fed *ad libitum* maintained weight throughout their dark cycle (Figure 5-21B, C). The amount of weight loss observed in mice after 12 hours of fasting is dependent on strain and gender; however, FVB/N males who fasted for 12 hours were found to lose 12% of their body weight [354,355]. In contrast, we only observed a 1.14 g body weight loss on average, accounting for an average of 5.6% loss in body weight. We then quantified the serum and tissue concentrations of amino acids using LC-MS. In the control mice fed *ad libitum*, the levels of every amino acid increased in the serum as expected (Figure 5-21D). Surprisingly, we observed an overall increase in many amino acids in the fasted cohort. In line with the pilot study, significant increases in serum BCAAs were observed (Figure 5-21E). However, in contrast to previous results, decreased levels of methionine and threonine were not observed. Only glutamine serum concentrations were significantly reduced after 12 hours of fasting (Figure 5-21E). Comparing the serum levels of fed and fasted mice at the end of the dark cycle, we observed decreased levels of many amino acids; however, no significant differences were observed (Figure 5-21F). Quantification of amino acid levels across the tissues collected revealed tissue-specific changes. In the MGT, the abundance of most amino acids are reduced compared to fed mice (Figure 5-21G).This is similar to what is observed in the serum of fasted mice compared to fed mice, which suggests that the changes observed in the MGT recapitulate the changes observed in the serum and likely reflect nutrient availability in the TME. Indeed, the abundance of amino acids in the TIF reflected dietary changes in lung adenocarcinoma and pancreatic ductal adenocarcinoma xenografts[430]. Unlike the MGT, the abundance of amino acids in the livers of fasted mice is more heterogeneous, with reductions in asparagine and alanine levels and an increase in the levels of glutamate and serine (Figure 5-21H). In contrast, significant increases in many amino acids are observed in the skeletal muscle. Indeed, levels of many EAAs are significantly increased (Figure 5-21I). Significant increases in BCAAs, methionine, phenylalanine, and tryptophan were observed (Figure 5-21I). Increases in NEAAs, asparagine, glutamate and proline were also observed. Muscles serve as the body's primary

reservoir for amino acids, releasing them during periods of need, such as fasting or starvation [356,357]. These data reflect system wide changes expected due to overnight fasting. Nevertheless, the decrease in amino acid levels in the MGT is similar to those observed in the *in vitro* amino acid starvation experiments, suggesting that overnight starvation could facilitate histidine preloading. This provides the necessary conditions to evaluate whether the role of histidine observed *in vitro* is replicated in tumours.

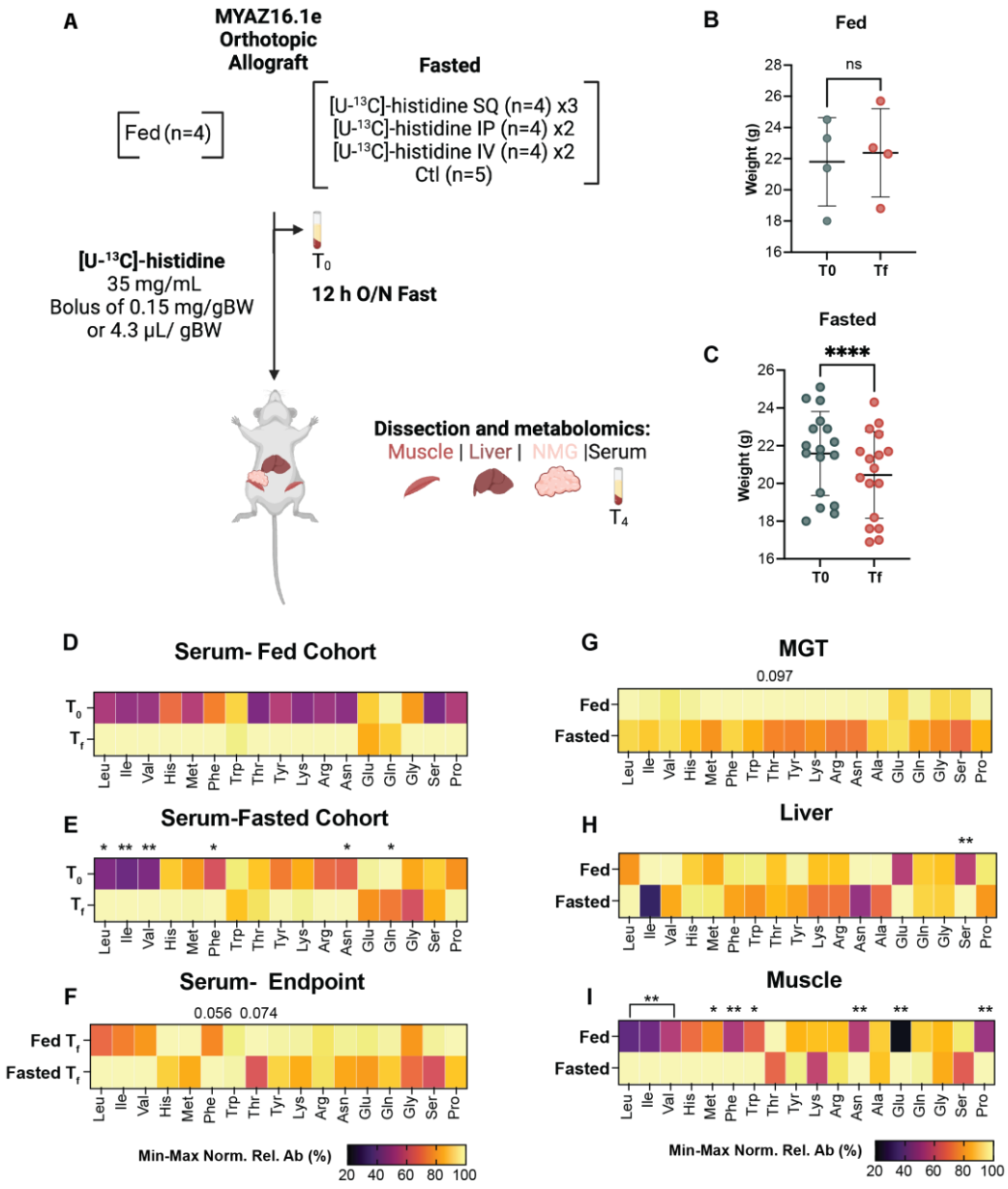



**Figure 5-21. Similar metabolic changes are observed in fasted tumours and amino acid starved tumour cells.**

**(A)** Schematic of experimental strategy: mice with MYAZ16.1e mammary tumours were fed *ad libitum* or fasted overnight for 12 hours with or without [U-$^{13}$C]-histidine administration as indicated. **(B-C)** Body weight of **(B)** fed (n=4) and **(C)** fasted (n= 17) mice at the start and end. Data presented as mean ± s.d. **(D-I)** LC-MS analysis of amino acid levels in serum and tissues. Heatmaps show the mean total abundance of indicated amino acid and colour scale represents the min-max normalized values for each individual amino acid: total abundance of serum amino acids in the **(D)** fed cohort and **(E)** fasted ctl cohort (n=5) at the beginning ($T_o$) and end ($T_f$) of 12 hours (multiple paired t-tests with Holm-Šídák correction, *p<0.05, **p<0.01), and **(F)** normalized total abundance in fed or fasted mice at the end ($T_f$) of 12 hours. **(G-I)** normalized abundance of amino acids in tissues of ctl (n=4) and fasted-ctl (n=5) mice (multiple paired t-tests with Holm- Šídák correction, *p≤0.05, **p≤0.01).

We assessed whether the new strategy of histidine administration (Figure 5-22A) was sufficient to increase the abundance of histidine in the MGT. Intravenous administration of histidine significantly increased the total abundance of histidine in the MGT and muscle but not the liver (Figure 5-22A-C). Indeed, IV histidine boluses led to a 2-fold increase in histidine abundance compared to fasted MGTs (Figure 5-22A). Significant increases in enrichment of $^{13}C$ in histidine were observed for all tissues for each administration route, with no significant differences detected between the routes, indicative of rapid equilibration of histidine in the tumour (Figure 5-22D-F). Therefore, this provided the conditions necessary to assess whether increased histidine accumulation in the tumour could replenish amino acid pools and increase mTORC1/4E-BP1 activity as observed *in vitro*. We then assessed mTORC1 signalling to ensure fasted tumours had decreased mTORC1 activation. Surprisingly, all tissues could maintain phosphorylation of RPS6 despite decreases in amino acid availability observed within the MGT (Figure 5-22G-I). After these initial attempts to optimise histidine preloading *in vivo*, we decided to discontinue this line of investigation due to challenges in achieving the necessary conditions that recapitulate the *in vitro* experiments. Longer-term fasting may be required for mTORC1 inhibition; however, given the high cost associated with sustained [U-$^{13}C$]-histidine administration, it was decided first to pursue a more controlled experimental strategy.

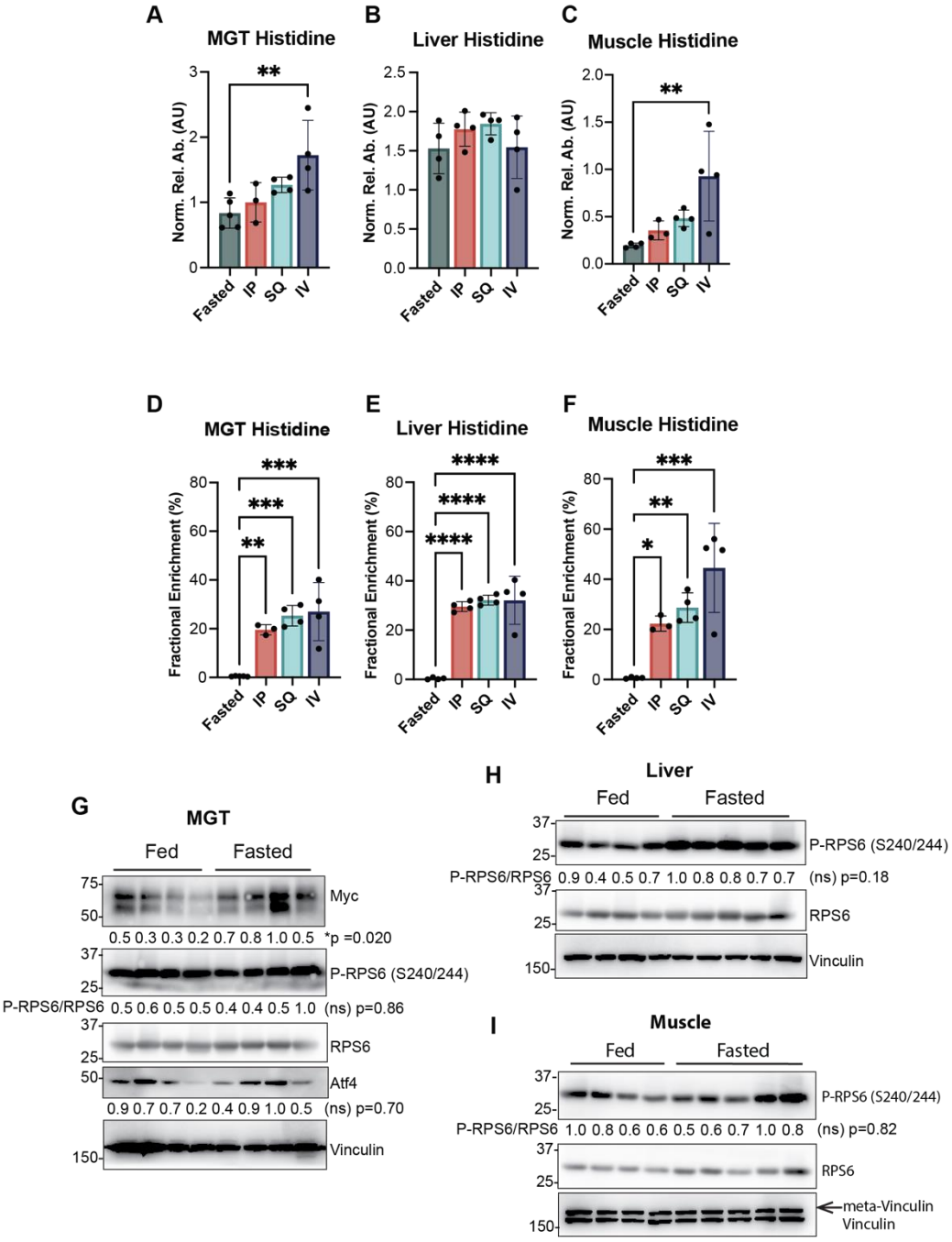



**Figure 5-22. mTORC1 signalling was unaffected in fasted mice.**
FVB/N mice with MYAZ16.1e mammary tumours were fasted overnight with [U-$^{13}$C]-histidine administered via IP (n=4), SQ (n=4), or IV (n=4) injection, or unbolused (n=5). LC-MS analysis of histidine in indicated tissues: **(A-C)** normalized total abundance of histidine in each tissue for each cohort. **(D-F)** $^{13}$C enrichment of histidine in each tissue for each cohort. Data are presented as mean ± s.d.; one-way ANOVA with Dunnett correction (*p≤0.05, **p≤0.01, ***p≤0.001, ****p≤0.0001). **(G-H)** WB of tissues from fed (n=4) or fasted-ctl (n=5) cohorts. Protein expression was normalized to vinculin, and min-max normalized. Unpaired two-tailed t-test.

We next sought to evaluate histidine exchange in an *ex vivo* tumour slice culture system. Tissue slices from fresh MMTV-Myc MGT were prepared and cultured as described and detailed in the Materials & Methods chapter (Figure 5-23A). After 24 hours of acclimation, tumour slices were starved of amino acids in the presence or absence of 1.6 mM histidine for indicated times and replenished with complete DMEM for 1 hour. Ten minutes before collection, tumour slices were administered 10 µg/mL puromycin. Protein lysates were prepared for western blot analysis. We assessed mTORC1 signalling in the *ex vivo* tumour slice culture by evaluating Rps6 and 4e-bp1 phosphorylation. Like 2D cell culture experiments, amino acid starvation reduced mTORC1 activity at 24 and 48 hours of starvation compared to control cells cultured in amino acid-replete conditions (Figure 5-23B). Furthermore, replenishing tumour slices reactivated mTORC1 signalling, as expected (Figure 5-23B). Notably, after 1 hour of replenishment, histidine-preloaded tumour slices had increased levels of phosphorylated 4e-bp1, as was observed in tumour cell lines preloaded with histidine (Figure 5-23B). This correlated with increased puromycin incorporation in histidine-preloaded tumour slices (Figure 5-23B). No significant differences were observed in Rps6 phosphorylation across conditions. However, differences may be observed at earlier time points of replenishment. As seen in cell experiments, amino acid-starved cells had increased Myc levels compared to histidine-preloaded cells; however, following 60 minutes of replenishment, these levels were more similar (Figure 5-23B). We may see these differences maintained at early time points of replenishment. As mentioned in previous chapters, MMTV-Myc tumours have significant intratumour heterogeneity; therefore, the cellular composition of each tumour slice could vary. To circumvent this possibility, three slices from the same tumour were combined per sample; however, I cannot negate the possibility that variations in Myc levels could exist at the initiation of starvation and could affect the results observed. Notably, while we observe an increase in puromycin incorporation after replenishment in histidine-preloaded cells, the opposite is true of amino acid-starved cells (Figure 5-23B). Indeed, greater puromycin incorporation was observed at 24 and 48 hours of starvation than after 1 hour of amino acid replenishment (Figure 5-23B). This could suggest underlying differences in the tumour slices across each condition. Furthermore, the lack of puromycin incorporation in control slices cultured in amino acid-replete conditions indicates a technical error (Figure 5-23B). Given similar

findings in the tumour slice culture system compared to tumour cell lines, histidine exchange was interrogated via LC-MS analysis. Tumour slices were prepared from three individual MMTV-Myc MGTs, and histidine preload conditions were achieved as previously described. Three technical replicates were combined per condition for each biological replicate. Like cells, supplementation of 1.6 mM histidine during starvation significantly increased intratumoural histidine levels. However, an insignificant decrease in histidine levels was observed following replenishment with histidine-free DMEM (Figure 5-23C). Notably, this is due to one tumour with increased histidine levels observed following amino acid replenishment (Figure 5-23C). This highlights a requirement for a greater sample number. However, despite this increase in histidine availability, increased uptake of high-affinity LAT1 substrates such as leucine was not observed (Figure 5-23D). Furthermore, no significant differences were observed in the net uptake of EAAs or NEAAs in amino acid-starved or histidine-preloaded cells (Figure 5-23E, F). Due to the variability observed between tumours, further optimisation with increased tumour sample size would be necessary to determine whether histidine is a bidirectional LAT1 substrate in tumours *in vivo*.

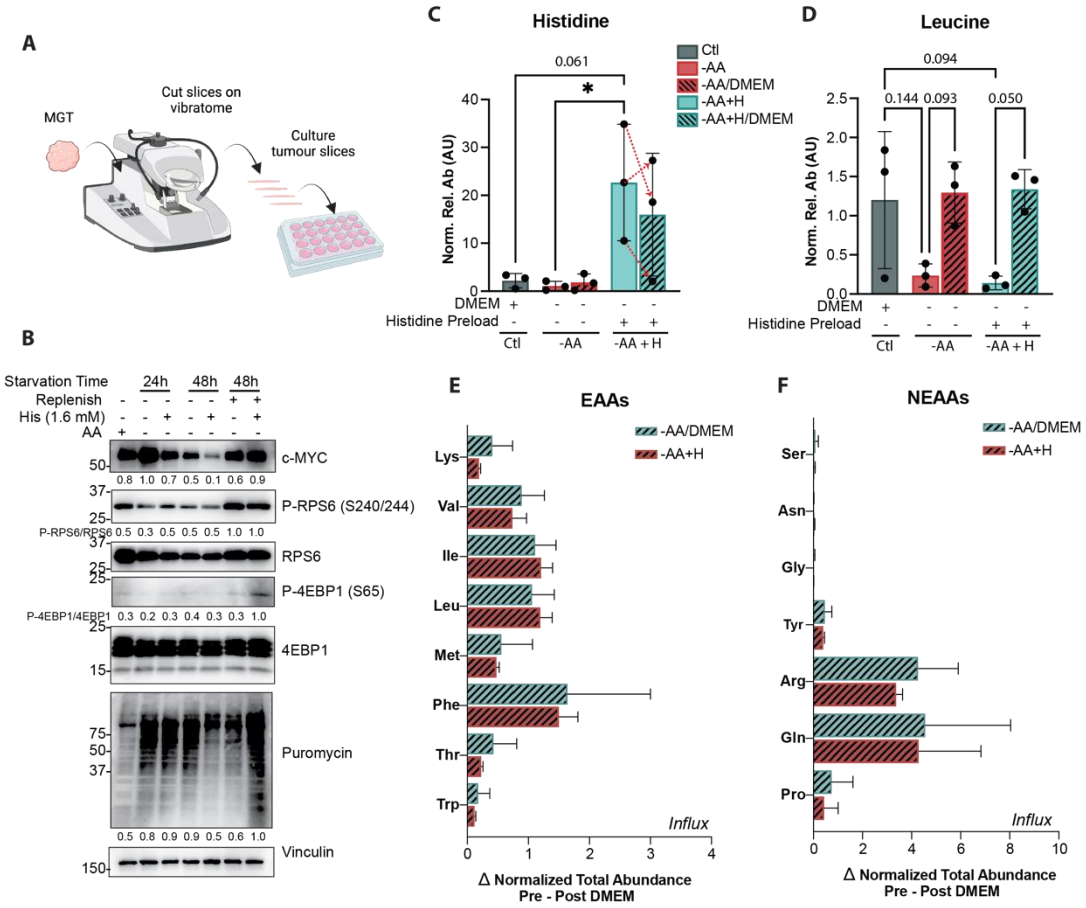



**Figure 5-23. Histidine availability enhances mTORC1/4E-BP1 signalling and protein translation in MGT *ex vivo* cultures.**
**(A)** Schematic of tumour slice preparation. **(B)** WB of MMTV-Myc tumour slices starved of amino acids or preloaded with 1.6 mM histidine for 24 or 48 hours. Tumolur slices that were cultured in these conditions for 48 hours were then replenished with DMEM for 1 hour. Protein quantification was normalized to vinculin and min-max normalized. Three tumour slices were grouped in each lysate. **(C-F)** LC-MS analysis of tumour slices starved of amino acids or preloaded with 1.6 mM histidine and replenished for 10 minutes with DMEM. Data represent 3 biological replicates (MMTV-Myc MGTs) each with 3 tumour slices combined. **(C-D)** intracellular total abundance of **(C)** histidine and **(D)** leucine (one-way ANOVA with Šídák correction, *p≤0.05). **(E-F)** The relative influx of indicated amino acids. The x-axis represents the net influx, calculated as the difference in total abundance after replenishment and before replenishment (two-way ANOVA with Šídák correction). All data are presented as mean ± s.d.

Given the identified role of histidine as the preferred bidirectional LAT1 substrate in tumour cells *in vitro* over glutamine, if histidine were exchanged within tumours, we would expect an accumulation of histidine upon Lat1 KO. Therefore, we generated inducible Lat1 KO MYAZ16.1e cells using the lentiviral guide system described in BT-549 cells above. Several clones with Lat1 KO were confirmed via western blot

(Figure 5-24A). Inhibition of Lat1 via JPH203 in MYAZ16.1e cells results in a significant decline in the rate of proliferation (Appendix 9). Therefore, we hypothesised that KO of Lat1 would lead to a significant decrease in proliferation in all the clones tested. Therefore, proliferation was compared in dox-on and dox-off conditions in clones 1,3 and 4. Lat1 KO in clones 1 and 3 significantly decreased the proliferation rate (Figure 5-24B, C). In contrast, a significant increase in proliferation was observed in clone 4 (Figure 5-24D). To confirm functional Lat1 KO, several clones were starved of leucine for 24 hours before administration of [U-$^{13}$C]-leucine for 10 minutes. Decreased leucine uptake was observed across all clones, suggesting leucine uptake was impacted due to Lat1 knockout (Figure 5-24E). Given that cells were starved of leucine before leucine administration, both dox-on and dox-off cells had similar enrichment in leucine (Figure 5-24F). Further investigation confirmed a significant decrease in leucine abundance and enrichment in clones 1 and 3 upon doxycycline administration compared to dox-off cells and MYAZ16.1e cells transduced with the Cas9 vector and an empty guide cassette (Figure 5-24G, H). This was consistent with an overall decrease in each Lat1 substrate in dox-on cells, except for histidine, the only Lat1 substrate that increased in clone 3 (Figure 5-24I). However, histidine levels did not significantly increase in clone 3, as would be expected if cells used histidine as an exchange substrate (Figure 5-24B). Similarly, no differences were observed in the intracellular levels of tyrosine or glutamine, the other lower-affinity bidirectional Lat1 substrates (Figure 5-24K, L). This lack of accumulation could be due to a sustained demand for EAAs, such as histidine for protein translation and overall cellular compensation to maintain histidine homeostasis. Since histidine is the only Lat1 substrate in clone 3 observed at increased levels upon Lat1 KO, it supports the hypothesis that it is an exchange substrate. Notably, although there was a significant reduction in leucine uptake in clone 4, the levels of amino acids differ in clone 4 compared to the ctl and clone 3 cells (Figure 5-24I). Indeed, the significantly reduced glutamine levels in dox-off clone 4 cells suggest that this clonal population may exhibit distinct compensatory mechanisms and altered amino acid metabolism compared to the ctl cells (a batch population of MYAZ16.1e cells expressing an empty guide cassette) and clone 3. Considering that the dox-off state of clone 4 is significantly different than that of the batch population the clone was derived from, alterations or adaptations may have occurred during clonal

selection. In support of this, dox-induced KO of Lat1 in this clonal population did not lead to a proliferative decline as observed in clone 3 (Figure 5-24D). Therefore, we injected clones 1 and 3 into FVB/N mice to interrogate the role of histidine in Lat1-mediated uptake of EAAs.

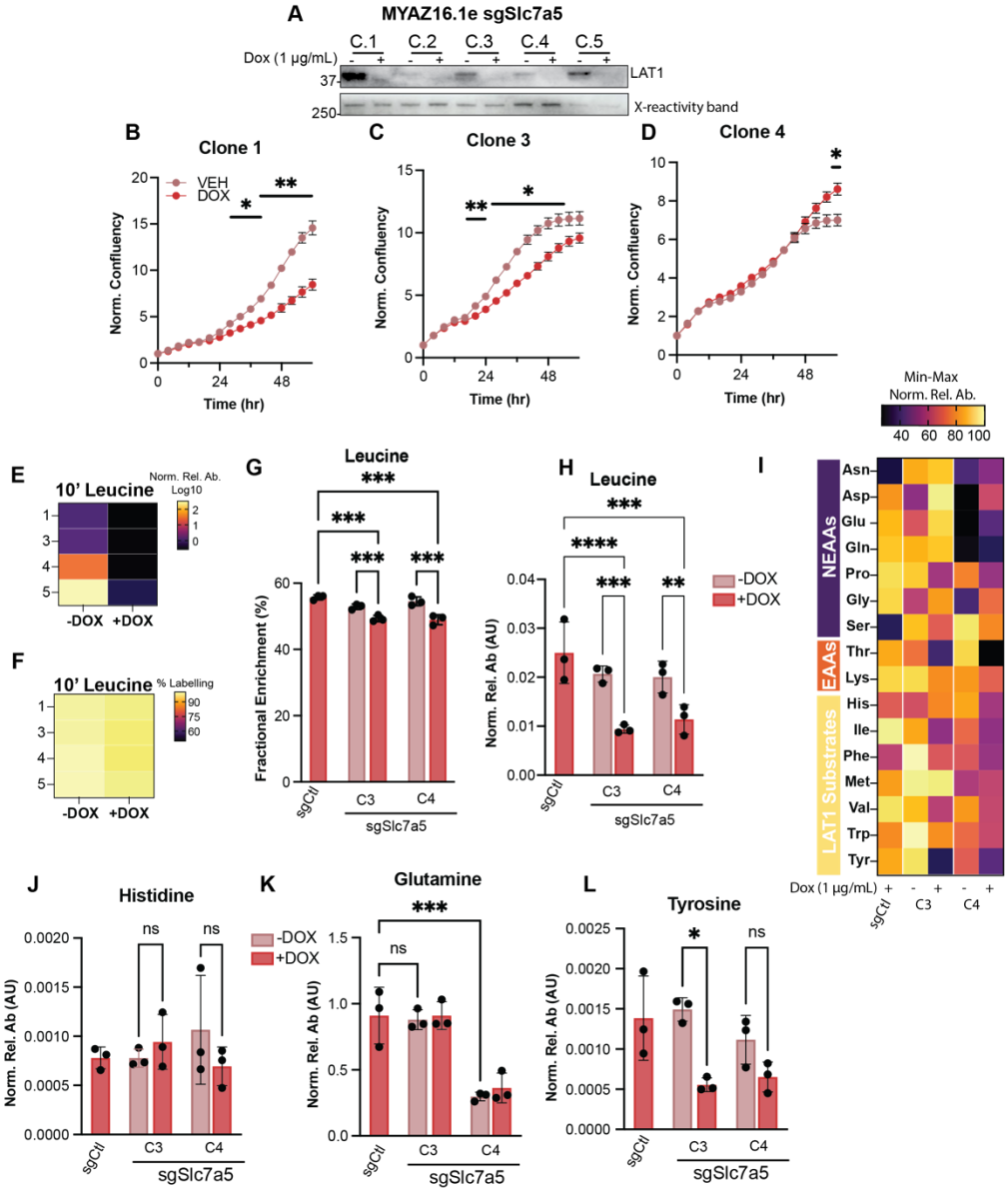



**Figure 5-24. LAT1 KO cells have reduced leucine uptake and proliferation.** MYAZ16.1e clones with doxycycline inducible knockout of Slc7a5/Lat1. All clones were administered 1 µg/mL doxycycline for 48 hours. **(A)** WB of Lat1 protein expression in several tested clones. The loading control is a cross-reactivity band for Lat1. **(B-D)** Normalized confluency in three tested clones. Confluency was measured every 4 hours and normalized to the starting confluency at 0 hr (repeated measures two-way ANOVA with Geisser-Greenhouse correction and Šídák for multiple comparisons). **(E-F)** heatmap of average leucine **(E)** abundance and **(F)** $^{13}C$ enrichment in indicated sgSlc7a5 clones starved of leucine for 24 hours and then administered 0.8 mM [U-$^{13}C$]-leucine for 10 minutes. The colour scale represents log10 transformed values. Representative of 1 replicate. **(G-L)** sgSlc7a5 clones 3 and 4 were cultured in the presence or absence of doxycycline for 48 hours and administered 0.8 mM [U-13]-leucine for 10 minutes: **(G)** $^{13}C$ enrichment of leucine, **(H)** total abundance of leucine, and **(I)** heatmap of mean total abundance of indicated amino acids. Colour scale represents min-max normalized values for each amino acid. **(J-L)** total abundance of **(J)** histidine, **(K)** glutamine, and **(L)** tyrosine. Data are presented as mean ± s.d. One-way ANOVA with Tukey correction. *p≤0.05, **p≤0.01, ***p≤0.001, ****p≤0.0001.

Orthotopic MGT allografts were generated by injecting cells into the mammary fat pad of Nod-SCID mice. The injected cells included: i) parental, ii) empty sgRNA vector (sgCtl), iii) clone 1 (C1) and iv) clone 3 (C3) (Figure 5-25A). After ten days, when tumours were palpable, mice were put onto a standard control or a 0.625 g/Kg doxycycline diet fed *ad libitum* (Figure 5-25A). Tumour growth was monitored until most mice reached a tumour volume of 500 $mm^3$ (Figure 5-25A). After this, the MGT and blood serum were collected for further analysis. *In vivo,* clone 1 grew slower than the dox-fed mice with parental and sgCtl tumours (Figure 5-25B, C). Furthermore, no differences were observed in tumour growth or final tumour weight (Figure 5-25B, C). In contrast, as expected, control-fed mice bearing C3 tumours increased at a rate similar to that of dox-fed parental and sgCtl tumours. When mice bearing C3 tumours were fed a dox diet, tumours grew slower (Figure 5-25B). However, at collection, there was no significant difference in tumour weight (Figure 5-25C). This agreed with *in vitro* results; while induction of Lat1 KO in clone 3 resulted in retarded proliferation, it did not ablate proliferation (Figure 5-24C). This was also observed upon Lat1 inhibition in the parental cell line (Appendix 9). Thus, highlighting the robust compensatory mechanisms in cells and tumours when Lat1 function is disrupted. Indeed, LAT2, which has broad tissue expression, is also expressed in tumours and shares overlapping substrate specificity with LAT1, including a higher affinity for glutamine. It is possible that LAT2 is upregulated in these tumours and compensates for LAT1 function[358]; however, this was not investigated in our study. Before conducting metabolomics analysis, we assessed Lat1 protein levels in these tumours to confirm efficient Lat1 KO. Lat1 expression was similar in parental and sgCtl tumours from dox-fed mice (Figure 5-25D). However, Lat1 protein expression was visible in C1 tumours from mice fed a dox diet, although significantly reduced compared to dox-fed sgCtl tumours (Figure 5-25E, F). Notably, Lat1 expression was decreased in C1 tumours from mice fed a control diet, compared to sgCtl tumours, suggesting that this system may be leaky *in vivo* (Figure 5-25E, F). Interestingly, despite the insufficient KO of Lat1, there was a significant increase in Atf4 expression in dox-diet C1 tumours compared to sgCtl tumours (Figure 5-25E, F). Therefore, the control-fed C1 tumours may grow slower than parental and sgCtl tumours due to a reduction in Lat1 protein expression. However, when assessing Lat1 protein expression in C3 tumours, a significant decrease in Lat1 protein expression was observed in dox-fed and

control-fed mice compared to sgCtl tumours (Figure 5-25G, H). Furthermore, while there was an insignificant reduction in phosphorylation of 4e-bp1, a significant decrease in Rps6 phosphorylation was observed in C3 tumours from dox-fed and control-fed mice (Figure 5-25G, H). However, only C3 tumours from dox-fed mice had higher Atf4 protein expression than sgCtl and control-diet C3 tumours (Figure 5-25G, H). However, in contrast to the tumour growth trends observed in C1 dox- and control-fed mice, C3 tumours grew at a similar rate to WT and sgCtl tumours (Figure 5-25B, C). Due to inefficient LAT1 KO *in vivo,* we decided not to proceed with a thorough investigation of these tumours. Indeed, even in the absence of doxycycline, there was a significant reduction in the expression of Lat1, similar to the levels achieved in the doxycycline-treated groups. Given the time constraint and the need to prioritise other approaches, I chose not to continue with further metabolic analysis of these tumours.

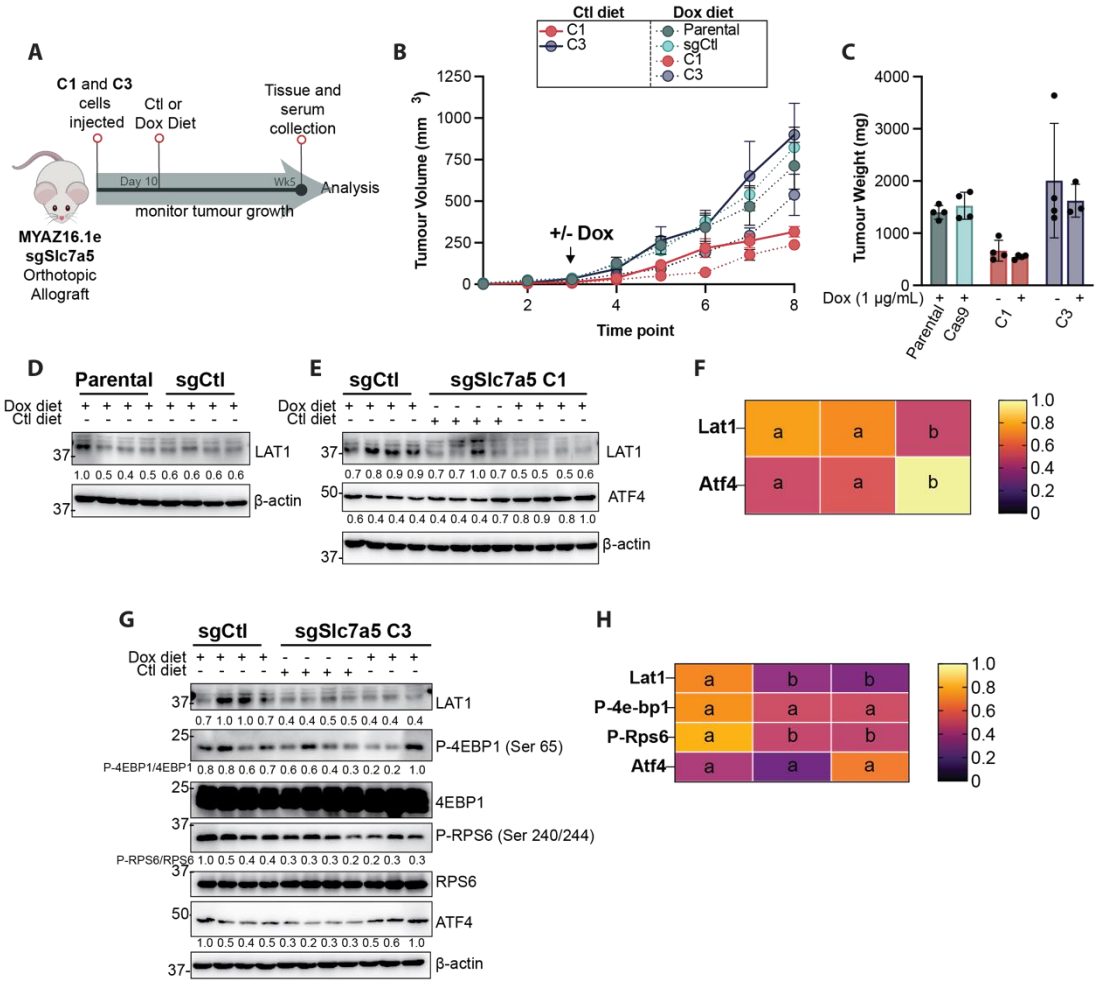



**Figure 5-25. LAT1 was not knocked out efficiently in vivo**
**(A)** Schematic of experimental timeline. FVB/n mice were injected with MYAZ16.1e sgSlc7a5 clones 1 (C1) and 3 (C3), wild-type (Parental), or expressing an empty sgRNA cassette (sgCtl), and put on a control (C1: n=4, C3: n=3) or doxycycline-containing (C1: n=4, C3: n=3, Parental: n=4, sgCtl: n=4) diet 10 days after injection. Tumour growth was monitored for 5 weeks and the MGT and serum were collected at the end. **(B)** Tumour volume over time (data presented as mean ± s.d.; repeated measures two-way ANOVA with Geisser-Greenhouse correction and Dunnett test for multiple comparisons). **(C)** Tumour weight at collection (data presented as mean ± s.d.; one-way ANOVA with Dunnett test). **(D)** WB of LAT1 expression in parental or sgCtl MGTs. **(E)** WB of LAT1 and ATF4 expression in sgCtl and C1 (dox-on and dox-off) MGTs. **(F)** Heatmap showing average normalized protein expression from panel E, letters represent statistically significant differences from sgCtl MGTs. P-values are as follows: LAT1: p=0.013; ATF4= p<0.0001 (two-way ANOVA with Tukey). **(G)** WB of LAT1, ATF4 and mTORC1 protein expression. **(H)** Heatmap showing average normalized protein expression from panel G. Letters represent statistically significant differences from sgCtl MGTs. P values are as follows: LAT1: p=0.0243, p=0.0159; P-Rps6: p=0.0339, p=0.0394. All proteins were normalized to β-actin expression.

Together, these attempts at assessing the importance of histidine as a Lat1 exchange substrate within tumours were unsuccessful. The *ex vivo* tumour slice

culture system provides a promising avenue to confirm the role of histidine in Lat1 exchange and mTORC1/4E-BP1 signalling in a model that more closely recapitulates the TME. Further work optimising experimental conditions with increased sample sizes will be necessary to validate *in vitro* results.

## 5.7 Discussion

As mentioned, LAT1-mediated uptake of EAAs, such as leucine, depends on coupling with the glutamine transporter ASCT2[142]. Fifteen years ago, Nicklin *et al.* (2009) showed that glutamine imported via ASCT2 was subsequently used for exchange through LAT1, essential for leucine uptake and mTORC1 signalling. However, preincubation experiments were done using 10 mM of glutamine, which is significantly higher than physiological serum levels. Therefore, this increase in glutamine availability could support glutamine catabolism and facilitate LAT1-mediated uptake of EAAs, but it may not be physiologically relevant. Indeed, ASCT2 KO was shown not to affect LAT1-activity in cancer cell lines [148]. In this chapter, our results confirm that histidine, rather than glutamine, is used as the primary LAT1 exchange factor in Myc-driven cancer cells. While our preincubation experiments initially used a supraphysiological (1.6 mM) concentration of histidine to assess the role of histidine as a LAT1 exchange substrate, further experiments under physiological histidine and glutamine concentrations were used to confirm this preference. Importantly, we observe that histidine-mediated LAT1 activity promotes activation of the mTORC1/4E-BP1 signalling axis, rapidly increasing global protein translation and promoting cellular proliferation. In contrast, when cells are starved of amino acids without histidine preload, there is increased asparagine release due to proteasomal degradation, and subsequently used for amino acid transport. Furthermore, these cells had enhanced mTORC1/RPS6 activation compared to histidine-preloaded cells, increased Myc protein and mRNA expression, and increased expression ribosomal biogenesis genes. Therefore, histidine availability under nutrient scarcity was sufficient to alter mTORC1 activity in response to AA availability. These results suggest that cancer cells that can accumulate more histidine have a survival advantage during nutrient scarcity, acting to improve the uptake of EAAs required for cellular proliferation and rapidly initiate protein translation.

One of the more surprising aspects of this chapter was enhanced activation of the mTORC1/4E-BP1 axis but reduced activation of mTORC1/RPS6 signalling. There are several reasons why this may occur. While RPS6 is directly downstream of the mTORC1 target, S6K1, it is also activated by various factors. Indeed, a published siRNA screen revealed 632 validated regulators of RPS6 phosphorylation[359]. Many of these were determined to be regulators of mTORC1 signalling. Intriguingly, the glutamine tRNA synthase (QARS) was observed to inhibit RPS6 phosphorylation in an mTORC1 dependent manner. Depletion of QARs significantly inhibited amino acid-stimulated RPS6 phosphorylation in several cancer cell lines. However, the exact mechanisms of this repression remain to be determined [359]. In our data, glutamine uptake was significantly increased in amino acid starved compared to histidine-preloaded BT-549 cells, consistent with increased RPS6 phosphorylation. In contrast, enhanced RPS6 activity or increased glutamine was not observed under amino acid starvation in MDA MB 231. Therefore, when glutamine is available to bind QARs, it may no longer inhibit the phosphorylation of RPS6, which could account for the increased RPS6 phosphorylation observed. However, this remains to be elucidated. Another possibility is that depending on the availability of amino acids, mTORC1 could be differentially activated. For example, glutamine and asparagine were found to activate mTORC1 independent of Rag GTPase activity and instead depend on the small GTPase, Arf1, for mTORC1 activation [360,361]. The data presented here showed a significant increase in leucine uptake in histidine-preloaded cells compared to starved cells and previous investigations have demonstrated that leucine was crucial for 4E-BP1 phosphorylation [362]. In support of this, LAT1 KO, which ablated leucine uptake in histidine-preloaded cells, attenuated mTORC1/4E-BP1 activation. Therefore, while maximal phosphorylation of 4E-BP1 is observed in the presence of all EAAs, leucine alone is sufficient for 4E-BP1 phosphorylation[362]. This contrasts with S6K1, which is stimulated by several amino acids[360]. Therefore, the mTORC1/S6K1/RPS6 pathway may respond to the availability of several individual amino acids (i.e., glutamine, leucine, arginine, histidine, serine, valine, methionine, alanine, asparagine, cysteine and threonine), whereas mTORC1/4E-BP1 signalling could be activated as a response to increases in the availability of specific amino acids, such as leucine. Notably, in a previous study using *Drosophila* models of neural tumourigenesis, including *nerfin-*

*1* and *Propspero* mutant clones in the CNS, dietary histidine was explicitly required for *nerfin-1* mediated dedifferentiation in a Myc-dependent manner[261]. In contrast, *Prospero* mutant clones, which do not depend on Myc for dedifferentiation, were relatively insensitive to histidine availability. Importantly, this study found that the growth of *nerfin-1* mutant clonal growth depended on 4E-BP but not S6K1, whereas the opposite trend was observed in *Prospero* mutant clones[261]. Therefore, neural lineages highly sensitive to dietary histidine availability (*nerfin-1* mutant clones) demonstrate a vital requirement for Myc- and eiF4E- mediated cellular growth. These data underscore that i) the intracellular milieu could differentially activate mTORC1 signalling, and ii) histidine availability primes Myc-driven cancer cells for increased activation of 4E-BP1, leading to a rapid increase in global protein translation. Given the critical role of 4E-BP1 in Myc-driven tumourigenesis[347], this relationship between histidine and 4E-BP1 warrants further investigation.

Unexpectedly, despite significant increases in EAA uptake, 4E-BP1 inhibition, and global protein translation in histidine-preloaded cells, only a slight, albeit significant, increase in proliferation was observed upon reintroduction of amino acids. One upstream mediator of the ISR is PERK, a key component of the unfolded protein response (UPR) due to the accumulation of misfolded or unfolded proteins in the ER. Aberrant MYC signalling in cancer results in increased protein translation; therefore, activation of PERK in MYC-driven transformation is required to sustain MYC-dependent transformation and tumour growth[363]. Furthermore, concurrent activation of ATF4 by GCN2 and PERK resulted in cooperative transcription of 4E-BP1 alongside MYC[347]. Induction of 4E-BP1 balances protein synthesis by inhibiting protein synthesis, thus relieving proteotoxic stress and sustaining MYC-driven tumourigenesis[347]. In our experiments, an increase in total 4E-BP1 levels was observed in histidine-preloaded cells, which balanced levels of phosphorylated 4E-BP1. Therefore, it is possible that the rapid increase in protein translation observed could lead to increased PERK/eIF2a/ATF4 signalling, 4E-BP1, and subsequent reduction in protein synthesis. While we see an initial increase in protein translation at 30 minutes to 2 hours of amino acid replenishment in cells that accumulate high concentrations of histidine, at 24 hours, these levels were lower than in starved cells or cells preloaded with physiological levels of histidine.

This could indicate that the rapid protein synthesis observed could lead to activation of the UPR. However, further analysis would be necessary to compare the PERK arm of the ISR in amino acid replenished starved and preloaded cells. Therefore, while increased global protein translation may initially provide a proliferative advantage to Myc-driven cancer cells, eventually, this is balanced by 4E-BP1 upregulation.

This chapter shows that MYAZ16.1e, BT-549, and MDA MB 231 cells have significantly increased uptake of EAAs such as leucine. While histidine preload increased mTORC1/4E-BP1 activation in MYAZ16.1e and BT-549 cells, this was not observed in MDA MB 231 cells. MDA MB 231 cells had significantly increased levels of LAT1 substrates such as tryptophan, isoleucine, leucine, phenylalanine, valine, and tyrosine, although to a lesser extent than BT-549 cells. However, MDA MB 231 cells did not accumulate as much histidine as BT-549 cells and only slightly reduced intracellular histidine levels upon nutrient replenishment, as observed in MYAZ16.1e and BT-549 cells. Therefore, it is unclear how preloaded MDA MB 231 cells mediate increased uptake of LAT1 substrates. To better understand the role of histidine in MDA MB 231 cells, it will be crucial to confirm how histidine exchange is affected by LAT1 KO. Notably, BT-549 cells have endogenous amplification of MYC, whereas MDA MB 231 cells do not. As mentioned above, Froldi *et al.* found that Myc levels dictated sensitivity to dietary histidine[261]. *Prospero* mutant clones that did not depend on Myc for dedifferentiation similarly were not sensitive to dietary histidine limitation. In contrast, histidine-sensitive *nerfin-1* clones depend on Myc for growth and dedifferentiation. These clones were also dependent on 4E-BP for growth. Therefore, this could indicate that this requirement for LAT1-mediated histidine exchange for mTORC1/4E-BP1 signalling could similarly depend on MYC for cellular growth and proliferation. Notably, MDA MB 231 cells can proliferate upon MYC knockdown (KD) *in vitro* and *in vivo*, making them more similar to the histidine-insensitive *Prospero* phenotype[364]. This is significant because it indicates that the importance of LAT1 for mTORC1 activation, and thus histidine, may depend on Myc status. Further assessment in cells with Myc ectopic expression will be necessary to confirm this hypothesis.

Of particular importance, in this chapter, we revealed that the concentration of glutamine was significantly lower in the TIF of Myc-driven mammary tumours than in the plasma. In contrast, histidine concentration significantly increased in the TIF relative to the plasma. This results in similar relative concentrations of histidine and glutamine in the TIF and tumour. Given the demand for glutamine catabolism and not histidine catabolism in Myc-driven cancer cells, coupled with increased LAT1 substrate affinity for histidine compared to glutamine, histidine is likely the primary LAT1 substrate in tumours. In cells, we observe that even cells preloaded with 6-fold less histidine than glutamine still preferentially used histidine for exchange through LAT1. We attempted to confirm the role of histidine in LAT1-mediated exchange *in vivo* using [U-$^{13}$C]-histidine preloading experiments and Lat1 KO tumours. Unexpectedly, we demonstrated that mTORC1 signalling was maintained, if not slightly enhanced, in the MGT, liver, and muscle of fasted mice relative to control mice. This contradicts other studies that demonstrated significant attenuation of mTORC1 signalling in livers and muscles following 12-24 hours of fasting in female and male mice[182,365]. In our experiments, mice were overnight fasted on wooden bedding, as they were usually housed. However, a study demonstrated that mice housed with wooden bedding consumed this bedding far more than other types (cellulose or corncob)[366]. Furthermore, all mice housed with or without bedding had a more minor reduction in weight following overnight fasting than mice housed on a metal grid that were prevented from consuming their faeces[366]. Therefore, it is possible that a combination of woodchip bedding and coprophagy could deliver enough sustenance to sustain mTORC1 signalling in the liver.

While significant research efforts have assessed LAT1 requirement in cancer cell proliferation and tumourigenesis, implicating LAT1 in mTORC1 signalling and cellular growth, this data is the first to show a preferential utilisation of histidine as a bidirectional LAT1 substrate in Myc-driven tumour cell lines. Furthermore, we showed differential activation of mTORC1 upon amino acid replenishment in histidine-preloaded cells compared to starved cells, suggesting that amino acid availability could alter downstream mTORC1 pathway activation and function. Histidine preload increased global protein translation, leading to a slight but significant proliferative advantage in Myc-dependent tumour cells. Given the

nutrient gradient often observed in poorly vascularised solid tumours, tumour cells with increased accumulation of histidine could be better suited to maintain EAA pools and protein translation than those less capable. Furthermore, tumour cells with high intracellular levels of histidine may have an improved ability to metastasise and colonise diverse tissue microenvironments and adapt to changes in amino acids available in the extracellular environment. Significantly, a recent study has demonstrated in a CRISPRa screen that aside from *SLC7A5*, overexpression (OE) of *SLC38A3* in cells cultured in low histidine media could rescue proliferation[367]. *SLC38A3* encodes SNAT3, which was thought to facilitate glutamine loading primarily but can also transport histidine and asparagine unidirectionally. However, *SLC38A3* OE did not rescue cells from glutamine limitation, suggesting it may be more critical for histidine loading[367]. Our RNA-seq data from large MMTV-Myc tumours had increased *SLC38A3* expression (Figure 3-1A); therefore, inhibiting SNAT3 could limit histidine accumulation in Myc-dependent tumours; however, SNAT3 inhibitors have not been developed to date. Overall, this data suggests that limiting histidine availability or targeting histidine import could represent a promising therapeutic strategy to limit the progression of Myc-dependent tumours.

**Summary**

To summarise, this Chapter has:

1) Evaluated histidine exchange in Myc-dependent tumour and breast cancer cell lines.
2) Identified histidine as a bidirectional LAT1 substrate.
3) Quantified concentrations of glutamine and histidine in the serum, TIF, and Myc-driven MGTs.
4) Demonstrated a preference for histidine as a LAT1 substrate over glutamine at physiological concentrations.
5) Shown increased activation of the mTORC1/4E-BP1 signalling pathway, leading to enhanced global protein translation and proliferation in histidine preloaded cells.

# Chapter 6. Histidine availability is a targetable metabolic vulnerability in Myc-driven tumourigenesis

## 6.1 Introduction

The integrated stress response (ISR) is the primary signalling network by which cells adapt to stress through reprogramming of translation, thereby restoring cellular homeostasis and supporting survival. This plasticity in cell state as a response to stress is imperative for cancer cell survival. Indeed, the aberrant proliferation and protein translation associated with cancer makes it especially vulnerable to intrinsic and extrinsic stressors. These stressors include, for example, low nutrient availability, low ATP, increased reactive oxygen species, activation of the UPR, or hypoxia. Therefore, as the name suggests the ISR integrates signals from four unique serine/threonine kinases which respond to these different types of stress, including heme-regulated inhibitor (HRI), double-stranded RNA-dependent protein kinase (PKR), PKR-like ER kinase (PERK), and general control non-derepressible 2 (GCN2). eIF2α, a subunit of the eIF2 complex which forms the ternary complex (eIF2-GTP-$tRNA_i^{Met}$) required for initiation of protein translation, is at the core of this signalling pathway. When any of these four upstream kinases are activated in response to stress, they converge onto eIF2α, leading to its phosphorylation (Figure 6-1. Regulation of ATF4 translation by the ISR.. This phosphorylation limits the formation of the ternary complex, resulting in a global reduction in protein synthesis. However, translation of a subset of mRNAs containing specific sequences in their 5' untranslated regions, known as upstream open reading frames (uORFs), is enhanced[368]. One key example is the the canonical ISR effector, the transcription factor ATF4[369]. ATF4 mRNA contains two uORFs, uORF1 and uORF2. Under normal conditions, uORF1 is translated efficiently, and the 40S ribosomal subunit reinitiates translation at uORF2, which overlaps with the main ORF (mORF) of ATF4[368]. This results in ribosome recycling at the end of uORF2 and repression of ATF4 mORF translation. However, during stress, phosphorylation of eIF2α at Ser51 reduces ternary complex availability, making reinitiation at uORF2 less likely[368]. As a result, the ribosome bypasses

uORF2 and instead reinitiates at the mORF, leading to increased translation of ATF4[368]. Activation of ATF4 reprograms cellular transcription, prioritizing the translation of specific pro-survival mRNA transcripts, such as those involved in amino acid synthesis and transport, that can restore homeostasis[370].

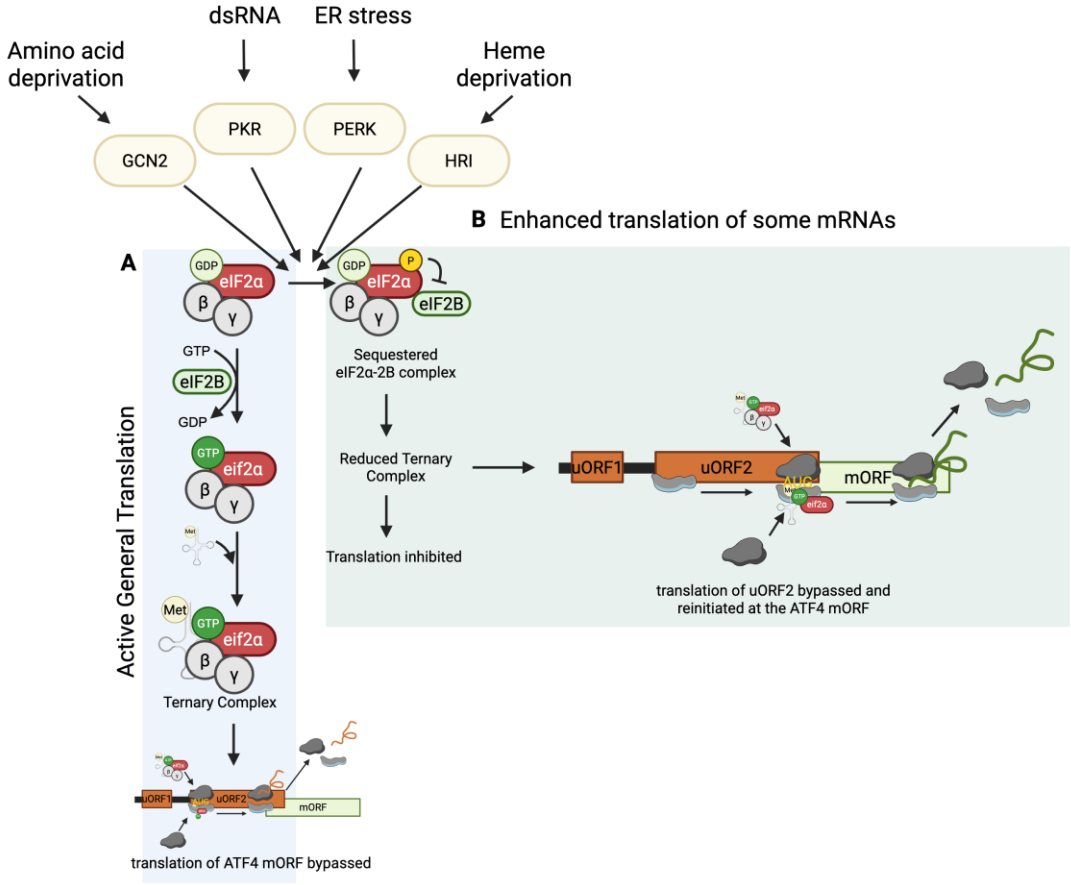



**Figure 6-1. Regulation of ATF4 translation by the ISR.**
**(A)** Under non-stressed conditions, eIF2α, together with eIF2β (β) and eIF2γ (γ), forms the eIF2 complex, which is activated by guanine nucleotide exchange from GDP to GTP via eIF2B. This allows the delivery of the initiator $tRNA_i^{Met}$ to the 40S ribosomal subunit, promoting general translation initiation. During this state, upstream open reading frames (uORFs) in transcripts such as ATF4 are efficiently translated. Translation of uORF2, which overlaps with the main ORF (mORF), prevents translation of ATF4. **(B)** In response to cellular stress, the ISR is activated via one of four kinases, GCN2, PKR, PERK, or HRI, which phosphorylate eIF2α at Ser51. Phosphorylated eIF2α forms an inhibitory complex with eIF2B (eIF2α-2B), inhibiting recycling of eIF2α to its GTP-bound form, thereby reducing ternary complex (eIF2-GTP-$tRNA_i^{Met}$) and inhibiting global protein translation. Under these conditions, translation of mRNAs containing uORFs is selectively enhanced. For ATF4, reduced ternary complex availability causes ribosomes to bypass the start codon of uORF2 and instead reinitiate translation at the mORF, resulting in increased ATF4 protein expression. Image created with biorender.com.

PERK and GCN2 are especially relevant to Myc-dependent transformation and tumourigenesis[224,240]. PERK is an ER resident transmembrane protein that is induced by the UPR. Maintaining protein quality and proper peptide folding is an important challenge in tumours that depends on the UPR. The UPR is activated by a number of factors; cell-extrinsic factors such as hypoxia[371], nutrient availability[372], ROS[373], and acidosis[374] are all common characteristics of the TME which perturb ER homeostasis. In addition to coping with these extrinsic factors, oncogene activation increases the demand for global protein synthesis, fuelling ER stress. Indeed, MYC hyperactivation induces proteotoxic stress, thus depending on the UPR and PERK-eIF2α-ATF4 signalling for survival. Indeed, activation of PERK in MYC-transformed cells and Eμ-*Myc*/+ transgenic mice prevented autophagy through preferential translation of SLC amino acid transporters and 4E-BP1[224]. However, balancing this demand for nutrients for protein synthesis requires concerted effort from multiple arms of the ISR. It is evident that, MYC-transformed cells also rely on GCN2 for optimal activation of the ISR and induction of ATF4. Indeed, both PERK and GCN2 KD enhance apoptosis in MYC-transformed cells[224]. GCN2 responds to amino acid restriction by recognizing and binding to uncharged tRNAs[375]. Importantly, Myc activation induces the transcription of tRNAs, accumulation of these tRNAs when amino acids are limited therefore activate GCN2.

GCN2 binds uncharged tRNAs through a C-terminal domain that is homologous with histidyl-tRNA synthetase[376]. This leads to allosteric rearrangement and subsequent autophosphorylation of GCN2, which then phosphorylates eIF2α in the ISR signalling cascade. Importantly, despite the homology to histidyl-tRNA synthetase, GCN2 can bind uncharged tRNAs indiscriminately. Furthermore, GCN2 is also activated by ribosome stalling and collision, highlighting its role in initiation and elongation stages of translation[164,377]. Activation of GCN2/eIF2α/ATF4 induces amino acid biosynthetic and transport pathways[369,378,379]. Indeed, in prostate cancer cells, 20 out of 27 expressed SLC transcripts were significantly reduced following treatment with the GCN2 inhibitor, GCN2iB[241]. Furthermore, amino acid uptake assays with leucine, arginine, and lysine demonstrated that GCN2iB treatment significantly impeded the uptake of these amino acids[241], thereby highlighting the important role of GCN2 in restoring amino acid levels. Importantly, while GCN2 can

be activated by deprivation of multiple individual amino acids, the outcome of that activation can be context dependent. ATF4 is a basic leucine zipper (bZIP) protein, for its function as a transcription factor it must form a heterodimer with another bZIP protein[380–383]. Indeed, ATF4 can heterodimerize to at least 30 other bZIP family members[381]. Depending on the heterodimer formed, ATF4 can regulate different sets of genes, leading to context-specific outcomes that are dependent on cell type and environment, providing the cell with the flexibility and plasticity required to cope with diverse stressors[384]. The mechanisms by which ATF4 signalling targets specific subsets of genes downstream of the ISR triggered by different kinases remain to be elucidated.

While the ISR is an Achilles heel in tumour progression, the flexibility of ATF4 transcriptional reprogramming adds a layer of complexity. These adaptations make tumours more challenging to treat[385]. Therefore, understanding these mechanisms is imperative for improved targeted treatment strategies. Importantly, LAT1 knockout and pharmacological inhibition have been demonstrated to activate the ISR[236,386]. ATF4 can also induce LAT1 expression during amino acid starvation by binding to an amino acid response element (AARE) located in the first intron of LAT1[387]. Therefore, this emphasizes the important role of SLC transporters, such as LAT1, in maintaining amino acid homeostasis. Given the important role of histidine in LAT1 function in Myc-driven cancer cells, we hypothesised that histidine is an important signal for amino acid sensing. Therefore, this chapter will assess the effect of histidine limitation on Myc-driven cancer cells and compare its deprivation to deprivation of individual high-affinity LAT1 substrates. Furthermore, we will determine whether histidine limitation is feasible therapeutic strategy targeting Myc-driven mammary tumours and characterize the effect of histidine limitation *in vivo*.

**Aims**

This chapter aims to address these aspects of my hypothesis:

1) Histidine is required to maintain amino acid homeostasis in Myc-dependent tumour cells.

2) Histidine requirement is a therapeutic vulnerability in Myc-driven mammary tumourigenesis.

## 6.2 Histidine is important in maintaining amino acid homeostasis.

In the previous chapter we determined that Myc-dependent cancer cells rely on histidine, rather than glutamine, as a bidirectional LAT1 substrate. Given the crucial role for LAT1 in amino acid homeostasis, as mentioned above, we hypothesised that histidine availability is necessary in the maintenance of EAA pools. We first assessed whether histidine deprivation influenced mTORC1 activation and the ISR pathway. MYAZ16.1e cells were cultured in low concentrations of histidine for up to 48 hours. Western blot analysis revealed an induction in the ISR as demonstrated by increased phosphorylation of eIF2α and a concomitant induction of Atf4 after 16 hours of histidine limitation (Figure 6-2A). Furthermore, attenuation of mTORC1 signalling was observed, as shown by decreased phosphorylation of RPS6 at 48 hours of histidine limitation and a parallel increase in expression of the lipidated form of LC-3, indicative of increased autophagosome formation (Figure 6-2A). Surprisingly, we also observed a significant increase in Myc protein expression (Figure 6-2A). ATF4 induction downstream of the ISR activates adaptive pathways to endure periods of stress, such as prolonged amino acid limitation. Given the previous reports on ASCT2 coupling with LAT1 to mediate uptake of EAAs, we assessed whether levels of *Slc1a5* (encoding Asct2), a previously demonstrated transcriptional target of ATF4[145,388], were altered upon histidine limitation. Indeed, we observed a significant increase in glycosylated-Asct2 after 16 hours of histidine limitation in MYAZ cell lines (Figure 6-2B, C). Asct2 must be glycosylated for plasma membrane trafficking to facilitate glutamine uptake, therefore, this indicated an increase in functional Asct2 at the plasma membrane. Asct2 localization was assessed via immunofluorescence (IF) in cells cultured under histidine limitation. Histidine limitation increased staining intensity at the plasma membrane after 16 hours (Figure 6-2D). Therefore, histidine limitation appears to induce the ISR, resulting in an increase in Asct2 expression at the plasma membrane.

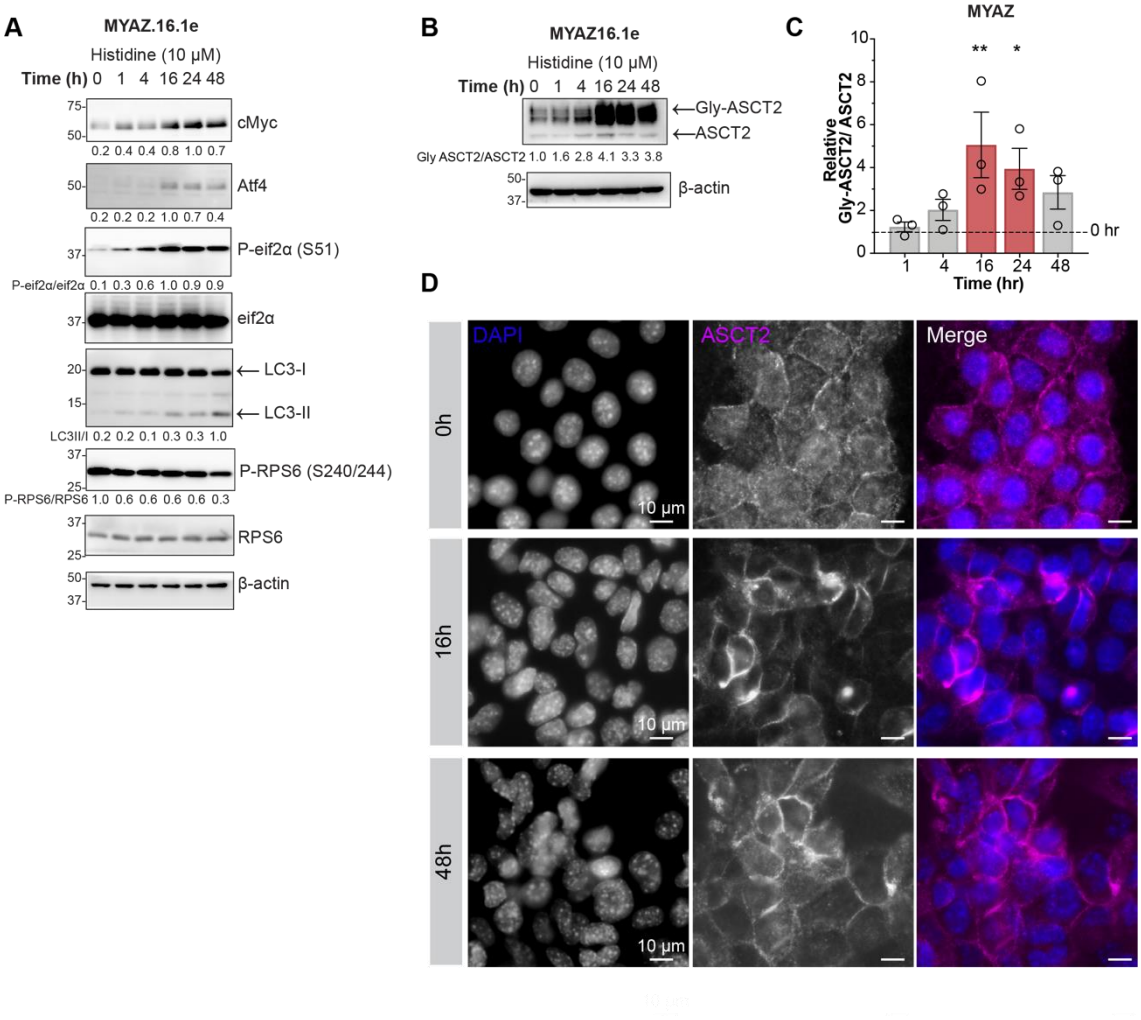



**Figure 6-2. Histidine limitation induces expression of ASCT2.**
MYAZ16.1e cells were cultured in 10 μM histidine for indicated times. **(A)** WB of proteins in the ISR and mTORC1 signalling pathways. Protein levels are normalised to β-actin and min-max normalized. Representative of 3 independent replicates. (**B)** WB of Asct2 expression. Protein levels were normalized to β-actin. The ratio of Glycosylated (Gly)-Asct2 relative to un-glycosylated Asct2 was determined and fold change to 0 hour was assessed. Representative of 3 independent replicates. **(C)** Quantification Gly-Asct2/Asct2 protein expression from panel B, relative to the levels at 0 hr (no histidine deprivation). One-way ANOVA with Šídák correction (*p≤0.05, **p≤0.01). **(D)** Representative IF images of ASCT2 localization in MYAZ16.1e cells cultured in 10 μM histidine for indicated times.

GCN2 responds to the deprivation of many amino acids partially by binding to their uncharged tRNAs. Therefore, Asct2 expression was assessed under histidine deprivation compared to the deprivation of other high-affinity Lat1 substrates, including leucine, isoleucine and methionine. MYAZ16.1e cells were starved of histidine, leucine, isoleucine, or methionine for 4 or 16 hours. Western blot analysis revealed that deprivation of all these amino acids individually is sufficient to

attenuate mTORC1 activation as demonstrated by decreased 4e-bp1 phosphorylation, and/or activation of the ISR, as shown by increased phosphorylation of eIF2α (Figure 6-3A). Notably, deprivation of histidine resulted in increased Myc expression at 16 hours, whereas Myc expression was significant induced at 4 hours in isoleucine starved cells. In contrast, leucine and methionine deprivation resulted in decreased Myc expression. Furthermore, all amino acids except of methionine induced phosphorylation of eIF2α, suggestive of differential activation of the GCN2/eIF2α pathway depending on the specific amino acid. Importantly, histidine deprivation specifically resulted in increased protein levels of glycosylated-Asct2 and, therefore, Asct2 localization to the plasma membrane (Figure 6-3A, B). To determine whether this increase in Asct2 protein levels was transcriptional, we quantified mRNA expression of *Slc1a5* in histidine-deprived cells compared to deprivation of the other EAAs above. Strikingly, histidine deprivation resulted in a significant increase in *Slc1a5* transcript expression compared to the other EAAs at 4 and 16 hours of deprivation (Figure 6-3C). Given the important role for histidine in mediating LAT1 function, we hypothesised that Lat1 expression would be enhanced to compensate for histidine limitation. Indeed, histidine limitation resulted in significant upregulation of *Slc7a5* compared to the other EAAs tested (Figure 6-3D). These results indicate that although mTORC1 and the ISR are affected by the limitation of most EAAs, histidine limitation appears to result in an enhanced response in Myc-driven tumour cells by upregulating the expression of Slc transporters, such as *Slc1a5 and Slc7a5*.

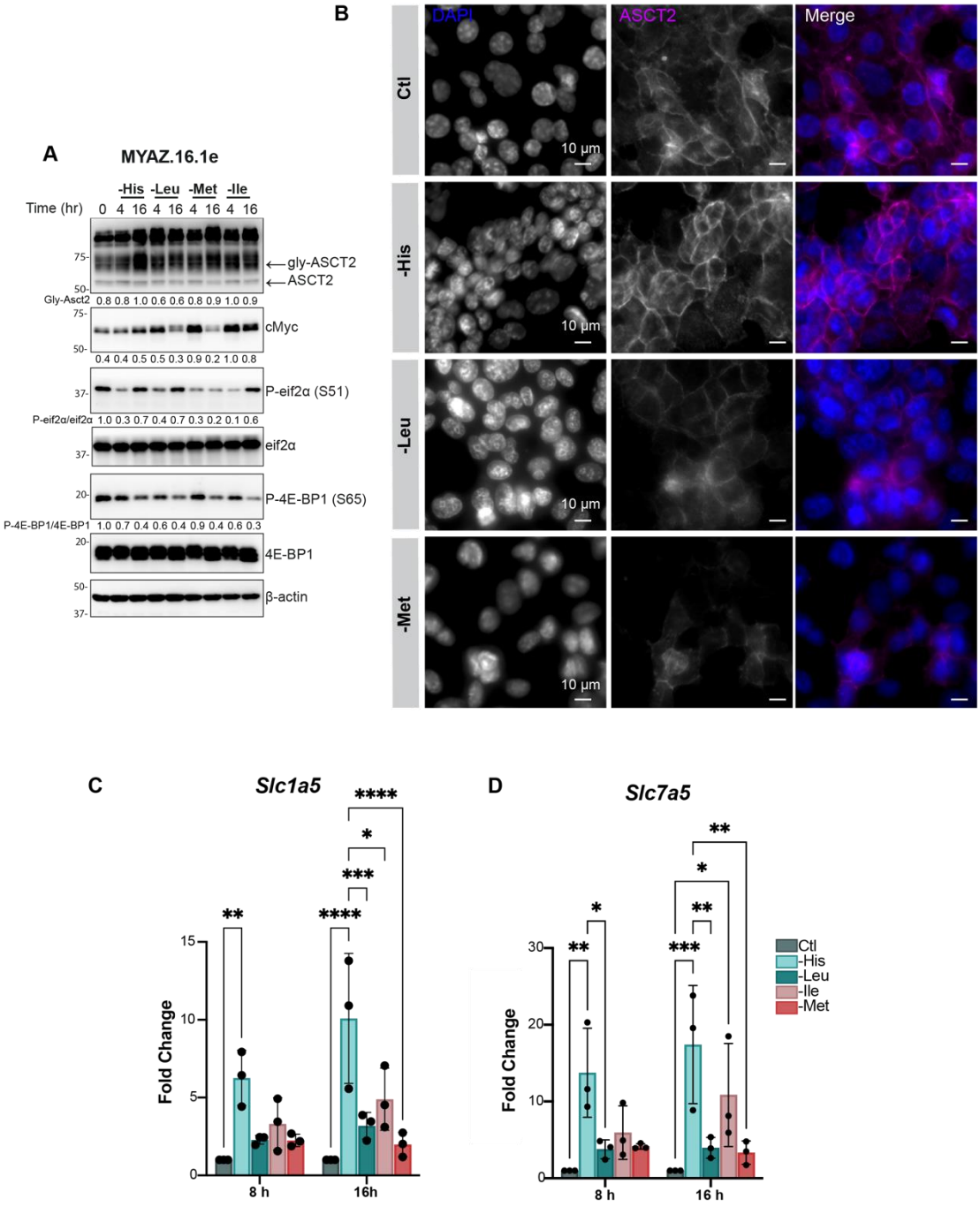



**Figure 6-3. Histidine limitation enhances transcription of amino acid transporters.** MYAZ16.1e cells were starved of histidine (his), leucine (leu), methionine (met), or isoleucine (ile) for the indicated times. **(A)** WB of ASCT2, Myc, eIF2α, and P-4E-BP1. Protein levels were normalized to β-actin and min-max normalized. Representative of 1 replicate. **(B)** Representative IF images of Asct2 expression in cells deprived of indicated amino acids for 24 hours. **(C-D)** RT-qPCR analysis of fold change in *Slc1a5* and *Slc7a5* gene expression, normalized to β-actin, relative to control cells (Ctl; cells cultured in complete DMEM). Data are presented as mean ±s.d.; two-way ANOVA with Tukey correction for 3 biological replicates (*p≤0.05, **p≤0.01, ***p≤0.001, ****p≤0.0001).

Histidine mediates uptake of EAAs and cationic amino acids in MYAZ16.1e cells, therefore, histidine limitation should result in decreased amino acid levels. However, considering the increase in amino acid transporters, we hypothesised that this compensates for histidine limitation and maintains amino acid pools. MYAZ16.1e cells were starved of histidine, or the indicated EAAs, for 8 hours or 24 hours, after which cells were collected for metabolite extraction and LC-MS analysis. Interestingly, histidine limitation resulted in a significant increase in the abundance of LAT1 substrates such as leucine, isoleucine, phenylalanine, tryptophan, and tyrosine compared to deprivation of the other EAAs (Figure 6-4A,C). This agrees with data from the previous chapter, where the uptake of these amino acids was significantly impeded by the ablation of LAT1. Furthermore, arginine and lysine are also increased during histidine deprivation compared to deprivation of other EAAs (Figure 6-4B). Notably, glutamine levels were maintained during histidine deprivation, whereas they significantly decrease upon deprivation of isoleucine, methionine, and amino acid replete conditions (Figure 6-4C). These data support the hypothesis that increased expression of SLC transporters under histidine deprivation increases or maintains pools of certain amino acids.

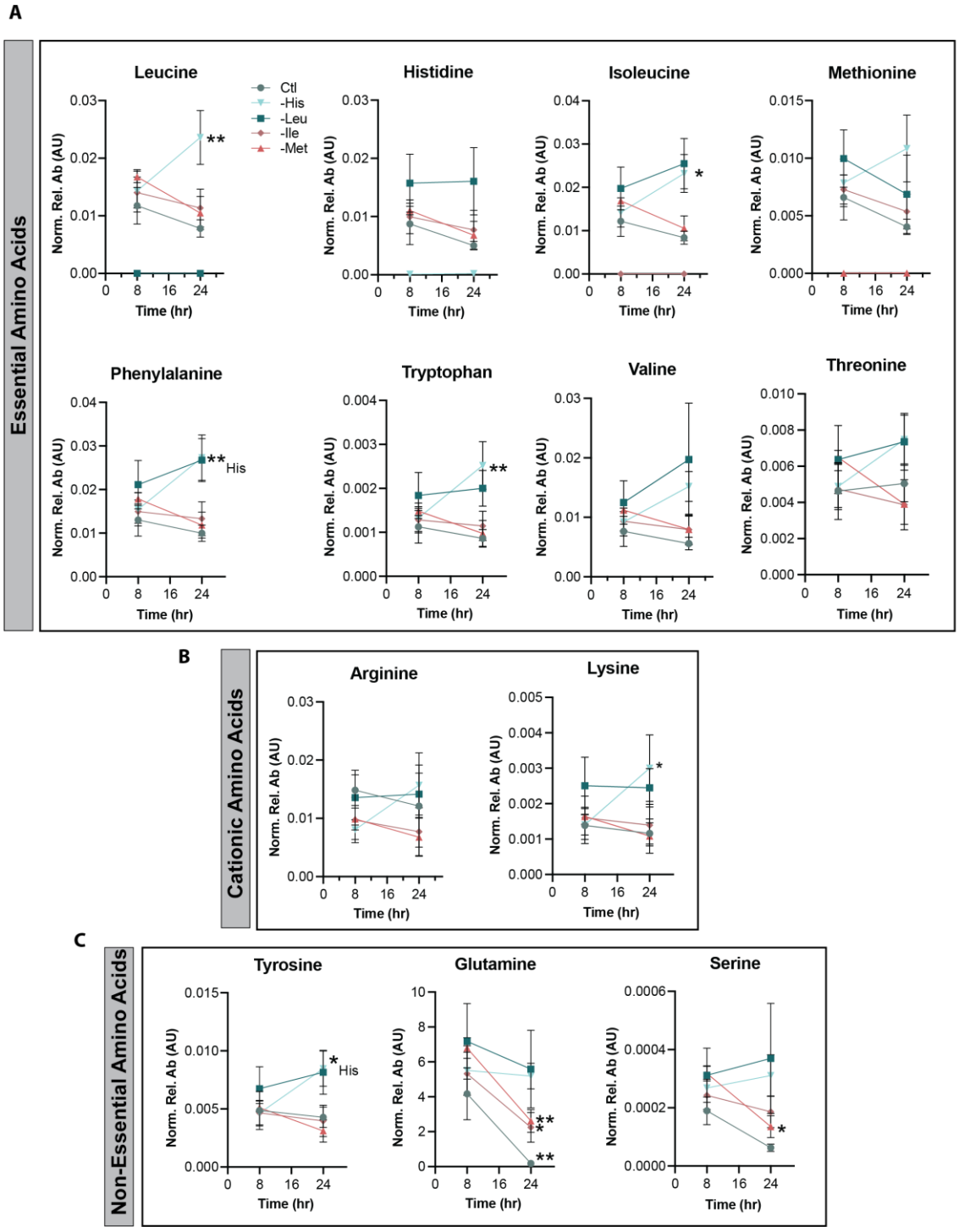



**Figure 6-4. Intracellular amino acid levels increase under histidine limitation.** MYAZ16.1e cells were cultured in MMEC media without histidine (his), isoleucine (ile), leucine (leu), or methionine (met) for indicated times and collected for LC-MS analysis. Normalized relative abundance of **(A)** EAAs, **(B)** cationic amino acids, and **(C)** NEAAs in DMEM. Data is presented as mean ± s.d. Two-way ANOVA with Šídák comparing 24 hour to 8 hr time point for each condition. *p≤0.05, **p≤0.01, ***p≤0.001, ****p≤0.0001. Representative of 1 replicate.

It is important to note that the 8-hour time point was used as the comparison because induction of the ISR under histidine deprivation was not observed at 8 hours. However, the ISR could be induced more quickly upon deprivation of leucine, isoleucine, or methionine. The levels of most amino acids appeared to be higher at 8 hours during leucine deprivation compared to deprivation of the other EAAs. Given that leucine availability is sensed by mTORC1[173,175], protein translation may be quickly inhibited upon leucine deprivation, thereby resulting in decreased utilization and increased amino acid levels. Indeed, the increase in levels of amino acids may not be a result of SLC-mediated amino acid uptake but rather induction of autophagy and proteasomal degradation. Therefore, markers for autophagy and proteasomal degradation were assessed by western blot in MYAZ16.1e cells deprived of histidine or leucine. Increased LC3-II levels were observed at 24 hours but not 8 hours of either histidine or leucine deprivation. This is indicative of increased autophagosome formation (Figure 6-5A). However, we also see an increase in the delipidated precursor, LC3-I. This suggests that LC-3 transcription may be upregulated upon deprivation of either histidine or leucine to stimulate autophagosome formation. This could also suggest that transcription of LC-3 exceeds autophagosome formation, or that autophagy is not proceeding efficiently. Like LC3-II, p62 is normally degraded through autophagy. Therefore, a reduction in p62 protein levels is a marker for autophagy. However, under leucine deprivation increased p62 protein expression coincided with increased LC3-II expression (Figure 6-5A, B). In contrast, p62 expression is reduced under histidine deprivation. This suggests that while autophagy is active in histidine starved cells, leucine deprivation resulted in a block in autophagic flux. Indeed, no change in LC3-II levels were observed upon treatment of leucine starved cells with BafA1, which inhibits the fusion of autophagosomes with lysosomes and leads to accumulation of LC3-II (Figure 6-5B). This suggests that while autophagy is initiated as a response to leucine deprivation, it is blocked at the stage of autophagosome-lysosome fusion. Notably, only a slight increase in LC3-II levels were observed upon histidine deprivation in BafA1 treated cells, therefore, it may also be the case that autophagolysosome formation could be a bottleneck in these cells during amino acid starvation.

The UPS is another major source of amino acids during amino acid shortage; therefore, we assessed whether there were any differences between proteasomal degradation in histidine and leucine deprived cells that could explain the difference in amino acid pools. MG-132 treatment was used to assess proteasome-mediated degradation of ubiquitin-linked proteins. Surprisingly, after 8 hours of starvation, neither histidine nor leucine-starved cells had increased UPS activity. Indeed, MG-132 treated control cells had greater levels of poly-ubiquitinated and K48-linked-polyubiquitinated proteins than histidine or leucine deprived cells (Figure 6-5C). Furthermore, in the absence of MG-132 treatment there are similar levels of K48-linked-polyubiquitinated proteins in histidine and leucine starved cells, suggesting that there is a similar level of degradation under these conditions (Figure 6-5C). However, leucine deprived cells appear to have decreased overall ubiquitination compared to histidine preloaded cells, as evidence by lower ubiquitin levels in leucine deprived cells compared to histidine deprived cells treated with MG-132 (Figure 6-5C). Therefore, differential UPS activity does not explain the difference in amino acid pools in histidine or leucine starved cells. To better understand whether the increase in amino acid pools observed in histidine-starved cells results from increased transporter expression, further experimentation with inhibition of specific transporters such as ASCT2 or LAT1 will be necessary. Nonetheless, these results suggest a unique cellular response downstream of histidine limitation compared to other EAAs, which results in increased amino acid transporter expression to maintain pools of specific amino acids.

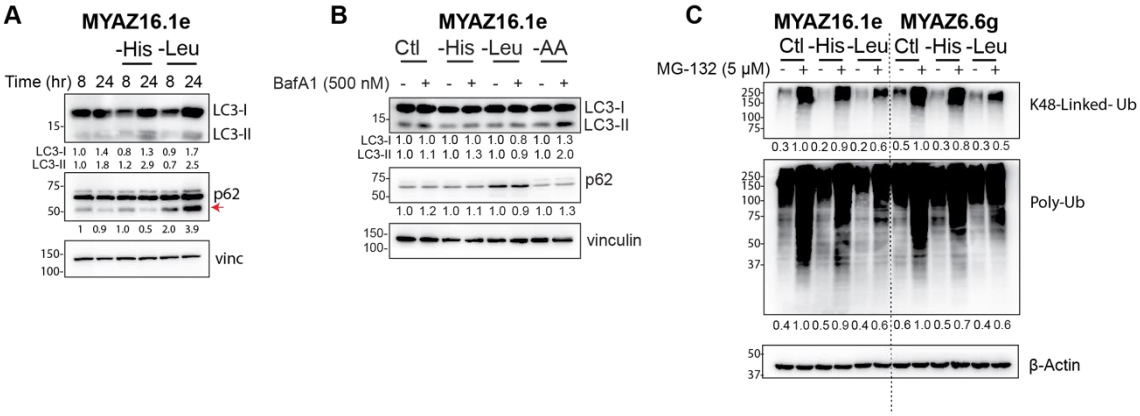



**Figure 6-5. Histidine and leucine deprivation induce macroautophagy and proteasomal degradation to similar extents.**
**(A)** WB of MYAZ16.1e cells starved of histidine (his) or leucine (leu) for indicated times. Protein expression is normalized to vinculin and is quantified as a fold change relative to 8-hour control condition. WB is representative of 2 replicates. **(B)** WB of MYAZ16.1e cells starved of his, leu, or amino acids for 24 hours in the presence of BafA1 or DMSO. Protein expression is normalized to vinculin and quantified as a fold change relative to the Ctl condition without BafA1. Representative of 1 replicate. **(C)** WB of MYAZ16.1e and -6.6g cells deprived of histidine or leucine for 8 hours with MG-132 or DMSO. Protein expression is normalized to β-actin and min-max normalized.

## 6.3 Myc and Atf4-mediated transcription facilitates SLC transporter response to histidine limitation

In the previous section histidine deprivation increased expression of *SLC* transporters, this was concomitant with an increase in Myc protein expression and Atf4 induction in Myc-dependent tumour cell lines. Myc and Atf4 are transcription factors that mediate transcription of a number of SLC transporters, and co-occupy promoter regions of many genes[145,163,224]. Therefore, the role of Myc and Atf4 in histidine deprived cells was assessed. MYAZ16.1e cells with conditional KO of Myc were prepared using the double lentiviral system described in the previous chapter. For these experiments, a multiclonal culture was used. Knockout of Myc was confirmed via western blot analysis of Myc protein levels upon administration of doxycycline. Control cells expressing the Cas9 vector and an empty guide cassette were unaffected by doxycycline administration, whereas expression of Myc was lost in sgMyc cells (Figure 6-6A). As expected, Myc expression is necessary for proliferation of these Myc-driven tumour cells (Figure 6-6B). However, the residual Myc protein expression in the dox-on condition in sgMyc cells could represent clones within the culture with incomplete Myc KO. However, there was sufficient reduction in Myc protein expression to assess the requirement for Myc in SLC

transporter expression. sgMyc cells were cultured in the presence or absence of doxycycline for 24 hours, after which they were starved of histidine for 16 hours. Notably, under histidine-replete conditions, dox-on cells had reduced levels of both *Slc1a5* and *Slc7a5,* indicating that Myc expression is important in maintaining the expression of these transporters, as was alluded to in previous chapters (Figure 6-6C). As expected, histidine deprivation significantly induced the expression of *Slc1a5* and *Slc7a5* in dox-off conditions. However, upon dox-induced KO of Myc, a significant decrease in this induction was observed (Figure 6-6C). Despite this, histidine deprivation still induced expression of *Slc1a5* and *Slc7a5* in dox-on cells (Figure 6-6C). This suggests that while Myc may be partially involved in mediating cellular response to histidine deprivation, it is not sufficient.

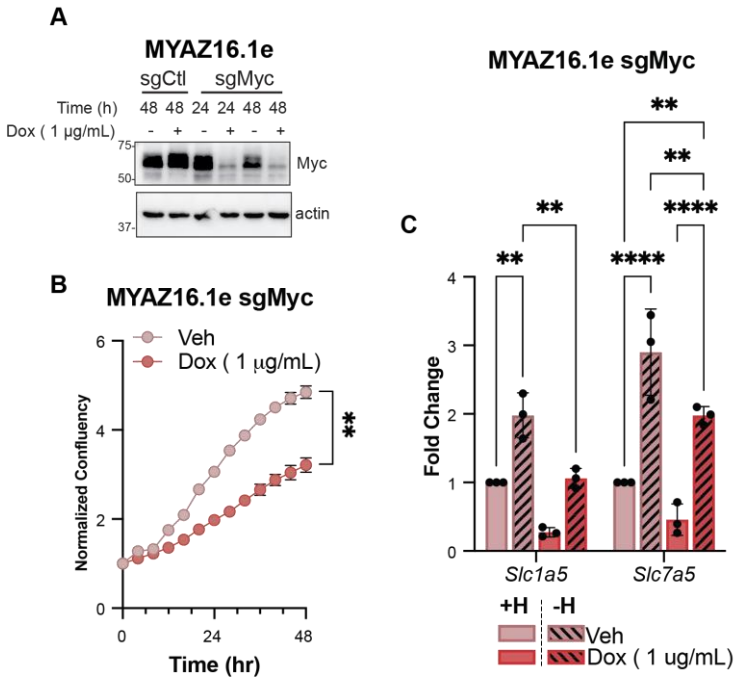



**Figure 6-6. Transcriptional response to histidine limitation is only partially dependent on Myc.**
**(A)** WB of MYAZ16.1e cells with doxycycline inducible sgMyc or an empty sgRNA (sgCtl) cultured in 1 µg/mL doxycycline for indicated times. **(B)** Confluency of sgMyc cells cultured with or without doxycycline for 48 hours and imaged every 4 hours (data are presented as mean ± s.d.; repeated measures two-way ANOVA with Geisser-Greenhouse correction and Šídák test for multiple comparisons. Representative of 2 independent replicates). **(C)** RT-qPCR of *Slc7a5* and *Slc1a5* gene expression in MYAZ16.1e sgMyc cells cultured with or without doxycycline in the presence or absence of histidine for 24 hours. Gene expression was normalized to *β-actin* and fold change is relative to his replete dox-off gene expression. Data are presented as mean ± s.d.; two-way ANOVA with Tukey correction. **p≤0.01, ****p≤0.0001. Representative of 1 replicate.

We next assessed whether *Atf4* induction was necessary in mediating this response. To investigate the role of Atf4 in histidine deprivation, we employed a previously validated short hairpin RNA (shRNA)-mediated knockdown in MYAZ16.1e cells. Indeed, Atf4 transcript levels were significantly reduced in shAtf4 transduced cells compared to control cells expressing an shRNA against luciferase (shLuc) (Figure 6-7A). Therefore, these cells were cultured in the presence or absence of histidine for 16 hours. A striking increase in *Atf4* transcript levels were observed in shLuc cells upon histidine deprivation (Figure 6-7B). In contrast, there was no significant difference in Atf4 levels upon histidine deprivation in shAtf4 cells, and these cells had significantly reduced expression of Atf4. Similarly, Atf4 KD had no effect on expression of *Slc1a5* or *Slc7a5* in control conditions, however, under histidine deprivation there was a significant decrease in the induction of these transporters (Figure 6-7C, D). However, there was still an insignificant increase in *Slc1a5* and a significant increase in *Slc7a5 expression* upon histidine deprivation in shAtf4 cells. Therefore, like Myc, Atf4 appears to be partially involved in mediating the transcriptional response to histidine deprivation. However, this could be due to incomplete KD of Atf4.

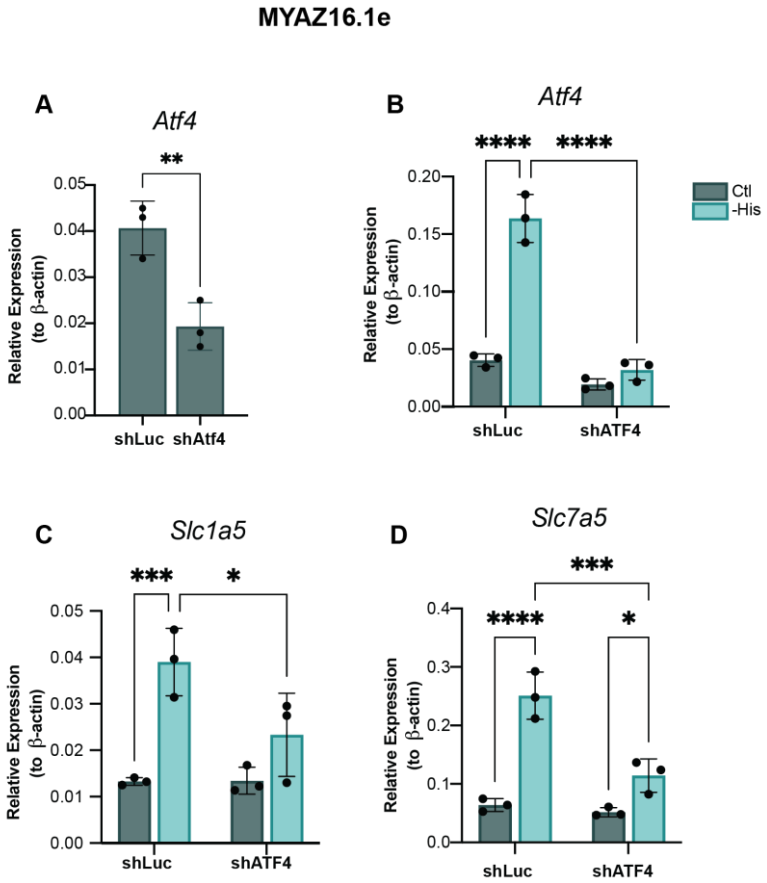



**Figure 6-7. Transcriptional response to histidine limitation is partially dependent on Atf4.**
MYAZ16.1e cells expressing shLuc or shAtf4 were cultured in the presence (ctl) or absence of histidine (-his) for 24 hours. **(A)** RT-qPCR of *Atf4* mRNA expression in shLuc and shAtf4 cells cultured in his replete (ctl) conditions (unpaired two-tailed t-test). **(B-D)** RT-qPCR of *Atf4, Slc1a5,* and *Slc7a5* gene expression normalized to *β-actin* (two-way ANOVA with Šídák correction). All data are presented as mean ± s.d. *p≤0.05, ***p≤0.001, ****p≤0.0001. Representative of 1 replicate.

Given the increase in Myc-expression upon histidine deprivation, we sought to investigate whether histidine deprivation may alter Myc expression in cells lacking endogenous Myc amplification. Therefore, 67NR cells, which are derived from a spontaneous murine mammary tumour in a BALB/c mouse and have low Myc expression, were used. 67NR cells were deprived of histidine, isoleucine, leucine, or methionine for 16 hours, after which they were collected for RT-qPCR. As observed in MYAZ cell lines, histidine deprivation significantly induced transcription of Myc compared to cells cultured in histidine replete conditions, and cells starved of the other individual EAAs (Figure 6-8A). A similar trend was observed for *Slc1a5* and *Slc7a5*, but not *Slc38a1* (encoding Snat1) (Figure 6-8A). This was confirmed in histidine deprived cells at the protein level. Indeed, cells deprived of histidine had

significantly higher protein expression of Myc, Asct2, and Lat1 (Figure 6-8B). Furthermore, these were induced in a dose-dependent manner, from 24 μM to 0 μM of histidine (Figure 6-8C). This concentration is akin to 12% the concentration of histidine in DMEM, 20% the concentration in PLASMAX, or roughly 50% of the concentration we measured in the serum of FVB/N mice. Therefore, under histidine limitation it appears that cells increase Myc expression, resulting in a cellular phenotype that closely resembles that of a Myc-driven cancer cell (high Asct2 and Lat1 expression).

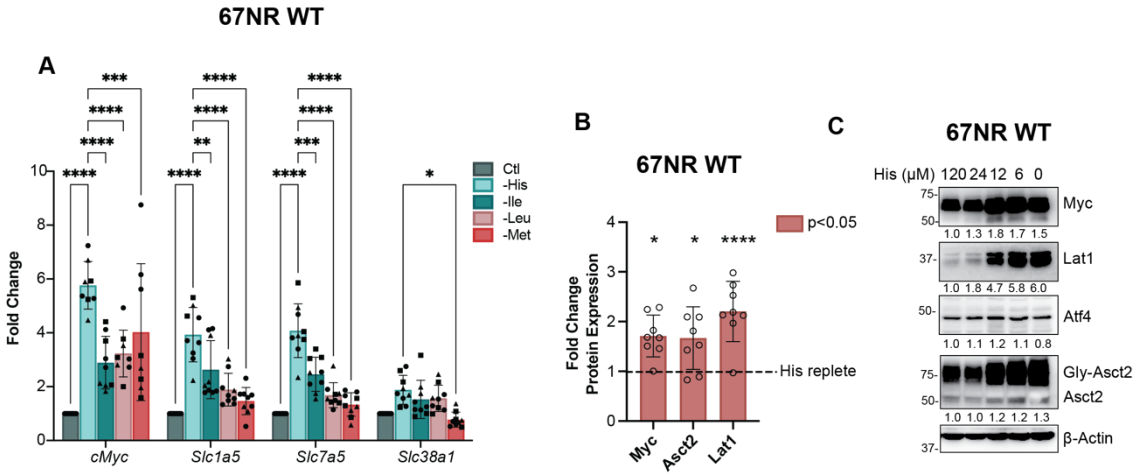



**Figure 6-8. Histidine limitation induces Myc and Slc transporters in Myc-low cells.** **(A)** RT-qPCR of *Slc* gene expression in 67NR cells starved of indicated amino acids for 24 hours normalized to *β-actin* with fold change relative to amino acid replete conditions (Ctl). Data presented as mean ± s.d.; two-way ANOVA with Dunnett (*p≤0.05, **p≤0.01, ***p≤0.001, ****p≤0.0001), representative of 3 independent replicates. **(B)** Quantification of protein expression in 67NR cells starved of histidine for 24 hours. Representative of 8 independent replicates as a fold change compared to his replete conditions. Data presented as mean ± s.d.; one-way ANOVA with Šídák correction (p≤0.05, ****p≤0.0001). **(C)** WB of 67NR cells cultured in indicated concentrations of histidine for 24 hours. Protein expression normalized to β-actin and quantified as a fold change of 120 μM histidine.

Using 67NR cells with doxycycline-inducible ectopic MYC expression, generated by a previous post-doctoral fellow from our lab, Dr. Peter Kreuzaler, we assessed whether the expression of *Slc7a5*, *Slc1a5*, and *Slc38a1* were induced by Myc expression. As expected, dox administration led to significant increase in Myc expression (Figure 6-9A). Furthermore, *Slc1a5* and *Slc7a5* mRNA expression was significantly upregulated as well, however, *Slc38a1* expression was not dependent on Myc overexpression. Therefore, given the 6-fold increase in Myc mRNA levels in histidine deprived cells, we hypothesised that Myc would be important in mediating

the induction of *Slc1a5* and *Slc7a5* observed. We attempted to generate a conditional KO of Myc in 67NR cells, using the same sgRNA previously validated in MYAZ16.1e cells. However, despite expression of the Cas9 and sgRNA cassettes, we were unable to efficiently KO Myc in any of the 10 clones tested. In two clones there was a 50% decrease in Myc protein levels upon dox administration for 24 hours (Figure 6-9B). Under dox-off conditions, histidine deprivation for 24 hours induced expression of Myc, Asct2, and Lat1. In Myc KO cells, histidine deprivation appeared to increase expression of these proteins, with a potential decrease in Lat1 protein levels compared to dox-off cells. Overall, the results obtained from the 67NR Myc KO clones were inconclusive, as efficient gene disruption was not achieved within the timeframe of this project. Although preliminary data suggests that Myc induction is not necessary for induction of Asct2 downstream of histidine limitation, and may be partially required for Lat1 upregulation, further optimization of this knockout approach will be essential to validate these observations. As described in other cell models, Myc overexpression induces the ISR and Atf4 [224]. Indeed, we observed a significant increase in Atf4 mRNA expression upon ectopic expression of MYC in 67NR cells. Furthermore, Atf4 was partially involved in the induction of *Slc1a5* and *Slc7a5* under histidine deprivation in MYAZ16.1e cells. Therefore, to examine the role of Atf4 in histidine deprivation, we utilised the same Atf4 targeting shRNA as was used in MYAZ16.1e cells. We observed a significant reduction in Atf4 mRNA levels in shAtf4 expressing cells compared to shLuc cells (Figure 6-9C). Like MYAZ16.1e cells, Atf4 levels were significantly increased under histidine deprivation in shLuc cells, but this was ablated in shAtf4 cells (Figure 6-9D). However, while histidine deprived shAtf4 cells had significantly reduced expression of *Myc*, *Slc1a5*, and *Slc7a5* compared to histidine deprived shLuc cells, they were significantly higher than shAtf4 cells cultured in histidine replete conditions (Figure 6-9E-G). In contrast, *Slc38a1* was not upregulated in histidine deprived shAtf4 cells or WT cells as observed previously, however, there was significant upregulation in histidine deprived shLuc cells (Figure 6-9H). This could be due to off-target effects, but it was not investigated further. Therefore, Atf4 induction may be partially responsible for mediating the transcription of SLC transporters in response to histidine limitation.

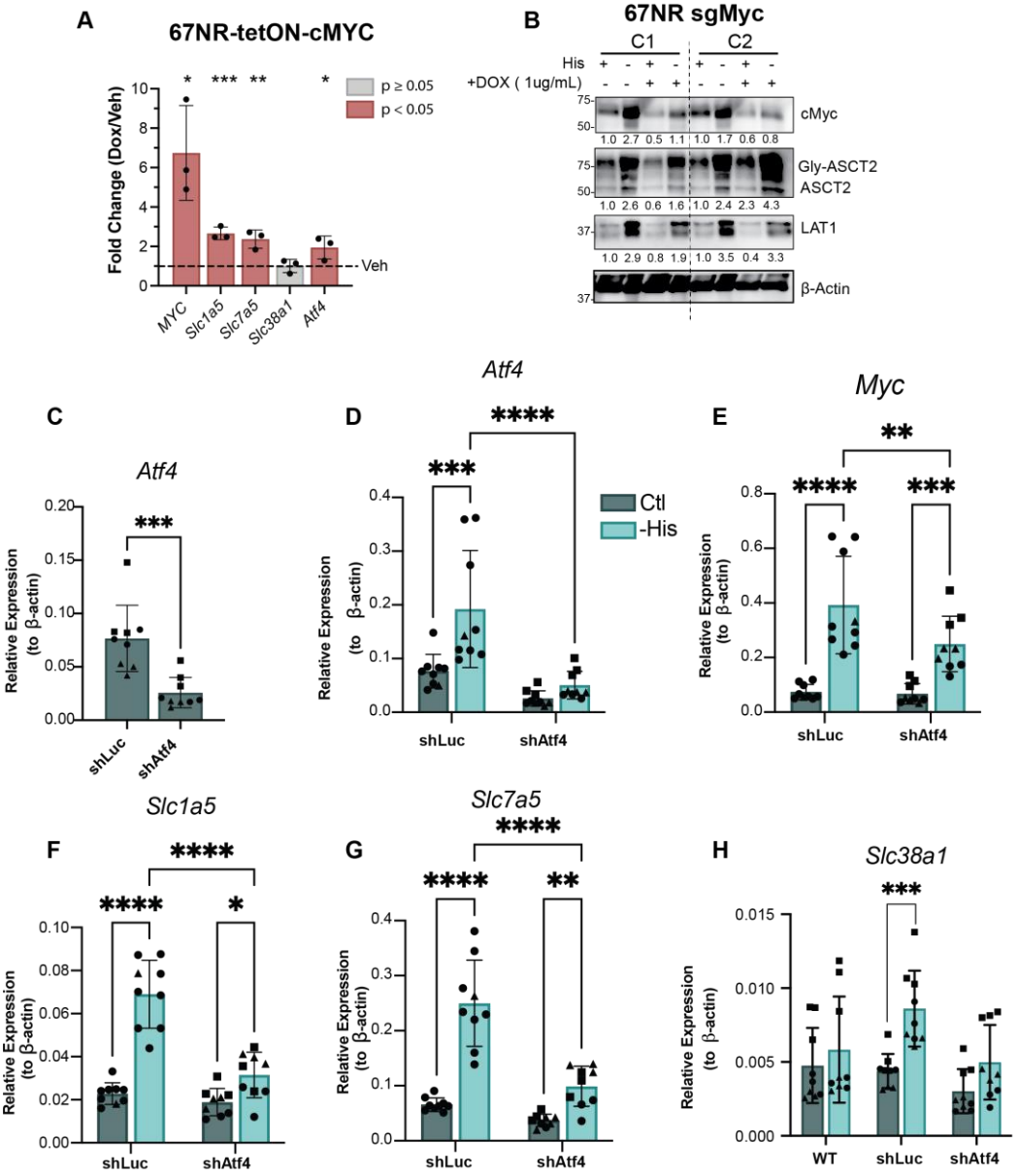



**Figure 6-9. Transcriptional response to histidine limitation is partially dependent on Atf4 in 67NR cells.**

**(A)** RT-qPCR of 67NR cells with ectopic expression of doxycycline inducible MYC. Gene expression is normalized to *β-actin* and relative to vehicle treated cells. Data presented as mean ± s.d. One-way ANOVA with Šídák correction. Representative of 1 replicate. **(B)** WB of lysates from 67NR clones expressing doxycycline inducible sgRNA against Myc. Protein expression was normalized to β-actin and fold-change is relative to dox-off and his replete conditions. **(C-H)** 67NR cells expressing shLuc or shAtf4 were cultured in the presence (ctl) or absence of histidine (-his) for 24 hours. **(C)** RT-qPCR of Atf4 mRNA expression in shLuc and shAtf4 cells cultured in his replete (ctl) conditions. Data presented as mean ± s.d. unpaired two-tailed t-test. **(D-H)** RT-qPCR of gene expression normalized to *β-actin*. Data presented as mean ± s.d.; two-way ANOVA with Šídák correction. *p≤0.05, **p≤0.01, ***p≤0.001, ****p≤0.0001. Representative of 3 independent replicates.

Given this induction in Atf4 and amino acid transporters upon histidine limitation in Myc-low cells, we sought to determine whether this sensitizes 67NR cells to treatments targeting these nodes. 67NR cells were cultured in 100% (120 μM), 20 % (24 μM), or 10% (12 μM) histidine in the presence of vehicle or the LAT1 inhibitor, JPH-203. Importantly, 67NR cells are not sensitive to histidine limitation. Indeed, these cells can maintain proliferation for up to 72 hours in 10% histidine (Figure 6-10A). Furthermore, 67NR cells are not sensitive to LAT1 inhibition with 10 μM JPH-203. However, when histidine is limited, it synergizes with JPH-203 and results in a significant proliferative defect. Therefore, histidine limitation sensitizes 67NR cells to LAT1 inhibition. Indeed, reducing histidine to 20% led to a significant decrease in the $IC_{50}$ of JPH-203, from 24.4 μM to 8.9 μM, highlighting an increase in sensitivity (Figure 6-10B). This was similarly observed in 67NR cells when cultured in 100% histidine (120 μM) or 10% histidine (12 μM) in the presence of increasing doses of the eIF2α inhibitor, ISRIB. Under control conditions, ISRIB had little effect on proliferation, however, under histidine limitation a dose dependent decrease in cellular proliferation was observed (Figure 6-10C). Therefore, reduced histidine availability was sufficient to sensitize 67NR cells to ISR inhibition.

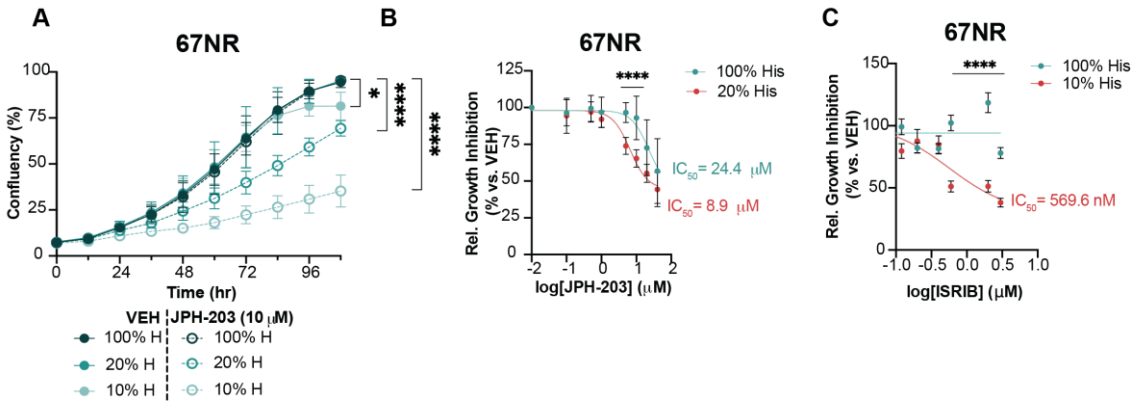



**Figure 6-10. Histidine limitation sensitizes 67NR cells to LAT1 inhibition.**
**(A)** Confluency of 67NR cells every 12 hours. Data presented as mean ± s.d.; repeated measures two-way ANOVA with Geisser-Greenhouse correction and Tukey test for multiple comparisons. Representative of 2 independent replicates. **(B)** Absolute $IC_{50}$ curve of JPH-203 in DMEM containing 100% or 20% histidine at 72 hours. Data presented as mean ± s.d.; two-way ANOVA with Šídák correction (****p≤0.0001). Representative of 3 independent replicates. **(C)** $IC_{50}$ curve of ISRIB in 67NR cells cultured in 100% or 10% histidine. Data presented as mean ± s.d.; two-way ANOVA with Šídák correction (****p≤0.0001). Representative of 2 independent replicates.

In conclusion these results point to an important role for both the ISR and Myc in protecting cells from histidine limitation. Furthermore, here we show that histidine limitation can sensitize Myc-low expressing cells to inhibition of LAT1 or the ISR, which may represent a promising therapeutic approach. A more thorough examination of the transcriptional response to histidine limitation and the mechanistic underpinnings of increased Myc expression could further elucidate potential therapeutic targets in tumours with or without Myc amplification.

## 6.4 LAT1 inhibition does not reduce tumour burden in Myc- or ErbB2-driven mammary gland tumours.

We have shown that histidine is important for LAT1-mediated transport of EAA in Myc-dependent tumour cells. Therefore, we investigated whether this can be exploited by inhibiting Lat1 during Myc-driven mammary tumourigenesis. Indeed, inhibition of Lat1 via the selective inhibitor JPH203 has shown anti-tumour efficacy in breast cancer xenografts [389]. In collaboration with Dr Asad Mahmood, a clinical PhD student in our lab, we assessed the anti-tumour efficacy of Lat1 inhibition on Myc-driven MGTs compared to the Lat1-low ErbB2-driven model. MMTV-Myc and MMTV-ErbB2 MGTs were disassociated, and cells were orthotopically injected into mammary gland four as described in the Materials & Methods Chapter. The mice were then randomly redistributed between the vehicle and JPH203 treatment groups. Mice were administered a daily IP injection of the vehicle or 20 mg/kg JPH203 for 21 days. At collection, mice were given an IV bolus of [U-$^{13}$C]-leucine for 5 minutes to assess JPH203 efficacy. Afterwards, the MGT and serum were collected for metabolite extraction and LC-MS analysis (Figure 6-11A). Surprisingly, mice bearing Myc-overexpressing tumours did not have significantly reduced tumour growth when treated with JPH203 compared to vehicle treated mice (Figure 6-11B). At collection, mice appeared to have slightly reduced tumour burden, as assessed by tumour weight; however, this was insignificant (Figure 6-11C, D). Blood serum enrichment of $^{13}$C-leucine confirmed that both groups received a similar amount (Figure 6-11E). However, leucine enrichment in the serum was slightly higher in JPH203-treated mice (Figure 6-11E). Given that leucine levels have not reached steady-state after a 5-minute bolus, this difference could indicate that JPH203-treated mice have reduced overall leucine uptake. However, contrary

to this hypothesis, Myc-driven MGTs also tended to increase leucine enrichment, suggesting increased leucine uptake (Figure 6-11F). The total and the m+6 isotopologue abundance of leucine was quantified; no difference in total abundance was observed in JPH203 treated compared to vehicle-treated mice (Figure 6-11G). Furthermore, the m+6 leucine abundance was similar in mice that received vehicle or JPH203 treatment, suggesting that Lat1 may be redundant for leucine uptake *in vivo* or that the inhibitor is not effective in blocking Lat1 transporter activity (Figure 6-11H). JPH203 is a competitive inhibitor; therefore, it is possible that high levels of Lat1 substrates in the extracellular milieu could block JPH203 activity. We identified JPH203 within the tumour samples with LC-MS and observed significant heterogeneity in the intratumoural abundance of the administered drug across the treatment group (Figure 6-11I). This variation could result from technical errors in drug administration and differential drug distribution or uptake within the tumours, contributing to the overall lack of treatment effectiveness in reducing tumour growth. Similar results were observed in the ErbB2 cohort. JPH203 treatment did not reduce tumour growth compared to the vehicle treatment in ErbB2-driven MGTs (Figure 6-11J, K). These data could suggest that Lat1 inhibition is insufficient to reduce Myc-driven tumour growth despite high Lat1 expression in these tumours. This could be due to the compensatory action of other EAA transporters, such as those in the Lat family, or it could result from competition with Lat1 substrates such as histidine. However, the variability in JPH203 within the MGTs of treated mice suggests that this could be due to insufficient concentrations of the drug or technical errors and requires optimisation. Importantly, this may indicate that a combined treatment strategy with histidine limitation, as was assessed *in vitro*, could improve the anti-tumour efficacy of JPH203. Therefore, we sought to determine whether dietary restriction of histidine could be a therapeutic strategy for Myc-driven tumourigenesis.

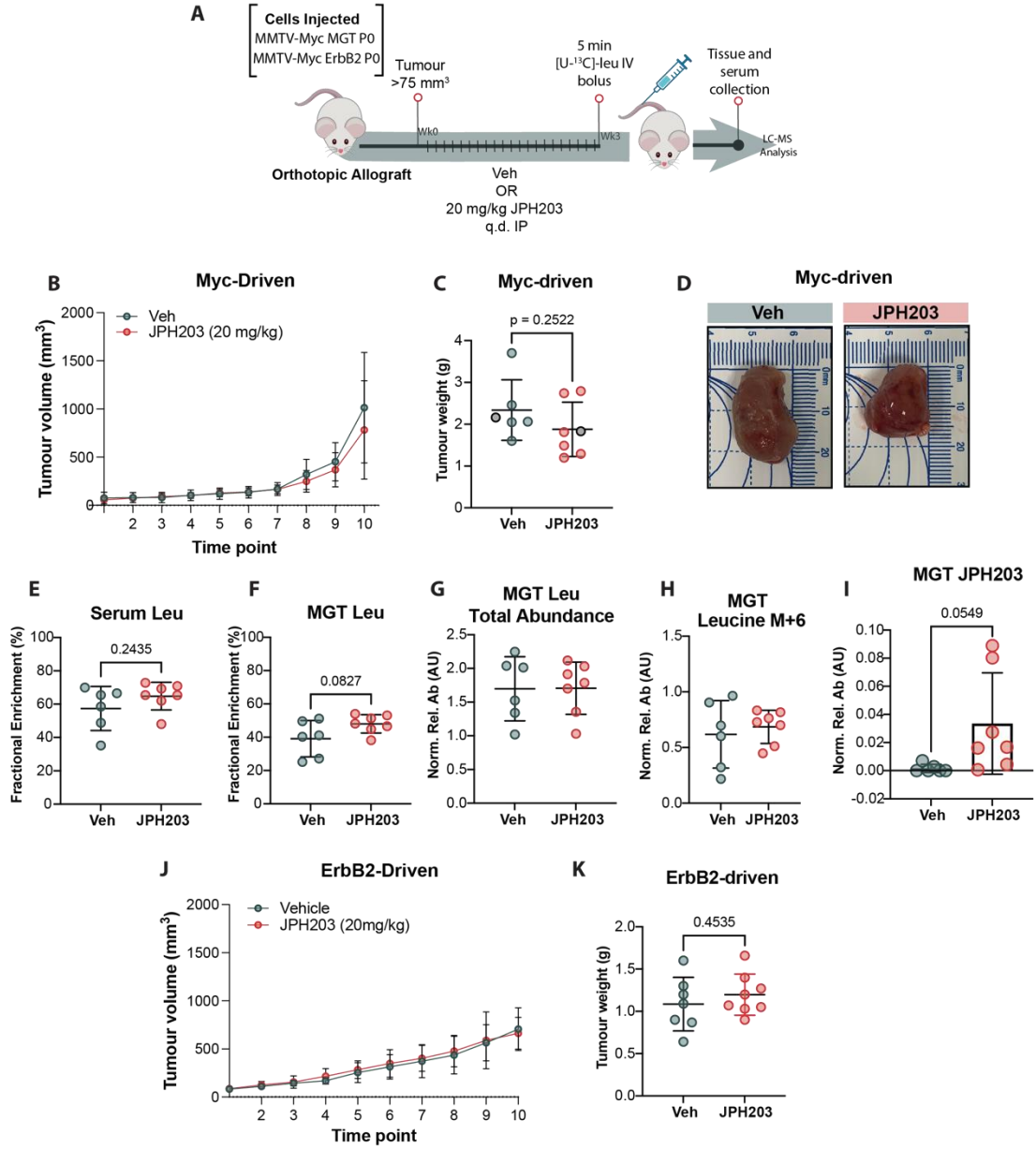



**Figure 6-11. LAT1 inhibition is insufficient to inhibit Myc-driven tumour growth.** **(A)** Experimental timeline of JPH203 treatment. **(B)**Tumour growth in Myc-driven MGT mice treated with vehicle (n=6) or JPH203 (n=7), with measurements every 2-3 days for 21 days (baseline volume at treatment start). **(C)** Tumour weights at collection; black point denotes representative tumours shown in panel D. **(D)** Representative images of tumours from panel C. **(E-H)** LC-MS analysis of leucine: **(E)** $^{13}C$ enrichment in serum, **(F)** $^{13}C$ enrichment in MGTs, **(G)** total abundance in the MGT, and **(H)** abundance of the m+6 isotopologue. **(I)** LC-MS analysis of JPH203 abundance in the MGT. **(J)** Tumour growth in ErbB2-driven MGT mice treated with vehicle (n=7) or JPH203 (n=8) over 21 days. **(K)** Tumour weights at collection in ErbB2-driven MGT mice. All data are presented as mean ± s.d.; unpaired two-tailed t-test.

## 6.5 Histidine is required for Myc-dependent mammary tumourigenesis.

Given the importance of histidine in mediating LAT1 activity and amino acid homeostasis in Myc-driven mammary tumour and breast cancer cell lines, we sought to determine whether histidine limitation could limit tumour growth *in vivo*. Histidine is an essential amino acid, therefore, it cannot be produced by mammalian cells *de novo.* Thus, a histidine deficient diet may not be well tolerated. To test this, healthy female FVB/N mice were placed on a control diet (CD) or histidine-deficient diet (HDD) to interrogate whether the diet is tolerated. Importantly, total amino acid levels were maintained between the diets, therefore the intake for protein synthesis is the same. Mice were acclimated to the experimental diet by gradually increasing the proportion of the experimental diets from 25% to 75% over the course of one week (Figure 6-12A). After the diet was fully introduced the mice were monitored and regularly weighed (Figure 6-12A). Blood serum was collected prior to diet initiation, after acclimation, and at the endpoint (Figure 6-12A). After the acclimation period, the HDD resulted in rapid weight loss, with an average weight loss of 11.5% $\pm$ 2.9% within 1 week of being fed the HDD (Figure 6-12B). In contrast, mice fed a control diet on average gained 12.58% $\pm$ 7.2% (Figure 6-12B). Therefore, the humane endpoint of this was reached and the experiment was not continued. Despite a significant reduction in serum levels of histidine in HDD mice compared to CD mice (Figure 6-12C), histidine levels were not significantly altered in tissues, with only a slight decrease observed in the liver and NMG (Figure 6-12D). Thus, highlighting the robust compensatory mechanisms within tissues to maintain levels of amino acids. Therefore, a longer-term diet may be necessary to affect tissue levels, which is not feasible with the HDD. Importantly, the significant reduction in serum histidine during diet acclimation, without loss in body weight, suggested a 25 to 75% histidine diet may be sufficient. Therefore, we sought to determine how much dietary histidine could be reduced while balancing efficacy at reducing histidine levels without significant impact on body weight.

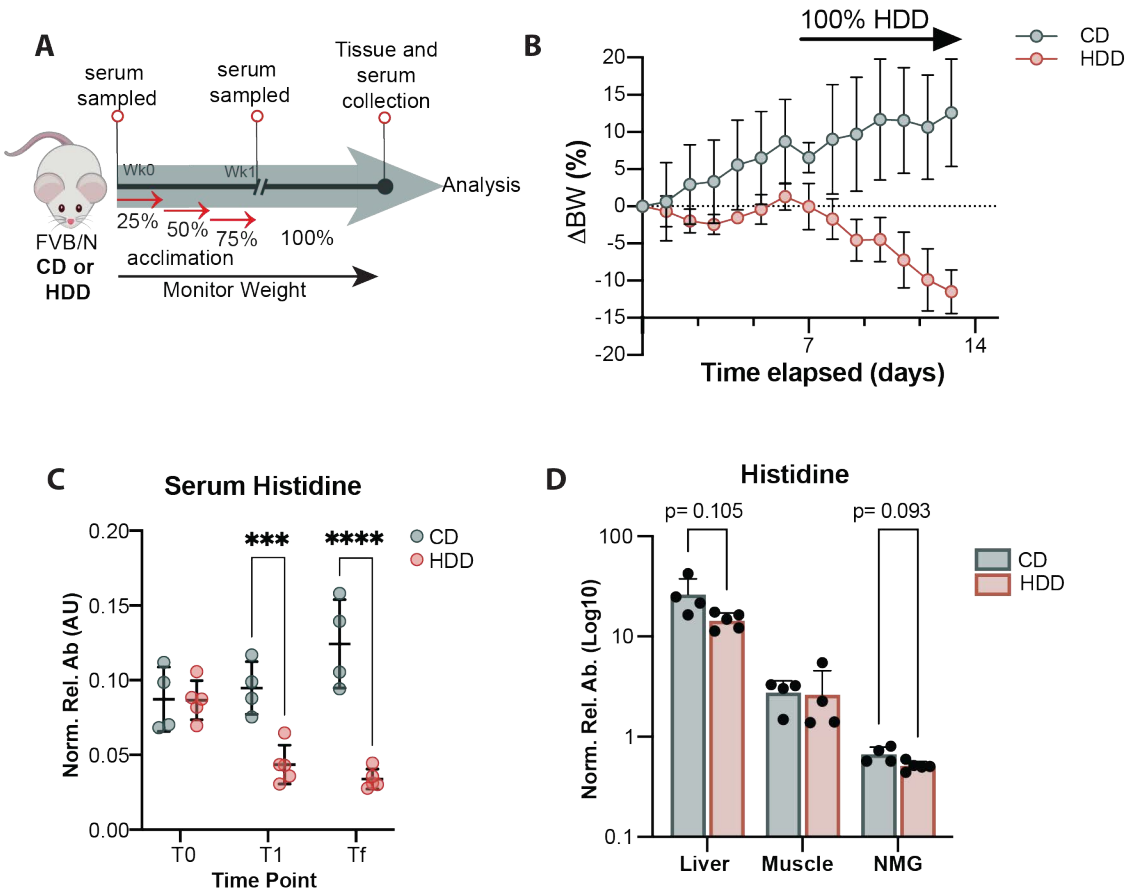



**Figure 6-12. A histidine deficient diet results in significant weight loss.**
**(A)** Schematic of experimental timeline of 5-6 week old FVB/N wild-type mice placed on a control diet (CD, n=4) or histidine-free diet (n=5,HDD). **(B)** Change in body weight over time of mice on CD or HDD. **(C-D)** LC-MS analysis of total abundance of histidine in the **(C)** serum (two-way ANOVA with Šídák correction) and **(D)** tissues (multiple unpaired two-tailed t-tests with Šídák correction). Data presented as mean ± s.d. ***p≤0.001,****p≤0.0001.

Wildtype healthy FVB/N female mice were similarly placed on either a 100%, 50%, 25% or 10% histidine diet, and the weight of animals was monitored for up to 8 weeks. These diets were prepared by mixing a proportion of the CD with the HDD used above, 1:1, 3:1, and 9:1 HDD to CD, respectively. Therefore, this diet had to be administered as a mashed diet. Substantial differences in body weight were observed in mice fed diets with different concentrations of histidine. Mice fed a 50% histidine diet gained weight faster than mice fed a control diet (Figure 6-13A). Importantly, dietary histidine has been demonstrated to prevent obesity and metabolic syndrome through the actions of histamine-mediated regulation of glucogenesis and food intake[390,391]. Furthermore, histidine supplementation was

found to improve insulin resistance in obese diabetic women[392]. Therefore, we assessed whether glucose homeostasis was affected in mice fed a 50% histidine diet compared to mice fed a 100% histidine diet via intraperitoneal glucose tolerance testing. Mice fed a 50% histidine diet had insignificantly increase blood glucose levels after 30 minutes of glucose administration compared to control mice (Appendix 10). Furthermore, while the levels of glucose were cleared rapidly, returning close to baseline levels in control mice, glucose levels declined much slower in mice on the 50% histidine diet (Appendix 10). This suggests that mice on the 50% histidine diet may have insulin resistance or reduced insulin secretion. In addition to this, 50% reduction in dietary histidine did not affect blood serum levels of histidine (Figure 6-13B). Therefore, this diet would not be suitable for our requirements. In stark contrast to the 50% histidine diet, after 1 week the 10% histidine diet resulted in weight loss, culminating in an average of -6.7 % $\pm$ 2.0% after 4 weeks (Figure 6-13A). While this diet resulted in a significant reduction in serum histidine levels (Figure 6-13B), it was not sufficient for use in our tumour models. However, mice fed a 25% histidine diet maintained body weight on par with mice on a 100% histidine diet and resulted in significant reduction in serum histidine levels (Figure 6-13A, B). Together these results highlight the important role for histidine in physiology, with small changes in dietary histidine mediating significantly different responses. Therefore, empirically determining a suitable concentration of histidine that does not adversely impact overall physiology but significantly reduces histidine availability was essential.

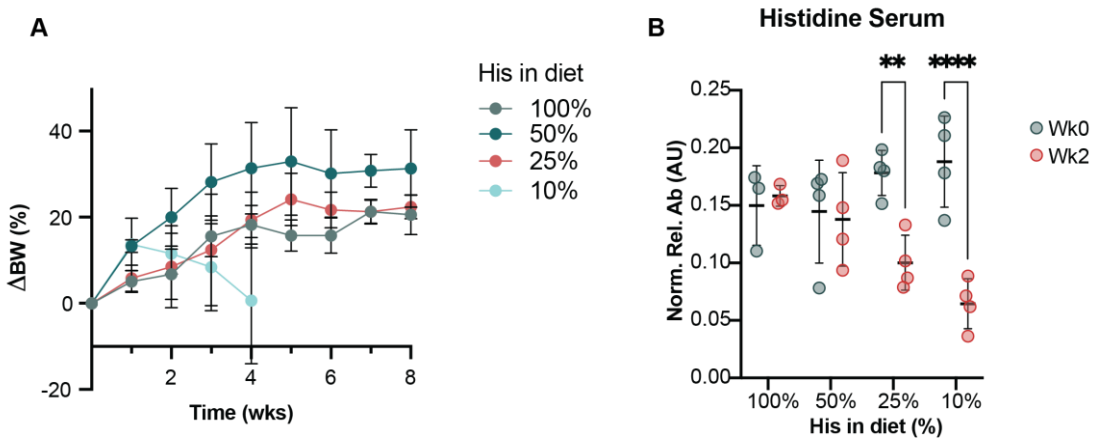



**Figure 6-13. A 25% histidine diet significantly reduces serum histidine without affecting body weight.**
**(A)** FVB/N wild-type mice were placed on indicated histidine diets (n=4 per group) at 5-6 weeks of age, and weight was measured on a weekly basis. Repeated measures two-way ANOVA with Geisser-Greenhouse correction and Tukey for multiple comparisons. **(B)** LC-MS analysis of total abundance of histidine in the serum before diet (Wk0) and after 2 weeks (Wk2) on the diet. Data presented as mean ± s.d. Two-way ANOVA with Šídák correction (**p≤0.01,****p≤0.0001).

To our knowledge, the requirement for dietary histidine for tumourigenesis has yet to be assessed, therefore, we sought to determine whether histidine limitation impacted Myc-driven tumourigenesis. We decided to slightly lower the histidine diet from 25% to 20%, to reduce levels of serum histidine further. Wild-type healthy female FVB/N mice were placed on a control diet (100% histidine; CD) or histidine reduced diet (20% histidine; HRD) as detailed above. In short, mice were acclimated to the experimental diet gradually over one week and then placed on the experimental diets for two additional weeks before SQ orthotopic injection of MYAZ16.1e cells into the MFP (Figure 6-14A). Tumour growth and weight was monitored throughout the experiment. When most tumours reached a volume of >500 $mm^3$, mice were administered an IP bolus of puromycin for 30 minutes before tissue, tumour, and serum collection. Interestingly, despite the promising results in wild-type animals fed a 25% histidine diet, tumour-bearing mice on the HRD diet had significantly reduced max and final weights compared to the CD cohort (Figure 6-14B). Dietary deprivation of EAAs has been noted to result in reduced food consumption[393], therefore, in a pilot study the average daily chow consumption was compared in mice fed the CD or HRD. Each cage of mice was given approximately 50 g of food at the beginning of each week and at the end of each week the

remaining food was weighed. The difference between start and final food weight, was interpreted as the amount of food ingested on average by all mice. From this, the average consumption per mouse per day was calculated. In the first week following acclimation to the experimental diets, it appeared that mice fed the HRD had reduced food intake compared to the CD fed mice, however, this seemed to quickly stabilize and no significant differences in food consumption were observed over 5 weeks (Appendix 11). Therefore, any changes in body weight observed, do not appear to be a result of reduced food intake in the HRD cohort. However, visual inspection indicated that these diets were particularly friable, and much of the diet could be observed discarded within the bedding. Thus, we cannot completely discount the possibility that the HRD mice could reduce food intake. Furthermore, rats force fed diets lacking individual EAAs still lost weight in an EAA-specific manner[394], therefore, this weight loss could be independent of reduced food intake. Nonetheless, we were encouraged by the fact that mice fed the HRD did not significantly lose weight throughout the experiment. Importantly, this diet achieved significant reduction in serum and tumour histidine levels (Figure 6-14C, D). Furthermore, mice fed the HRD had significantly retarded tumour growth compared to CD mice (Figure 6-14E-G). Despite reduced body weights, tumour growth is still inhibited even when normalized to corresponding animal body weights (Figure 6-14H). These results were consistent and reproducible in another cohort (Appendix 12).

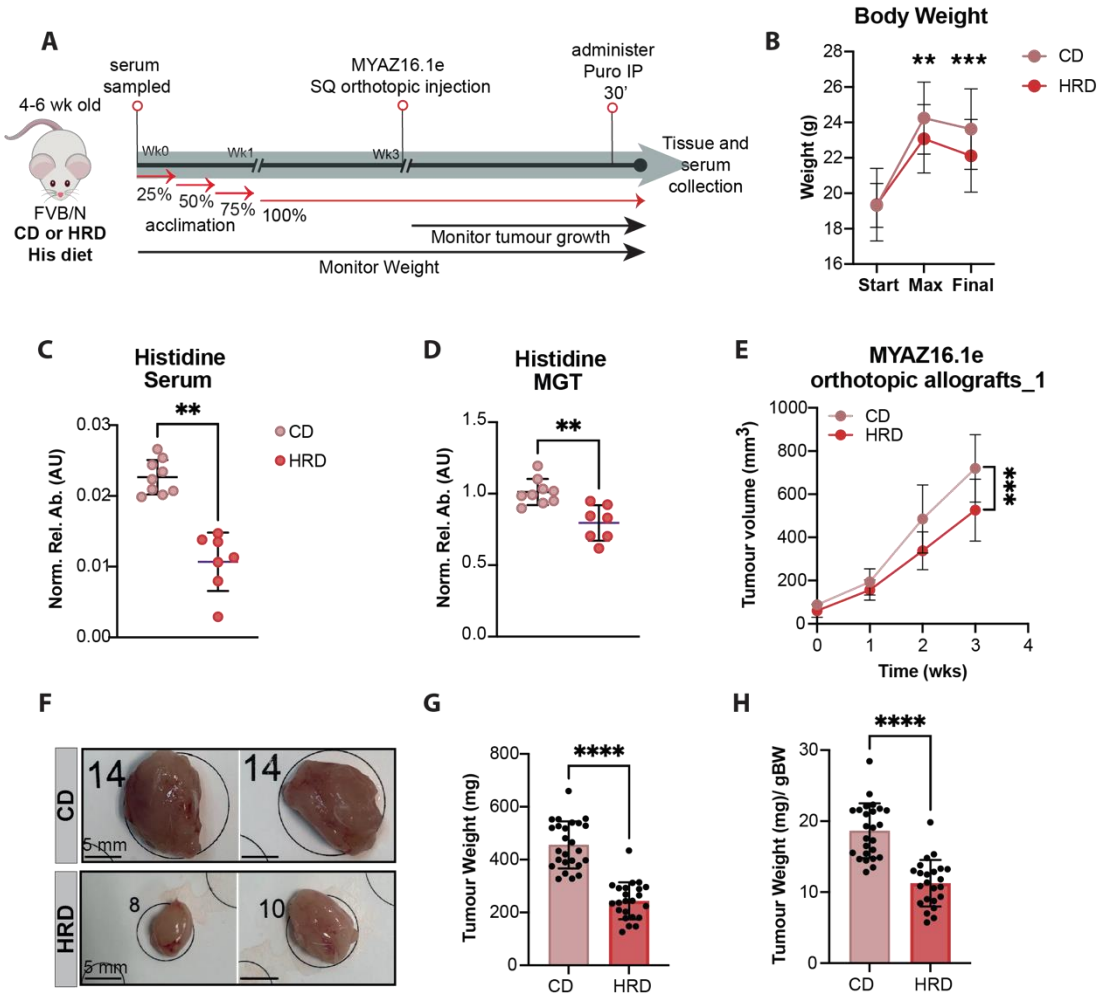



**Figure 6-14. The HRD significantly attenuates Myc-driven mammary tumourigenesis.**
**(A)** Schematic of experimental timeline of FVB/N mice placed on a CD (control diet, n=25) or HRD (histidine reduced diet, n=25) at 4-6 weeks of age, and MGTs were initiated through an orthotopic subcutaneous injection of MYAZ16.1e cells. **(B)** Body weight of 2 cohorts of mice on CD (n=41) and HRD (n=40). Data are presented as mean ± s.d.; two-way ANOVA with Šídák correction. **(C-D)** LC-MS analysis of total histidine abundance in the **(C)** serum and **(D)** MGT. on the CD (n=9) and HRD (n=7); unpaired two-tailed t-test. **(e)** Tumour volume of mice on the CD (n=25) and HRD (n=25). Data are presented as mean ± s.d.; repeated measures two-way ANOVA with Geisser-Greenhouse correction and Šídák for multiple comparisons. **(F)** Images of representative tumours. **(G)** Tumour weight at collection and **(H)** Tumour weight normalized to bodyweight. Data are presented as mean ± s.d.; unpaired two-tailed t-test. **p≤0.01, ***p≤0.001, ****p≤0.0001.

Since histidine is essential for protein translation and cells cannot synthesize histidine *de novo*, we first aimed to confirm that the observed effect of dietary histidine limitation on tumour growth was not merely due to insufficient histidine to support its proteinogenic role. Therefore, a cohort of mice fed the CD and HRD

were administered a bolus of puromycin to assess nascent global protein translation. Protein lysates were prepared from the tumours and puromycin incorporation was analysed by western blot. No differences in puromycin incorporation were visible in the MGTs or livers of HRD mice (Figure 6-15A-C). Therefore, this lends support to histidine requirement outside of its proteinogenic role in Myc-driven tumourigenesis.

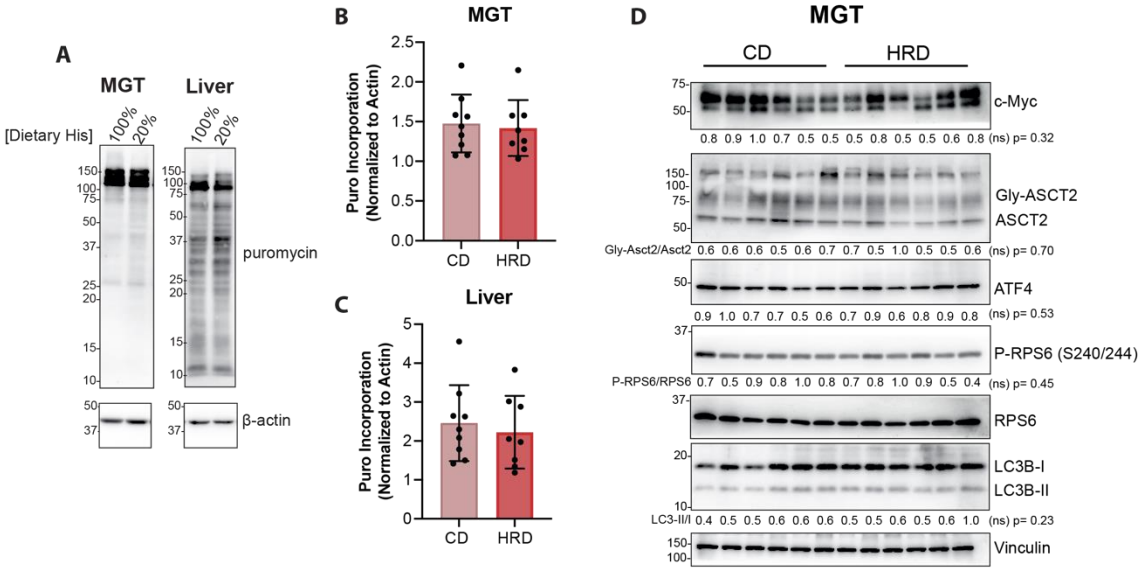



**Figure 6-15. The HRD impacts tumour growth independent of protein translation.** FVB/N mice bearing orthotopic allografts of MYAZ16.1e mammary tumours were put on a CD (control diet (100% his)) or HRD (histidine reduced diet (20% His)) and a subset were injected with 0.02 mg/gBW puromycin before collection (CD: n=9, HRD: n=8). **(A)** Representative WB of puromycin incorporation into proteins in a MGT and liver from each diet treatment. **(B-C)** Quantification of puromycin protein expression in panel A for each sample normalized to β-actin; unpaired two-tailed t-test. **(D)** WB of MGTs from mice fed a CD (n=6) or HRD (n=6). Protein levels were normalized to vinculin and then min-max normalized; unpaired two-tailed t-test.

In the *in vitro* experiments presented above, histidine deprivation induced Myc, Asct2, and Atf4, and attenuated mTORC1 signalling. Therefore, we assessed whether dietary histidine limitation had similar effects on tumours. Contrary to the effect of histidine limitation *in vitro*, no significant differences were observed in tumours from mice fed a HRD compared to CD (Figure 6-15D). In a separate experimental cohort (Appendix 12), HRD mice had a significant reduction in puromycin incorporation in the MGT and an insignificant reduction in the liver compared to CD mice (Figure 6-16A, B). Therefore, this suggests that histidine may be limiting for global protein synthesis and decreased tumourigenesis could result from insufficient histidine availability for protein synthesis. Furthermore, in

this cohort, Myc and glycosylated/total Asct2 protein levels were increased in HRD tumours (Figure 6-16A), resembling the results from cellular experiments with histidine limitation. However, Lat1 levels were heterogeneous, and no induction of Atf4 was observed (Figure 6-16A). Furthermore, rather than attenuated mTORC1 signalling, significantly increased Rps6 phosphorylation was observed and an apparent increase in 4e-bp1 phosphorylation, although this was not quantified due to increased background levels (Figure 6-16A). This is in apparent contradiction to the reduced protein synthesis evident in tumours from mice fed a 20% histidine diet. However, other reports have suggested that autophagy during amino acid starvation can restore mTORC1 activation[395,396].It is unclear why the effect on protein translation differs between these two experimental cohorts. In the second experimental cohort (Appendix 12), CD tumours grew slightly slower and were collected 4.3 weeks post injection, compared to 3.6 weeks in the previous cohort. This does not seem substantially different; however, it is possible that these additional five days may result in these differences in protein translation and that future experimental endpoints should be based on the total time on the HRD rather than tumour size.

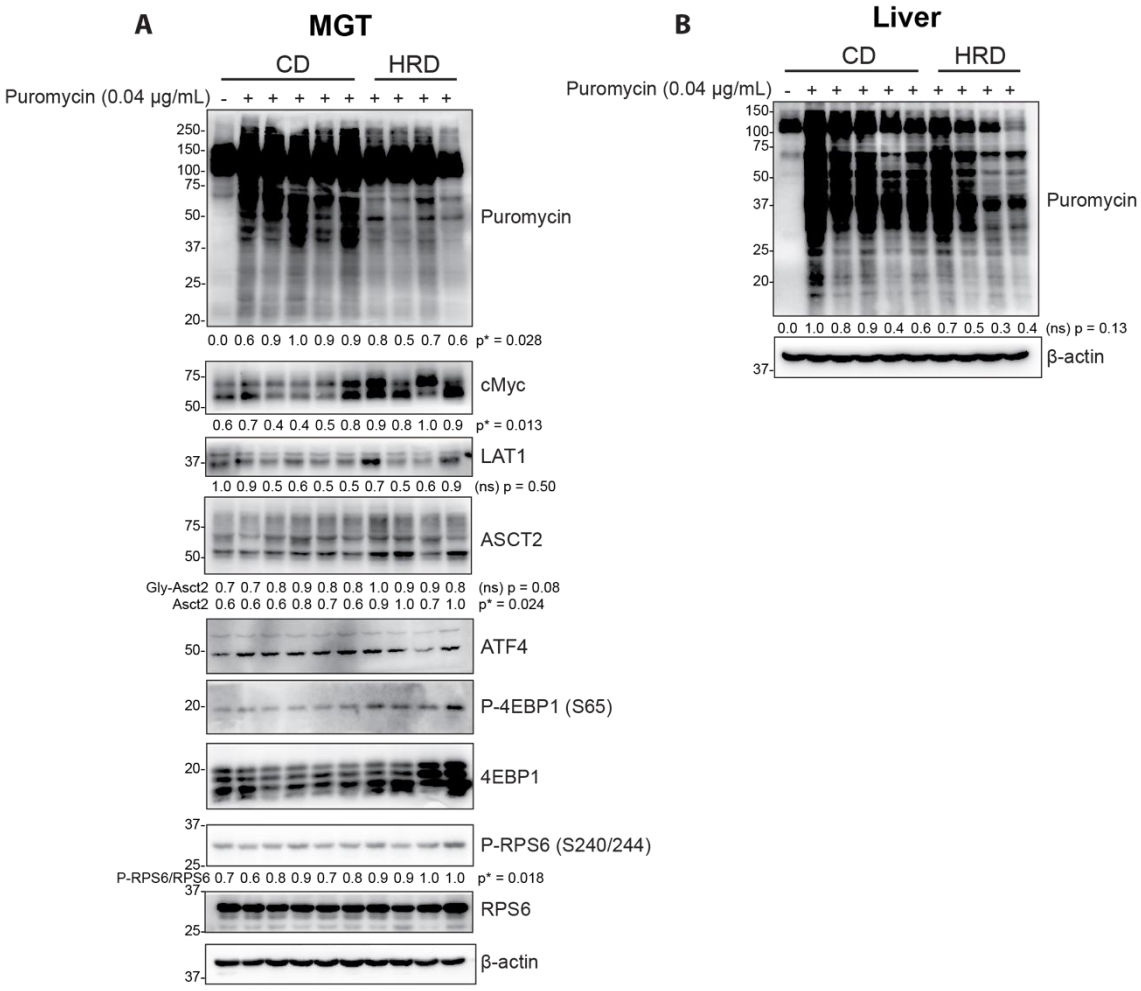



**Figure 6-16. Significant reduction of protein translation was observed in another cohort of mice fed a HRD.**
Another cohort of FVB/N mice bearing orthotopic allografts of MYAZ16.1e mammary tumours were put on a CD (n=16) or HRD (n=15) and a subset were injected with 0.02 mg/gBW puromycin prior to collection (CD: n=5, HRD: n=4). **(A-B)** WB of **(A)** MGTs and **(B)** livers of puromycin injected mice with a negative control in the first lane. Protein levels were normalized to β-actin and then min-max normalized; unpaired two-tailed t-test reported. *p≤0.05.

## 6.6 Dietary histidine limitation invokes systemic changes in metabolism.

### 6.6.1 Amino acid profiles are altered in mice fed a histidine reduced diet.

Histidine is a bidirectional LAT1 substrate, therefore, histidine limitation could affect intratumoural amino acid pools. We assessed the abundance of amino acids in the MGT, liver, and serum of CD or HRD mice. A striking decrease in most amino acids was observed across the serum, MGT, and liver of HRD mice, indicative of

substantial rewiring of amino acid metabolism (Figure 6-17A, C, F). Indeed, aside from histidine there were significant reductions in phenylalanine, threonine, lysine, tyrosine, and BCAAs (leucine, isoleucine, and valine) in the serum of HRD fed mice compared to CD mice (Figure 6-17A, B). This could be due to reduced consumption of the HRD as mentioned. Previous studies demonstrate that rats can detect EAA imbalance in diets, which can lead to chronic hypophagia[397]. Indeed, rats fed a threonine-deficient diet altered their food consumption patterns, characterised by increased inter-meal intervals and decreased meal size and ingestion rate[398]. However, if not given the option of an alternative diet, aversive food behaviour toward the histidine reduced diet would be maladaptive. Although we attempted to measure food intake in the pilot study, the use of metabolic chambers would more accurately quantify food intake to determine whether limitation of histidine, rather than deprivation, has a similar effect. In another study comparing amino acid levels in serum from mice fed different amino acid deficient diets, the altered serum amino acid profile was not a result of reduced food intake[399]. Indeed, diet-restricted mice that were given less food to match the intake of the EAA deficient diet groups had significantly different amino acid profiles [399]. However, this study reported significantly increased serum levels of threonine, phenylalanine, lysine, glutamine, glycine, proline, serine and tyrosine, in murine serum after 2 weeks of being fed a histidine free diet. We did not observe similar changes in our histidine-reduced diet cohort. Therefore, it is unclear what is driving this altered amino acid profile in the serum of mice fed a HRD.

Tumours from mice on the HRD had overall reduced amino acid levels (Figure 6-17C). However, despite the reduced availability of many EAAs in the serum of these mice, only threonine levels were significantly affected aside from histidine in the MGT (Figure 6-17C, D). Threonine is not a LAT1 substrate, furthermore, histidine exchange did not mediate uptake of threonine *in vitro*. Therefore, it is unlikely that this reduction in threonine levels resulted from decreased availability of histidine for LAT1-mediated exchange. In contrast to the MGT, significant changes in amino acid abundance were observed in the liver (Figure 6-17E). Surprisingly, histidine levels were maintained (Figure 6-17D), however the levels of the majority of other EAAs were significantly reduced, especially BCAAs such as valine (Figure 6-17C,E). During EAA deprivation, liver and skeletal muscle tissues enter a

catabolic state, degrading proteins to provide necessary amino acids. Indeed, dietary histidine deprivation has been shown to induce autophagy in both the liver and skeletal muscle of mice[399]. However, autophagy can only partially restore amino acid abundance[400]. In fact, in mouse myotobes, 80% of EAA remained undetectable during amino acid starvation, even with activation of autophagy, suggesting incomplete replenishment[395]. Therefore, how prolonged histidine limitation effects the metabolism within these tissues, and therefore systemic metabolism, is not understood. Overall, these changes highlight the challenges in utilizing EAA limited diets as a targeted tumour treatment and reveal the breadth of changes in amino acid metabolism in the MGT, liver, and serum. This suggests that even a 50% reduction in serum histidine levels can lead to systemic metabolic changes.

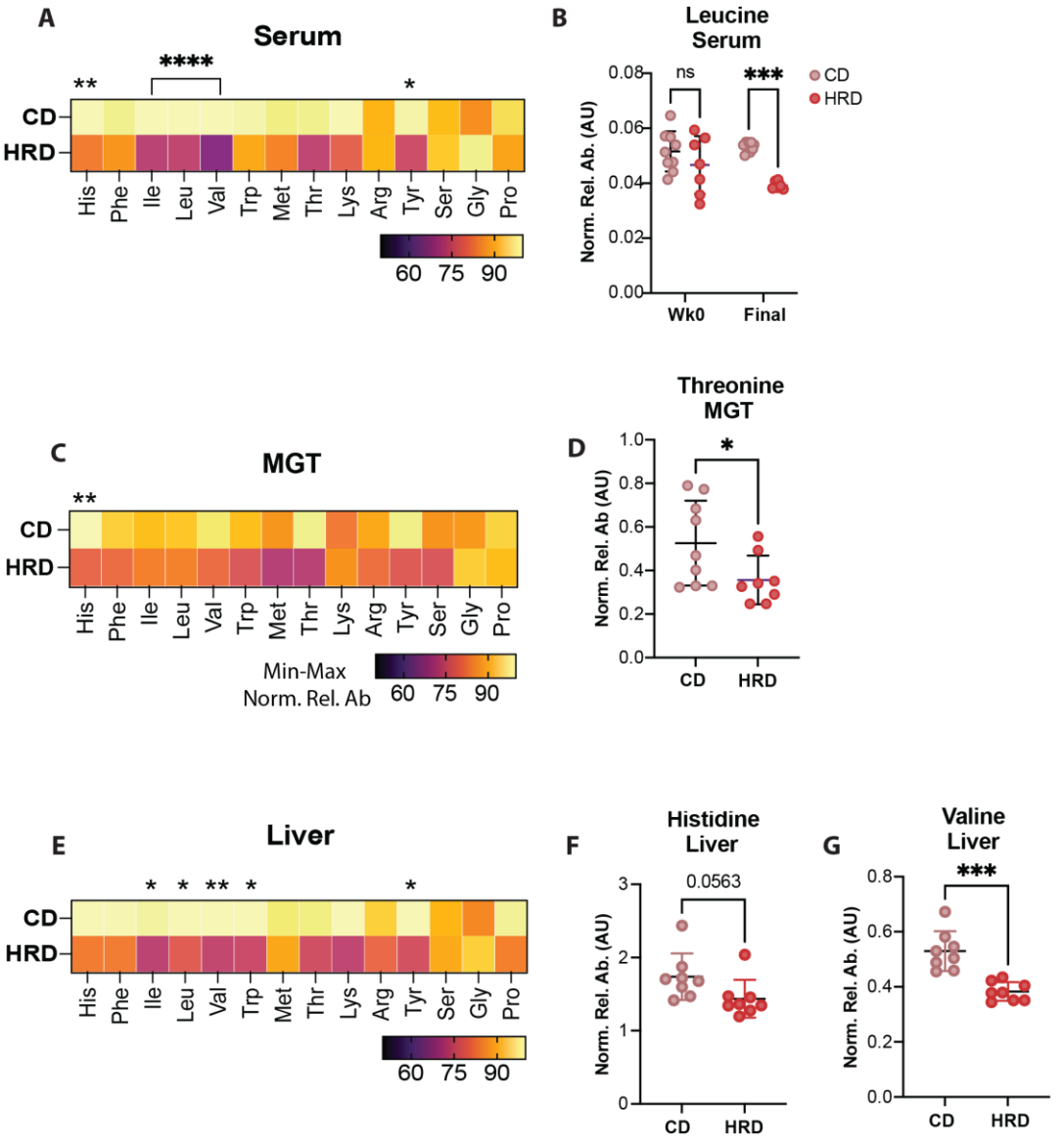



**Figure 6-17. The HRD significantly alters amino acid profiles in the serum, MGT, and liver.**

Amino acid profiles in serum and tissues from mice bearing MYAZ16.1e mammary tumours fed a CD (n=9) or HRD (n=8). (**A, C, E**) Heatmaps showing mean total abundance of indicated amino acids in CD- and HRD-fed mice. Colour intensity represents min-max normalized values as a percentage of the minimum (0) and the maximum value for each amino acid (multiple unpaired two-tailed t-tests). (**B, D, F, G**) Representative plots displaying the mean ± s.d. for the significant differences identified in panels A, C, E: **(B)** total abundance of leucine in serum (two-way ANOVA with Šídák correction). **(D)** Total abundance of threonine in the MGT; **(F-G)** total abundance of **(F)** histidine and **(G)** valine in the liver. (D, E, F analysed by unpaired two-tailed t-tests). *p≤0.05, **p≤0.01, ***p≤0.001, ****p≤0.0001.

### 6.6.2 Rewiring of glutamine metabolism

Other studies have demonstrated that glutamine is released by tissues such as skeletal muscles during starvation, serving as the primary nitrogen carrier in the blood[401,402]. Furthermore, conversion of glutamine to glutamate and subsequent transamination into NEAAs was demonstrated to work in concert with autophagy to restore mTORC1 signalling even when EAA are absent[403]. Therefore, we interrogated whether glutamine catabolism was affected in tumours from mice fed a HRD. In HRD-fed mice, serum glutamine levels were insignificantly increased (Figure 6-18A), this suggests that the histidine limitation may indeed result in nitrogen sparing by the liver and skeletal muscles. Strikingly, significant differences in levels of Krebs cycle intermediates, and NEAAs, aspartate and asparagine, were observed in MGTs, but not livers, of HRD mice compared to CD mice (Figure 6-18B, C). Significant increases in levels of succinate, fumarate, malate, and aspartate were observed, whereas asparagine abundance was reduced (Figure 6-18D-H). This was indicative of potential glutamine rewiring in tumours from mice fed a reduced histidine diet.

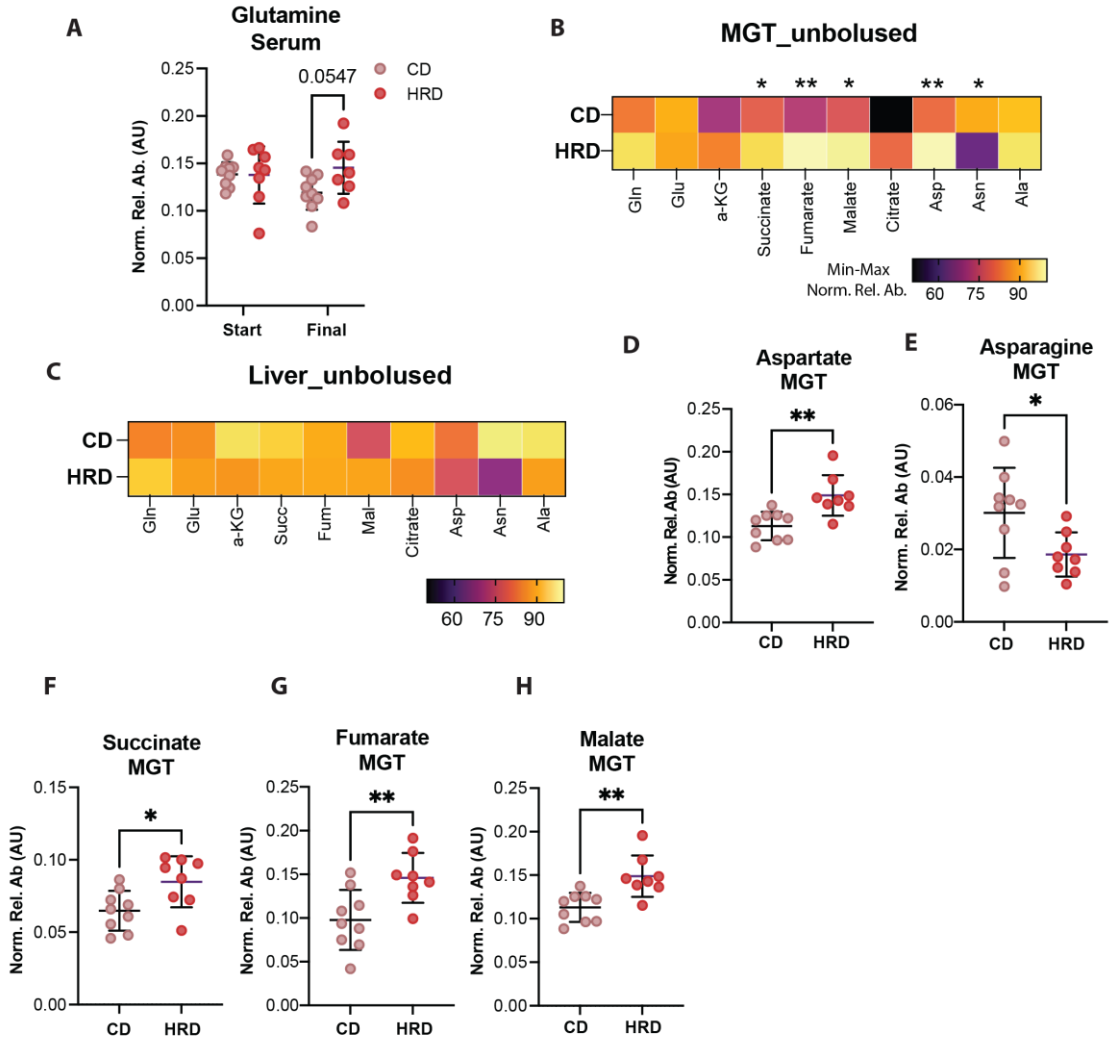



**Figure 6-18. Glutamine metabolism is rewired in MGTs from mice fed a HRD.** LC-MS analysis of the abundance of Krebs cycle intermediates and amino acids in serum and tissues from mice bearing MYAZ16.1e mammary tumours fed a CD (n=9) or HRD (n=8). **(A)** Glutamine abundance in the serum (two-way ANOVA with Šídák correction). **(B-C)** Heatmaps showing mean total abundance of indicated amino acids in CD and HRD-fed mice in the **(C)** MGT and **(D)** liver. Colour intensity represents min-max normalized values as a percentage of the minimum (0) and the maximum value for each amino acid (multiple unpaired two-tailed t-tests). **(D-H)** Representative plots displaying the mean ± s.d. for the significant differences identified in the MGT in panel B (unpaired two-tailed t-test). *p≤0.05, **p≤0.01.

Stable isotope tracing of glutamine was employed to interrogate glutamine catabolism. One cohort of mice on the CD and HRD, were administered two consecutive 15-minute IV boluses of 0.086 mg/gBW [U-$^{13}$C]-glutamine prior to collection to assess whether glutamine catabolism was altered. Like the unbolused cohort, glutamine-bolused mice on the HRD had a significant reduction in histidine

levels in the MGT (Figure 6-19A). Furthermore, similar levels of $^{13}C$ enrichment in glutamine were achieved in both diet groups in the serum and tumour (Figure 6-19B, C). However, when the abundance of Krebs cycle intermediates was assessed, the abundance of these metabolites was increased in the CD and HRD in the group that received the [U-$^{13}C$]-glutamine bolus compared to the unbolused group (Figure 6-18B,Figure 6-19D). Indeed, aside from aspartate, the significant differences previously observed in the HRD cohort were attenuated (Figure 6-19D). This indicates that steady state was not reached in these experiments, and that increased glutamine availability pushes synthesis of these intermediates. Glutamine contributes to aspartate pools via two primary pathways: i) through GLUD1-mediated conversion of glutamate into α-ketoglutarate, which enters the Krebs cycle, and ii) via the mitochondrial aspartate transaminase (GOT2), where glutamate and oxaloacetate are converted to α-ketoglutarate and aspartate (Figure 1-4). Previous work in pancreatic ductal adenocarcinoma (PDAC) cells has demonstrated that glutamine-derived aspartate can be converted into oxaloacetate by GOT1 in the cytoplasm and subsequently into malate, which can be oxidised into pyruvate to produce NADPH[130]. This rewiring of glutamine metabolism was essential for redox balance in PDAC cells[130]. Tracing of $^{13}C$ from glutamine revealed that glutamine is incorporated into Krebs cycle intermediates, with similar enrichment between CD and HRD mice (Figure 6-19E). Therefore, levels of key enzymes in these pathways were assessed to determine whether there was an increased capacity for Got2-mediated aspartate synthesis and Got1-mediated oxaloacetate production in tumours from mice fed a HRD. Indeed, a significant increase in Got1 and Got2 protein expression was observed in tumours from mice fed a HRD (Figure 6-19F). Furthermore, a decrease in Asns protein levels, which agrees with the reduction of asparagine levels observed in HRD mice (Figure 6-19D, Figure 6-18B, E). This suggests that aspartate pools are redirected to oxaloacetate rather than asparagine synthesis. A reduction in Gls1 protein levels is also apparent (Figure 6-19F). Got1 activity produces oxaloacetate and glutamate in the cytosol, therefore, it is possible that this recycling of glutamate between Got2 and Got1 can maintain glutamate pools with less input from glutaminolysis. However, despite these differences observed at the protein level, changes in *Got1*, *Got2*, and *Gls1* mRNA expression was not apparent (Figure 6-19G). Therefore, at this point, it is

unclear what is driving these changes. Further research investigating the overall contribution of glutamine to aspartate pools at steady state in tumours from mice fed a CD or HRD are necessary to draw any conclusions. During this project, cells with genetic knockdown of Got1 and Got2 were successfully generated. However, due to time constraints, further investigation into this line of work was beyond the scope of this project. However, understanding the interplay between glutamine rewiring and histidine limitation within the tumour is an interesting question. It is tempting to speculate that histidine limitation in the MGT rewires glutamine metabolism to meet the demand for LAT1-mediated exchange of glutamine in place of histidine. However, given the breadth of systemic changes that result from a histidine restricted diet, it is likely that these changes are driven by other factors.

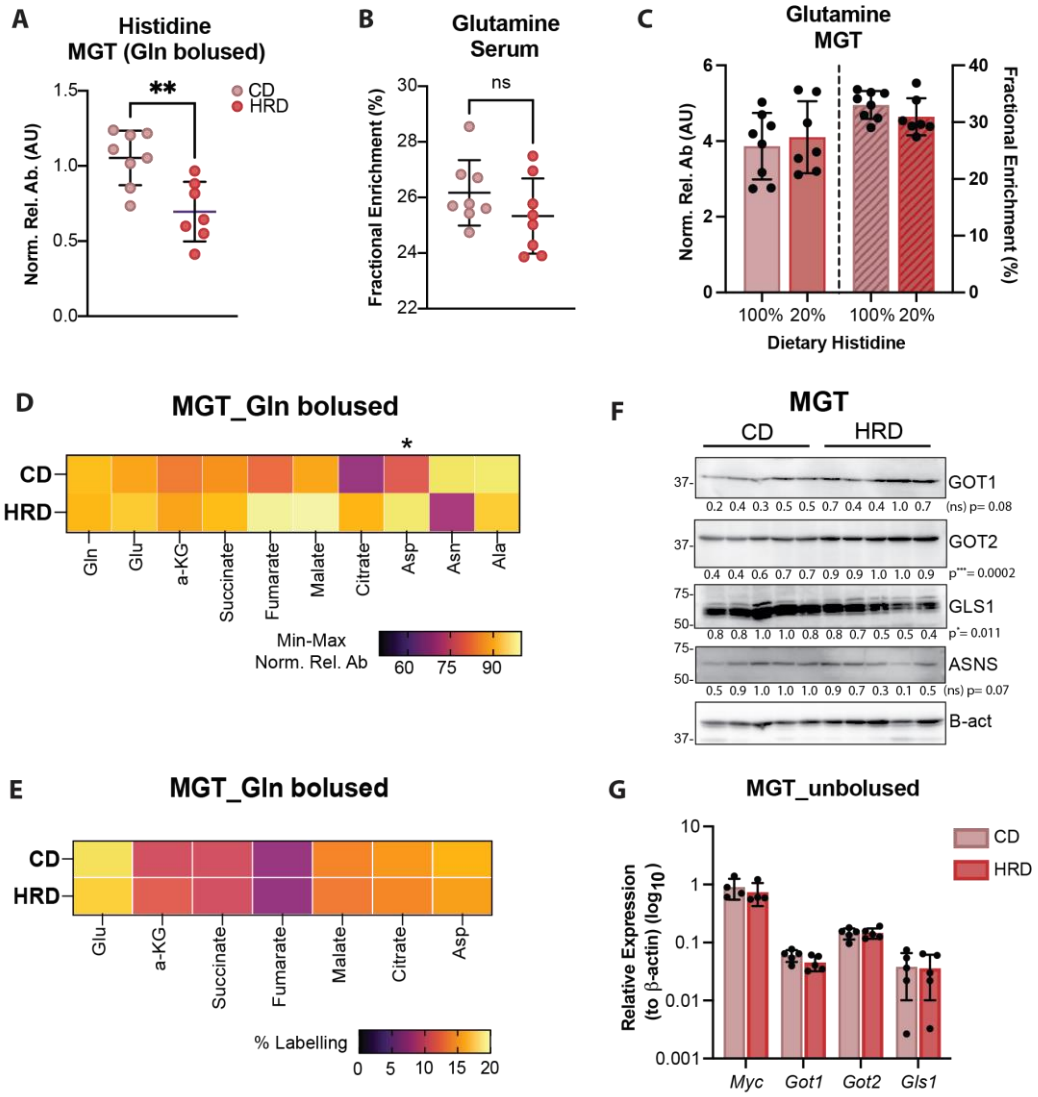



**Figure 6-19. GOT1 and GOT2 are upregulated in MGTs from mice fed a HRD.** LC-MS analysis of the abundance of Krebs cycle intermediates and amino acids in serum and tissues from mice bearing MYAZ16.1e mammary tumours fed a CD (n=8) or HRD (n=7) and received a total IV bolus of 0.34 mg/gBW [U-$^{13}$C]-glutamine. **(A)** Histidine abundance in the MGT (Unpaired t-test). **(B)** $^{13}$C glutamine enrichment in the serum (unpaired two-tailed t-test). **(C)** The total abundance (left y-axis) and 13C enrichment (right y-axis) of glutamine in the MGT. **(D-E)** Heatmaps showing mean **(D)** total abundance and **(E)** $^{13}$C enrichment of indicated metabolites in CD and HRD-fed mice in the MGT. Colour intensity represents min-max normalized values as a percentage of the minimum (0) and the maximum value for each metabolite (Multiple unpaired two-tailed t-tests). **(F)** WB of MGTs from CD (n=5) and HRD (n=5) fed mice. Protein levels were normalized to β-actin and then min-max normalized (unpaired two-tailed t-test). **(G)** RT-qPCR of *Myc*, *Got1*, *Got2* and *Gls1* gene expression in MGTs from CD (n=5) and HRD (n=5) fed mice (two-way ANOVA with Šídák correction). Data in bar plots are presented as mean ± s.d. *p≤0.05, **p≤0.01. ***p≤0.001.

## 6.7 Dietary histidine limitation is less effective in immunocompromised mice.

Despite significantly reduced tumour growth in mice fed a HRD, we did not observe any differences in Ki67 or cleaved caspase 3 (CC3) expression in tumours from mice fed a HRD compared to CD (Figure 6-20A).

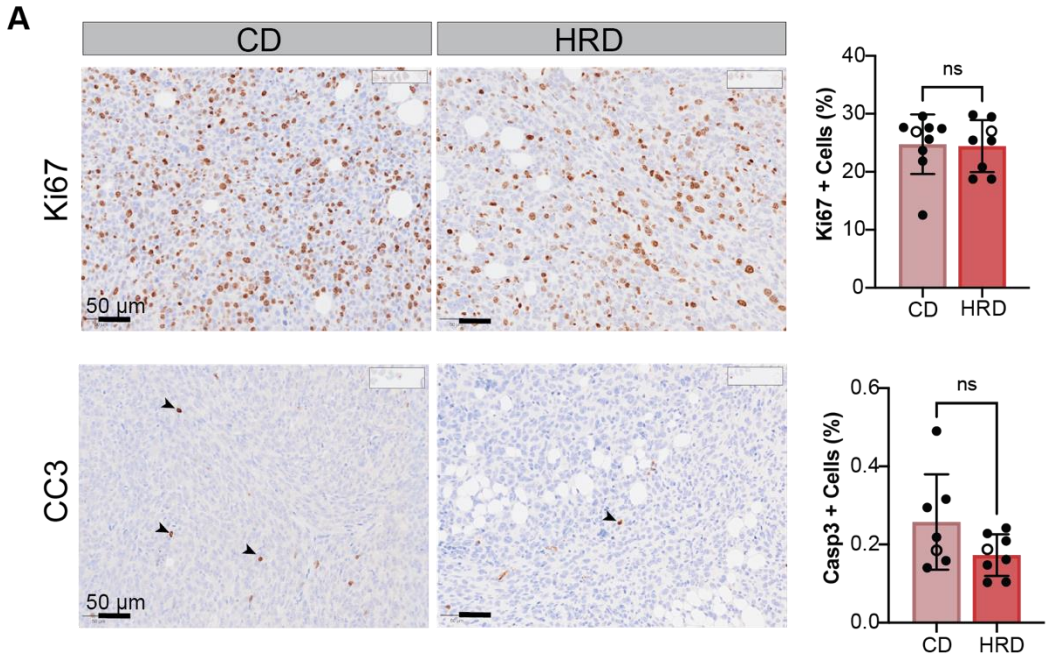



**Figure 6-20. The HRD does not alter cell proliferation or induce apoptosis in MGTs. (A)** IHC and quantification of Ki67 and CC3 staining in MYAZ16.1e MGTs from CD (n=9) and HRD (n=8) fed mice. Arrows depict positive staining for CC3. Bar plots are presented as mean ± s.d. and individual tumours are shown with the unfilled data points depicting the representative IHC on the left. Unpaired two-tailed t-test.

Considering the significant body of literature on the role of LAT1 in immune cell function, we interrogated whether dietary histidine limitation affected the immune compartment of tumours. Indeed, tumours from mice fed a reduced histidine diet had significantly increased immune cell infiltration, as demonstrated by an increased percentage of CD45-positive cells (Figure 6-21A). LAT1 has been shown to be crucial for the function of activated cytotoxic T-cells[404]. Therefore, the percentage of CD3, a marker for both T-helper and T-effector cells, and CD8, a marker for cytotoxic T-cells was quantified. There was a significant increase in

the percentage of CD3-positive cells in the entire population of cells within tumours from mice fed a HRD; however, when this was normalized to the CD45-positive population, CD3-positive cells were not significantly altered within the immune population between diet groups (Figure 6-21A). Furthermore, no differences were observed in the percentage of CD8 positive T-cells (Figure 6-21A). More thorough immune cell profiling will be necessary to determine whether specific immune populations are contributing to retarded tumour growth in HRD mice.

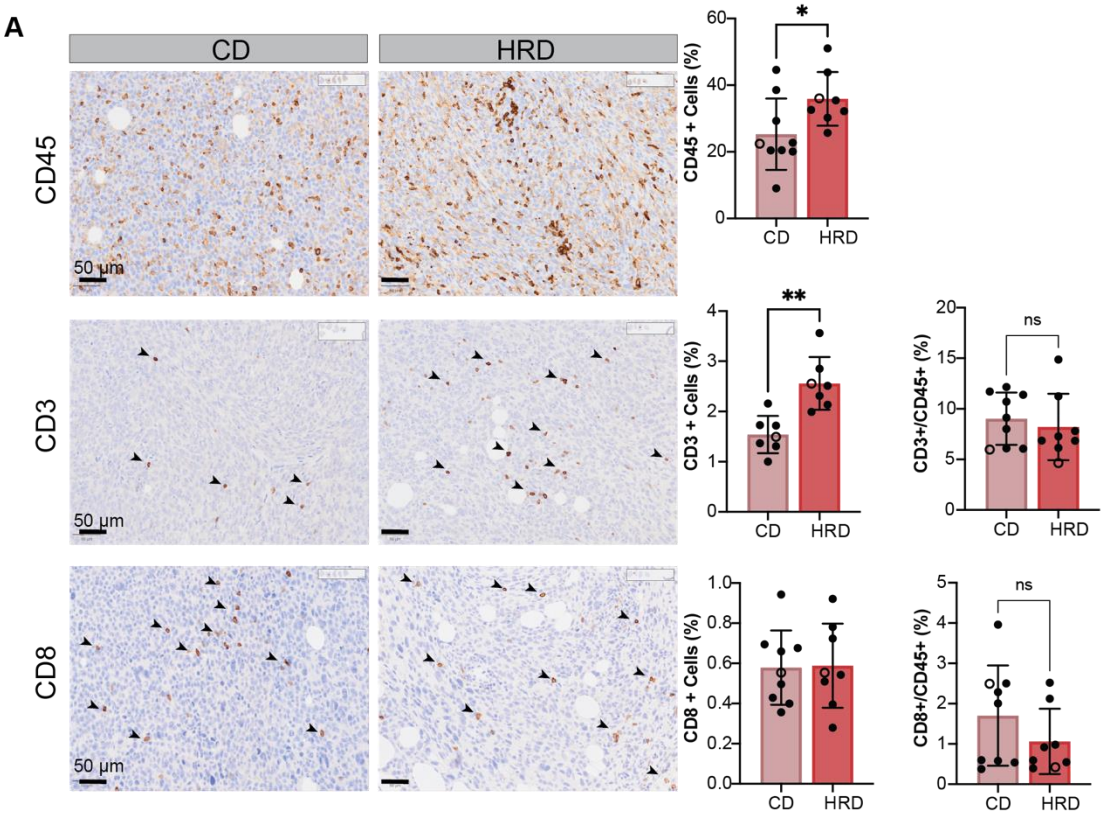



**Figure 6-21. Mammary tumours from mice fed a HRD have increased immune infiltration.**
**(A)** IHC and quantification of CD45, CD3, and CD8 staining in MYAZ16.1e MGTs from CD (n=9) and HRD (n=8) fed mice. Arrows depict positive staining for CD3 and CD8. Bar plots are presented as mean ± s.d. and individual tumours are shown with the unfilled data points depicting the representative IHC on the left. Unpaired two-tailed t-test. *p≤0.05, **p≤0.01.

To elucidate potential immune cell interactions within the TME, cytokines were profiled within tumours using a membrane-based antibody array against cytokines and chemokines. It is important to note that TIF was not collected during this experiment, therefore, bulk tumour protein lysates were used. While there was

significant variability in cytokine levels in CD and HRD tumours, significant alterations were only found for a few cytokines, including IFN-γ, IL-4, and TARC (Figure 6-22A-D). Significantly, these cytokines were expressed at low levels, with mean pixel densities ranging from 0 to 5 (Figure 6-22B-D), compared to high expressing cytokines such as ICAM-1 (Figure 6-22A,E). Therefore, these changes were not evident by the human eye and only picked up by computer analysis. Therefore, we attempted to confirm increased IFN-γ levels with an ELISA, which had a sensitivity as low as 1.9 pg/mL. However, this failed to confirm an increase in IFN-γ levels in the HRD tumours (Figure 6-22F). Indeed, most samples had levels below the range of the assay (Figure 6-22F). Therefore, further optimization of the assay may be necessary. Alternatively, the cytokine array may be insufficient to accurately compare small changes in low expressing cytokines, and these changes may be artifacts. However, the concomitant increase in IFN-γ and decrease in IL-4 was intriguing. IL-4 is required for M2-polarised macrophages, whereas M1-polarised macrophages require IFN-γ. M1-polarised macrophages promote antitumoural activity, whereas M2-polarised macrophages are linked to pro-tumour effects by promoting an immunosuppressive environment[405]. Relevant to this project, a recent study found that breast cancer patients taking antihistamines for allergies during immune checkpoint blockade therapies had improved OS[406]. The study demonstrated that the histamine-HRH1 axis on tumour-associated macrophages (TAMs) promoted M2-like polarization, leading to impaired cytotoxic T-cell function[406]. By blocking this pathway, either through HRH1 knockout or antihistamine treatment, the polarization shifted toward an M1-like phenotype, enhancing T-cell-mediated antitumour immunity[406]. Considering that histidine is a necessary precursor for histamine synthesis, we assessed histamine levels within the MGTs of mice fed a CD or HRD. However, histamine levels were not significantly reduced in the HRD cohort (Figure 6-22G).

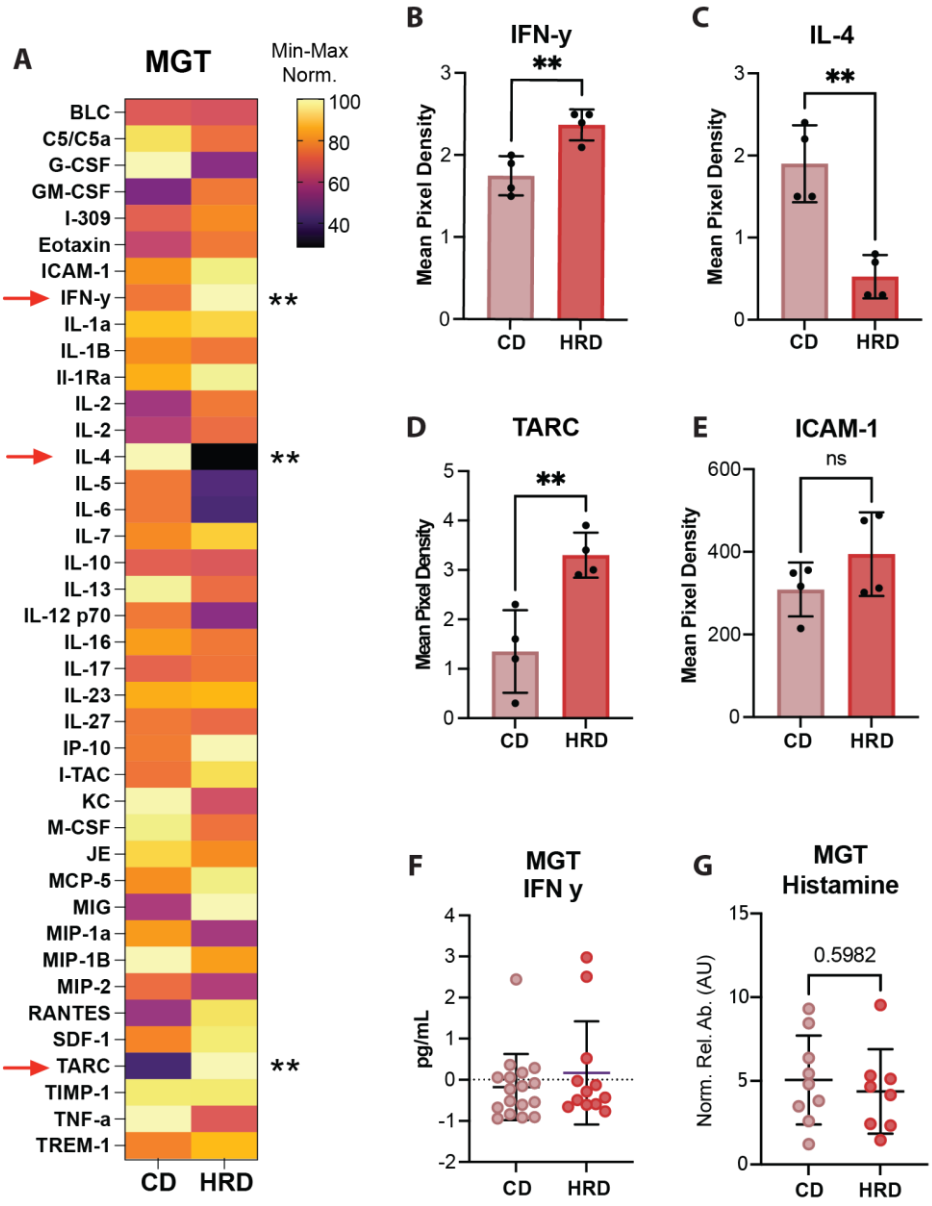



**Figure 6-22. The HRD increases IFNy and reduces IL-4 levels in the MGT.**
**(A-E)** Cytokine array of MYAZ16.1e MGTs from CD (n=4) and HRD (n=4) fed mice. **(A)** Heatmap showing mean pixel density of indicated cytokines and chemokines in CD and HRD-fed mice in the MGT. Colour intensity represents min-max normalized values as a percentage of the minimum (0) and the maximum value (multiple unpaired two-tailed t-tests). **(B-D)** Representative bar plots displaying the mean ± s.d. for the significant differences identified in the MGT in panel A (unpaired two-tailed t-test; **p≤0.01). **(E)** Quantification of pixel-density of ICAM-1 from panel A. **(F)** IFN**γ** ELISA binding assay in MGTs from CD (n=17) and HRD (n=12) tumours. Most tumours were below the detection limit (Y=0). **(G)** LC-MS analysis of histamine levels in the MGTs of CD (n=9) and HRD (n=8) fed mice (mean ± s.d.; unpaired two-tailed t-test).

Histamine is primarily produced by mast cells within the mammary gland and TME[407]. Therefore, since LC-MS analysis was performed on bulk tumour tissue, the effect of a HRD on histamine production may be diluted, as the mast cell population comprises only a small percentage of the total cell population within the tumour. Because tumours from the HRD cohort had increased infiltration of CD45-positive cells compared to the control diet cohort, IHC staining was performed for specific macrophage markers, including CD11b, CD11c, CD68, and CD163, to assess whether there were changes in macrophage populations. CD11b and CD68 identify overall changes to the population of macrophages, CD11c is a marker for dendritic cells and M1-polarised macrophages, and CD163 identifies M2-polarised macrophages. Tumours from the histidine reduced diet group displayed increased staining for all markers (Figure 6-23A). The HRD should reduce histamine production within the TME, thus a polarization of TAMs towards the M1-like phenotype is expected. However, it appears as though HRD tumours have increased M2-polarised macrophages compared to CD tumours (Figure 6-23A). Furthermore, M2-polarised macrophages are primarily observed around the periphery of tumours from the CD cohort, whereas they are completely infiltrated in the HRD tumours (Figure 6-23B). Notably, increased CD11c staining is observed in HRD tumours (Figure 6-23A). To determine whether this is due to changes in dendritic cells or M1-polarised macrophages, profiling with more specific immune markers will be necessary. Together these data highlight that the immune system may be involved in affecting tumour growth in mice fed a HRD, however, whether this is due to LAT1 function, histidine limitation, or a result of an altered TME remains to be explored.

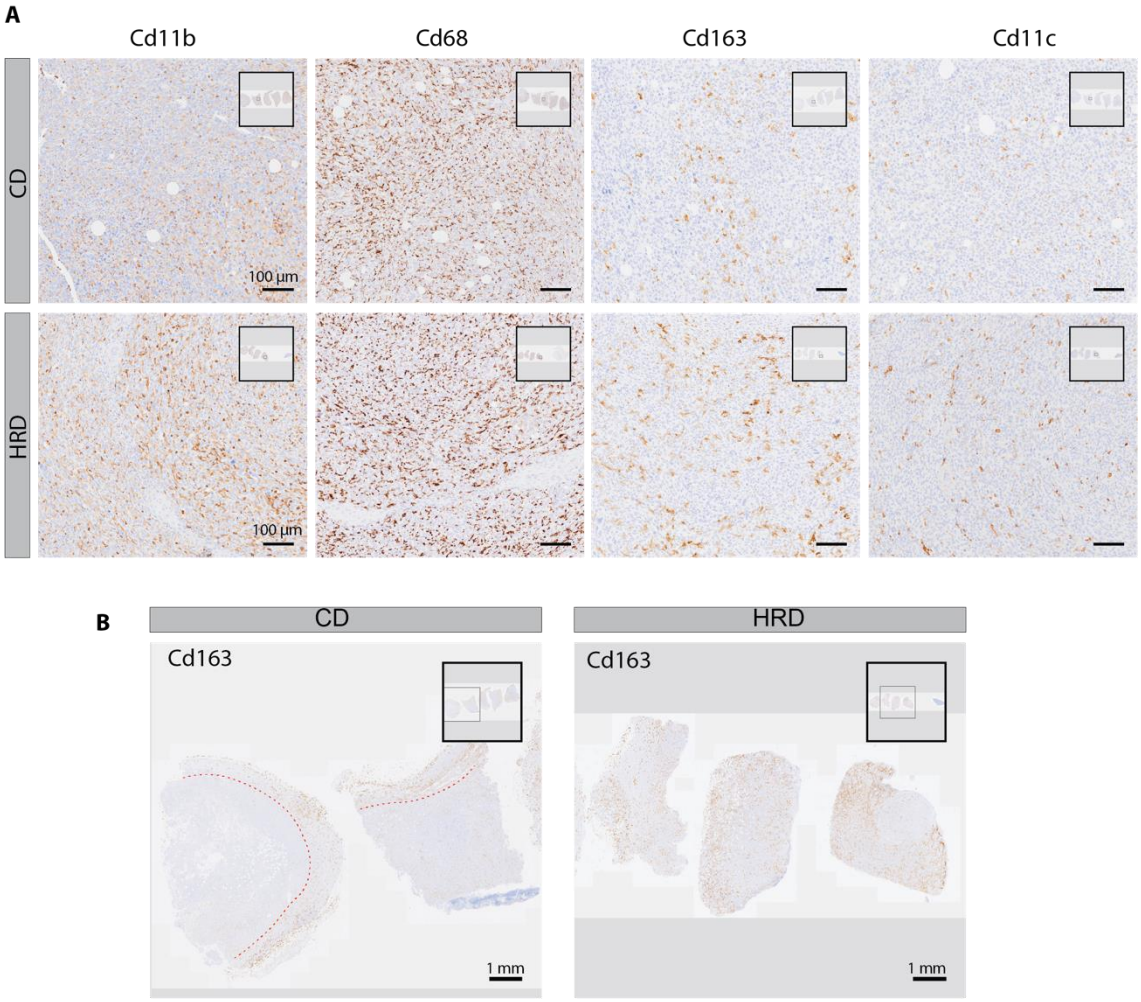



**Figure 6-23. MGTs from mice fed a HRD have increased TAMs**
**(A)** IHC and quantification of CD11b, Cd68, Cd163, and Cd11c staining in MYAZ16.1e MGTs from CD (n=9) and HRD (n=8) fed mice. **(B)** Whole tumour section view of infiltration. The red dashed line in the CD tumours marks the edge of the positive staining for Cd163 and illustrates the lack of immune cell infiltration into the MGT.

To better understand the contribution of the immune system to tumour growth in mice fed a histidine reduced diet, we repeated the experiment in MYAZ16.1e orthotopic allografts in immunocompromised NOD-SCID mice, which are deficient in adaptive immunity and exhibit defective macrophage function[408]. This makes them a suitable model for investigating the overall contribution of the immune system in tumours from the histidine-reduced diet cohort. As was described previously, NOD-SCID female mice were acclimated to a 100%(CD) or 20% (HRD) histidine experimental diet gradually over one week and were fed 100% of each experimental diet for two weeks before orthotopic subcutaneous injection of MYAZ16.1e into the MFP (Figure 6-24A). Tumour growth and body weight were monitored. Mice fed a HRD had a striking decrease in their ability to gain weight

compared to mice on the CD (Figure 6-24B). Furthermore, HRD mice exhibited significant weight loss from their maximum weight (Figure 6-24B). Indeed, on average a 6.2% ± 3.3% decline in body weight from their maximum weight was found in HRD mice compared to 0.16% ± 0.32 %(med(0)) in CD mice. Importantly, histopathological analysis of quadriceps from mice on these diets indicated that mice fed a HRD had severe muscle loss, indicative of muscle atrophy under dietary histidine limitation (Figure 6-24C). Therefore, the diet appears to be less well tolerated in immunocompromised mice. However, because the experiments in immunocompetent and immunocompromised mice were not done in parallel, we cannot exclude the possibility that other variables may have led to reduced weight gain. As was observed in immunocompetent mice, tumour growth was retarded in mice fed a HRD, but unlike immunocompetent mice this decrease in tumour volume and weight was not statistically significant (Figure 6-24D-F). Furthermore, only an insignificant reduction in tumour weight was observed when the tumour weight was normalized to individual body weight (Figure 6-24G). These results suggest that reduced dietary intake of histidine enhances the antitumour response of the immune system, which contributes to inhibition of tumour growth. However, a slight reduction in tumour growth in weight normalized NOD-SCID mice fed a histidine reduced diet indicates that histidine limitation likely impacts the tumour directly as well.

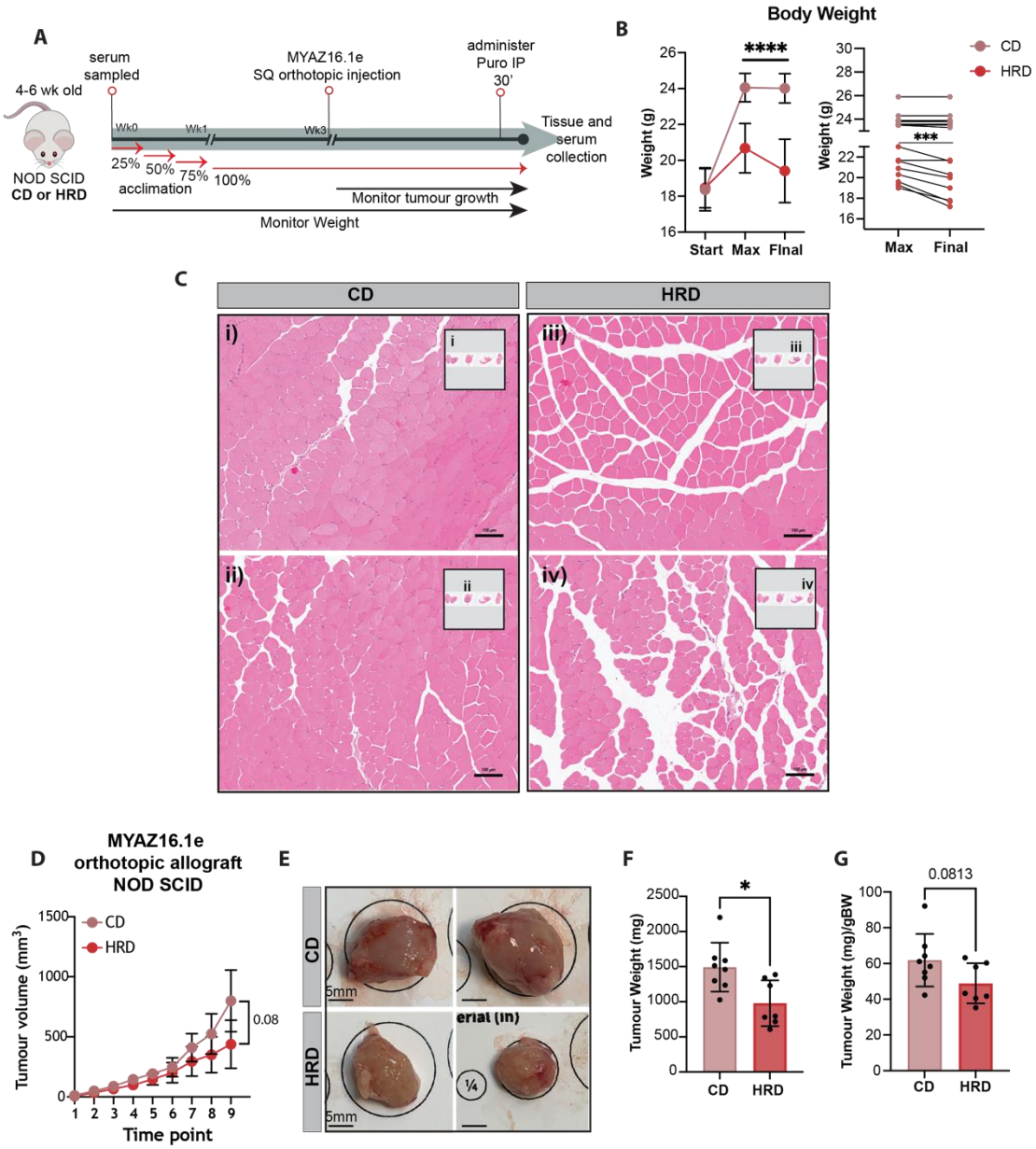



**Figure 6-24. The immune system contributes to the anti-tumour efficacy of the HRD.**

**(A)** Schematic of experimental timeline of Nod-Scid mice placed on a CD (control diet, n=8) or HRD (histidine reduced diet, n=8) at 4-6 weeks of age, and MGTs were initiated through an orthotopic subcutaneous injection of MYAZ16.1e cells. **(B)** Body weight (left) and change in weight of individual mice (right). Data are presented as mean ± s.d.; two-way ANOVA with Šídák correction. **(C)** Representative H&E images of cross sections of quadricep muscles. Scales bars are 100 µm. **(D)** Tumour volume of mice on the CD (n=8) and HRD (n=8). Data are presented as mean ± s.d.; repeated measures two-way ANOVA with Geisser-Greenhouse correction and Šídák for multiple comparisons. **(E)** Images of representative tumours. **(F)** Tumour weight at collection and **(G)** Tumour weight normalized to grams bodyweight. Data are presented as mean ± s.d. unpaired two-tailed t-test. *p≤0.05, ****p≤0.0001.

## 6.8 Discussion

In a study published April of this year, *SLC7A5* was identified as essential for proliferation of cells cultured in low histidine containing media in a CRISPRi screen[367]. In this chapter we demonstrated that upon histidine limitation, specifically, Myc and Atf4 induction co-regulate transcription of Slc transporters such as *Slc7a5* and *Slc1a5*. This was shown to maintain glutamine and EAA pools, which could be a necessary compensatory response to the loss of a bidirectional LAT1 substrate. Furthermore, histidine limitation in Myc-low cells insensitive to histidine deprivation results in significant induction of *Slc7a5*/Lat1 downstream of Atf4, which sensitizes them to treatment with LAT1 and ISR inhibitors. Together these results suggest that histidine is important in maintaining EAA homeostasis and that cancer cells induce the Myc and the ISR to cope with histidine limitation through upregulation of amino acid transporters. Therefore, we tested whether chronic dietary histidine limitation was a viable treatment strategy to target Myc-driven mammary tumours *in vivo*. These data revealed a significant requirement for histidine in Myc-driven tumourigenesis, however, defining the mechanism by which dietary histidine limitation impeded tumour growth has been challenging. Dietary histidine limitation resulted in significant metabolic rewiring across multiple organs. Furthermore, histidine limitation promoted an antitumour immune response which significantly contributed to the inhibition of Myc-driven tumour growth under histidine restriction. This chapter also highlights potential avenues of treatment strategies, combining histidine limitation with inhibitors targeting the ISR or amino acid uptake, such as the LAT1 inhibitor, JPH-203. However, it also serves as a cautionary reminder, underscoring key considerations when employing EAA limitation as a therapeutic strategy.

Histidine limitation, but not limitation of isoleucine or leucine, resulted in significant increase in Myc transcription and protein levels. At odds with this, *SLC7A5* knockout was demonstrated to reduce translation of MYC and downstream MYC-dependent transcription[163]. However, while histidine is the preferred bidirectional LAT1 substrate in Myc-dependent cancer cells, LAT1 can still utilise glutamine and tyrosine for EAA uptake[229]. Therefore, upregulation of LAT1 would facilitate uptake of EAAs, including histidine, when histidine is limited, which could support

translation of Myc. Alternatively, Froldi et al., demonstrated an important link between Myc-dependent cellular growth and histidine sensitivity[261]. Indeed, neural mutant clones that did not depend on Myc/eiF4E for cellular growth were insensitive to dietary histidine limitation. In contrast, clones that were dependent on Myc/eiF4E for cellular growth were sensitive to histidine[261]. However, when Myc was overexpressed in these clones, they became less sensitive to histidine limitation[261]. Our results reinforce this relationship between histidine and Myc. Indeed, induction of Myc upon histidine limitation, facilitates transcription of *Slc* transporters, which are important in coping with histidine limitation. Furthermore, inhibiting the function of these transporters was found to render cells sensitive to histidine limitation. However, Myc was only partially involved in the transcriptional response downstream of histidine limitation, and Atf4 was found to be partially involved. Therefore, Myc and Atf4 may act in concert to regulate the response to histidine limitation. Myc overexpression activates the ISR/ATF4 pathway through PERK and GCN2. Indeed, both arms were found to be necessary for optimal ATF4 expression in MYC-transformed cells[224]. MYC-mediated transcriptional activity results in upregulation of tRNAs. This is necessary to meet the demands of protein translation in MYC-transformed cells, however, it also activates the ISR pathway through GCN2, which responds to uncharged tRNAs. Indeed, ectopic expression of MYC significantly induced expression of uncharged tRNAs, including histidyl-tRNAs, which prime or activate the GCN2/eIF2α/ATF4 arm of the ISR[224]. Therefore, upon deprivation of amino acids such as histidine, accumulation of uncharged tRNAs bind to GCN2 and lead to its activation. Indeed, deprivation and limitation of histidine resulted in eIF2α phosphorylation and Atf4 induction in Myc-driven tumour cell lines, in agreement with previous reports[378,409]. Therefore, both intrinsic factors such as Myc amplification and extrinsic factors, such as amino acid limitation, can activate the ISR. Prior studies have demonstrated that GCN2-dependent genes, including many SLC transporters, are closely associated with amino acid deprivation and transport pathways[241]. In one study, leucine deprivation in GCN2+/+ mouse embryonic fibroblasts resulted in 731 differentially regulated genes, 61% of these were found to be GCN2/ATF4 dependent, highlighting the scale of transcriptional reprogramming that occurs upon activation of the ISR[410]. However, of the GCN2-dependent genes which were upregulated, only 5 of these genes were classified as being related to amino acid transport, including *Slc6a9*,

*Slc1a5*, *Slc7a5*, *Slc43a1*, and *Slc6a6*[410]. In our data, leucine deprivation led to an approximately 2-fold increase in *Slc1a5* and *Slc7a5* transcript expression in Myc-driven tumour cells. However, histidine deprivation resulted in significantly greater induction of these genes. This raises the question of whether the transcriptional program downstream of the GCN2/eIF2α/ATF4 pathway is differentially regulated depending on which amino acid is limited and whether it is more sensitive to deprivation of certain amino acids. GCN2 contributes to mTORC1 inhibition during leucine or arginine deprivation through ATF4-independent mechanisms[411], highlighting the complexity in responses to specific amino acid shortages. Indeed, activation of GCN2 in response to EAA deprivation elicits a highly cell-type-specific transcriptional response[412–414]. For example, one study that quantified the expression of ASNS, a hallmark gene of ISR activation, across different tissues under single EAA deficiencies found significant variation in the response depending on both the tissue and the specific EAA[399]. This suggests that the cellular response to amino acid deprivation may be selective, based on the specific requirement of individual amino acid for cell function. Given the important role for GCN2 in maintaining amino acid homeostasis[241] , LAT1-mediated EAA homeostasis[236], and the role of histidine as the preferred bidirectional LAT1 substrate, it is especially interesting that GCN2 recognizes and binds uncharged tRNAs to a domain that is homologous to histidyl-tRNA synthetase, which is conserved across all species with GCN2 homologs[376]. This might suggest that GCN2 has evolutionarily been a sensor for histidine levels, which may be an important indicator of AA homeostasis. However, inconsistent with this hypothesis, purified GCN2 was found to bind various uncharged tRNAs with comparable affinities, whereas charged tRNAs bound with lower affinity[164]. This suggests that GCN2 can only distinguish between charged and uncharged forms of tRNA. However, while activation of GCN2 may not differ between amino acids, the outcome of ATF4 activation is considered highly context dependent[370]. Indeed, ATF4 can trigger transcription of apoptotic genes or adaptive genes[370]. Furthermore, GCN2-independent signalling mechanisms have been identified in response to amino acid availability[410]. Future work will be necessary to understand the mechanisms leading to this differential response to histidine limitation compared to limitation of other EAAs, such as leucine, isoleucine, and methionine in Myc-dependent cancer cells.

Clinical trials with the LAT1 inhibitor, JPH203, have demonstrated an anti-tumour effect on biliary tract cancer (BTC)[415,416]. The success in BTC aligns with previous studies demonstrating that LAT1 is overexpressed in 64% of resected BTC samples and is correlated with poor prognosis[324,417]. Therefore, this suggests that JPH203 treatment may be more effective in tumours with high LAT1 expression. Importantly, the phase I study, which included different solid tumours, had a small sample size (n=17), with only one patient with breast cancer. Considering that LAT1 has been identified as an independent prognostic marker in breast cancer, it is likely that JPH203 treatment could be effective in this tumour type as well[219,286,322]. In this chapter we demonstrated that limiting histidine in a Myc/Lat1 low mammary tumour cell line, 67NR, resulted in significant upregulation of *Slc7a5*/Lat1 mRNA and protein expression. This sensitised these cells to treatment with JPH203, reducing the $IC_{50}$ of JPH203 from 25.4 μM to 8.4 μM when combined with histidine limitation, indicating a >2-fold increase in potency. This suggests that reducing histidine plasma levels, whether through dietary intervention or through enzymatic degradation, may increase the antitumour efficacy of JPH203 and could broaden its use to a wider range of tumours, including those that may have lower LAT1 expression.

Dietary approaches as alternative, or complementary, to drug treatments in cancer have gained significant attention, with recent progress demonstrating the potential for defined diets in targeting metabolic vulnerabilities within tumours. While much of this research focuses on caloric restriction, fats, and carbohydrates, in recent years the role of amino acids in metabolism has garnered interest. Much of the work in this area has focused on NEAAs, as cancers have an increased reliance on dietary NEAAs despite the capacity to synthesize them. Limiting the availability of amino acids from circulation can be achieved through degradative enzymes or by diet. For a substantial period of time, asparaginase was the only degradative enzyme in cancer treatment, used to target asparagine and has been a mainstay in treatment of ALL[418–420]. More recently, enzymes targeting degradation of methionine (I-Met)[421,422], cysteine/cystine (Cyst(e)inase)[423–425], and arginine (ADI-PEG20)[426–428] have shown promise in different cancer models. However, degradative enzymes for every amino acid do not yet exist or have not been tested. Furthermore, more work is required to understand how these degradative enzymes remodel metabolism and

how tumours adapt to them. Compared to NEAAs, dietary restriction of EAA has received less attention, likely due to a narrower therapeutic window, as EAA are essential for both normal and cancer cells. However, while neither healthy tissues nor tumours can survive in the absence of EAAs for long, tumours have an increased requirement for EAAs and, therefore, would be more sensitive than normal tissues to the restriction of individual amino acids. Indeed, methionine-restricted diets have been generally well tolerated in humans and have been effective at reducing methionine plasma levels[189,190]. However, restriction of other amino acids could be less well-tolerated[394]. Therefore, further research is necessary to determine whether individual EAA restricted diets are feasible. Furthermore, dietary deprivation of any individual EAA has been demonstrated to lead to a myriad of effects, some of which were tissue or EAA specific [394,399]. Therefore, further research is needed in this area to better understand the adaptive metabolic responses associated with dietary restriction of EAAs for cancer treatment. In this chapter, we sought to determine whether dietary histidine restriction could be a therapeutic approach for the treatment of Myc-dependent mammary tumours. We observed reduced tumour growth in mice fed a HRD compared to those fed a CD. However, the HRD led to reduced body weight, significant alterations in the serum and liver amino acid profile, and muscle atrophy. The potential effect of histidine restriction on the liver could be a cause for concern. Mice fed leucine deficient diets rely on GCN2-mediated adaptation in the liver to maintain fatty acid homeostasis and prevent severe liver steatosis[413]. However, induction of the ISR was found to be absent in the livers of mice fed histidine-, phenylalanine-, or methionine-deficient diets, compared to diets deficient in the other EAAs[399]. In contrast to this study, deprivation of any of the nine EAAs was capable of repression fatty acid synthase (*FAS*) in a GCN2-dependent manner in HepG2 HCC cells[429]. Therefore, more work will be necessary to understand how a HRD affects the liver metabolome, as we observed. Muscles store amino acids in proteins, which are released through proteolysis when amino acids are needed in the body. When the balance between muscle protein synthesis and degradation is skewed towards catabolism, skeletal muscle mass is lost. Indeed, muscle atrophy was observed in mice fed any diet deficient in a single EAA, with differing potencies underlying the individual role of these amino acids in muscle protein synthesis[399]. Branched chain amino acids, threonine and tryptophan have been demonstrated to

be important in maximizing muscle protein synthesis[430]. This is consistent with the observed effect of each individual EAA deficient diet on muscle atrophy in this order of potency: Ile$^-$>Val$^-$>Thr$^-$>Leu$^-$>Trp$^-$>His$^-$>Phe$^-$>Met$^-$>Lys[399-]. Therefore, histidine limitation may be more well tolerated than limitation of other EAAs.

In comparison to the liver, the levels of most amino acids were not significantly altered in the MGT of HRD mice. However, we observed significant changes in the abundance of Krebs cycle intermediates and NEAAs, aspartate and asparagine. We observed an increase in protein expression of mitochondrial and cytoplasmic aspartate transaminases, Got1 and Got2, along with a reduction in Gls1 and Asns in MGTs from mice fed a HRD. In PDAC cells, reprogramming of glutamine metabolism to produce aspartate via GOT2, followed by the conversion of aspartate to malate through GOT1, and subsequent production of NADPH through malate to pyruvate conversion, was crucial for maintaining redox homeostasis[130]. However, this failed to be replicated in vivo, and GOT2 KD was found to be dispensable for redox balance and growth of xenografts[431]. We observed increased $^{13}$C enrichment of glutamate, aspartate, malate and citrate compared to α-ketoglutarate, succinate, and fumarate from [U-$^{13}$C]-glutamine in HRD and CD tumours. Therefore, aspartate may replenish the Krebs cycle and contribute to malate and citrate pools. However, we did not observe any differences in $^{13}$C enrichment in the CD or HRD group, despite significant differences in the abundance of Krebs cycle intermediates observed in the HRD. However, the [U-$^{13}$C]-glutamine bolus increased the total abundance of these metabolites, making it difficult to discern differences in glutamine flux. Aside from the Krebs cycle and malate-aspartate-shuttle, aspartate is essential for macromolecule synthesis (Figure 1-4). Indeed, another study demonstrated that starvation-induced autophagy in yeast led to increased glutamate levels to replenish nitrogen reserves and aspartate synthesis, which was necessary for protein translation and nucleotide synthesis[432]. Understanding how tumour cells reprogram glutamine metabolism under histidine limitation could reveal new insights into strategies that help tumour cells cope with histidine restriction or nutrient deprivation and may open novel therapeutic avenues that warrant further exploration. Indeed, it would be interesting to determine whether shifting glutamine away from Krebs cycle anaplerosis, could provide free glutamine for exchange through Lat1 to

compensate for histidine limitation. Intriguingly, we observed a reduction in Gls1, which suggests that there is reduced glutamine catabolism in tumours from mice fed a HRD.

A major hindrance to antitumour immunity is competition for nutrients within the TME. Indeed, increased uptake of amino acids by tumour cells, facilitated by overexpression of SLC transporters, outcompete immune cells and dampen their effector functions[264,433]. Early studies have demonstrated the critical role for leucine in the antitumour function of immune cells[434]. As mentioned previously, leucine has a crucial role in immune cell activity by regulating mTORC1[173,175]. Therefore, given the capacity of LAT1 for leucine uptake, LAT1 is essential for T-cell function. Consistently, SLC7A5 KO in T-cells impedes lineage differentiation through mTORC1-dependent mechanisms[435]. Furthermore, T-cell receptor activation results in rapid activation of the mTORC1 signalling pathway underlying the increased biosynthetic demands of activated T-cells[436]. In accordance with this, T-cell receptor activation induces the expression of amino acid transporters such as ASCT2[437] and LAT1[435]. Indeed, induction of LAT1 upon T-cell activation is necessary for EAA uptake and full activation[404]. Genetic and pharmacological inhibition of LAT1 was demonstrated to impair EAA uptake and function of activated T-cells. Therefore, histidine limitation could affect LAT1-mediated uptake of EAAs in T-cells along with tumour cells. However, opposing this view, the immune response appeared to be heightened in tumours from mice fed a HRD. Compared to immunocompetent mice, the HRD had only a minor effect on tumour growth in immunocompromised mice when normalized to body weight. Furthermore, HRD tumours from immunocompetent mice had an increased proportion of CD45-positive cells compared to CD tumours, indicative of an active immune response. This appears to be inconsistent with reduced LAT1 function, however, immune cells such as T-cells may use glutamine rather than histidine as a bidirectional LAT1 substrate. Notably, inhibition of ASCT2 in CD4+ T-helper cells resulted in reduced glutamine and leucine levels[437]. Thereby suggesting that ASCT2/glutamine are important in maintaining cellular leucine levels, which aligns with ASCT2 and LAT1 coupled activity[142]. Therefore, T-cells may cope with a reduction in histidine availability through the utilization of different exchange substrates. Interestingly, we observed significantly increased serum glutamine,

which may be reflected in the TIF, which could bolster LAT1 activity and compensate for histidine limitation. In addition, glutamine has been recognised as essential for several immune functions and is highly contested in the TME[158]. Therefore, changes in the TME due to metabolic reprogramming within the serum and the tumour could affect immune function. However, we did not observe significant differences in the proportion of CD3+ or CD8+ T-cells in MGTs from CD or HRD-fed mice. Importantly, histidine is decarboxylated by HDC to produce histamine. Mast cells use histidine to produce histamine which has been described to affect various aspects of immune function by modulating the activity of a diverse array of immune cells in cancer through its interaction with cell surface histamine receptors[438]. Notably, tumours from mice fed a HRD had increased macrophage infiltration compared to those from CD mice. Recent work has highlighted that histamine polarizes TAMs towards the M2-like pro-tumour phenotype [406]. Although we did not observe a reduction in histamine levels in the bulk tumour tissue of HRD fed mice, it is possible that reduced histidine availability could limit histamine production by mast cells and alter immune function in the TME. However, currently, we do not have enough data to determine whether histidine limitation abrogates histamine production and affects the activity of TAMs. Given histamine's broad impact on both immune and tumour cells, further research is needed to determine whether specific immune populations are responsible for the observed antitumour response in tumours under histidine limitation.

In the last decade, efforts to understand the role of amino acid metabolism in tumourigenesis have expanded beyond glutamine. It is well understood that metabolic requirements in tumours are dependent on the oncogenic driver as well as the tissue of origin[93]. We have elucidated an important role for histidine in Myc-driven tumourigenesis that can be targeted as a metabolic vulnerability. However, the ideal amino acid candidate as a therapeutic target would affect cancer cells but not healthy cells. Given the increased demand for histidine in Myc-driven tumours, histidine limitation should be biased against the tumour. However, due to the systemic effects observed due to dietary histidine limitation, more research will be necessary to assess the feasibility of dietary limitation of histidine as a therapeutic strategy. However, importantly, dietary limitation of other EAAs, such as phenylalanine and methionine have proven tolerable and effective[190,189,439]. While

using inhibitors targeted against specific amino acid transporters to limit amino acid uptake, such as LAT1, have demonstrated efficacy *in vitro* and *in vivo* at inhibiting tumour growth, they have been less effective in clinical trials[415,416]. Indeed, much of the current strategies targeting amino acids such as glutamine, arginine, and asparagine in cancer have revealed robust compensatory mechanisms evoked by the tumour that lead to resistance[440]. However, enzymatic degradation of amino acids like asparagine have been effective. Nonetheless, much of the success in targeting amino acid metabolism in cancer likely lies in combinatorial treatment strategies. This requires a mechanistic understanding of the role of the amino acid target within specific systems and contexts. In this chapter, we revealed that Myc and Atf4-coregulation of amino acid transporters such as Slc7a5/Lat1 is induced upon histidine limitation, and histidine limitation can be used to sensitize cells to Lat1 inhibition. Therefore, the development and thorough testing of enzymes that can deplete histidine may be a potential avenue that could improve the efficacy of JPH203 for the treatment of breast cancers and could perhaps be applicable to other Myc-dependent cancers. Overall, the data presented in this chapter indicates that histidine limitation could be a promising therapeutic strategy for Myc-driven breast cancers that warrants more attention.

**Summary**

To summarize, this Chapter has:

1) Evaluated the impact of histidine limitation on the ISR in Myc-driven tumour cells.
2) Identified histidine as an important mediator of amino acid homeostasis.
3) Identified histidine limitation as a complementary strategy to enhance the effectiveness of LAT1 or ISR inhibition.
4) Demonstrated the requirement for histidine in Myc-driven mammary tumourigenesis.
5) Highlighted the challenges associated with limitation of EAAs such as histidine.

# Chapter 7. Discussion

The existing literature suggests that glutamine, a low-affinity LAT1 substrate, is the primary amino acid responsible for LAT1 function[142], supported by concurrent upregulation of ASCT2 and LAT1 in cancer[151,327]. However, metabolism is inherently flexible, and the tumour microenvironment, tissue of origin, and oncogenic lesion dictate these metabolic pathways[93]. Therefore, this project aimed to determine whether MYC, an oncogene that leads to metabolic reprogramming and "glutamine addiction"[97,111,244], depends on histidine, a high-affinity LAT1 substrate, to maintain the activity of this essential amino acid transporter and support MYC-driven tumourigenesis. In this thesis, we have demonstrated that Myc-driven mammary tumours have increased levels of histidine compared to the normal mammary gland and ErbB2-driven mammary tumours. Furthermore, while glutamine is primarily catabolised for anaplerosis in the Krebs cycle, histidine is a metabolic dead-end in these tumour cells. Importantly, Myc-driven tumour cells use histidine rather than glutamine as the bidirectional Lat1 substrate, supporting the transport of EAA and mTORC1/4E-BP1 signalling. Given this important role for histidine in EAA uptake in Myc-driven tumour cells, histidine limitation resulted in enhanced upregulation of SLC transporters that maintain amino acid homeostasis. This revealed synthetic lethalities with histidine restriction in these tumour cells. Finally, we show that the availability of histidine is a vulnerability in MYC-driven tumourigenesis that can be targeted therapeutically. However, we highlight the challenges involved in targeting the role of histidine via dietary intervention.

In the previous chapters, I have provided a detailed analysis and interpretation of the results within the context of each chapter. In this chapter, I will combine the previous chapters' insights into a broader understanding of the role of histidine in Myc-driven tumours and beyond. Specifically, I will address whether histidine could be a feasible therapeutic target and its potential applicability outside Myc-driven TNBC subtypes. Key points include histidine's role as a LAT1 substrate in the context of glutamine limitation, how histidine supports cancer cell survival in nutrient-deprived environments, and the specificity and implications of the ISR to histidine availability. I will also critically discuss the limitations of using *in vitro* cell models to study SLC transporter mechanisms and metabolic vulnerabilities in

tumours. Finally, I will outline future directions that can further advance this research.

## 7.1 MYC-driven metabolic reprogramming: glutamine utilisation and LAT1 substrates

Understanding which transporters are essential for tumour growth and how a cancer cell's external [TME] and internal [metabolism] environments underscore transporter adaptations is critical for identifying strategies targeting transporter function. Therefore, we aimed to assess whether Myc-induced glutamine addiction altered LAT1 transporter function. Here, we found that Myc-driven tumours have increased demand for histidine due to limited glutamine availability in their environment and increased catabolism. Indeed, Myc-driven tumours had increased histidine levels and uptake compared to the normal mammary gland and ErbB2-driven tumours, suggesting an increased requirement for this amino acid. Notably, Myc-driven tumourigenesis correlated with increased expression of specific amino acid transporters such as *Slc7a5*/Lat1, indicating an increased requirement for Lat1 substrates. This dependency for LAT1 transport in MYC-overexpressing cells has been shown to support MYC translation and metabolic reprogramming[163]. Our data suggests that histidine uptake in cancer cells may depend on exogenous glutamine availability, intracellular glutamine levels, and the requirement for glutamine to fuel the Krebs cycle. This supported our hypothesis that glutamine-limited Myc-driven tumours have an increased requirement for histidine to support LAT1 transport. However, systems-level quantitative modelling of transporter function in cells has previously revealed that the concentration of most amino acids within the cytosol is consistently maintained, and the effect of metabolism (glutaminolysis was modelled in this case) was negligible over time[201]. This would suggest that Myc-hyperactivation, despite increasing glutamine metabolism, would be met by increased glutamine uptake, and glutamine levels would remain stable. This is supported by the increased expression of the glutamine transporter, Asct2, that we observe. However, this assumption is modelled under conditions where the availability of amino acids in the cellular environment is constant. While serum levels of glutamine were ~8-fold higher than histidine, this was reduced to ~2-fold in the TIF and MGT. Therefore, the reduced availability of glutamine in our tumour

model may limit the availability of glutamine to sustain LAT1 transport. Despite this, we found that under all conditions we tested, histidine was the preferred LAT1 substrate in Myc-dependent tumour cells. Indeed, even when cells were cultured with serum levels of glutamine and histidine at which glutamine was 8x the concentration of histidine in the medium, cells utilised glutamine for Krebs cycle anaplerosis and NEAA biosynthesis and histidine for LAT1 transport. Therefore, these data directly contradict the work from Nicklin et al. (2009), which has been the mainstay hypothesis on LAT1 transporter function. While glutamine is a highly abundant amino acid in the serum and can be used as an exchange substrate through LAT1, the oncogenic lesion may determine LAT1 substrate preference. Indeed, while glutamine is involved in several metabolic pathways, histidine is not degraded in Myc-driven mammary tumour cells; therefore, utilising histidine rather than glutamine as an efflux substrate would be significantly less expensive to the cell. These dynamics likely differ depending on the metabolic requirements and the tissue of origin. For example, when we compared the requirement for histidine in TNBC cells to luminal BC cell lines with low GLS1 and high GS expression, there was a significant reduction in histidine uptake. Furthermore, the requirements for histidine can differ across tissues. Indeed, the liver is capable of degrading histidine into glutamate[252]. Therefore, this may shift histidine away from facilitating LAT1 transport in MYC-driven liver cancer compared to Myc-driven mammary tumourigenesis, where histidine is not degraded. In addition to this, the levels of metabolites within the TME depend on the tumour location. Indeed, recent work demonstrates that TIF composition significantly differs in lung cancer and PDAC xenografts[441]. This highlights that SLC transporters are not passive players but adapt and contribute to tumourigenesis depending on their metabolic environment[442,367].

## 7.2 Histidine in mTORC1/4E-BP1 activation in MYC-dependent cancers

mTORC1 regulation downstream of nutrient availability is complex; many amino acids and nutrients are sensed by mTORC1 through independent mechanisms, some of which are dependent on Rag GTPase heterodimers and some of which activated mTORC1 through Rag GTPase-independent pathways[443]. How all these

different nutrient-sensing pathways are integrated to regulate mTORC1 activity remains to be determined. Furthermore, whether these nutrient sensing mechanisms modulate different canonical and non-canonical mTORC1 activity is unknown. Froldi *et al.* (2019) demonstrated a differential requirement for S6K and eIF4E downstream of Tor for the growth of *Drosophila* neural mutant clones dictated by Myc-dependency[261]. Importantly, Myc/eIF4E clones were sensitive to histidine restriction. Differential dependence on mTORC1 downstream targets has not been ascribed to different amino acid sensing mechanisms, and no direct histidine sensors have been found. Therefore, it is unclear how histidine supports Myc/eIF4E-dependent growth. We similarly observed a preferential increase in activation of mTORC1/4E-BP1 compared to mTORC1/S6K1/RPS6 signalling axis in histidine-preloaded Myc-dependent cancer cells, which enhanced global protein translation and cellular growth. While the role of 4E-BP1 in regulating eIF4E and 5'-cap-dependent mRNA translation is well understood, the role of RPS6 is less understood. Initially thought important in ribosome biogenesis, altering all five phosphorylation sites on RPS6 did not affect ribosomal biogenesis or translation[348]. Therefore, the functional significance of RPS6 activation downstream of mTORC1/S6K1 in starved cells is unclear. Further investigation is needed to determine whether differential activation remains true for S6K1 downstream of mTORC1. Before identifying leucine sensors, leucine was hypothesised to bind directly to 4E-BP1 and block its inhibitory activity[362]. Indeed, 4E-BP1 inhibition downstream of amino acids was completely leucine-dependent[362]. However, leucine has similarly been demonstrated to activate mTORC1/S6K1. One caveat is that sensors have not been uncovered for all amino acids; only leucine, arginine, methionine, and threonine sensors have been described[173–176,178,181,444]. Notably, aminoacyl-tRNAs for leucine and threonine have been described as cytoplasmic leucine[173] and threonine[445] sensors, respectively. Glutamine and asparagine have been demonstrated to activate mTORC1 through Rag GTPase-independent mechanisms at the lysosome; how cells sense these individual amino acids remains to be determined[360]. Therefore, aminoacyl-tRNAs for other amino acids may act as amino acid sensors upstream of mTORC1. How mTORC1 integrates input from these different amino acid sensing pathways and whether it results in differential activation downstream of mTORC1 activation will be necessary to

understand the pathological significance of mTORC1 signalling in response to individual amino acids.

We observed rapid uptake and utilisation of LAT1 substrates and/or cationic amino acids in histidine-preloaded cells. This facilitated increased protein translation but only afforded a slight growth advantage. During nutrient starvation, cells upregulate the expression of 'loaders', SLC transporters that allow for a net uptake of small and polar amino acids such as glutamine[201]. While 'harmonisers' (i.e., LAT1) transport substrates rapidly, loaders can allow up to 100-fold accumulation of their substrates in the cytosol[201]. Therefore, histidine preload may increase protein translation due to rapid LAT1 exchange. Still, the intracellular content of amino acids in starved cells may eventually be compensated for through 'loaders' such as SNAT1/2. Therefore, this demonstrates the robust mechanisms by which cells maintain amino acid homeostasis over time. Nonetheless, cells with higher levels of intracellular histidine can boost global protein translation and proliferation. It's been shown that the core of tumours has significantly less glutamine than the periphery, whereas histidine levels were not altered throughout the tumour[246]. Therefore, cells that can accumulate high levels of intracellular histidine to support exchange through LAT1 may be more capable of maintaining amino acid homeostasis and supporting protein translation and proliferation. Furthermore, mTORC1 signalling drives a translational program that supports epithelial-to-mesenchymal transition to promote metastasis[446]. Moreover, MYC activation can drive resistance to mTOR inhibition in metastatic breast cancer by restoring protein synthesis[447]. This potentially centres histidine as a critical metabolite in sustaining protein translation in tumours with MYC hyperactivation.

## 7.3 Implications for histidine in AA homeostasis in MYC-dependent cancers

MYC-hyperactivated cells depend on the GCN2/eIF2α/ATF4 and PERK/eIF2α/ATF4 signalling pathways of the ISR to prevent cell death and sustain protein translation[224,240]. Activation of ATF4 regulates genes that promote cell survival in nutrient-adverse conditions or during oncogene-induced stress. MYC induces the expression of aminoacyl-tRNA synthetases, which activate the GCN2

arm of the ISR[224]. This increases the transcription of SLC amino acid transporters, critical targets of ATF4 in response to amino acid limitation[241]. This increase in SLC transporters maintains amino acid levels to sustain MYC-driven tumourigenesis. The absence of any one individual EAA, except for methionine[448], results in similar transcriptional changes across multiple cell lines[442]. Indeed, specific SLC transporters were found enriched upon restriction of any amino acid, including members of the SLC1 (*SLC1A4/5*), SLC7 (*SLC7A1, SLC7A3, SLC7A5, SLC7A11*), and SLC38 (*SLC38A1/2*)[442]. Indeed, the upregulation of these transporters is essential for rescuing nutrient limitation directly (by supplying the limited nutrient via the high-affinity transporter) or indirectly (by providing a metabolite that compensates for the metabolic requirement of the limited compound)[442]. In two independent CRISPR screens under limitation or depletion of individual amino acids, SLC7A5 was found to be essential for limitation of histidine, tyrosine, phenylalanine, and methionine in one screen, and additionally isoleucine, leucine, phenylalanine, tryptophan, and tyrosine in the other[367,442]. These differences highlight cell-specific requirements for individual amino acids and the presence of potential redundant transporters for some amino acids more than others. However, SLC7A5 was the most significantly enriched in cells cultured under histidine limitation in both of these studies[367,442]. This emphasises that SLC7A5 is a high-affinity histidine transporter in multiple cell lines, and SLC7A5 upregulation during histidine limitation is essential for cell survival in histidine-limited conditions[367,442]. We similarly observed increased Lat1 expression in cells deprived of EAAs such as histidine, leucine, isoleucine, and methionine. However, the resulting induction of SLC transporters varied depending on the individual amino acid restricted. Indeed, histidine limitation resulted in a striking increase that may result from the co-regulation of these transporters by Myc and Atf4. Whether histidine restriction leads to distinct transcriptional responses downstream or results in advanced transcription of similar targets is not known at this time, and a more thorough investigation of the transcriptional response in these conditions will be required to answer this. Notably, we observed that the enhanced transcription of these SLC transporters under histidine limitation compared to leucine, isoleucine, and methionine could maintain or even increase intracellular levels of specific amino acids. However, a significant caveat is that we did not use stable isotopes to replace the amino acids within our media. It is not entirely clear whether this

increase results from uptake, increased protein degradation, or macroautophagy. While this warrants further investigation, we did not observe significant differences in autophagosome formation or UPS activity between cells starved of histidine or leucine, which indicates that upregulation of these transporters acts to maintain levels of histidine as well as other amino acids that (i) may be necessary in compensating for histidine's role as an exchange substrate (i.e; glutamine and asparagine) or (ii) increases uptake of EAA to maintain EAA homeostasis under histidine limitation.

While we were undertaking this project, Chidley *et al*. (2024) demonstrated that the knockdown of SLC7A5 was not sufficient to reduce proliferation rates in leukaemia cell lines under amino acid-replete conditions but demonstrated a robust proliferative defect when any high-affinity LAT1 substrate was limited (i.e., his, ile, leu, met, phe, trp, tyr or val)[367]. This lack of sensitivity to SLC7A5 ablation contrasts the stark sensitivity observed in leaukemia cells with MYC amplification, which were significantly sensitive to the ablation of LAT1[163]. However, our results recapitulate this. While Myc-dependent tumour cells were sensitive to histidine limitation and Lat1 inhibition, we found that Myc-low mammary tumour cells were insensitive to both. However, when we limited histidine in the media, these cells became sensitive to Lat1 inhibition. Given the results from Chidley et al., this is likely not specific to histidine. However, given that histidine limitation leads to a marked increased amino acid response compared to deprivation of other LAT1 substrates (leu, ile, and met), histidine restriction may be a better strategy to sensitise cells to inhibition of this transporter. Furthermore, in Rebsamen *et al*. (2022) similar gain-of-function CRISPR screen, SLC7A5 was only enriched under histidine, tyrosine, phenylalanine, and methionine deprivation in Hek293T and HeLa cells[442]. Therefore, cells may have multiple mechanisms to maintain levels of amino acids, such as leucine, which is necessary to maintain mTORC1 signalling, compared to histidine. These dependencies are likely to be cell-type and environment-specific; for example, in the gain-of-function CRISPR screen from Chidley et al. (2024), SNAT3 was a significant contributor to histidine uptake along with LAT1 in histidine-limited cells but was not critical to maintain histidine levels when knocked down[367]. SNAT3 acts as a 'controller', where the uptake of amino acids such as asparagine, glutamine, and histidine is coupled to Na+-symport and

H+-antiport, creating an electroneutral transport process[201]. This mechanism limits amino acid uptake, as the ion gradients across the membrane constrain the accumulation. Therefore, SNAT3-mediated histidine import may contribute significantly less histidine than LAT1 and be less essential under histidine limitation, making complementary LAT1 inhibition a promising combination therapy.

Another unique property of histidine limitation is the increase in Myc transcription and translation in both Myc-high and -low cells. This contrasts with the findings of Yue et al. (2017), who demonstrated that LAT1 ablation restricted MYC translation and significantly reduced MYC protein levels[163]. Furthermore, Froldi et al. (2019) provided indirect evidence that histidine restriction downregulates Myc[261]. Their study demonstrated that histidine supplementation failed to promote clonal growth in a Myc hypomorphic background[261]. At the same time, overexpression of Myc rescued the reduction of clonal growth under histidine limitation[261]. Therefore, it is unclear mechanistically how histidine limitation increased Myc mRNA and protein expression in our model. However, we observe increased Slc transporter induction and intracellular amino acid levels. Therefore, this may support Myc translation for some time to help cells overcome histidine limitation, as demonstrated by Froldi and colleagues. Indeed, we found that Myc KO cells had a reduced transcriptional response to histidine limitation, suggesting that Myc has a part in this amino acid response. It was previously demonstrated that Myc levels can be maintained under glutamine limitation by supplementing with asparagine, restoring Myc expression[449]. Therefore, a similar phenomenon may occur here with histidine due to increased amino acid uptake. Overall, it appears that unique feedback between histidine levels and Myc expression exists, and understanding the mechanisms that underlie this relationship may elucidate further therapeutic targets that may be synthetically lethal with histidine restriction. Notably, the increase in Myc and the subsequent induction in SLC transporters make the cells more vulnerable to inhibition of SLC transporters; therefore, while maintaining MYC levels under histidine deprivation could be a compensatory mechanism, it may also be a targetable vulnerability.

## 7.4 Therapeutic targeting of histidine: dietary restriction, transport inhibition in MYC-dysregulated breast cancer and beyond

The prime example of targeting amino acid availability in cancer is the use of the asparagine degrading enzyme, asparaginase, in ALL[450]. Indeed, asparaginase effectively treats leukaemia due to insufficient ASNS activity in immature lymphocytes and leukaemia blasts to meet cellular demands, making them auxotrophic for asparagine[451]. The lack of efficacy in asparaginase for treating other cancers also emphasises the importance of interrogating the specific needs of tumour types when targeting amino acids as a therapeutic strategy. Further highlighting the complexity of amino acid targeting strategies Indeed, even within ALL, significant heterogeneity exists in the response to asparaginase treatment due to compensatory mechanisms that drive resistance[266,451,452].

The connection between diet and health has been acknowledged for centuries, famously captured in Hippocrates' (c. 460- c. 370 BCE) words, "Let food be thy medicine and medicine be thy food," emphasising the enduring relationship between nutrition and health and disease. Therefore, the role of diet in cancer, including breast cancer has received significant attention[12,453–456]. However, much of this research has focused on the role of carbohydrates and fats, with less consideration of protein[296]. Notably, the role of protein in disease has been considered as a whole, but each amino acid impacts cellular and physiological processes that require consideration. Many of these studies compare the efficacy of plant-based or Mediterranean to Western diets in reducing breast cancer risk and mortality[457]. A recently published comprehensive analysis of amino acids in different food sources as well as in ten defined human diets (i.e., plant-based, vegetarian, Mediterranean, American, ketogenic, paleo, etc.) found that there was significant variation in amino acid composition in food and diet compared to carbohydrates and fats[296]. Therefore, identifying the role of these amino acids in disease and elucidating strategies that target them is essential.

The current strategies that exist in targeting amino acids are (i) blocking uptake, (ii) inhibiting biosynthesis, and (iii) amino acid depletion[450]. Histidine is an essential amino acid that cannot be synthesised *de novo;* therefore, histidine targeting strategies must either block uptake or deplete it. Blocking LAT1 with JPH203 has demonstrated efficacy in some preclinical models but has been disappointing in translation[415,416]. This is partly due to redundancy in amino acid transporters and the flexibility in expression of these transporters afforded by the ISR, thereby making them challenging targets[241]. Indeed, despite the upregulation of *Slc7a5*/Lat1 in Myc-driven compared to ErbB2-driven tumourigenesis, Lat1 inhibition with JPH-203 was ineffective at reducing tumour growth, despite demonstrating anti-proliferative effects *in vitro*. Additionally, others have found that LAT1 ablation did not affect cell proliferation[247,367], which we also observe in a Myc-low cell line. These results varied within *in vitro* and *in vivo* systems; however, some groups have found that while ablation of ASCT2 or LAT1 did not display efficacy *in vitro*, they could delay tumour growth *in vivo*, reflecting changes in the tumour microenvironment[148,247]. Given that JPH203 is a competitive inhibitor, and we observe an increase in many EAAs in the TIF of Myc-driven mammary tumours, this lack of efficacy could be due to insufficient levels of JPH203 within the TME, therefore, whether this is due to technical limitations or compensatory mechanisms remains to be determined. However, we and others[367] have shown that limiting LAT1 substrates, such as histidine, improves the anti-proliferative ability of JPH203. Therefore, combining strategies that reduce histidine availability with JPH203 may be promising. Furthermore, this expands the range of tumours that may benefit from LAT1 inhibition beyond MYC-dependent tumours.

Diets free of individual EAAs have resulted in significant weight loss and increased skeletal muscle catabolism and are associated with systemic metabolic changes to varying degrees[394,404]. Valine, for example, is not well tolerated, with animals force-fed valine-free diets not recovering even when switched back to a complete diet[394]. However, dietary restriction of EAAs has proven effective and feasible. Reducing histidine levels could be achieved through multiple strategies, such as (i) a histidine-restricted semisynthetic diet and (ii) an enzyme that degrades histidine. A histidine-restricted diet was found to reduce serum histidine levels in patients with histidinemia, a genetic disorder characterised by a deficiency in the enzyme HAL,

which is necessary for histidine degradation in the liver; individuals with this condition typically have elevated serum histidine levels[458]. Therefore, this could be an effective strategy. Indeed, a methionine-restricted diet in Phase I clinical trials for metastatic cancer, using a specially formulated methionine-free medical diet as the primary protein source and supplemented with low-methionine foods, was well tolerated[189]. Notably, histidine was found to be one of the amino acids which varied most significantly across different diets, with considerably lower levels of histidine in plant-based diets[296]. Therefore, a similar strategy to methionine restriction could successfully limit histidine serum levels. Pre-clinical and clinical methionine limitation has observed manageable weight loss at around 0.5 kg/week in humans[189]. Furthermore, methionine limitation to 0.1% in mouse chow, the same as our 20% histidine diet, in a preclinical model of TNBC resulted in significant weight loss by day 6 of the diet[459]. However, these studies did not assess the impact of the diet on amino acid profiles, skeletal muscle, or the immune system. In our study, we observed a significant reduction in weight gain. However, the weight was overall net positive over eight weeks of dietary limitation, along with systemic changes in metabolism in the serum, tumour, and liver of mice on the HRD. Furthermore, the reduced weight gain was not the sole factor that determined tumour growth, as normalising tumour weight for the overall body weight of each mouse still resulted in a significant reduction in tumour growth. Notably, the antitumour efficacy of the HRD may be partially due to an enhanced immune response. This suggests that HRD may be a well-tolerated and effective strategy. However, whether these changes are due to disrupting histidine's role as a bidirectional LAT1 substrate remains unclear, and how metabolic reprogramming within the tumour systemically affects tumour growth remains to be discerned. An ideal treatment would effectively treat multiple tumour types and be specific and targeted. Therefore, significant effort remains to determine the off-target effects mediated by the HRD. If this diet targets histidine's role in LAT1 transport in Myc-driven mammary tumours, we can better predict treatment efficacy. For example, we found that luminal breast cancer cell lines had reduced uptake of histidine, which correlated with reduced GLS1 expression and increased GS expression and activity. Therefore, a HRD in luminal tumours may be less effective than TNBC with MYC amplification. Similarly, using the HRD in liver cancer may be less effective due to the significant contribution of histidine to glutamate pools in this tissue.

Identifying tumour types that are glutamine-auxotrophic and MYC-amplified may elucidate those that may benefit from a HRD diet or a combined approach with LAT1 inhibition.

Using amino acid degrading enzymes in cancer treatment has expanded beyond asparagine, with targeted degraders for methionine and arginine in Phase I/II clinical trials[450,460]. Therefore, a histidine-degrading enzyme may be on the horizon. One caveat to arginase treatment has been the ability of cells to compensate through the arginine salvage pathway by converting ornithine back to arginine[461]. Histidine cannot be synthesised by cells. Therefore, histidine degradation may be compensated less well. Indeed, we observed significantly reduced levels of histidine within mammary tumours of mice fed a HRD, suggesting that compensatory pathways are insufficient to maintain levels of histidine. However, how histidine limitation affects cells within the TME remains to be determined. A holistic understanding of the effects of histidine limitation on the cells within the TME will be necessary to determine whether cancer cells are disproportionately sensitive to limitation of this EAA.

## 7.5 Limitations

Chidley et al. (2024) found that while overall phenotypes of SLC amino acid transporter dependency in subcutaneous tumours correlated to results in cells cultured in HPLM (human plasma-like medium) and RPMI, some transporters were significantly different *in vivo* compared to *in vitro*[367]. Highlighting the impact of the TME on which SLC transporters become essential for tumour growth. A significant limitation of this work is the use of DMEM for cell experiments, which contains supraphysiological levels of 15 amino acids ranging from 1.0x to 6.7x the concentration of these amino acids found in Plasmax, a media composition modelled after physiological plasma levels of metabolites[462]. Furthermore, DMEM lacks NEAAs such as alanine, aspartate, glutamate, and proline, as well as various other components compared to media that more closely reflect physiological plasma, such as HPLM[463] and Plasmax[462]. However, even these plasma-like mediums cannot fully reflect the TME. For example, we observed a significant reduction in levels of arginine, lysine, and tryptophan, as others have observed[441],

in the TIF of Myc-driven tumours. Therefore, the requirement for SLC transporters that take up these amino acids may be more significant in the tumour than in the cells cultured with supraphysiological or serum levels of these amino acids. Similarly, because LAT1 transport depends on its cytosolic and extracellular affinities, the tumour microenvironment may affect LAT1 activity. For example, tryptophan, a high-affinity LAT1 substrate, is significantly reduced in the TIF relative to the serum. Therefore, LAT1 may become more essential for tryptophan transport than leucine, affecting its role in mTORC1 regulation. While we altered histidine and glutamine concentrations to resemble physiological serum levels in our mouse model, using Plasmax or HPLM may alter these dynamics. Alanine is one of the most abundant amino acids in the serum, and we find the levels are even higher in the TIF; alanine can be used as a carbon source to fuel the Krebs cycle[464]. Therefore, alanine utilisation may compensate for our reduced glutamine levels and provide enough free glutamine for LAT1 exchange. Determining whether histidine is a bidirectional substrate *in vivo* will be critical to identifying histidine availability as a metabolic vulnerability in tumours.

Another significant limitation of this study is that it centres the cancer cell outside the context of interactions with cells in the TME. LAT1 is essential to immune cell function; immune cells compete with cancer cells for nutrients within the TME[404,435]. Therefore, cells that can accumulate more histidine or glutamine may be better able to compete for EAAs within the TME. Indeed, upregulation of SLC43A2 in tumours was found to outcompete T-cells for methionine, limiting methionine metabolism in T-cells and negatively affecting T-cell function[264]. Therefore, MYC-driven LAT1 expression may support immune evasion. Understanding whether histidine sustains LAT1 function in tumour cells and how this impacts immunometabolism may further emphasise histidine availability as a metabolic vulnerability. Indeed, if histidine is used as a bidirectional substrate specifically in Myc-driven tumour cells, histidine limitation may disproportionally impact tumour cells while sparing T-cells that utilise an alternative bidirectional LAT1 substrate such as glutamine or tyrosine. This may suggest combining a HRD with immunotherapy may be a more effective strategy. We observed an increase in immune cell infiltration and reduced efficacy in the inhibitory capacity of the HRD on tumour growth in immunocompromised mice compared to immunocompetent

mice. While mechanistic studies assessing the effect of histidine limitation on immune cells were not in this project's scope, they may reveal further vulnerabilities that can be exploited and are an essential consideration for future studies.

## 7.6 Future Directions

One of the difficulties in this project was translating these mechanistic results into the *in vivo* tumour system. Using the ex vivo system was a promising strategy that more closely recapitulates the TME. However, it still does not recapitulate the *in vivo* system. During this PhD we backcrossed Slc7a5$^{fl/fl}$-Rosa$^{eYFP}$ C57BL/6 mice onto the MMTV-Myc-Cre-Rosa$^{eYFP}$ background and Slc7a5$^{fl/+}$-Rosa$^{eYFP}$ onto the MMTV-Nic-Slc7a5$^{fl/+}$ FVB/N background to generate MMTV-Myc$^{+/+}$-Cre$^{+/+}$-Slc7a5$^{fl/fl}$-Rosa$^{eYFP+/-}$ and MMTV-Nic-Slc7a5$^{fl/fl}$-Rosa$^{eYFP+/-}$ mice, and their WT siblings on the FVB/N genetic background. This experiment will help us answer three questions: (i) do Myc-driven tumours depend on Slc7a5/Lat1 for tumour growth, and does this differ from ErbB2-driven tumours? (ii) Are Myc-driven tumours more sensitive to histidine restriction than ErbB2-drive tumours, and does LAT1 ablation synergise with the HRD to inhibit tumour growth? (iii) is histidine used for LAT1 exchange? Does histidine accumulate further in Myc-driven mammary tumours, and does this differ from ErbB2-driven tumours? This will enable us to confirm Myc-dependency for histidine and LAT1 in a tumour model, assess the specificity of the HRD, and confirm the role of histidine in LAT1 function.

Notably, positron emission tomography (PET) tracers specific to LAT1 have been developed in recent years. These include $^{18}$F labelled amino tracers such as O-(2-[$^{18}$F]fluoroethyl)-l-tyrosine ([$^{18}$F]FET) and 3, 4-dihydroxy-6-[$^{18}$F]-fluoro-l-phenylalanine ([$^{18}$F] FDOPA), and many more with varying specificity[465,466]. Using these tracers in the models described above would allow us to determine whether tumours that lack histidine have a reduced capacity for uptake of the LAT1-targeted PET tracers or whether tumour cells compensate for reduced histidine by using a different substrate to maintain LAT1 activity. Using these LAT1-specific PET tracers *in vivo* would provide significant *in situ* evidence on the role of histidine in Myc-driven tumourigenesis and monitor therapy response.

Cells that can accumulate histidine have increased uptake of LAT1 substrates, enhanced mTORC1/4E-BP1 pathway activation, and increased global protein translation, which provides a proliferative advantage. Therefore, whether this potentiates the metastatic capacity of Myc-driven tumour cells is an interesting question that warrants further investigation. Given more time, *in vitro* experiments could assess the invasive and migratory properties of cells with higher histidine levels than those without. This can be validated *in vivo* using a metastatic mouse model and feeding them a HRD. Given the metastatic potential of TNBC subtypes, identifying mechanisms that support metastasis is essential. Furthermore, cells with an increased ability to accumulate histidine and use it as a LAT1 exchange substrate may be more resistant to therapies. Therefore, identifying whether histidine promotes epithelial-to-mesenchymal transition and metastasis will be critical.

## 7.7 Concluding Remarks

Overall, the evidence presented in this thesis highlights histidine's important role in amino acid homeostasis in Myc-dependent tumour cells (Figure 7-1). Our proposed mechanistic model demonstrates that Myc-hyperactivation increases the expression of amino acid transporters to sustain metabolic programs and protein translation. Specifically, Myc-driven mammary tumours and cells have increased Asct2 and Lat1 mRNA and protein expression, indicating an enhanced requirement for glutamine and EAAs in these tumours. We find that Myc-driven tumours are faced with a TME that is limited in glutamine but enriched in histidine. Therefore, Myc-driven cancer cells are glutamine addicted and primarily use glutamine to fuel the Krebs cycle via glutaminolysis. This limits the availability of cytosolic glutamine that can be used to maintain Lat1-mediated EAA transport. Therefore, increased intracellular histidine accumulated in Myc-driven tumours sustains EAA uptake in Myc-driven cancer cells by acting as the preferential exchange substrate. Uptake of EAAs sustains mTORC1/4E-BP1 signalling and global protein translation, which supports the proliferation of Myc-driven tumour cells and may support tumour progression. This project has highlighted histidine availability as a potential

metabolic vulnerability in Myc-driven tumour cells and emphasises the therapeutic potential of targeting histidine in these tumours.

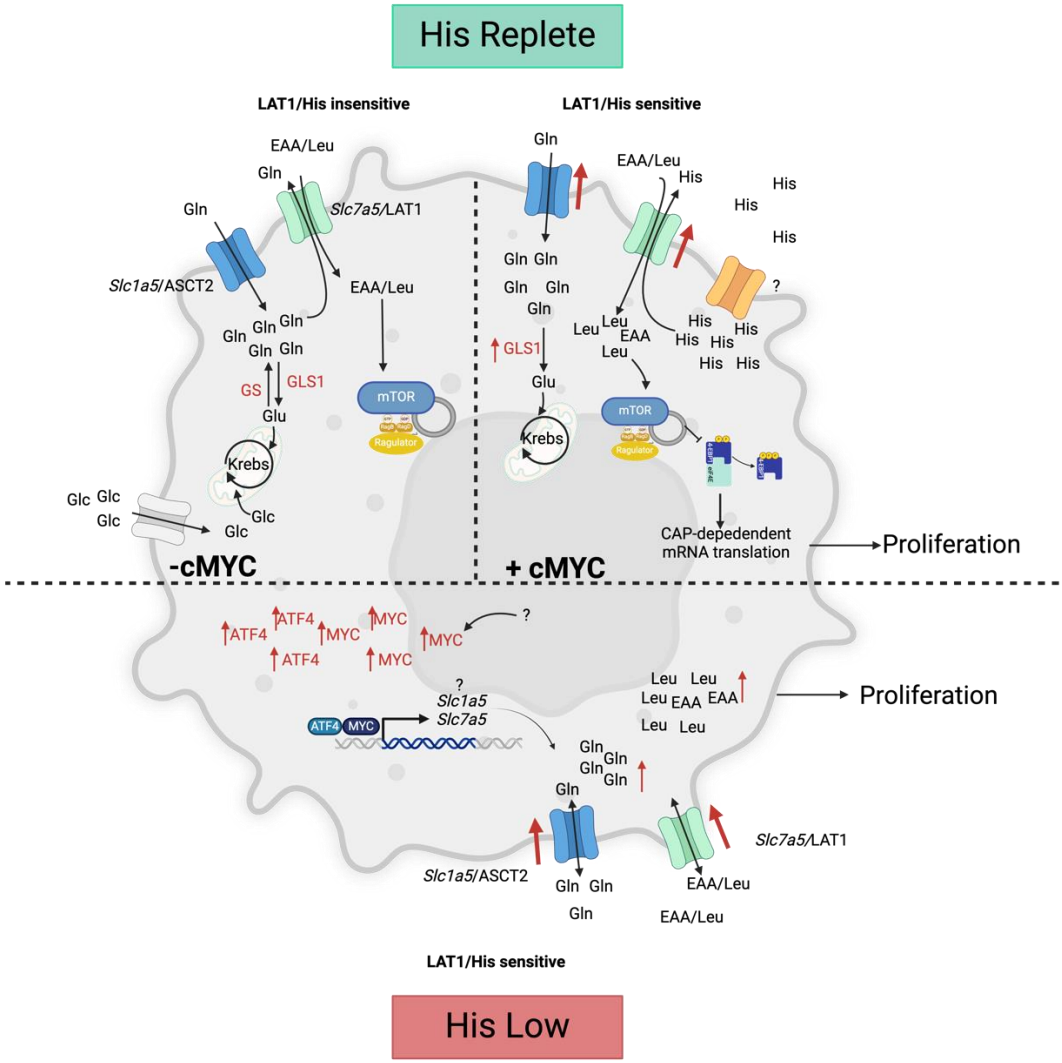



**Figure 7-1.Proposed model of the role of histidine in Myc-independent and dependent cancer cells.** Figure made with biorender.com

# Reference List


1. Sung, H. *et al.* Global Cancer Statistics 2020: GLOBOCAN Estimates of Incidence and Mortality Worldwide for 36 Cancers in 185 Countries. *CA: A Cancer Journal for Clinicians* **71**, 209–249 (2021).
2. Arnold, M. *et al.* Current and future burden of breast cancer: Global statistics for 2020 and 2040. *Breast* **66**, 15–23 (2022).
3. Breast cancer statistics. *Cancer Research UK* https://www.cancerresearchuk.org/health-professional/cancer-statistics/statistics-by-cancer-type/breast-cancer (2015).
4. Bleyer, A. & Welch, H. G. Effect of Three Decades of Screening Mammography on Breast-Cancer Incidence. *New England Journal of Medicine* **367**, 1998–2005 (2012).
5. Cancer incidence by stage. *NHS England Digital* https://digital.nhs.uk/data-and-information/publications/statistical/cancer-registration-statistics/england-2021---summary-counts-only/cancer-incidence-by-stage.
6. Wang, R. *et al.* The Clinicopathological features and survival outcomes of patients with different metastatic sites in stage IV breast cancer. *BMC Cancer* **19**, 1091 (2019).
7. Bowen, R. L., Duffy, S. W., Ryan, D. A., Hart, I. R. & Jones, J. L. Early onset of breast cancer in a group of British black women. *Br J Cancer* **98**, 277–281 (2008).
8. DeSantis, C. E. *et al.* Breast cancer statistics, 2019. *CA: A Cancer Journal for Clinicians* **69**, 438–451 (2019).
9. Gathani, T., Clayton, G., MacInnes, E. & Horgan, K. The COVID-19 pandemic and impact on breast cancer diagnoses: what happened in England in the first half of 2020. *Br J Cancer* **124**, 710–712 (2021).
10. Sprague, B. L. *et al.* Changes in Mammography Use by Women's Characteristics During the First 5 Months of the COVID-19 Pandemic. *JNCI: Journal of the National Cancer Institute* **113**, 1161–1167 (2021).
11. McCarthy, A. M. *et al.* Relationship of established risk factors with breast cancer subtypes. *Cancer Medicine* **10**, 6456–6467 (2021).
12. Villarini, A. *et al.* Lifestyle and breast cancer recurrences: the DIANA-5 trial. *Tumori* **98**, 1–18 (2012).
13. Mao, X. *et al.* Association of reproductive risk factors and breast cancer molecular subtypes: a systematic review and meta-analysis. *BMC Cancer* **23**, 644 (2023).
14. Orrantia-Borunda, E., Anchondo-Nuñez, P., Acuña-Aguilar, L. E., Gómez-Valles, F. O. & Ramírez-Valdespino, C. A. Subtypes of Breast Cancer. in *Breast Cancer* (ed. Mayrovitz, H. N.) (Exon Publications, Brisbane (AU), 2022).
15. Yersal, O. & Barutca, S. Biological subtypes of breast cancer: Prognostic and therapeutic implications. *World J Clin Oncol* **5**, 412–424 (2014).
16. Hu, Z. *et al.* The molecular portraits of breast tumors are conserved across microarray platforms. *BMC Genomics* **7**, 96 (2006).
17. van 't Veer, L. J. *et al.* Gene expression profiling predicts clinical outcome of breast cancer. *Nature* **415**, 530–536 (2002).
18. Crimini, E. *et al.* Precision medicine in breast cancer: From clinical trials to clinical practice. *Cancer Treatment Reviews* **98**, 102223 (2021).

19. Zagami, P. & Carey, L. A. Triple negative breast cancer: Pitfalls and progress. *npj Breast Cancer* **8**, 1–10 (2022).
20. Goldhirsch, A. *et al.* Personalizing the treatment of women with early breast cancer: highlights of the St Gallen International Expert Consensus on the Primary Therapy of Early Breast Cancer 2013. *Ann Oncol* **24**, 2206–2223 (2013).
21. Abdelaziz, M. A., Ebrahim, E. M. & Zikry, M. S. E.-D. Evaluation of Pattern of Relapse in Luminal Breast Cancer. *Al-Azhar International Medical Journal* **4**, (2023).
22. Hwang, K.-T. *et al.* Impact of Breast Cancer Subtypes on Prognosis of Women with Operable Invasive Breast Cancer: A Population-based Study Using SEER Database. *Clinical Cancer Research* **25**, 1970–1979 (2019).
23. Voduc, K. D. *et al.* Breast Cancer Subtypes and the Risk of Local and Regional Relapse. *JCO* **28**, 1684–1691 (2010).
24. Sørlie, T. *et al.* Gene expression patterns of breast carcinomas distinguish tumor subclasses with clinical implications. *Proc Natl Acad Sci U S A* **98**, 10869–10874 (2001).
25. Li, Z., Hu, P., Tu, J. & Yu, N. Luminal B breast cancer: patterns of recurrence and clinical outcome. *Oncotarget* **7**, 65024–65033 (2016).
26. Curigliano, G. *et al.* Understanding breast cancer complexity to improve patient outcomes: The St Gallen International Consensus Conference for the Primary Therapy of Individuals with Early Breast Cancer 2023. *Annals of Oncology* **34**, 970–986 (2023).
27. Jallah, J. K., Dweh, T. J., Anjankar, A. & Palma, O. A Review of the Advancements in Targeted Therapies for Breast Cancer. *Cureus* **15**, e47847.
28. Viale, G. *et al.* Prognostic and predictive value of centrally reviewed expression of estrogen and progesterone receptors in a randomized trial comparing letrozole and tamoxifen adjuvant therapy for postmenopausal early breast cancer: BIG 1-98. *J Clin Oncol* **25**, 3846–3852 (2007).
29. Shirman, Y., Lubovsky, S. & Shai, A. HER2-Low Breast Cancer: Current Landscape and Future Prospects. *Breast Cancer (Dove Med Press)* **15**, 605–616 (2023).
30. Modi, S. *et al.* Trastuzumab Deruxtecan in Previously Treated HER2-Low Advanced Breast Cancer. *N Engl J Med* **387**, 9–20 (2022).
31. Yoon, J., Knapp, G., Quan, M. L. & Bouchard-Fortier, A. Cancer-Specific Outcomes in the Elderly with Triple-Negative Breast Cancer: A Systematic Review. *Curr Oncol* **28**, 2337–2345 (2021).
32. Peshkin, B. N., Alabek, M. L. & Isaacs, C. BRCA1/2 MUTATIONS AND TRIPLE NEGATIVE BREAST CANCERS. *Breast Dis* **32**, 10.3233/BD-2010–0306 (2010).
33. Xiong, N., Wu, H. & Yu, Z. Advancements and challenges in triple-negative breast cancer: a comprehensive review of therapeutic and diagnostic strategies. *Front. Oncol.* **14**, (2024).
34. Yin, L., Duan, J.-J., Bian, X.-W. & Yu, S. Triple-negative breast cancer molecular subtyping and treatment progress. *Breast Cancer Research* **22**, 61 (2020).
35. Holloway, C. M. B., Jiang, L., Whitehead, M., Racz, J. M. & Groome, P. A. Organized screening detects breast cancer at earlier stage regardless of molecular phenotype. *J Cancer Res Clin Oncol* **144**, 1769–1775 (2018).

36. Subhan, M. A. *et al.* Recent Advances with Precision Medicine Treatment for Breast Cancer including Triple-Negative Sub-Type. *Cancers (Basel)* **15**, 2204 (2023).
37. O'Reilly, D., Sendi, M. A. & Kelly, C. M. Overview of recent advances in metastatic triple negative breast cancer. *World J Clin Oncol* **12**, 164–182 (2021).
38. Bernsdorf, M. *et al.* Effect of adding gefitinib to neoadjuvant chemotherapy in estrogen receptor negative early breast cancer in a randomized phase II trial. *Breast Cancer Res Treat* **126**, 463–470 (2011).
39. Schuler, M. *et al.* A phase II trial to assess efficacy and safety of afatinib in extensively pretreated patients with HER2-negative metastatic breast cancer. *Breast Cancer Res Treat* **134**, 1149–1159 (2012).
40. Suder, A. *et al.* A phase I study of daily afatinib, an irreversible ErbB family blocker, in combination with weekly paclitaxel in patients with advanced solid tumours. *European Journal of Cancer* **51**, 2275–2284 (2015).
41. Lin, P.-H. *et al.* Neoadjuvant afatinib with paclitaxel for triple-negative breast cancer and the molecular characteristics in responders and non-responders. *Journal of the Formosan Medical Association* **121**, 2538–2547 (2022).
42. Garrido-Castro, A. C. *et al.* Phase 2 study of buparlisib (BKM120), a pan-class I PI3K inhibitor, in patients with metastatic triple-negative breast cancer. *Breast Cancer Res* **22**, 120 (2020).
43. Warburg, O. On the Origin of Cancer Cells. *Science* **123**, 309–314 (1956).
44. Vander Heiden, M. G. & DeBerardinis, R. J. Understanding the Intersections between Metabolism and Cancer Biology. *Cell* **168**, 657–669 (2017).
45. Gong, Y. *et al.* Metabolic-Pathway-Based Subtyping of Triple-Negative Breast Cancer Reveals Potential Therapeutic Targets. *Cell Metabolism* **33**, 51-64.e9 (2021).
46. Dong, Y., Tu, R., Liu, H. & Qing, G. Regulation of cancer cell metabolism: oncogenic MYC in the driver's seat. *Sig Transduct Target Ther* **5**, 1–11 (2020).
47. Cancer Genome Atlas Network. Comprehensive molecular portraits of human breast tumours. *Nature* **490**, 61–70 (2012).
48. Chandriani, S. *et al.* A core MYC gene expression signature is prominent in basal-like breast cancer but only partially overlaps the core serum response. *PLoS One* **4**, e6693 (2009).
49. Elend, M. & Eilers, M. Cell growth: downstream of Myc - to grow or to cycle? *Curr Biol* **9**, R936-938 (1999).
50. Shim, H. *et al.* c-Myc transactivation of LDH-A: implications for tumor metabolism and growth. *Proc Natl Acad Sci U S A* **94**, 6658–6663 (1997).
51. Shim, H., Chun, Y. S., Lewis, B. C. & Dang, C. V. A unique glucose-dependent apoptotic pathway induced by c-Myc. *Proc Natl Acad Sci U S A* **95**, 1511–1516 (1998).
52. Osthus, R. C. *et al.* Deregulation of glucose transporter 1 and glycolytic gene expression by c-Myc. *J Biol Chem* **275**, 21797–21800 (2000).
53. Conacci-Sorrell, M., McFerrin, L. & Eisenman, R. N. An Overview of MYC and Its Interactome. *Cold Spring Harb Perspect Med* **4**, a014357 (2014).
54. Sheiness, D. & Bishop, J. M. DNA and RNA from Uninfected Vertebrate Cells Contain Nucleotide Sequences Related to the Putative Transforming Gene of Avian Myelocytomatosis Virus. *Journal of Virology* **31**, 514–521 (1979).

55. Ramsay, G., Graf, T. & Hayman, M. J. Mutants of avian myelocytomatosis virus with smaller gag gene-related proteins have an altered transforming ability. *Nature* **288**, 170–172 (1980).
56. Bister, K., Ramsay, G. M. & Hayman, M. J. Deletions Within the Transformation-Specific RNA Sequences of Acute Leukemia Virus MC29 Give Rise to Partially Transformation-Defective Mutants. *Journal of Virology* **41**, 754–766 (1982).
57. Dalla-Favera, R. *et al.* Human c-myc onc gene is located on the region of chromosome 8 that is translocated in Burkitt lymphoma cells. *Proceedings of the National Academy of Sciences* **79**, 7824–7827 (1982).
58. Taub, R. *et al.* Translocation of the c-myc gene into the immunoglobulin heavy chain locus in human Burkitt lymphoma and murine plasmacytoma cells. *Proceedings of the National Academy of Sciences* **79**, 7837–7841 (1982).
59. Blackwell, T. K., Kretzner, L., Blackwood, E. M., Eisenman, R. N. & Weintraub, H. Sequence-Specific DNA Binding by the c-Myc Protein. *Science* **250**, 1149–1151 (1990).
60. Blackwood, E. M. & Eisenman, R. N. Max: A Helix-Loop-Helix Zipper Protein That Forms a Sequence-Specific DNA-Binding Complex with Myc. *Science* **251**, 1211–1217 (1991).
61. Llombart, V. & Mansour, M. R. Therapeutic targeting of “undruggable” MYC. *eBioMedicine* **75**, (2022).
62. Jha, R. K., Kouzine, F. & Levens, D. MYC function and regulation in physiological perspective. *Front Cell Dev Biol* **11**, 1268275 (2023).
63. Bretones, G., Delgado, M. D. & León, J. Myc and cell cycle control. *Biochimica et Biophysica Acta (BBA) - Gene Regulatory Mechanisms* **1849**, 506–516 (2015).
64. Gregory, M. A. & Hann, S. R. c-Myc Proteolysis by the Ubiquitin-Proteasome Pathway: Stabilization of c-Myc in Burkitt’s Lymphoma Cells. *Molecular and Cellular Biology* **20**, 2423 (2000).
65. Farrell, A. S. & Sears, R. C. MYC Degradation. *Cold Spring Harb Perspect Med* **4**, a014365 (2014).
66. Sun, X.-X., Li, Y., Sears, R. C. & Dai, M.-S. Targeting the MYC Ubiquitination-Proteasome Degradation Pathway for Cancer Therapy. *Front. Oncol.* **11**, (2021).
67. Flinn, E. M., Busch, C. M. & Wright, A. P. myc boxes, which are conserved in myc family proteins, are signals for protein degradation via the proteasome. *Mol Cell Biol* **18**, 5961–5969 (1998).
68. Yada, M. *et al.* Phosphorylation-dependent degradation of c-Myc is mediated by the F-box protein Fbw7. *EMBO J* **23**, 2116–2125 (2004).
69. Welcker, M. *et al.* The Fbw7 tumor suppressor regulates glycogen synthase kinase 3 phosphorylation-dependent c-Myc protein degradation. *Proc Natl Acad Sci U S A* **101**, 9085–9090 (2004).
70. Gregory, M. A., Qi, Y. & Hann, S. R. Phosphorylation by glycogen synthase kinase-3 controls c-myc proteolysis and subnuclear localization. *J Biol Chem* **278**, 51606–51612 (2003).
71. Stine, Z. E., Walton, Z. E., Altman, B. J., Hsieh, A. L. & Dang, C. V. MYC, Metabolism, and Cancer. *Cancer Discov* **5**, 1024–1039 (2015).
72. D’Cruz, C. M. *et al.* c-MYC induces mammary tumorigenesis by means of a preferred pathway involving spontaneous Kras2 mutations. *Nat Med* **7**, 235–239 (2001).

73. Schaub, F. X. *et al.* Pan-Cancer Alterations of the MYC oncogene and its Proximal Network across The Cancer Genome Atlas. *Cell Syst* **6**, 282-300.e2 (2018).
74. Hann, S. R. Role of post-translational modifications in regulating c-Myc proteolysis, transcriptional activity and biological function. *Semin Cancer Biol* **16**, 288–302 (2006).
75. Deming, S. L., Nass, S. J., Dickson, R. B. & Trock, B. J. C-myc amplification in breast cancer: a meta-analysis of its occurrence and prognostic relevance. *Br J Cancer* **83**, 1688–1695 (2000).
76. Blancato, J., Singh, B., Liu, A., Liao, D. J. & Dickson, R. B. Correlation of amplification and overexpression of the c-myc oncogene in high-grade breast cancer: FISH, in situ hybridisation and immunohistochemical analyses. *Br J Cancer* **90**, 1612–1619 (2004).
77. Escot, C. *et al.* Genetic alteration of the c-myc protooncogene (MYC) in human primary breast carcinomas. *Proc Natl Acad Sci U S A* **83**, 4834–4838 (1986).
78. Perou, C. M. *et al.* Molecular portraits of human breast tumours. *Nature* **406**, 747–752 (2000).
79. AlSultan, D. *et al.* The novel low molecular weight MYC antagonist MYCMI-6 inhibits proliferation and induces apoptosis in breast cancer cells. *Invest New Drugs* **39**, 587–594 (2021).
80. Grushko, T. A. *et al.* MYC Is Amplified in BRCA1-Associated Breast Cancers. *Clinical Cancer Research* **10**, 499–507 (2004).
81. Xu, J., Chen, Y. & Olopade, O. I. MYC and Breast Cancer. *Genes Cancer* **1**, 629–640 (2010).
82. Chen, Y. & Olopade, O. I. MYC in breast tumor progression. *Expert Rev Anticancer Ther* **8**, 1689–1698 (2008).
83. Han, Y., Yu, X., Li, S., Tian, Y. & Liu, C. New Perspectives for Resistance to PARP Inhibitors in Triple-Negative Breast Cancer. *Front. Oncol.* **10**, (2020).
84. Robson, M. E. *et al.* OlympiAD final overall survival and tolerability results: Olaparib versus chemotherapy treatment of physician's choice in patients with a germline BRCA mutation and HER2-negative metastatic breast cancer. *Ann Oncol* **30**, 558–566 (2019).
85. Carey, J. P. W. *et al.* Synthetic Lethality of PARP Inhibitors in Combination with MYC Blockade Is Independent of BRCA Status in Triple-Negative Breast Cancer. *Cancer Res* **78**, 742–757 (2018).
86. Fallah, Y., Brundage, J., Allegakoen, P. & Shajahan-Haq, A. N. MYC-Driven Pathways in Breast Cancer Subtypes. *Biomolecules* **7**, 53 (2017).
87. Dang, C. V. MYC on the Path to Cancer. *Cell* **149**, 22–35 (2012).
88. Duffy, M. J., O'Grady, S., Tang, M. & Crown, J. MYC as a target for cancer treatment. *Cancer Treatment Reviews* **94**, (2021).
89. Wang, C. *et al.* Alternative approaches to target Myc for cancer treatment. *Sig Transduct Target Ther* **6**, 1–14 (2021).
90. Massó-Vallés, D. & Soucek, L. Blocking Myc to Treat Cancer: Reflecting on Two Decades of Omomyc. *Cells* **9**, 883 (2020).
91. Toyoshima, M. *et al.* Functional genomics identifies therapeutic targets for MYC-driven cancer. *Proceedings of the National Academy of Sciences* **109**, 9545–9550 (2012).

92. Cermelli, S., Jang, I. S., Bernard, B. & Grandori, C. Synthetic Lethal Screens as a Means to Understand and Treat MYC-Driven Cancers. *Cold Spring Harb Perspect Med* **4**, a014209 (2014).
93. Yuneva, M. O. *et al.* The Metabolic Profile of Tumors Depends on Both the Responsible Genetic Lesion and Tissue Type. *Cell Metabolism* **15**, 157–170 (2012).
94. Kessler, J. D. *et al.* A SUMOylation-dependent transcriptional subprogram is required for Myc-driven tumorigenesis. *Science* **335**, 348–353 (2012).
95. Liu, L. *et al.* Deregulated MYC expression induces dependence upon AMPK-related kinase 5. *Nature* **483**, 608–612 (2012).
96. Bello-Fernandez, C., Packham, G. & Cleveland, J. L. The ornithine decarboxylase gene is a transcriptional target of c-Myc. *Proc Natl Acad Sci U S A* **90**, 7804–7808 (1993).
97. Yuneva, M., Zamboni, N., Oefner, P., Sachidanandam, R. & Lazebnik, Y. Deficiency in glutamine but not glucose induces MYC-dependent apoptosis in human cells. *J Cell Biol* **178**, 93–105 (2007).
98. Iurlaro, R., León-Annicchiarico, C. L. & Muñoz-Pinedo, C. Chapter Three - Regulation of Cancer Metabolism by Oncogenes and Tumor Suppressors. in *Methods in Enzymology* (eds. Galluzzi, L. & Kroemer, G.) vol. 542 59–80 (Academic Press, 2014).
99. Sun, L. *et al.* cMyc-mediated activation of serine biosynthesis pathway is critical for cancer progression under nutrient deprivation conditions. *Cell Res* **25**, 429–444 (2015).
100. Nikiforov, M. A. *et al.* A functional screen for Myc-responsive genes reveals serine hydroxymethyltransferase, a major source of the one-carbon unit for cell metabolism. *Mol Cell Biol* **22**, 5793–5800 (2002).
101. Ji, X. *et al.* xCT (SLC7A11)-mediated metabolic reprogramming promotes non-small cell lung cancer progression. *Oncogene* **37**, 5007–5019 (2018).
102. Singh, K. B., Hahm, E.-R., Kim, S.-H., Wendell, S. G. & Singh, S. V. A novel metabolic function of Myc in regulation of fatty acid synthesis in prostate cancer. *Oncogene* **40**, 592–602 (2021).
103. Zhou, W. *et al.* Over-expression of BCAT1, a c-Myc target gene, induces cell proliferation, migration and invasion in nasopharyngeal carcinoma. *Molecular Cancer* **12**, 53 (2013).
104. Edwards-Hicks, J. *et al.* MYC sensitises cells to apoptosis by driving energetic demand. *Nat Commun* **13**, 4674 (2022).
105. Kim, G. W. *et al.* Glutamine Synthetase as a Therapeutic Target for Cancer Treatment. *Int J Mol Sci* **22**, 1701 (2021).
106. Cruzat, V., Macedo Rogero, M., Noel Keane, K., Curi, R. & Newsholme, P. Glutamine: Metabolism and Immune Function, Supplementation and Clinical Translation. *Nutrients* **10**, 1564 (2018).
107. de Oliveira, D. C. *et al.* Glutamine metabolism and its effects on immune response: molecular mechanism and gene expression. *Nutrire* **41**, 14 (2016).
108. Kung, H.-N., Marks, J. R. & Chi, J.-T. Glutamine Synthetase Is a Genetic Determinant of Cell Type–Specific Glutamine Independence in Breast Epithelia. *PLoS Genet* **7**, e1002229 (2011).
109. Gross, M. I. *et al.* Antitumor activity of the glutaminase inhibitor CB-839 in triple-negative breast cancer. *Mol. Cancer Ther.* **13**, 890–901 (2014).
110. Castegna, A. & Menga, A. Glutamine Synthetase: Localization Dictates Outcome. *Genes (Basel)* **9**, 108 (2018).

111. Wise, D. R. & Thompson, C. B. Glutamine addiction: a new therapeutic target in cancer. *Trends Biochem Sci* **35**, 427–433 (2010).
112. Dang, C. V. Rethinking the Warburg effect with Myc micromanaging glutamine metabolism. *Cancer Res* **70**, 859–862 (2010).
113. Gao, P. *et al.* c-Myc suppression of miR-23a/b enhances mitochondrial glutaminase expression and glutamine metabolism. *Nature* **458**, 762–765 (2009).
114. Wang, Z. *et al.* Targeting Glutaminolysis: New Perspectives to Understand Cancer Development and Novel Strategies for Potential Target Therapies. *Front. Oncol.* **10**, (2020).
115. Edwards, D. N. *et al.* Selective glutamine metabolism inhibition in tumor cells improves antitumor T lymphocyte activity in triple-negative breast cancer. *J Clin Invest* **131**, (2021).
116. Méndez-Lucas, A. *et al.* Identifying strategies to target the metabolic flexibility of tumours. *Nat Metab* **2**, 335–350 (2020).
117. Sun, L. *et al.* Dual inhibition of glycolysis and glutaminolysis as a therapeutic strategy in the treatment of ovarian cancer. *Oncotarget* **8**, 63551–63561 (2017).
118. Singleton, D. C. *et al.* Pyruvate anaplerosis is a mechanism of resistance to pharmacological glutaminase inhibition in triple-receptor negative breast cancer. *BMC Cancer* **20**, 470 (2020).
119. Yang, J. *et al.* Targeting cellular metabolism to reduce head and neck cancer growth. *Sci Rep* **9**, 4995 (2019).
120. Elgogary, A. *et al.* Combination therapy with BPTES nanoparticles and metformin targets the metabolic heterogeneity of pancreatic cancer. *Proc Natl Acad Sci U S A* **113**, E5328-5336 (2016).
121. Biancur, D. E. *et al.* Compensatory metabolic networks in pancreatic cancers upon perturbation of glutamine metabolism. *Nat Commun* **8**, 15965 (2017).
122. Reis, L. M. D. *et al.* Dual inhibition of glutaminase and carnitine palmitoyltransferase decreases growth and migration of glutaminase inhibition-resistant triple-negative breast cancer cells. *J Biol Chem* **294**, 9342–9357 (2019).
123. Timmerman, L. A. *et al.* Glutamine Sensitivity Analysis Identifies the xCT Antiporter as a Common Triple-Negative Breast Tumor Therapeutic Target. *Cancer Cell* **24**, 450–465 (2013).
124. Muir, A. *et al.* Environmental cystine drives glutamine anaplerosis and sensitizes cancer cells to glutaminase inhibition. *eLife* **6**, e27713 (2017).
125. Okazaki, S. *et al.* Glutaminolysis-related genes determine sensitivity to xCT-targeted therapy in head and neck squamous cell carcinoma. *Cancer Sci* **110**, 3453–3463 (2019).
126. Udupa, S. *et al.* Upregulation of the Glutaminase II Pathway Contributes to Glutamate Production upon Glutaminase 1 Inhibition in Pancreatic Cancer. *PROTEOMICS* **19**, 1800451 (2019).
127. Lukey, M. J. *et al.* Liver-Type Glutaminase GLS2 Is a Druggable Metabolic Node in Luminal-Subtype Breast Cancer. *Cell Reports* **29**, 76-88.e7 (2019).
128. Still, E. R. & Yuneva, M. O. Hopefully devoted to Q: targeting glutamine addiction in cancer. *Br J Cancer* **116**, 1375–1381 (2017).
129. Thornburg, J. M. *et al.* Targeting aspartate aminotransferase in breast cancer. *Breast Cancer Research* **10**, R84 (2008).

130. Son, J. *et al.* Glutamine supports pancreatic cancer growth through a KRAS-regulated metabolic pathway. *Nature* **496**, 101–105 (2013).
131. Korangath, P. *et al.* Targeting Glutamine Metabolism in Breast Cancer with Aminooxyacetate. *Clin Cancer Res* **21**, 3263–3273 (2015).
132. Guo, W., Tan, H.-Y., Li, S., Wang, N. & Feng, Y. Glutamic-Pyruvic Transaminase 1 Facilitates Alternative Fuels for Hepatocellular Carcinoma Growth—A Small Molecule Inhibitor, Berberine. *Cancers (Basel)* **12**, 1854 (2020).
133. Coloff, J. L. *et al.* Differential Glutamate Metabolism in Proliferating and Quiescent Mammary Epithelial Cells. *Cell Metab* **23**, 867–880 (2016).
134. Lane, A. N. & Fan, T. W.-M. Regulation of mammalian nucleotide metabolism and biosynthesis. *Nucleic Acids Research* **43**, 2466 (2015).
135. Zhang, J. *et al.* Asparagine Plays a Critical Role in Regulating Cellular Adaptation to Glutamine Depletion. *Molecular Cell* **56**, 205–218 (2014).
136. Polet, F. *et al.* Reducing the serine availability complements the inhibition of the glutamine metabolism to block leukemia cell growth. *Oncotarget* **7**, 1765–1776 (2015).
137. Alkan, H. F. *et al.* Cytosolic Aspartate Availability Determines Cell Survival When Glutamine Is Limiting. *Cell Metab* **28**, 706-720.e6 (2018).
138. Pavlova, N. N. *et al.* As Extracellular Glutamine Levels Decline, Asparagine Becomes an Essential Amino Acid. *Cell Metabolism* **27**, 428-438.e5 (2018).
139. Tajan, M. *et al.* A Role for p53 in the Adaptation to Glutamine Starvation through the Expression of SLC1A3. *Cell Metab* **28**, 721-736.e6 (2018).
140. Recouvreux, M. V. *et al. Glutamine Mimicry Suppresses Tumor Progression through Asparagine Metabolism in Pancreatic Ductal Adenocarcinoma*. http://biorxiv.org/lookup/doi/10.1101/2022.10.31.514261 (2022) doi:10.1101/2022.10.31.514261.
141. Jiang, J., Srivastava, S. & Zhang, J. Starve Cancer Cells of Glutamine: Break the Spell or Make a Hungry Monster? *Cancers (Basel)* **11**, 804 (2019).
142. Nicklin, P. *et al.* Bidirectional Transport of Amino Acids Regulates mTOR and Autophagy. *Cell* **136**, 521–534 (2009).
143. Chen, J., Cui, L., Lu, S. & Xu, S. Amino acid metabolism in tumor biology and therapy. *Cell Death Dis* **15**, 1–18 (2024).
144. Bröer, A., Rahimi, F. & Bröer, S. Deletion of Amino Acid Transporter ASCT2 (SLC1A5) Reveals an Essential Role for Transporters SNAT1 (SLC38A1) and SNAT2 (SLC38A2) to Sustain Glutaminolysis in Cancer Cells. *J Biol Chem* **291**, 13194–13205 (2016).
145. Ren, P. *et al.* ATF4 and N-Myc coordinate glutamine metabolism in MYCN-amplified neuroblastoma cells through ASCT2 activation. *J Pathol* **235**, 90–100 (2015).
146. Bröer, A. *et al.* Ablation of the ASCT2 (SLC1A5) gene encoding a neutral amino acid transporter reveals transporter plasticity and redundancy in cancer cells. *J Biol Chem* **294**, 4012–4026 (2019).
147. van Geldermalsen, M. *et al.* ASCT2/SLC1A5 controls glutamine uptake and tumour growth in triple-negative basal-like breast cancer. *Oncogene* **35**, 3201–3208 (2016).
148. Cormerais, Y. *et al.* The glutamine transporter ASCT2 (SLC1A5) promotes tumor growth independently of the amino acid transporter LAT1 (SLC7A5). *J Biol Chem* **293**, 2877–2887 (2018).

149. Zhang, Z. *et al.* ASCT2 (SLC1A5)-dependent glutamine uptake is involved in the progression of head and neck squamous cell carcinoma. *Br J Cancer* **122**, 82–93 (2020).
150. Ye, J. *et al.* Targeting of glutamine transporter ASCT2 and glutamine synthetase suppresses gastric cancer cell growth. *J Cancer Res Clin Oncol* **144**, 821–833 (2018).
151. Lopes, C., Pereira, C. & Medeiros, R. ASCT2 and LAT1 Contribution to the Hallmarks of Cancer: From a Molecular Perspective to Clinical Translation. *Cancers (Basel)* **13**, 203 (2021).
152. Bröer, A., Fairweather, S. & Bröer, S. Disruption of Amino Acid Homeostasis by Novel ASCT2 Inhibitors Involves Multiple Targets. *Front Pharmacol* **9**, 785 (2018).
153. Corti, A. *et al.* γ-Glutamyltransferase enzyme activity of cancer cells modulates L-γ-glutamyl-p-nitroanilide (GPNA) cytotoxicity. *Sci Rep* **9**, 891 (2019).
154. Ma, H. *et al.* Inhibition of Glutamine Uptake Improves the Efficacy of Cetuximab on Gastric Cancer. *Integr Cancer Ther* **20**, 15347354211045349 (2021).
155. Quek, L.-E. *et al.* Glutamine addiction promotes glucose oxidation in triple-negative breast cancer. *Oncogene* **41**, 4066–4078 (2022).
156. Conger, K. O. *et al.* ASCT2 is a major contributor to serine uptake in cancer cells. *Cell Rep* **43**, 114552 (2024).
157. Cruzat, V. & Tirapegui, J. Glutamine and Skeletal Muscle. in 12 (2015). doi:10.1007/978-1-4939-1932-1_38.
158. Wang, B., Pei, J., Xu, S., Liu, J. & Yu, J. A glutamine tug-of-war between cancer and immune cells: recent advances in unraveling the ongoing battle. *Journal of Experimental & Clinical Cancer Research* **43**, 74 (2024).
159. Tanaka, K. *et al.* Glioma cells require one-carbon metabolism to survive glutamine starvation. *Acta Neuropathologica Communications* **9**, 16 (2021).
160. Endicott, M., Jones, M. & Hull, J. Amino acid metabolism as a therapeutic target in cancer: a review. *Amino Acids* **53**, 1169–1179 (2021).
161. Ruggero, D. The role of Myc-induced protein synthesis in cancer. *Cancer Res* **69**, 8839–8843 (2009).
162. Panda, S., Banerjee, N. & Chatterjee, S. Solute carrier proteins and c-Myc: a strong connection in cancer progression. *Drug Discovery Today* **25**, 891–900 (2020).
163. Yue, M., Jiang, J., Gao, P., Liu, H. & Qing, G. Oncogenic MYC Activates a Feedforward Regulatory Loop Promoting Essential Amino Acid Metabolism and Tumorigenesis. *Cell Reports* **21**, 3819–3832 (2017).
164. Dong, J., Qiu, H., Garcia-Barrio, M., Anderson, J. & Hinnebusch, A. G. Uncharged tRNA Activates GCN2 by Displacing the Protein Kinase Moiety from a Bipartite tRNA-Binding Domain. *Molecular Cell* **6**, 269–279 (2000).
165. Liu, G. Y. & Sabatini, D. M. mTOR at the nexus of nutrition, growth, ageing and disease. *Nat Rev Mol Cell Biol* **21**, 183–203 (2020).
166. Fingar, D. C., Salama, S., Tsou, C., Harlow, E. & Blenis, J. Mammalian cell size is controlled by mTOR and its downstream targets S6K1 and 4EBP1/eIF4E. *Genes Dev* **16**, 1472–1487 (2002).
167. Proud, C. G. Phosphorylation and Signal Transduction Pathways in Translational Control. *Cold Spring Harb Perspect Biol* **11**, a033050 (2019).

168. Sancak, Y. *et al.* The Rag GTPases bind raptor and mediate amino acid signaling to mTORC1. *Science* **320**, 1496–1501 (2008).
169. Shaw, R. J. mTOR signaling: RAG GTPases transmit the amino acid signal. *Trends Biochem Sci* **33**, 565–568 (2008).
170. Sancak, Y. *et al.* Ragulator-Rag complex targets mTORC1 to the lysosomal surface and is necessary for its activation by amino acids. *Cell* **141**, 290–303 (2010).
171. Bar-Peled, L. *et al.* A Tumor suppressor complex with GAP activity for the Rag GTPases that signal amino acid sufficiency to mTORC1. *Science* **340**, 1100–1106 (2013).
172. Bar-Peled, L. & Sabatini, D. M. Regulation of mTORC1 by amino acids. *Trends Cell Biol* **24**, 400–406 (2014).
173. Han, J. M. *et al.* Leucyl-tRNA Synthetase Is an Intracellular Leucine Sensor for the mTORC1-Signaling Pathway. *Cell* **149**, 410–424 (2012).
174. Chantranupong, L. *et al.* The CASTOR Proteins Are Arginine Sensors for the mTORC1 Pathway. *Cell* **165**, 153–164 (2016).
175. Wolfson, R. L. *et al.* Sestrin2 is a leucine sensor for the mTORC1 pathway. *Science* **351**, 43–48 (2016).
176. Gu, X. *et al.* SAMTOR is an S-adenosylmethionine sensor for the mTORC1 pathway. *Science* **358**, 813–818 (2017).
177. Gollwitzer, P., Grützmacher, N., Wilhelm, S., Kümmel, D. & Demetriades, C. A Rag GTPase dimer code defines the regulation of mTORC1 by amino acids. *Nat Cell Biol* **24**, 1394–1406 (2022).
178. Jung, J., Genau, H. M. & Behrends, C. Amino Acid-Dependent mTORC1 Regulation by the Lysosomal Membrane Protein SLC38A9. *Mol Cell Biol* **35**, 2479–2494 (2015).
179. Tsun, Z.-Y. *et al.* The folliculin tumor suppressor is a GAP for the RagC/D GTPases that signal amino acid levels to mTORC1. *Mol Cell* **52**, 495–505 (2013).
180. Son, S. M. *et al.* Leucine Signals to mTORC1 via Its Metabolite Acetyl-Coenzyme A. *Cell Metab* **29**, 192-201.e7 (2019).
181. Chen, J. *et al.* SAR1B senses leucine levels to regulate mTORC1 signalling. *Nature* **596**, 281–284 (2021).
182. Cangelosi, A. L. *et al.* Zonated leucine sensing by Sestrin-mTORC1 in the liver controls the response to dietary leucine. *Science* **377**, 47–56 (2022).
183. Takahara, T., Amemiya, Y., Sugiyama, R., Maki, M. & Shibata, H. Amino acid-dependent control of mTORC1 signaling: a variety of regulatory modes. *Journal of Biomedical Science* **27**, 87 (2020).
184. Venkateswaran, N. *et al.* MYC promotes tryptophan uptake and metabolism by the kynurenine pathway in colon cancer. *Genes Dev* **33**, 1236–1251 (2019).
185. Venkateswaran, N. *et al.* Tryptophan fuels MYC-dependent liver tumorigenesis through indole 3-pyruvate synthesis. *Nat Commun* **15**, 4266 (2024).
186. Niland, C. N., Ghosh, A., Cahill, S. M. & Schramm, V. L. Mechanism and Inhibition of Human Methionine Adenosyltransferase 2A. *Biochemistry* **60**, 791–801 (2021).
187. Aoki, Y. *et al.* Oncogenes and Methionine Addiction of Cancer: Role of c-MYC. *Cancer Genomics & Proteomics* **20**, 165–170 (2023).

188. Zhao, L. *et al.* mTORC1-c-Myc pathway rewires methionine metabolism for HCC progression through suppressing SIRT4 mediated ADP ribosylation of MAT2A. *Cell & Bioscience* **12**, 183 (2022).
189. Epner, D. E., Morrow, S., Wilcox, M. & Houghton, J. L. Nutrient Intake and Nutritional Indexes in Adults With Metastatic Cancer on a Phase I Clinical Trial of Dietary Methionine Restriction. *Nutrition and Cancer* **42**, 158–166 (2002).
190. Durando, X. *et al.* Dietary Methionine Restriction with FOLFOX Regimen as First Line Therapy of Metastatic Colorectal Cancer: A Feasibility Study. *Oncology* **78**, 205–209 (2010).
191. Colas, C., Ung, P. M.-U. & Schlessinger, A. SLC Transporters: Structure, Function, and Drug Discovery. *Medchemcomm* **7**, 1069–1081 (2016).
192. Pizzagalli, M. D., Bensimon, A. & Superti-Furga, G. A guide to plasma membrane solute carrier proteins. *FEBS J* **288**, 2784–2835 (2021).
193. Smorodina, E. *et al.* Structural informatic study of determined and AlphaFold2 predicted molecular structures of 13 human solute carrier transporters and their water-soluble QTY variants. *Sci Rep* **12**, 20103 (2022).
194. Nishimura, M. & Naito, S. Tissue-specific mRNA expression profiles of human solute carrier transporter superfamilies. *Drug Metab Pharmacokinet* **23**, 22–44 (2008).
195. Chrostowski, M. K., McGonnigal, B. G., Stabila, J. P. & Padbury, J. F. LAT-1 Expression in Pre- and Post-implantation Embryos and Placenta. *Placenta* **30**, 270–276 (2009).
196. Vidal, S. M., Malo, D., Vogan, K., Skamene, E. & Gros, P. Natural resistance to infection with intracellular parasites: Isolation of a candidate for *Bcg*. *Cell* **73**, 469–485 (1993).
197. Vulturar, R. *et al.* One Molecule for Mental Nourishment and More: Glucose Transporter Type 1—Biology and Deficiency Syndrome. *Biomedicines* **10**, 1249 (2022).
198. Zhang, J. *et al.* Review of the Correlation of LAT1 With Diseases: Mechanism and Treatment. *Front Chem* **8**, 564809 (2020).
199. Colas, C., Ung, P. M.-U. & Schlessinger, A. SLC transporters: structure, function, and drug discovery. *Med. Chem. Commun.* **7**, 1069–1081 (2016).
200. He, L., Vasiliou, K. & Nebert, D. W. Analysis and update of the human solute carrier (SLC) gene superfamily. *Hum Genomics* **3**, 195–205 (2009).
201. Gauthier-Coles, G. *et al.* Quantitative modelling of amino acid transport and homeostasis in mammalian cells. *Nat Commun* **12**, 5282 (2021).
202. Olson, A. L. & Pessin, J. E. Structure, function, and regulation of the mammalian facilitative glucose transporter gene family. *Annu Rev Nutr* **16**, 235–256 (1996).
203. Fotiadis, D., Kanai, Y. & Palacín, M. The SLC3 and SLC7 families of amino acid transporters. *Molecular Aspects of Medicine* **34**, 139–158 (2013).
204. Bodoy, S., Fotiadis, D., Stoeger, C., Kanai, Y. & Palacín, M. The small SLC43 family: Facilitator system l amino acid transporters and the orphan EEG1. *Molecular Aspects of Medicine* **34**, 638–645 (2013).
205. Freidman, N. *et al.* Amino Acid Transporters and Exchangers from the SLC1A Family: Structure, Mechanism and Roles in Physiology and Cancer. *Neurochem Res* **45**, 1268–1286 (2020).
206. Bröer, S. & Gether, U. The solute carrier 6 family of transporters. *Br J Pharmacol* **167**, 256–278 (2012).

207. Bröer, S. The SLC38 family of sodium-amino acid co-transporters. *Pflugers Arch* **466**, 155–172 (2014).
208. Zhang, Y., Zhang, Y., Sun, K., Meng, Z. & Chen, L. The SLC transporter in nutrient and metabolic sensing, regulation, and drug development. *Journal of Molecular Cell Biology* **11**, 1–13 (2019).
209. Mir, A. *et al.* SLC gene mutations and pediatric neurological disorders: diverse clinical phenotypes in a Saudi Arabian population. *Hum Genet* **141**, 81–99 (2022).
210. Messana, T. *et al.* Glucose Transporter Type 1 Deficiency Syndrome: Developmental Delay and Early-Onset Ataxia in a Novel Mutation of the SLC2A1 Gene. *J Pediatr Neurosci* **13**, 496–499 (2018).
211. Kleta, R. *et al.* Mutations in SLC6A19, encoding B0AT1, cause Hartnup disorder. *Nat Genet* **36**, 999–1002 (2004).
212. Sebastio, G., Sperandeo, M. P. & Andria, G. Lysinuric protein intolerance: reviewing concepts on a multisystem disease. *Am J Med Genet C Semin Med Genet* **157C**, 54–62 (2011).
213. Poncet, N., Shi, Y.-B., Taylor, P. & Storey, K. LAT1 (Slc7a5) null mice are embryonic lethal and exhibit neural tube defects (896.5). doi:10.1096/fasebj.28.1_supplement.896.5.
214. Tsumura, H. *et al.* The targeted disruption of the CD98 gene results in embryonic lethality. *Biochemical and Biophysical Research Communications* **308**, 847–851 (2003).
215. Ye, J. *et al.* The GCN2-ATF4 pathway is critical for tumour cell survival and proliferation in response to nutrient deprivation. *The EMBO Journal* **29**, 2082–2096 (2010).
216. Hushmandi, K. *et al.* Amino acid transporters within the solute carrier superfamily: Underappreciated proteins and novel opportunities for cancer therapy. *Mol Metab* **84**, 101952 (2024).
217. Lyu, X.-D. *et al.* A Novel ASCT2 Inhibitor, C118P, Blocks Glutamine Transport and Exhibits Antitumour Efficacy in Breast Cancer. *Cancers (Basel)* **15**, 5082 (2023).
218. Lanzardo, S. *et al.* Immunotargeting of Antigen xCT Attenuates Stem-like Cell Behavior and Metastatic Progression in Breast Cancer. *Cancer Res* **76**, 62–72 (2016).
219. El Ansari, R. *et al.* The amino acid transporter SLC7A5 confers a poor prognosis in the highly proliferative breast cancer subtypes and is a key therapeutic target in luminal B tumours. *Breast Cancer Research* **20**, 21 (2018).
220. Sato, M. *et al.* L-type amino acid transporter 1 is associated with chemoresistance in breast cancer via the promotion of amino acid metabolism. *Sci Rep* **11**, 589 (2021).
221. Huang, R. *et al.* Targeting glutamine metabolic reprogramming of SLC7A5 enhances the efficacy of anti-PD-1 in triple-negative breast cancer. *Front Immunol* **14**, 1251643 (2023).
222. Wang, K. *et al.* Activation of SNAT1/SLC38A1 in human breast cancer: correlation with p-Akt overexpression. *BMC Cancer* **13**, 343 (2013).
223. Morotti, M. *et al.* Increased expression of glutamine transporter SNAT2/SLC38A2 promotes glutamine dependence and oxidative stress resistance, and is associated with worse prognosis in triple-negative breast cancer. *Br J Cancer* **124**, 494–505 (2021).

224. Tameire, F. *et al.* ATF4 couples MYC-dependent translational activity to bioenergetic demands during tumour progression. *Nat Cell Biol* **21**, 889–899 (2019).
225. Kanai, Y. *et al.* Expression Cloning and Characterization of a Transporter for Large Neutral Amino Acids Activated by the Heavy Chain of 4F2 Antigen (CD98)*. *Journal of Biological Chemistry* **273**, 23629–23632 (1998).
226. Yanagida, O. *et al.* Human L-type amino acid transporter 1 (LAT1): characterization of function and expression in tumor cell lines. *Biochimica et Biophysica Acta (BBA) - Biomembranes* **1514**, 291–302 (2001).
227. Kageyama, T. *et al.* The 4F2hc/LAT1 complex transports l-DOPA across the blood–brain barrier. *Brain Research* **879**, 115–121 (2000).
228. Lee, Y. *et al.* Cryo-EM structure of the human L-type amino acid transporter 1 in complex with glycoprotein CD98hc. *Nat Struct Mol Biol* **26**, 510–517 (2019).
229. Napolitano, L. *et al.* LAT1 is the transport competent unit of the LAT1/CD98 heterodimeric amino acid transporter. *Int. J. Biochem. Cell Biol.* **67**, 25–33 (2015).
230. Cormerais, Y. *et al.* Genetic Disruption of the Multifunctional CD98/LAT1 Complex Demonstrates the Key Role of Essential Amino Acid Transport in the Control of mTORC1 and Tumor Growth. *Cancer Res* **76**, 4481–4492 (2016).
231. Verrey, F. System L: heteromeric exchangers of large, neutral amino acids involved in directional transport. *Pflugers Arch - Eur J Physiol* **445**, 529–533 (2003).
232. Meier, C., Ristic, Z., Klauser, S. & Verrey, F. Activation of system L heterodimeric amino acid exchangers by intracellular substrates. *The EMBO Journal* **21**, 580–589 (2002).
233. del Amo, E. M., Urtti, A. & Yliperttula, M. Pharmacokinetic role of L-type amino acid transporters LAT1 and LAT2. *European Journal of Pharmaceutical Sciences* **35**, 161–174 (2008).
234. Tarlungeanu, D. C. *et al.* Impaired amino acid transport at the blood brain barrier is a cause of autism spectrum disorder. *Cell* **167**, 1481-1494.e18 (2016).
235. Bodoy, S. *et al.* Identification of LAT4, a Novel Amino Acid Transporter with System L Activity*. *Journal of Biological Chemistry* **280**, 12002–12011 (2005).
236. Cormerais, Y. *et al.* Genetic Disruption of the Multifunctional CD98/LAT1 Complex Demonstrates the Key Role of Essential Amino Acid Transport in the Control of mTORC1 and Tumor Growth. *Cancer Res.* **76**, 4481–4492 (2016).
237. CRUK Rosetta Grand Challenge Consortium *et al.* The amino acid transporter SLC7A5 is required for efficient growth of KRAS-mutant colorectal cancer. *Nat Genet* **53**, 16–26 (2021).
238. Kim, S.-Y. *et al.* Genetic Ablation of LAT1 Inhibits Growth of Liver Cancer Cells and Downregulates mTORC1 Signaling. *Int J Mol Sci* **24**, 9171 (2023).
239. Milkereit, R. *et al.* LAPTM4b recruits the LAT1-4F2hc Leu transporter to lysosomes and promotes mTORC1 activation. *Nat Commun* **6**, 7250 (2015).
240. Schmidt, S. *et al.* A MYC–GCN2–eIF2α negative feedback loop limits protein synthesis to prevent MYC-dependent apoptosis in colorectal cancer. *Nat Cell Biol* **21**, 1413–1424 (2019).
241. Cordova, R. A. *et al.* GCN2 eIF2 kinase promotes prostate cancer by maintaining amino acid homeostasis. *eLife* **11**, e81083 (2022).
242. Sun, L. *et al.* Rapamycin targets STAT3 and impacts c-Myc to suppress tumor growth. *Cell Chem Biol* **29**, 373-385.e6 (2022).

243. Hayashi, K., Jutabha, P., Endou, H. & Anzai, N. c-Myc is crucial for the expression of LAT1 in MIA Paca-2 human pancreatic cancer cells. *Oncology Reports* **28**, 862–866 (2012).
244. Wise, D. R. *et al.* Myc regulates a transcriptional program that stimulates mitochondrial glutaminolysis and leads to glutamine addiction. *Proc. Natl. Acad. Sci. U.S.A.* **105**, 18782–18787 (2008).
245. Krall, A. S., Xu, S., Graeber, T. G., Braas, D. & Christofk, H. R. Asparagine promotes cancer cell proliferation through use as an amino acid exchange factor. *Nat Commun* **7**, 11457 (2016).
246. Pan, M. *et al.* Regional glutamine deficiency in tumours promotes dedifferentiation through inhibition of histone demethylation. *Nat Cell Biol* **18**, 1090–1101 (2016).
247. Bothwell, P. J., Kron, C. D., Wittke, E. F., Czerniak, B. N. & Bode, B. P. Targeted Suppression and Knockout of ASCT2 or LAT1 in Epithelial and Mesenchymal Human Liver Cancer Cells Fail to Inhibit Growth. *International Journal of Molecular Sciences* **19**, (2018).
248. Napolitano, L. *et al.* Novel insights into the transport mechanism of the human amino acid transporter LAT1 (SLC7A5). Probing critical residues for substrate translocation. *Biochimica et Biophysica Acta (BBA) - General Subjects* **1861**, 727–736 (2017).
249. Scalise, M., Galluccio, M., Console, L., Pochini, L. & Indiveri, C. The Human SLC7A5 (LAT1): The Intriguing Histidine/Large Neutral Amino Acid Transporter and Its Relevance to Human Health. *Front Chem* **6**, (2018).
250. Bröer, S. & Bröer, A. Amino acid homeostasis and signalling in mammalian cells and organisms. *Biochemical Journal* **474**, 1935–1963 (2017).
251. Errasti-Murugarren, E. *et al.* L amino acid transporter structure and molecular bases for the asymmetry of substrate interaction. *Nat Commun* **10**, 1807 (2019).
252. Brosnan, M. E. & Brosnan, J. T. Histidine Metabolism and Function. *J Nutr* **150**, 2570S-2575S (2020).
253. Holeček, M. Histidine in Health and Disease: Metabolism, Physiological Importance, and Use as a Supplement. *Nutrients* **12**, 848 (2020).
254. Lin, W.-C. *et al.* Histidine-Dependent Protein Methylation Is Required for Compartmentalization of CTP Synthase. *Cell Reports* **24**, 2733-2745.e7 (2018).
255. Kanarek, N. *et al.* Histidine catabolism is a major determinant of methotrexate sensitivity. *Nature* **559**, 632–636 (2018).
256. Fukutake, N. *et al.* A Novel Multivariate Index for Pancreatic Cancer Detection Based On the Plasma Free Amino Acid Profile. *PLOS ONE* **10**, e0132223 (2015).
257. Zhong, L., Cheng, F., Lu, X., Duan, Y. & Wang, X. Untargeted saliva metabonomics study of breast cancer based on ultra performance liquid chromatography coupled to mass spectrometry with HILIC and RPLC separations. *Talanta* **158**, 351–360 (2016).
258. Kong, X. *et al.* Causal associations of histidine and 12 site-specific cancers: a bidirectional Mendelian randomization study. *Mol Genet Genomics* **298**, 1331–1341 (2023).
259. Park, Y. *et al.* Impact of Exogenous Treatment with Histidine on Hepatocellular Carcinoma Cells. *Cancers* **14**, 1205 (2022).

260. Kumar, N. *et al.* Histidine Enhances the Anticancer Effect of Gemcitabine against Pancreatic Cancer via Disruption of Amino Acid Homeostasis and Oxidant—Antioxidant Balance. *Cancers* **15**, 2593 (2023).
261. Froldi, F. *et al.* Histidine is selectively required for the growth of Myc-dependent dedifferentiation tumours in the Drosophila CNS. *The EMBO Journal* **38**, e99895 (2019).
262. Kreuzaler, P. *et al.* Vitamin B5 supports MYC oncogenic metabolism and tumor progression in breast cancer. *Nat Metab* **5**, 1870–1886 (2023).
263. Poncet, N. *et al.* The catalytic subunit of the system L1 amino acid transporter (slc7a5) facilitates nutrient signalling in mouse skeletal muscle. *PLoS ONE* **9**, e89547 (2014).
264. Bian, Y. *et al.* Cancer SLC43A2 alters T cell methionine metabolism and histone methylation. *Nature* **585**, 277–282 (2020).
265. Prakash, V. *et al.* Ribosome biogenesis during cell cycle arrest fuels EMT in development and disease. *Nat Commun* **10**, 2110 (2019).
266. Hinze, L. *et al.* Synthetic Lethality of Wnt Pathway Activation and Asparaginase in Drug-Resistant Acute Leukemias. *Cancer Cell* **35**, 664-676.e7 (2019).
267. Aubrey, B. J. *et al.* An Inducible Lentiviral Guide RNA Platform Enables the Identification of Tumor-Essential Genes and Tumor-Promoting Mutations In Vivo. *Cell Reports* **10**, 1422–1432 (2015).
268. Schmidt, E. K., Clavarino, G., Ceppi, M. & Pierre, P. SUnSET, a nonradioactive method to monitor protein synthesis. *Nat Methods* **6**, 275–277 (2009).
269. Tomayko, M. M. & Reynolds, C. P. Determination of subcutaneous tumor size in athymic (nude) mice. *Cancer Chemother Pharmacol* **24**, 148–154 (1989).
270. Ram, S. *et al.* Pixelwise H-score: A novel digital image analysis-based metric to quantify membrane biomarker expression from immunohistochemistry images. *PLOS ONE* **16**, e0245638 (2021).
271. Protein Array Analyzer for ImageJ - Gilles Carpentier Research Web Site: Computer Image Analysis. http://image.bio.methods.free.fr/ImageJ/?Protein-Array-Analyzer-for-ImageJ.html.
272. Naipal, K. A. T. *et al.* Tumor slice culture system to assess drug response of primary breast cancer. *BMC Cancer* **16**, 78 (2016).
273. Fets, L. *et al.* MCT2 mediates concentration-dependent inhibition of glutamine metabolism by MOG. *Nat Chem Biol* **14**, 1032–1042 (2018).
274. Ewels, P. A. *et al.* The nf-core framework for community-curated bioinformatics pipelines. *Nat Biotechnol* **38**, 276–278 (2020).
275. Dobin, A. *et al.* STAR: ultrafast universal RNA-seq aligner. *Bioinformatics* **29**, 15–21 (2013).
276. Li, B. & Dewey, C. N. RSEM: accurate transcript quantification from RNA-Seq data with or without a reference genome. *BMC Bioinformatics* **12**, 323 (2011).
277. Love, M. I., Huber, W. & Anders, S. Moderated estimation of fold change and dispersion for RNA-seq data with DESeq2. *Genome Biology* **15**, 550 (2014).
278. Andergassen, D. *et al.* Mapping the mouse Allelome reveals tissue-specific regulation of allelic expression. *eLife* **6**, e25125 (2017).
279. Darnell, A. M., Subramaniam, A. R. & O'Shea, E. K. Translational Control through Differential Ribosome Pausing during Amino Acid Limitation in Mammalian Cells. *Molecular Cell* **71**, 229-243.e11 (2018).

280. Broeker, C. D., Ortiz, M. M. O., Murillo, M. S. & Andrechek, E. R. Integrative multi-omic sequencing reveals the MMTV-Myc mouse model mimics human breast cancer heterogeneity. *Breast Cancer Research* **25**, 120 (2023).
281. Andrechek, E. R. *et al.* Genetic heterogeneity of Myc-induced mammary tumors reflecting diverse phenotypes including metastatic potential. *Proceedings of the National Academy of Sciences* **106**, 16387–16392 (2009).
282. Hollern, D. P. & Andrechek, E. R. A genomic analysis of mouse models of breast cancer reveals molecular features of mouse models and relationships to human breast cancer. *Breast Cancer Res* **16**, R59 (2014).
283. Kreuzaler, P. *et al.* Heterogeneity of Myc expression in breast cancer exposes pharmacological vulnerabilities revealed through executable mechanistic modeling. *Proc Natl Acad Sci U S A* **116**, 22399–22408 (2019).
284. Lieu, E. L., Nguyen, T., Rhyne, S. & Kim, J. Amino acids in cancer. *Experimental & Molecular Medicine* **52**, 15–30 (2020).
285. Zhao, Y., Pu, C. & Liu, Z. Essential amino acids deprivation is a potential strategy for breast cancer treatment. *The Breast* **62**, 152–161 (2022).
286. Li, Y. *et al.* SLC7A5 serves as a prognostic factor of breast cancer and promotes cell proliferation through activating AKT/mTORC1 signaling pathway. *Ann Transl Med* **9**, 892 (2021).
287. Slamon, D. J. *et al.* Studies of the HER-2/neu proto-oncogene in human breast and ovarian cancer. *Science* **244**, 707–712 (1989).
288. Park, S. *et al.* Protein expression profiling of primary mammary epithelial cells derived from MMTV-neu mice revealed that HER2/NEU-driven changes in protein expression are functionally clustered. *IUBMB Life* **62**, 41–50 (2010).
289. Yap, C.-S., Peterson, A. L., Castellani, G., Sedivy, J. M. & Neretti, N. Kinetic profiling of the c-Myc transcriptome and bioinformatic analysis of repressed gene promoters. *Cell Cycle* **10**, 2184–2196 (2011).
290. Paulusma, C. C., Lamers, W. H., Broer, S. & van de Graaf, S. F. J. Amino acid metabolism, transport and signalling in the liver revisited. *Biochemical Pharmacology* **201**, 115074 (2022).
291. Boldyrev, A. A., Aldini, G. & Derave, W. Physiology and Pathophysiology of Carnosine. *Physiological Reviews* **93**, 1803–1845 (2013).
292. Maslinski, C., Kierska, D., Fogel, W. A., Kinnunen, A. & Panula, P. Histamine: Its metabolism and localization in mammary gland. *Comparative Biochemistry and Physiology Part C: Comparative Pharmacology* **105**, 269–273 (1993).
293. Cantoni, G. L. The role of S-adenosylhomocysteine in the biological utilization of S-adenosylmethionine. *Prog Clin Biol Res* **198**, 47–65 (1985).
294. Wang, Q. & Holst, J. L-type amino acid transport and cancer: targeting the mTORC1 pathway to inhibit neoplasia. *Am J Cancer Res* **5**, 1281–1294 (2015).
295. Tessari, P. Nonessential amino acid usage for protein replenishment in humans: a method of estimation. *Am J Clin Nutr* **110**, 255–264 (2019).
296. Dai, Z., Zheng, W. & Locasale, J. W. Amino acid variability, tradeoffs and optimality in human diet. *Nat Commun* **13**, 6683 (2022).
297. Maugeri, S. *et al.* The Anti-Cancer Activity of the Naturally Occurring Dipeptide Carnosine: Potential for Breast Cancer. *Cells* **12**, 2592 (2023).
298. Tiedje, K. E., Stevens, K., Barnes, S. & Weaver, D. F. Beta-alanine as a small molecule neurotransmitter. *Neurochem Int* **57**, 177–188 (2010).
299. Caruso, G., Caraci, F. & Jolivet, R. B. Pivotal role of carnosine in the modulation of brain cells activity: Multimodal mechanism of action and

therapeutic potential in neurodegenerative disorders. *Progress in Neurobiology* **175**, 35–53 (2019).
300. Prakash, M. D. *et al.* Anti-Cancer Effects of Carnosine—A Dipeptide Molecule. *Molecules* **26**, 1644 (2021).
301. Hussein, M. M. A. *et al.* Evaluation of anti-cancer effects of carnosine and melittin-loaded niosomes in MCF-7 and MDA-MB-231 breast cancer cells. *Front. Pharmacol.* **14**, (2023).
302. Lei, L. *et al.* Zinc-Carnosine Metallodrug Network as Dual Metabolism Inhibitor Overcoming Metabolic Reprogramming for Efficient Cancer Therapy. *Nano Lett* **23**, 2659–2668 (2023).
303. Kamal, M. A., Jiang, H., Hu, Y., Keep, Richard. F. & Smith, D. E. Influence of genetic knockout of Pept2 on the in vivo disposition of endogenous and exogenous carnosine in wild-type and Pept2 null mice. *American Journal of Physiology-Regulatory, Integrative and Comparative Physiology* **296**, R986–R991 (2009).
304. Maslinski, C., Kierska, D., Fogel, W. A., Kinnunen, A. & Panula, P. Histamine in Mammary Gland: Pregnancy and Lactation*. *Comparative Biochemistry and Physiology Part A: Physiology* **116**, 57–64 (1997).
305. Kierska, D., Fogel, W. A. & Maslinski, C. Histamine concentration and metabolism in mouse mammary gland during the estrous cycle. *Inflamm. res.* **46**, 63–64 (1997).
306. Garcia-Caballero, M., Neugebauer, E., Rodriguez, F., De Castro, I. N. & Vara-Thorbeck, C. Histamine synthesis and content in benign and malignant breast tumours. Its effects on other host tissues. *Surgical Oncology* **3**, 167–173 (1994).
307. Medina, V. *et al.* Histamine-mediated signaling processes in human malignant mammary cells. *Cancer Biology & Therapy* **5**, 1462–1471 (2006).
308. Bolton, E., King, J. & Morris, D. L. H2-antagonists in the treatment of colon and breast cancer. *Semin Cancer Biol* **10**, 3–10 (2000).
309. Nicoud, M. B. *et al.* Study of the antitumour effects and the modulation of immune response by histamine in breast cancer. *Br J Cancer* **122**, 348–360 (2020).
310. He, L., Zhu, Z., Chen, S., Wang, Y. & Gu, H. Mammary tumor growth and metastasis are reduced in c-Kit mutant Sash mice. *Cancer Med* **5**, 1292–1297 (2016).
311. Cricco, G. P. *et al.* Histamine as an autocrine growth factor in experimental mammary carcinomas. *Agents Actions* **43**, 17–20 (1994).
312. Vila-Leahey, A. *et al.* Ranitidine modifies myeloid cell populations and inhibits breast tumor development and spread in mice. *Oncoimmunology* **5**, e1151591 (2016).
313. Martinel Lamas, D. J. *et al.* Enhancement of ionizing radiation response by histamine in vitro and in vivo in human breast cancer. *Cancer Biol Ther* **16**, 137–148 (2015).
314. Martinel Lamas, D. J. *et al.* Therapeutic potential of histamine $H_4$ receptor agonists in triple-negative human breast cancer experimental model. *Br J Pharmacol* **170**, 188–199 (2013).
315. Speisky, D. *et al.* Histamine H4 Receptor Expression in Triple-negative Breast Cancer: An Exploratory Study. *J Histochem Cytochem* **70**, 311–322 (2022).

316. Still, E. R. The requirement and regulation of the glutamine transporter, ASCT2 in mammary gland tumorigenesis. *Doctoral thesis, UCL (University College London).* 1–237 (UCL (University College London), 2018).
317. Hendriks, B. S., Opresko, L. K., Wiley, H. S. & Lauffenburger, D. Coregulation of Epidermal Growth Factor Receptor/Human Epidermal Growth Factor Receptor 2 (HER2) Levels and Locations: Quantitative Analysis of HER2 Overexpression Effects1. *Cancer Research* **63**, 1130–1137 (2003).
318. Chen, R. *et al.* The general amino acid control pathway regulates mTOR and autophagy during serum/glutamine starvation. *Journal of Cell Biology* **206**, 173–182 (2014).
319. Gambardella, G. *et al.* A single-cell analysis of breast cancer cell lines to study tumour heterogeneity and drug response. *Nat Commun* **13**, 1714 (2022).
320. Watford, M. Glutamine and Glutamate Metabolism across the Liver Sinusoid. *The Journal of Nutrition* **130**, 983S-987S (2000).
321. Tărlungeanu, D. C. *et al.* Impaired Amino Acid Transport at the Blood Brain Barrier Is a Cause of Autism Spectrum Disorder. *Cell* **167**, 1481-1494.e18 (2016).
322. Furuya, M., Horiguchi, J., Nakajima, H., Kanai, Y. & Oyama, T. Correlation of L-type amino acid transporter 1 and CD98 expression with triple negative breast cancer prognosis. *Cancer Science* **103**, 382–389 (2012).
323. Sakata, T. *et al.* L-type amino-acid transporter 1 as a novel biomarker for high-grade malignancy in prostate cancer. *Pathol Int* **59**, 7–18 (2009).
324. Kaira, K. *et al.* Prognostic significance of L-type amino acid transporter 1 expression in resectable stage I–III nonsmall cell lung cancer. *Br J Cancer* **98**, 742–748 (2008).
325. Imai, H. *et al.* L-type amino acid transporter 1 expression is a prognostic marker in patients with surgically resected stage I non-small cell lung cancer. *Histopathology* **54**, 804–813 (2009).
326. Imai, H. *et al.* Inhibition of L-type amino acid transporter 1 has antitumor activity in non-small cell lung cancer. *Anticancer Res* **30**, 4819–4828 (2010).
327. Yazawa, T. *et al.* Clinical significance of coexpression of L-type amino acid transporter 1 (LAT1) and ASC amino acid transporter 2 (ASCT2) in lung adenocarcinoma. *Am J Transl Res* **7**, 1126–1139 (2015).
328. Kaira, K. *et al.* Expression of amino acid transporter (LAT1 and 4F2hc) in pulmonary pleomorphic carcinoma. *Hum Pathol* **84**, 142–149 (2019).
329. Oda, K. *et al.* l-Type amino acid transporter 1 inhibitors inhibit tumor cell growth. *Cancer Science* **101**, 173–179 (2010).
330. Enomoto, K. *et al.* A novel therapeutic approach for anaplastic thyroid cancer through inhibition of LAT1. *Sci Rep* **9**, 14616 (2019).
331. Häfliger, P. *et al.* The LAT1 inhibitor JPH203 reduces growth of thyroid carcinoma in a fully immunocompetent mouse model. *Journal of Experimental & Clinical Cancer Research* **37**, 234 (2018).
332. Krick, T. *et al.* Amino Acid metabolism conflicts with protein diversity. *Mol Biol Evol* **31**, 2905–2912 (2014).
333. Inoki, K., Li, Y., Xu, T. & Guan, K.-L. Rheb GTPase is a direct target of TSC2 GAP activity and regulates mTOR signaling. *Genes Dev* **17**, 1829–1834 (2003).
334. Castro, A. F., Rebhun, J. F., Clark, G. J. & Quilliam, L. A. Rheb Binds Tuberous Sclerosis Complex 2 (TSC2) and Promotes S6 Kinase Activation in

a Rapamycin- and Farnesylation-dependent Manner *. *Journal of Biological Chemistry* **278**, 32493–32496 (2003).
335. Gingras, A.-C. *et al.* Regulation of 4E-BP1 phosphorylation: a novel two-step mechanism. *Genes Dev* **13**, 1422–1437 (1999).
336. Hara, K. *et al.* Regulation of eIF-4E BP1 phosphorylation by mTOR. *J Biol Chem* **272**, 26457–26463 (1997).
337. Thoreen, C. C. *et al.* A unifying model for mTORC1-mediated regulation of mRNA translation. *Nature* **485**, 109–113 (2012).
338. Pende, M. *et al.* S6K1(-/-)/S6K2(-/-) mice exhibit perinatal lethality and rapamycin-sensitive 5'-terminal oligopyrimidine mRNA translation and reveal a mitogen-activated protein kinase-dependent S6 kinase pathway. *Mol Cell Biol* **24**, 3112–3124 (2004).
339. Ballou, L. M., Jenö, P. & Thomas, G. Protein phosphatase 2A inactivates the mitogen-stimulated S6 kinase from Swiss mouse 3T3 cells. *J Biol Chem* **263**, 1188–1194 (1988).
340. Thomas, G., Martin-Perez, J., Siegmann, M. & Otto, A. M. The effect of serum, EGF, PGF2α and insulin on S6 phosphorylation and the initiation of protein and DNA synthesis. *Cell* **30**, 235–242 (1982).
341. Chauvin, C. *et al.* Ribosomal protein S6 kinase activity controls the ribosome biogenesis transcriptional program. *Oncogene* **33**, 474–483 (2014).
342. Ruvinsky, I. *et al.* Ribosomal protein S6 phosphorylation is a determinant of cell size and glucose homeostasis. *Genes Dev* **19**, 2199–2211 (2005).
343. Rullo-Tubau, J. *et al.* Structure and mechanisms of transport of human Asc1/CD98hc amino acid transporter. *Nat Commun* **15**, 2986 (2024).
344. Chiu, M. *et al.* GPNA inhibits the sodium-independent transport system L for neutral amino acids. *Amino Acids* **49**, 1365–1372 (2017).
345. Müller, M. *et al.* The coordinated action of the MVB pathway and autophagy ensures cell survival during starvation. *eLife* **4**, e07736 (2015).
346. Roux, P. P. *et al.* RAS/ERK signaling promotes site-specific ribosomal protein S6 phosphorylation via RSK and stimulates cap-dependent translation. *J Biol Chem* **282**, 14056–14064 (2007).
347. Tameire, F. *et al.* ATF4 couples MYC-dependent translational activity to bioenergetic demands during tumour progression. *Nat Cell Biol* **21**, 889–899 (2019).
348. Hannan, K. M. *et al.* mTOR-Dependent Regulation of Ribosomal Gene Transcription Requires S6K1 and Is Mediated by Phosphorylation of the Carboxy-Terminal Activation Domain of the Nucleolar Transcription Factor UBF†. *Molecular and Cellular Biology* **23**, 8862–8877 (2003).
349. Warner, J. R., Vilardell, J. & Sohn, J. H. Economics of ribosome biosynthesis. *Cold Spring Harb Symp Quant Biol* **66**, 567–574 (2001).
350. Mayer, C., Zhao, J., Yuan, X. & Grummt, I. mTOR-dependent activation of the transcription factor TIF-IA links rRNA synthesis to nutrient availability. *Genes Dev* **18**, 423–434 (2004).
351. Jiao, L. *et al.* Ribosome biogenesis in disease: new players and therapeutic targets. *Sig Transduct Target Ther* **8**, 1–22 (2023).
352. Mori, T. *et al.* c-Myc overexpression increases ribosome biogenesis and protein synthesis independent of mTORC1 activation in mouse skeletal muscle. *American Journal of Physiology-Endocrinology and Metabolism* **321**, E551–E559 (2021).

353. Charkey, L. W., Kano, A. K. & Hougham, D. F. Effects of Fasting on Blood Non-Protein Amino Acids in Humans1. *The Journal of Nutrition* **55**, 469–480 (1955).
354. Jensen, T., Kiersgaard, M., Sørensen, D. & Mikkelsen, L. Fasting of mice: a review. *Lab Anim* **47**, 225–240 (2013).
355. Sokolović, M. *et al.* Fasting induces a biphasic adaptive metabolic response in murine small intestine. *BMC Genomics* **8**, 361 (2007).
356. Argilés, J. M., Campos, N., Lopez-Pedrosa, J. M., Rueda, R. & Rodriguez-Mañas, L. Skeletal Muscle Regulates Metabolism via Interorgan Crosstalk: Roles in Health and Disease. *J Am Med Dir Assoc* **17**, 789–796 (2016).
357. Wolfe, R. R. The underappreciated role of muscle in health and disease2. *The American Journal of Clinical Nutrition* **84**, 475–482 (2006).
358. Rodriguez, C. F. *et al.* Structural basis for substrate specificity of heteromeric transporters of neutral amino acids. *Proceedings of the National Academy of Sciences* **118**, e2113573118 (2021).
359. Papageorgiou, A., Rapley, J., Mesirov, J. P., Tamayo, P. & Avruch, J. A genome-wide siRNA screen in mammalian cells for regulators of S6 phosphorylation. *PLoS One* **10**, e0116096 (2015).
360. Meng, D. *et al.* Glutamine and asparagine activate mTORC1 independently of Rag GTPases. *Journal of Biological Chemistry* **295**, 2890–2899 (2020).
361. Jewell, J. L. *et al.* Differential regulation of mTORC1 by leucine and glutamine. *Science* **347**, 194–198 (2015).
362. Fox, H. L., Pham, P. T., Kimball, S. R., Jefferson, L. S. & Lynch, C. J. Amino acid effects on translational repressor 4E-BP1 are mediated primarily by L-leucine in isolated adipocytes. *Am J Physiol* **275**, C1232-1238 (1998).
363. Hart, L. S. *et al.* ER stress-mediated autophagy promotes Myc-dependent transformation and tumor growth. *J Clin Invest* **122**, 4621–4634 (2012).
364. Wolfer, A. *et al.* MYC regulation of a 'poor-prognosis' metastatic cancer cell state. *Proc Natl Acad Sci U S A* **107**, 3698–3703 (2010).
365. Naito, T., Kuma, A. & Mizushima, N. Differential Contribution of Insulin and Amino Acids to the mTORC1-Autophagy Pathway in the Liver and Muscle*. *Journal of Biological Chemistry* **288**, 21074–21081 (2013).
366. Gregor, A. *et al.* Cage bedding modifies metabolic and gut microbiota profiles in mouse studies applying dietary restriction. *Sci Rep* **10**, 20835 (2020).
367. Chidley, C. *et al.* A CRISPRi/a screening platform to study cellular nutrient transport in diverse microenvironments. *Nat Cell Biol* **26**, 825–838 (2024).
368. Somers, J., Pöyry, T. & Willis, A. E. A perspective on mammalian upstream open reading frame function. *Int J Biochem Cell Biol* **45**, 1690–1700 (2013).
369. Harding, H. P. *et al.* Regulated Translation Initiation Controls Stress-Induced Gene Expression in Mammalian Cells. *Molecular Cell* **6**, 1099–1108 (2000).
370. Wortel, I. M. N., van der Meer, L. T., Kilberg, M. S. & van Leeuwen, F. N. Surviving Stress: Modulation of ATF4-Mediated Stress Responses in Normal and Malignant Cells. *Trends Endocrinol Metab* **28**, 794–806 (2017).
371. Koumenis, C. ER stress, hypoxia tolerance and tumor progression. *Curr Mol Med* **6**, 55–69 (2006).
372. Denzel, M. S. & Antebi, A. Hexosamine pathway and (ER) protein quality control. *Curr Opin Cell Biol* **33**, 14–18 (2015).
373. Vladykovskaya, E. *et al.* Lipid peroxidation product 4-hydroxy-trans-2-nonenal causes endothelial activation by inducing endoplasmic reticulum stress. *J Biol Chem* **287**, 11398–11409 (2012).

374. Dong, L., Krewson, E. A. & Yang, L. V. Acidosis Activates Endoplasmic Reticulum Stress Pathways through GPR4 in Human Vascular Endothelial Cells. *Int J Mol Sci* **18**, 278 (2017).
375. Wek, S. A., Zhu, S. & Wek, R. C. The histidyl-tRNA synthetase-related sequence in the eIF-2 alpha protein kinase GCN2 interacts with tRNA and is required for activation in response to starvation for different amino acids. *Mol Cell Biol* **15**, 4497–4506 (1995).
376. Wek, R. C., Jackson, B. M. & Hinnebusch, A. G. Juxtaposition of domains homologous to protein kinases and histidyl-tRNA synthetases in GCN2 protein suggests a mechanism for coupling GCN4 expression to amino acid availability. *Proc Natl Acad Sci U S A* **86**, 4579–4583 (1989).
377. Ishimura, R., Nagy, G., Dotu, I., Chuang, J. H. & Ackerman, S. L. Activation of GCN2 kinase by ribosome stalling links translation elongation with translation initiation. *eLife* **5**, e14295 (2016).
378. Siu, F., Bain, P. J., LeBlanc-Chaffin, R., Chen, H. & Kilberg, M. S. ATF4 Is a Mediator of the Nutrient-sensing Response Pathway That Activates the Human Asparagine Synthetase Gene*. *Journal of Biological Chemistry* **277**, 24120–24127 (2002).
379. Harding, H. P. *et al.* An integrated stress response regulates amino acid metabolism and resistance to oxidative stress. *Mol Cell* **11**, 619–633 (2003).
380. Podust, L. M., Krezel, A. M. & Kim, Y. Crystal structure of the CCAAT box/enhancer-binding protein beta activating transcription factor-4 basic leucine zipper heterodimer in the absence of DNA. *J Biol Chem* **276**, 505–513 (2001).
381. Newman, J. R. S. & Keating, A. E. Comprehensive identification of human bZIP interactions with coiled-coil arrays. *Science* **300**, 2097–2101 (2003).
382. Ameri, K. & Harris, A. L. Activating transcription factor 4. *The International Journal of Biochemistry & Cell Biology* **40**, 14–21 (2008).
383. Reinke, A. W., Baek, J., Ashenberg, O. & Keating, A. E. Networks of bZIP protein-protein interactions diversified over a billion years of evolution. *Science* **340**, 730–734 (2013).
384. Kilberg, M. S., Shan, J. & Su, N. ATF4-dependent transcription mediates signaling of amino acid limitation. *Trends in Endocrinology & Metabolism* **20**, 436–443 (2009).
385. Lines, C. L., McGrath, M. J., Dorwart, T. & Conn, C. S. The integrated stress response in cancer progression: a force for plasticity and resistance. *Front Oncol* **13**, 1206561 (2023).
386. Quan, L. *et al.* Amino acid transporter LAT1 in tumor-associated vascular endothelium promotes angiogenesis by regulating cell proliferation and VEGF-A-dependent mTORC1 activation. *Journal of Experimental & Clinical Cancer Research* **39**, 266 (2020).
387. Wang, Q. *et al.* Androgen receptor and nutrient signaling pathways coordinate the demand for increased amino acid transport during prostate cancer progression. *Cancer Res* **71**, 7525–7536 (2011).
388. Quirós, P. M. *et al.* Multi-omics analysis identifies ATF4 as a key regulator of the mitochondrial stress response in mammals. *J Cell Biol* **216**, 2027–2045 (2017).
389. Saito, Y. *et al.* LLGL2 rescues nutrient stress by promoting leucine uptake in ER + breast cancer. *Nature* **569**, 275–279 (2019).

390. Kimura, K. *et al.* Histidine augments the suppression of hepatic glucose production by central insulin action. *Diabetes* **62**, 2266–2277 (2013).
391. Kasaoka, S. *et al.* Histidine supplementation suppresses food intake and fat accumulation in rats. *Nutrition* **20**, 991–996 (2004).
392. Feng, R. N. *et al.* Histidine supplementation improves insulin resistance through suppressed inflammation in obese women with the metabolic syndrome: a randomised controlled trial. *Diabetologia* **56**, 985–994 (2013).
393. Romano, C. *et al.* Influence of Diets with Varying Essential/Nonessential Amino Acid Ratios on Mouse Lifespan. *Nutrients* **11**, 1367 (2019).
394. Sugimura, T., Birnbaum, S. M., Winitz, M. & Greenstein, J. P. Quantitative nutritional studies with water-soluble, chemically defined diets. VIII. The forced feeding of diets each lacking in one essential amino acid. *Arch Biochem Biophys* **81**, 448–455 (1959).
395. Yu, X. & Long, Y. C. Autophagy modulates amino acid signaling network in myotubes: differential effects on mTORC1 pathway and the integrated stress response. *FASEB J* **29**, 394–407 (2015).
396. Yu, L. *et al.* Termination of autophagy and reformation of lysosomes regulated by mTOR. *Nature* **465**, 942–946 (2010).
397. Koehnle, T. J., Russell, M. C. & Gietzen, D. W. Rats rapidly reject diets deficient in essential amino acids. *J Nutr* **133**, 2331–2335 (2003).
398. Feurté, S. *et al.* Feeding patterns and meal microstructure during development of a taste aversion to a threonine devoid diet. *Nutr Neurosci* **5**, 269–278 (2002).
399. Kamata, S. *et al.* Dietary deprivation of each essential amino acid induces differential systemic adaptive responses in mice. *Mol Nutr Food Res* **58**, 1309–1321 (2014).
400. Blackshear, P. J., Holloway, P. A. & Alberti, K. G. Factors regulating amino acid release from extrasplanchnic tissues in the rat. Interactions of alanine and glutamine. *Biochem J* **150**, 379–387 (1975).
401. Cruzat, V. F. Chapter 18 - Glutamine and Skeletal Muscle. in *Nutrition and Skeletal Muscle* (ed. Walrand, S.) 299–313 (Academic Press, 2019). doi:10.1016/B978-0-12-810422-4.00017-8.
402. Cersosimo, E. *et al.* Role of glutamine in adaptations in nitrogen metabolism during fasting. *Am J Physiol* **250**, E622-628 (1986).
403. Tan, H. W. S., Sim, A. Y. L. & Long, Y. C. Glutamine metabolism regulates autophagy-dependent mTORC1 reactivation during amino acid starvation. *Nat Commun* **8**, (2017).
404. Hayashi, K., Jutabha, P., Endou, H., Sagara, H. & Anzai, N. LAT1 Is a Critical Transporter of Essential Amino Acids for Immune Reactions in Activated Human T Cells. *The Journal of Immunology* **191**, 4080–4085 (2013).
405. Yao, Z. *et al.* Imatinib prevents lung cancer metastasis by inhibiting M2-like polarization of macrophages. *Pharmacol Res* **133**, 121–131 (2018).
406. Li, H. *et al.* The allergy mediator histamine confers resistance to immunotherapy in cancer patients via activation of the macrophage histamine receptor H1. *Cancer Cell* **40**, 36-52.e9 (2022).
407. Borriello, F., Iannone, R. & Marone, G. Histamine Release from Mast Cells and Basophils. *Handb Exp Pharmacol* **241**, 121–139 (2017).
408. Shultz, L. D. *et al.* Multiple defects in innate and adaptive immunologic function in NOD/LtSz-scid mice. *The Journal of Immunology* **154**, 180–191 (1995).

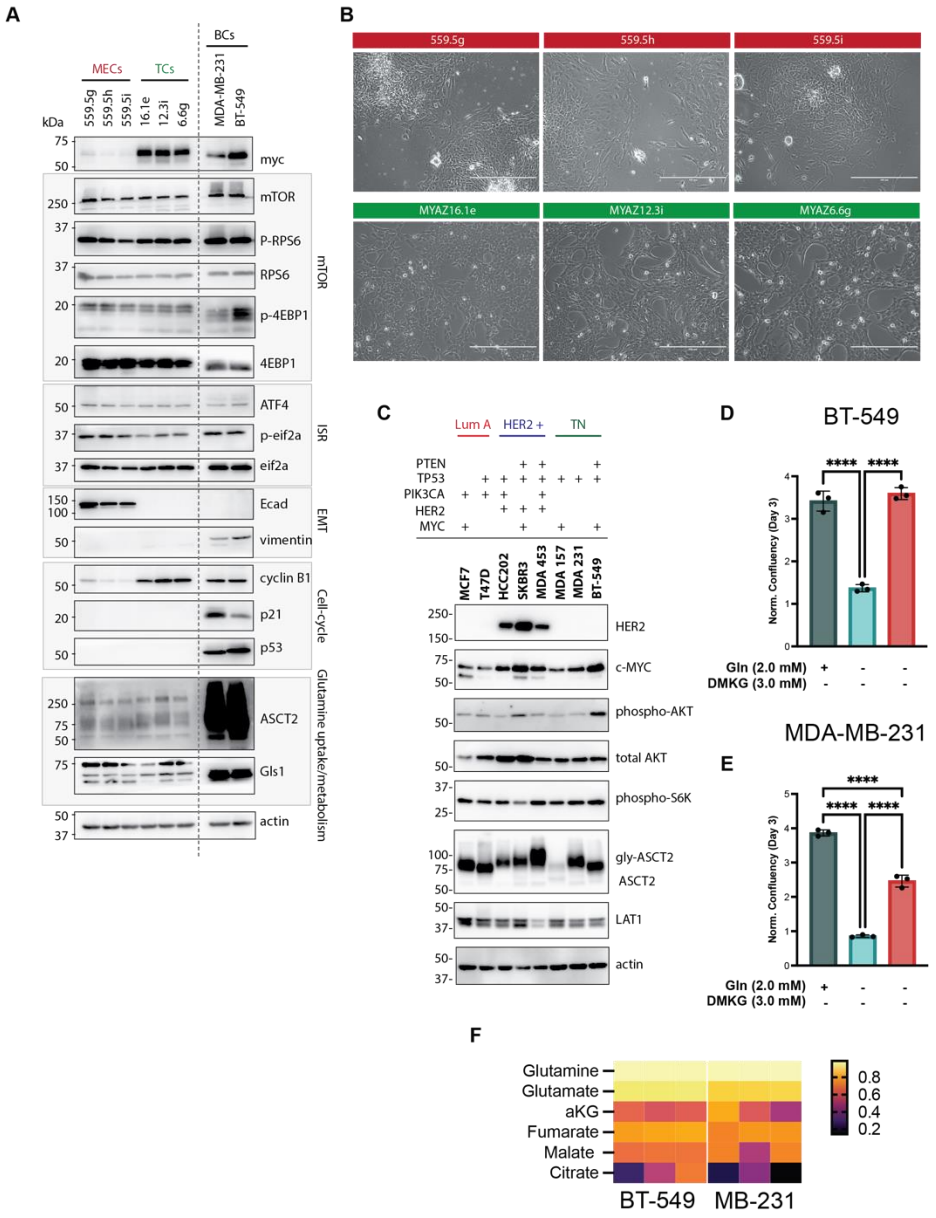
409. Shan, J., Fu, L., Balasubramanian, M. N., Anthony, T. & Kilberg, M. S. ATF4-dependent Regulation of the JMJD3 Gene during Amino Acid Deprivation Can Be Rescued in Atf4-deficient Cells by Inhibition of Deacetylation. *J Biol Chem* **287**, 36393–36403 (2012).
410. Deval, C. *et al.* Amino acid limitation regulates the expression of genes involved in several specific biological processes through GCN2-dependent and GCN2-independent pathways. *The FEBS Journal* **276**, 707–718 (2009).
411. Averous, J. *et al.* GCN2 contributes to mTORC1 inhibition by leucine deprivation through an ATF4 independent mechanism. *Sci Rep* **6**, 27698 (2016).
412. Costa-Mattioli, M. *et al.* Translational control of hippocampal synaptic plasticity and memory by the eIF2alpha kinase GCN2. *Nature* **436**, 1166–1173 (2005).
413. Guo, F. & Cavener, D. R. The GCN2 eIF2alpha kinase regulates fatty-acid homeostasis in the liver during deprivation of an essential amino acid. *Cell Metab* **5**, 103–114 (2007).
414. Xiao, F. *et al.* Leucine deprivation increases hepatic insulin sensitivity via GCN2/mTOR/S6K1 and AMPK pathways. *Diabetes* **60**, 746–756 (2011).
415. Okano, N. *et al.* First-in-human phase I study of JPH203, an L-type amino acid transporter 1 inhibitor, in patients with advanced solid tumors. *Invest New Drugs* **38**, 1495–1506 (2020).
416. Furuse, J. *et al.* Phase II Placebo-Controlled Study of the Effect and Safety of Nanvuranlat in Patients with Advanced Biliary Tract Cancers Previously Treated by Systemic Chemotherapy. *Clin Cancer Res* (2024) doi:10.1158/1078-0432.CCR-24-0461.
417. Yanagisawa, N. *et al.* High expression of L-type amino acid transporter 1 as a prognostic marker in bile duct adenocarcinomas. *Cancer Medicine* **3**, 1246–1255 (2014).
418. Kidd, J. G. Regression of transplanted lymphomas induced in vivo by means of normal guinea pig serum. I. Course of transplanted cancers of various kinds in mice and rats given guinea pig serum, horse serum, or rabbit serum. *J Exp Med* **98**, 565–582 (1953).
419. Broome, J. D. Evidence that the L-Asparaginase Activity of Guinea Pig Serum is responsible for its Antilymphoma Effects. *Nature* **191**, 1114–1115 (1961).
420. Appel, I. M. *et al.* Pharmacokinetic, pharmacodynamic and intracellular effects of PEG-asparaginase in newly diagnosed childhood acute lymphoblastic leukemia: results from a single agent window study. *Leukemia* **22**, 1665–1679 (2008).
421. Wilder, C. S. *et al.* Enzymatic depletion of l-Met using an engineered human enzyme as a novel therapeutic strategy for melanoma. *Mol Carcinog* **62**, 1531–1545 (2023).
422. Lu, W.-C. *et al.* Enzyme-mediated depletion of serum l-Met abrogates prostate cancer growth via multiple mechanisms without evidence of systemic toxicity. *Proc Natl Acad Sci U S A* **117**, 13000–13011 (2020).
423. Saha, A. *et al.* Cysteine depletion sensitizes prostate cancer cells to agents that enhance DNA damage and to immune checkpoint inhibition. *J Exp Clin Cancer Res* **42**, 119 (2023).
424. Badgley, M. A. *et al.* Cysteine depletion induces pancreatic tumor ferroptosis in mice. *Science* **368**, 85–89 (2020).

425. Cramer, S. L. *et al.* Systemic depletion of L-cyst(e)ine with cyst(e)inase increases reactive oxygen species and suppresses tumor growth. *Nat Med* **23**, 120–127 (2017).
426. Burrage, L. C. *et al.* Human recombinant arginase enzyme reduces plasma arginine in mouse models of arginase deficiency. *Hum Mol Genet* **24**, 6417–6427 (2015).
427. Agrawal, V. *et al.* In-vivo evaluation of human recombinant Co-arginase against A375 melanoma xenografts. *Melanoma Res* **24**, 556–567 (2014).
428. Keshet, R., Szlosarek, P., Carracedo, A. & Erez, A. Rewiring urea cycle metabolism in cancer to support anabolism. *Nat Rev Cancer* **18**, 634–645 (2018).
429. Dudek, S. M. & Semenkovich, C. F. Essential Amino Acids Regulate Fatty Acid Synthase Expression through an Uncharged Transfer RNA-dependent Mechanism *. *Journal of Biological Chemistry* **270**, 29323–29329 (1995).
430. Lv, X. *et al.* Elucidating the underlying mechanism of amino acids to regulate muscle protein synthesis: Effect on human health. *Nutrition* **103–104**, 111797 (2022).
431. Kerk, S. A. *et al.* Metabolic requirement for GOT2 in pancreatic cancer depends on environmental context. *eLife* **11**, e73245 (2022).
432. Liu, K., Sutter, B. M. & Tu, B. P. Autophagy sustains glutamate and aspartate synthesis in Saccharomyces cerevisiae during nitrogen starvation. *Nat Commun* **12**, 57 (2021).
433. Kedia-Mehta, N. & Finlay, D. K. Competition for nutrients and its role in controlling immune responses. *Nat Commun* **10**, 2123 (2019).
434. Jose, D. G. & Good, R. A. Quantitative effects of nutritional protein and calorie deficiency upon immune responses to tumors in mice. *Cancer Res* **33**, 807–812 (1973).
435. Sinclair, L. V. *et al.* Control of amino-acid transport by antigen receptors coordinates the metabolic reprogramming essential for T cell differentiation. *Nat. Immunol.* **14**, 500–508 (2013).
436. Chi, H. Regulation and function of mTOR signalling in T cell fate decisions. *Nat Rev Immunol* **12**, 325–338 (2012).
437. Nakaya, M. *et al.* Inflammatory T cell responses rely on amino acid transporter ASCT2 facilitation of glutamine uptake and mTORC1 kinase activation. *Immunity* **40**, 692–705 (2014).
438. Sarasola, M. de la P., Táquez Delgado, M. A., Nicoud, M. B. & Medina, V. A. Histamine in cancer immunology and immunotherapy. Current status and new perspectives. *Pharmacol Res Perspect* **9**, e00778 (2021).
439. Al Hafid, N. & Christodoulou, J. Phenylketonuria: a review of current and future treatments. *Transl Pediatr* **4**, 304–317 (2015).
440. Fung, M. K. L. & Chan, G. C.-F. Drug-induced amino acid deprivation as strategy for cancer therapy. *Journal of Hematology & Oncology* **10**, 144 (2017).
441. Sullivan, M. R. *et al.* Quantification of microenvironmental metabolites in murine cancers reveals determinants of tumor nutrient availability. *eLife* **8**, e44235 (2019).
442. Rebsamen, M. *et al.* Gain-of-function genetic screens in human cells identify SLC transporters overcoming environmental nutrient restrictions. *Life Science Alliance* **5**, (2022).

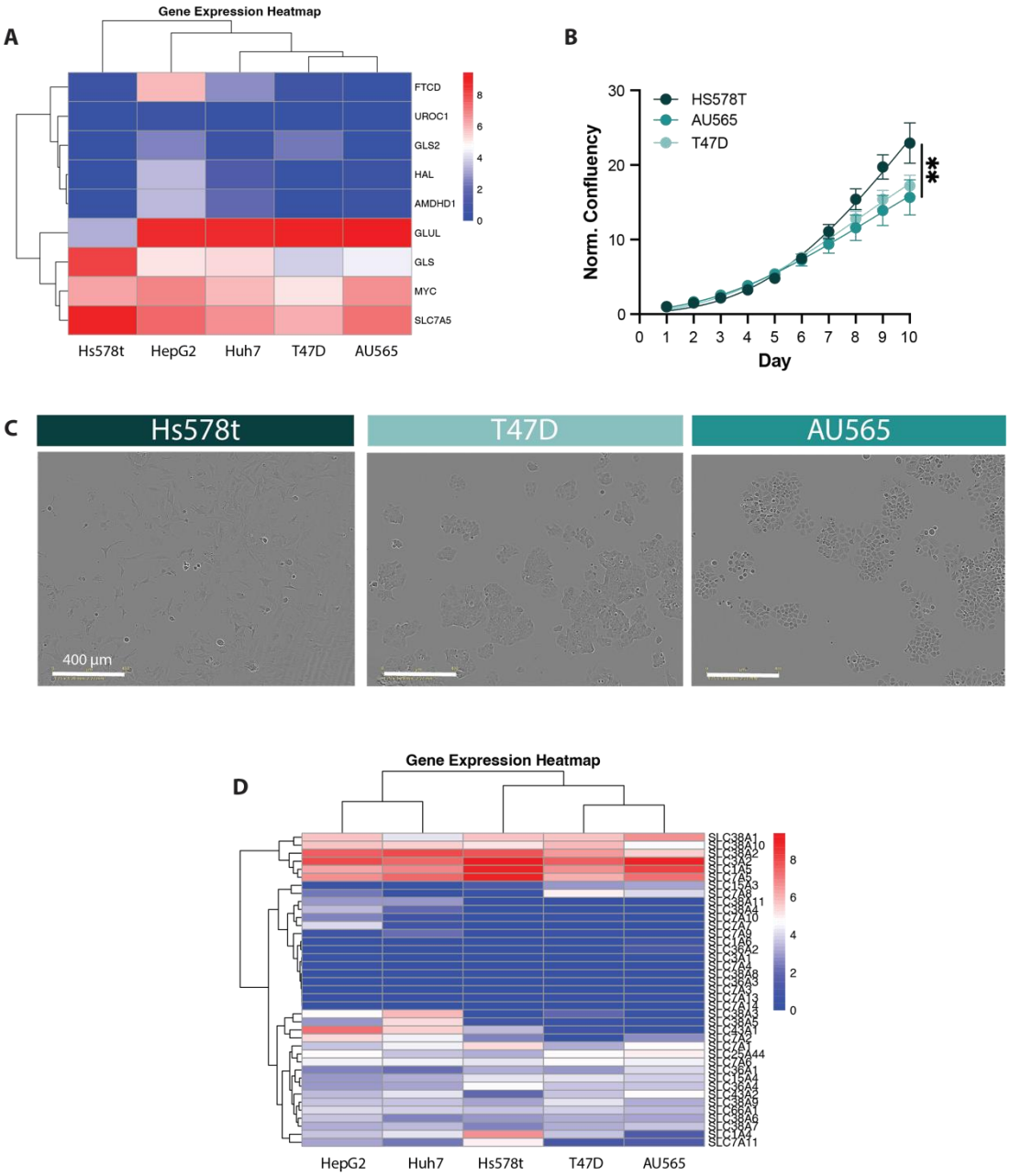
443. Jiang, C. *et al.* Nutrient sensing of mTORC1 signaling in cancer and aging. *Seminars in Cancer Biology* **106–107**, 1–12 (2024).
444. Jiang, J., Pavlova, N. N. & Zhang, J. Asparagine, a critical limiting metabolite during glutamine starvation. *Molecular & Cellular Oncology* **5**, e1441633 (2018).
445. Kim, S.-H. *et al.* Mitochondrial Threonyl-tRNA Synthetase TARS2 Is Required for Threonine-Sensitive mTORC1 Activation. *Molecular Cell* **81**, 398-407.e4 (2021).
446. Hsieh, A. C. *et al.* The translational landscape of mTOR signalling steers cancer initiation and metastasis. *Nature* **485**, 55–61 (2012).
447. Bhin, J. *et al.* MYC is a clinically significant driver of mTOR inhibitor resistance in breast cancer. *J Exp Med* **220**, e20211743 (2023).
448. Mazor, K. M. *et al.* Effects of single amino acid deficiency on mRNA translation are markedly different for methionine versus leucine. *Sci Rep* **8**, 8076 (2018).
449. Chiodi, I., Perini, C., Berardi, D. & Mondello, C. Asparagine sustains cellular proliferation and c-Myc expression in glutamine-starved cancer cells. *Oncology Reports* **45**, 1–12 (2021).
450. Butler, M., Meer, L. T. van der & Leeuwen, F. N. van. Amino Acid Depletion Therapies: Starving Cancer Cells to Death. *Trends in Endocrinology & Metabolism* **32**, 367–381 (2021).
451. Chiu, M., Taurino, G., Bianchi, M. G., Kilberg, M. S. & Bussolati, O. Asparagine Synthetase in Cancer: Beyond Acute Lymphoblastic Leukemia. *Front. Oncol.* **9**, (2020).
452. Sun, J. *et al.* SLC1A3 contributes to L-asparaginase resistance in solid tumors. *EMBO J* **38**, e102147 (2019).
453. Campbell, J. D. *et al.* Distinct patterns of somatic genome alterations in lung adenocarcinomas and squamous cell carcinomas. *Nat. Genet.* **48**, 607–616 (2016).
454. Cava, E. *et al.* Breast Cancer Diet “BCD”: A Review of Healthy Dietary Patterns to Prevent Breast Cancer Recurrence and Reduce Mortality. *Nutrients* **14**, 476 (2022).
455. Bu, Y. *et al.* Dietary patterns and breast cancer risk, prognosis, and quality of life: A systematic review. *Front Nutr* **9**, 1057057 (2023).
456. Castro-Espin, C. *et al.* Dietary patterns related to biological mechanisms and survival after breast cancer diagnosis: results from a cohort study. *Br J Cancer* **128**, 1301–1310 (2023).
457. Becerra-Tomás, N. *et al.* Postdiagnosis dietary factors, supplement use and breast cancer prognosis: Global Cancer Update Programme (CUP Global) systematic literature review and meta-analysis. *International Journal of Cancer* **152**, 616–634 (2023).
458. Widhalm, K. & Virmani, K. Long-term follow-up of 58 patients with histidinemia treated with a histidine-restricted diet: no effect of therapy. *Pediatrics* **94**, 861–866 (1994).
459. Jeon, H. *et al.* Methionine deprivation suppresses triple-negative breast cancer metastasis in vitro and in vivo. *Oncotarget* **7**, 67223–67234 (2016).
460. Pokrovsky, V. S., Abo Qoura, L., Morozova, E. & Bunik, V. I. Predictive markers for efficiency of the amino-acid deprivation therapies in cancer. *Front Med (Lausanne)* **9**, 1035356 (2022).

461. Rogers, L. C. *et al.* Intracellular arginine-dependent translation sensor reveals the dynamics of arginine starvation response and resistance in ASS1-negative cells. *Cancer & Metabolism* **9**, 4 (2021).
462. Vande Voorde, J. *et al.* Improving the metabolic fidelity of cancer models with a physiological cell culture medium. *Sci. Adv.* **5**, eaau7314 (2019).
463. Cantor, J. R. *et al.* Physiologic Medium Rewires Cellular Metabolism and Reveals Uric Acid as an Endogenous Inhibitor of UMP Synthase. *Cell* **169**, 258-272.e17 (2017).
464. Parker, S. J. *et al.* Selective alanine transporter utilization creates a targetable metabolic niche in pancreatic cancer. *Cancer Discov* **10**, 1018–1037 (2020).
465. Verhoeven, J. *et al.* New fluoroethyl phenylalanine analogues as potential LAT1-targeting PET tracers for glioblastoma. *Sci Rep* **9**, 2878 (2019).
466. Nozaki, S. *et al.* 18F-FIMP: a LAT1-specific PET probe for discrimination between tumor tissue and inflammation. *Sci Rep* **9**, 15718 (2019).

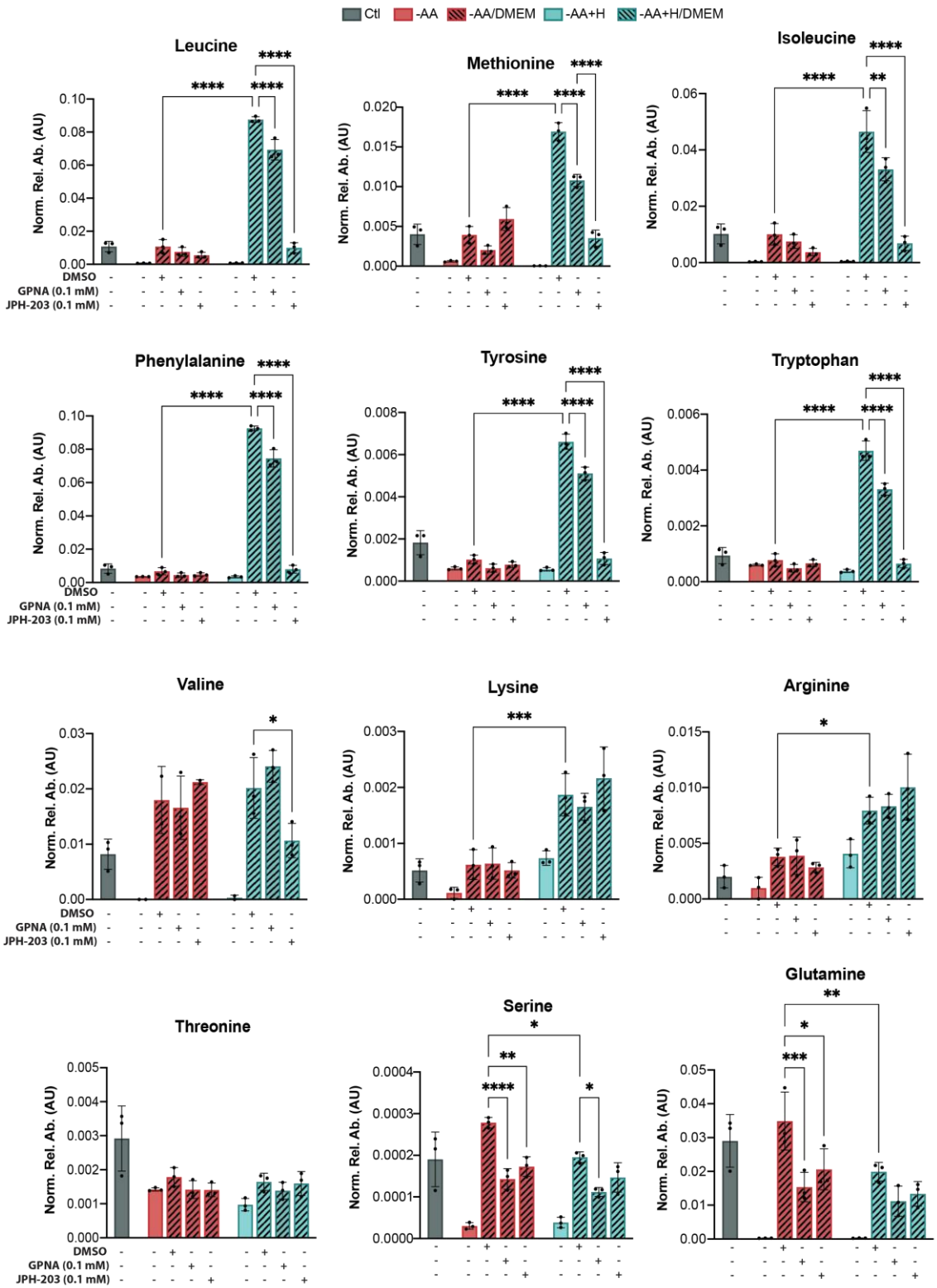
# Appendix




**Appendix 1. Characterization of cell lines used.**
**(A)** WB of mammary epithelial cells (MECs) freshly isolated and plated for 5 days, mammary tumour cell lines MYAZ16.1e, -6.6g, and 12.3i, and TNBC cells, BT-549 and MDA-MB-231. **(B)** Representative brightfield images of MECs and MYAZ mammary tumour cell lines. Scale bar is 400 µm. **(C)** WB of BC cell lines comparing MYC amplification, ASCT2, and LAT1 protein expression. **(D-E)** Confluency of **(D)** BT-549 and **(E)** MDA MB 231 TNBC cells, cultured under indicated conditions after 72 hours, normalized to starting confluency. Representative of 1 replicate. Data is presented as mean ± s.d.; one-way ANOVA with Šídák correction(****p≤0.0001). **(F)** Heatmaps showing mean $^{13}C$ enrichment of Krebs cycle intermediates in BT-549 and MDA MB 231 cells cultured in 2.0 mM [U-$^{13}C$]-glutamine for 24 hours. Colour intensity reflects the proportion of incorporation of $^{13}C$ from glutamine into each metabolite.

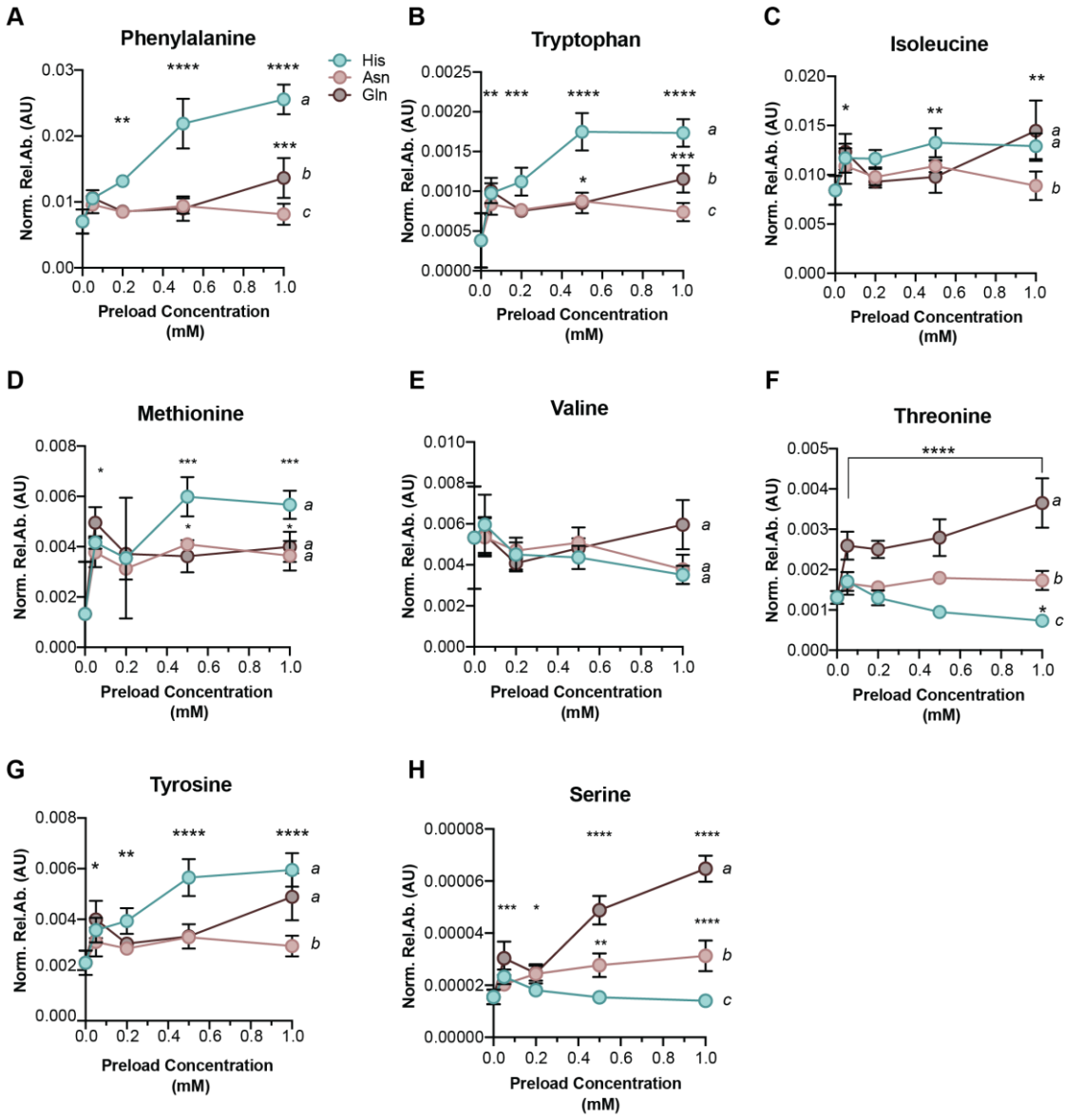



**Appendix 2. RNA-sequencing of HCC and BC cell lines**
**(A)** Heatmap of relative gene expression of enzymes in histidine metabolism and glutaminolysis and glutamine biosynthesis from DepMap Expression Public 24Q2 dataset in HepG2, Huh7, Hs578t, T47D, and AU565 cell lines. Colour scale represents RNA-seq based log2 transformed gene expression levels (log(TPM+1)) with no scaling applied. Hierarchical clustering was applied to genes and samples. **(B)** Confluency of BC cells normalized to starting confluency images every 24 hours. Repeated measures two-way ANOVA with Gessier-Greenhouse correction and Tukey for multiple comparisons, representative of 1 replicate (**p<0.01). **(C)** Brightfield images of BC cell lines from panel B. **(D)** Heatmap of gene expression of *Slc* amino acid transporters from DepMap Expression Public 24Q2 dataset in HepG2, Huh7, Hs578t, T47D, and AU565 cell lines. Colour scale represents RNA-seq based log2 transformed gene expression levels (log(TPM+1)) with no scaling applied. Hierarchical clustering was applied to genes and samples.

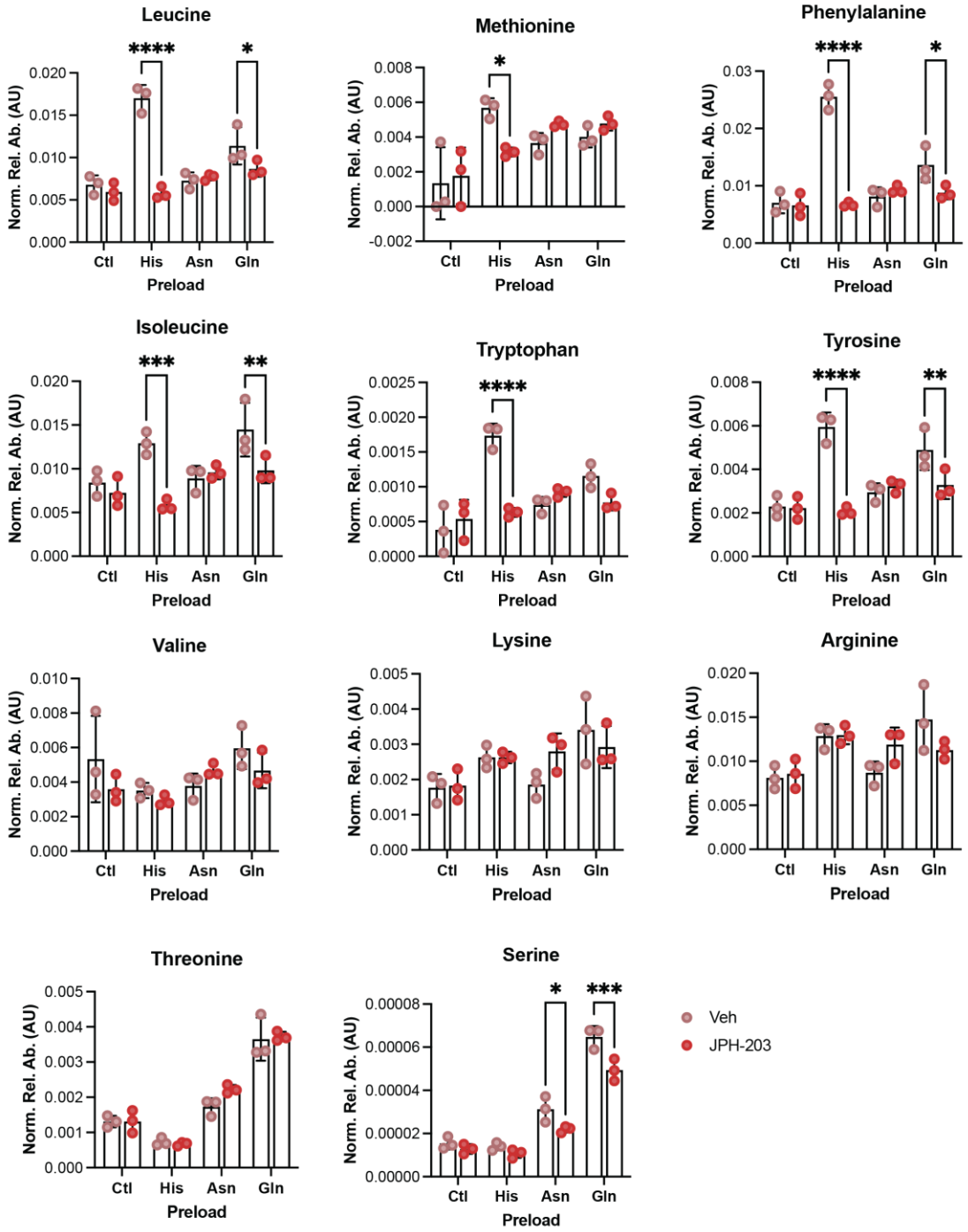



**Appendix 3. Histidine-mediated exchange for specific amino acids blocked by LAT1 inhibition.**

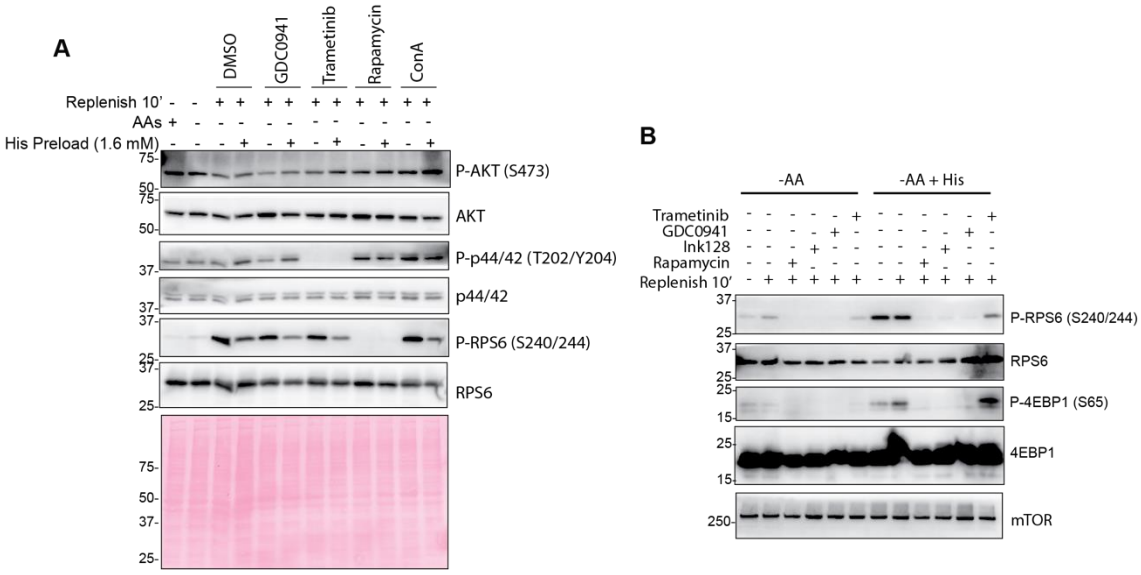
Total abundance of amino acids in MYAZ16.1e cells amino acid starved or preloaded with 1.6 mM histidine for 48 hours and replenished with DMEM in the presence of indicated inhibitors for 2.5 minutes. Two-way ANOVA with Tukey correction. *p≤0.005, **p≤0.01,***p≤0.001, ****p≤0.0001.




**Appendix 4. Histidine is a more efficient exchange factor for EAAs than glutamine.** LC-MS analysis of intracellular amino acid levels. MYAZ16.1e cells were amino acid starved or preloaded with indicated concentrations of asparagine, glutamine, or histidine for 48 hours and subsequently replenished with DMEM for 2.5 minutes. **(A-H)** Normalized relative abundance of indicated amino acids, the 0.0 mM condition depicts amino acid starved cells replenished with DMEM. Data is presented as mean ± s.d. and is representative of 2 independent replicates (two-way ANOVA; *p≤0.05, **p≤0.01, ***p≤0.001, ****p≤0.0001). Statistical significance compared to amino acid starved cells was corrected with Tukey hypothesis testing and is presented with stars. Statistical significance comparing preload conditions is indicated by letters and is corrected by Dunnett hypothesis testing.

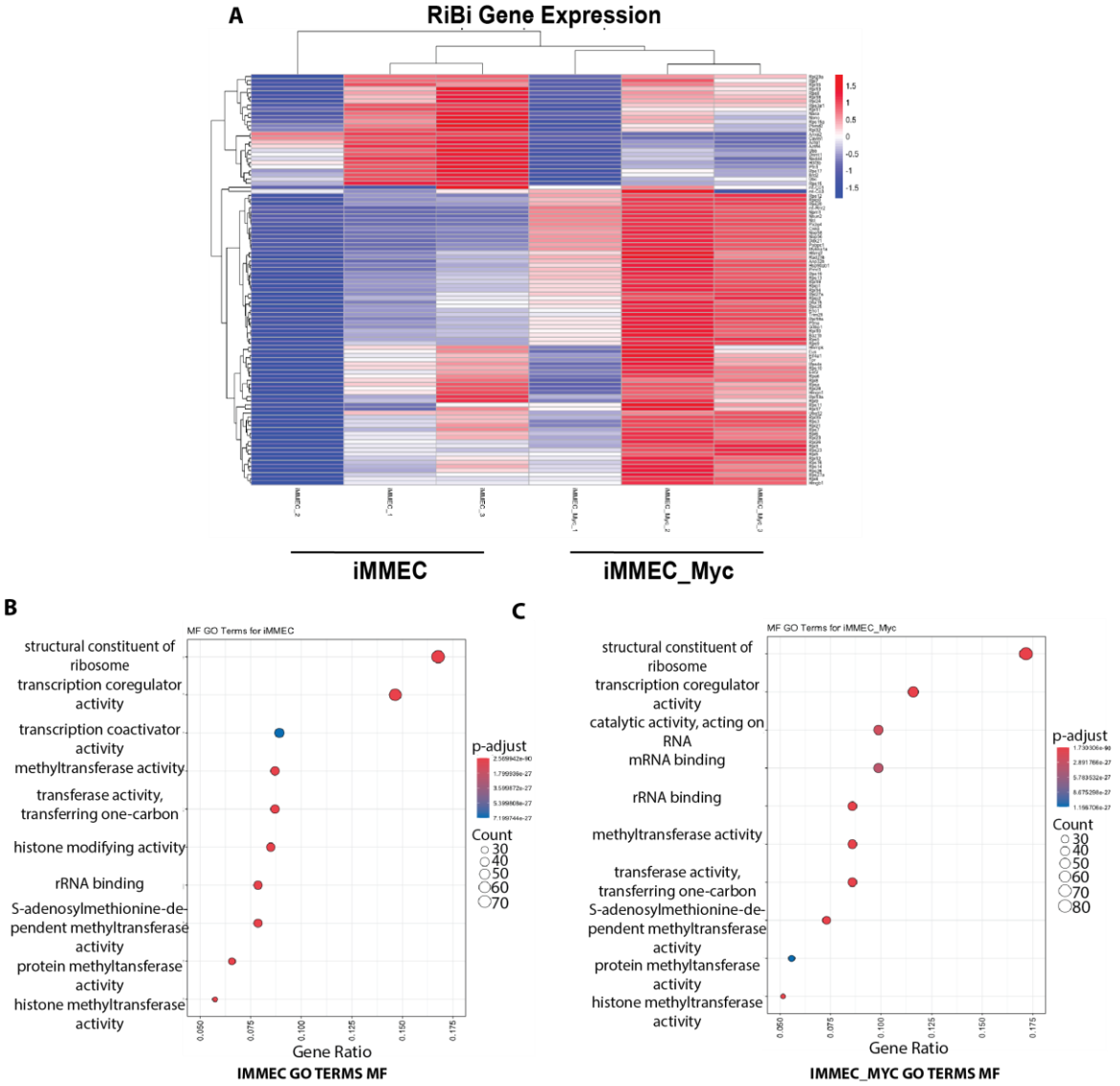



**Appendix 5. Histidine is a more efficient LAT1 exchange substrate than asparagine or glutamine.**
Intracellular total abundance of indicated amino acids in MYAZ16.1e cells starved or preloaded with 1.0 mM of histidine, asparagine, or glutamine, and replenished with DMEM with vehicle (0.1% DMSO) or JPH203 for 2.5 minutes. Data are presented as mean ± s.d.; two-way ANOVA with Šídák method (*p≤0.05, **p≤0.01, ***p≤0.001, ****p≤0.0001), representative of 1 replicate.

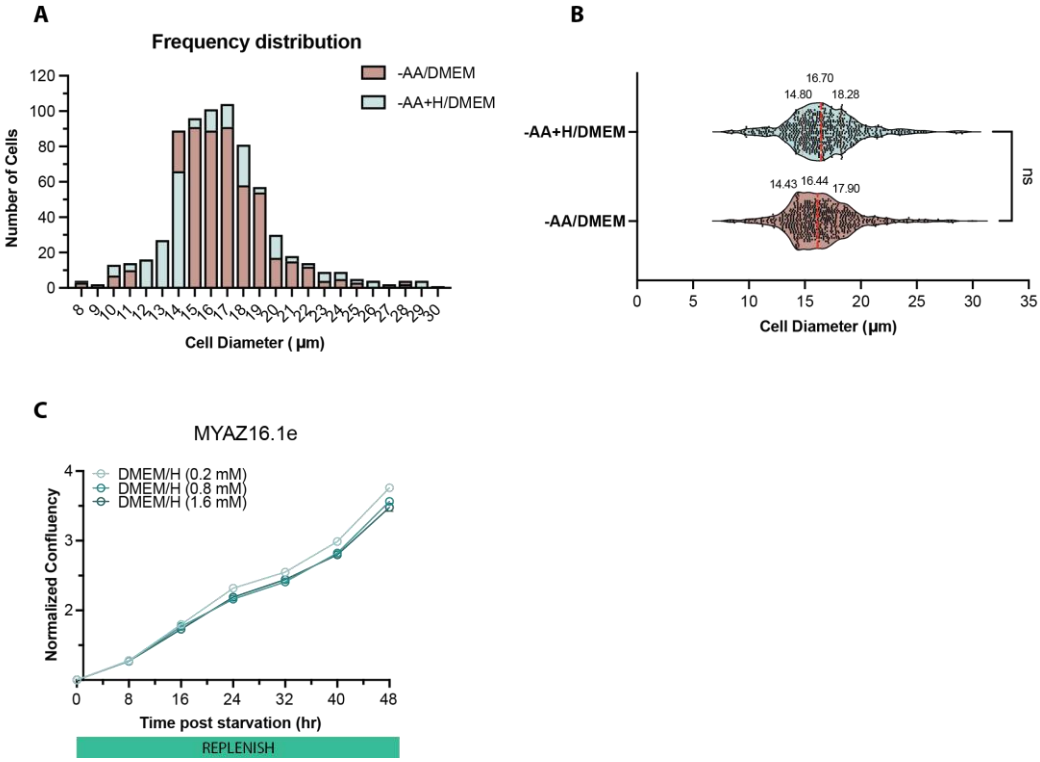



**Appendix 6. Differential activation of RPS6 and inhibition of 4E-BP1 is mediated through mTORC1.**

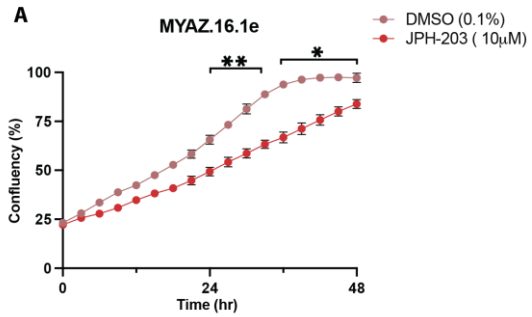
Cells were starved of amino acids or preloaded with 1.6 mM histidine for 48 hours and replenished with DMEM for 10 minutes **(A, B)** Representative WBs assessing RPS6 and 4E-BP1 phosphorylation in BT-549 cells treated with indicated inhibitors for 1 hour prior to and maintained during 10 minutes of DMEM replenishment.



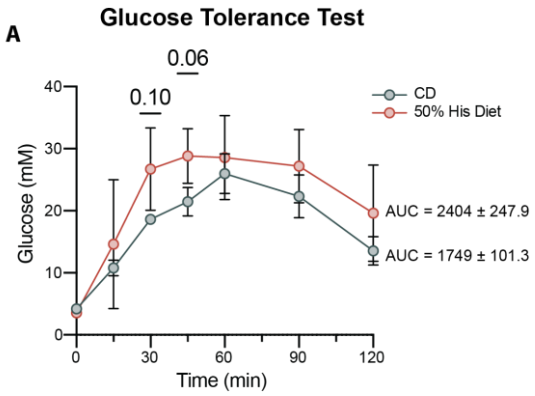

**Appendix 7. MYC regulates ribosome biogenesis.**
RNA sequencing of immortalized mouse mammary epithelial cells (iMMECs) with exogenous expression of Myc (iMMEC_Myc) or the empty vector controls (iMMEC). **(A)** Heatmap depicting the top 100 genes related to ribosome biogenesis, identified by Ensembl IDs, based on average expression across samples. The colour scale represents Z-scores of gene expression values, which were scaled by gene. Hierarchical clustering was applied to the genes. **(B-C)** Dot plots of Gene Ontology (GO) enrichment analysis of molecular function (MF) GO terms for the top 100 differentially expressed genes in **(B)** iMMEC and **(C)** iMMEC_Myc cells. The top 100 genes for each cell line were selected by average expression. Size of dot indicates the number of genes associated with each term and the colour scale indicates the adjusted p-values. P-values were adjusted for multiple testing using the Benjamini-Hochberg method. GO terms are displayed on the y-axis and their significance is reflected on the x-axis.



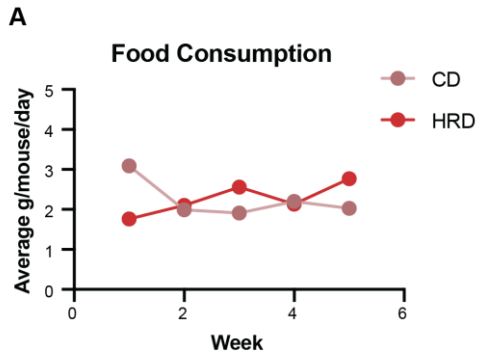

**Appendix 8. Histidine preload does not significantly affect cell size.**
MYAZ16.1e cells were starved of amino acids (-AA) or preloaded with 1.6 mM histidine (-AA+H) for 48 hours prior to 24 hours of DMEM replenishment. **(A, B)** Frequency and distribution of cell size measured by automated haemocytometer. N=604 starved cells and N=676 preloaded cells (unpaired t-test). **(C)** Confluency of MYAZ16.1e cells starved of amino acids for 48 hours and replenished with DMEM containing indicated concentrations of histidine normalized to the confluency before initiating replenishment. Data represent mean ± s.d. representative of 1 independent replicate.



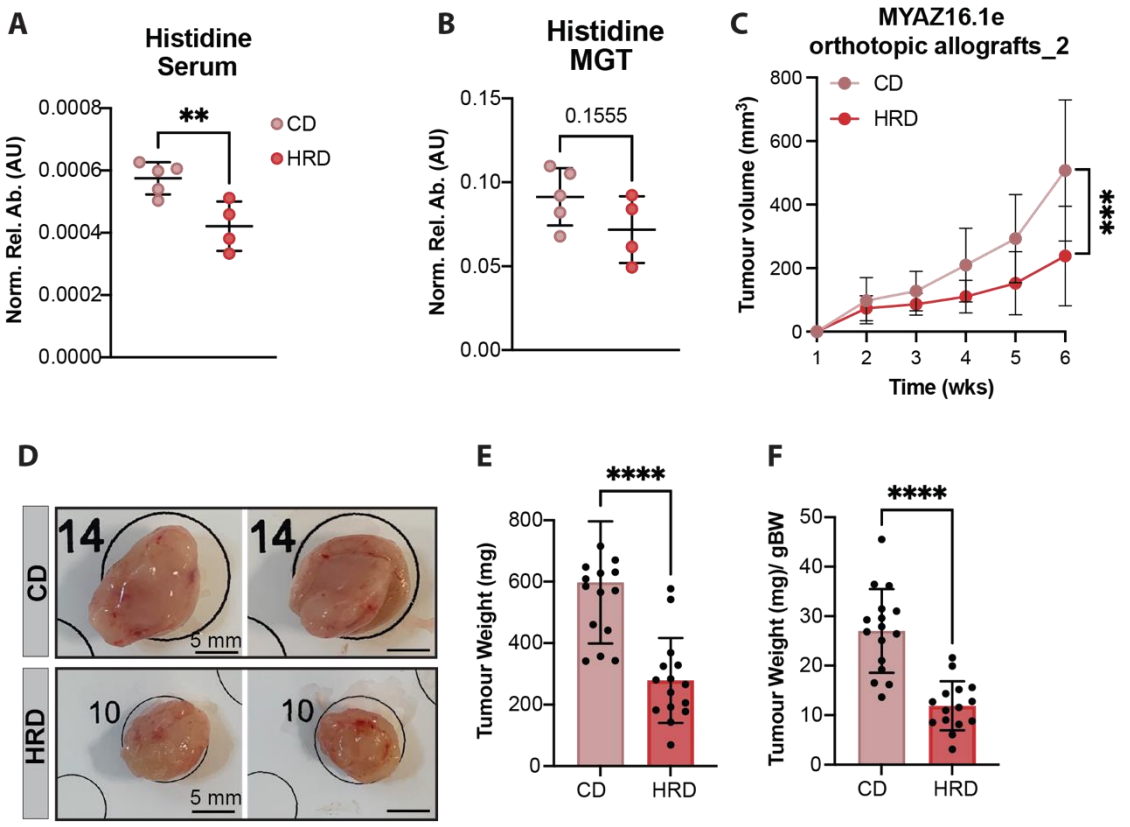

**Appendix 9. LAT1 inhibition by JPH203 significantly retards cell proliferation.**
**(A)** Confluency of MYAZ16.1e cells was imaged every 4 hours for 48 hours in the presence of DMSO or 10 µMJPH203. Data are presented as mean ± s.d.; repeated measures two-way ANOVA with Geisser-Greenhouse correction and Šídák for multiple comparisons. Representative of 1 replicate, *p≤0.05, **p≤0.01.




**Appendix 10. Mice fed a 50% histidine diet have impaired glucose clearance.**
**(A)** Blood glucose levels in FVB/N wild-type mice placed on a CD (100% histidine) or 50% histidine diet (n=4 per group). Mice were fasted overnight and injected with 2 mg/kg body weight glucose via IP injection and blood glucose levels were measured at baseline and every 15 minutes for the first hour and every half hour thereafter for a total of 2 hours. Data are presented as mean ± s.d.; repeated measures two-way ANOVA with Geisser-Greenhouse correction and Šídák for multiple comparisons.




**Appendix 11. Mice fed a HRD do not have significantly altered food consumption.**
**(A)** Average daily food consumption was measured in FVB/N mice bearing MYAZ16.1e orthotopic mammary tumours fed either a CD (n=5) and HRD (20% histidine, n=5) for 4 weeks, following a 1-week diet acclimation period. Average daily food consumption was calculated by measuring the difference in the weight of the diet at the start and end of each week, then dividing by the days and number of animals per cage




**Appendix 12. A HRD significantly reduces Myc-driven tumour growth.**
An additional cohort of FVB/N mice placed on a CD (control diet, n=16) or HRD (histidine reduced diet, n=15) at 4-6 weeks of age, and MGTs were initiated through an orthotopic subcutaneous injection of MYAZ16.1e cells. **(A, B)** LC-MS analysis of total histidine abundance in the **(A)** serum and **(B)** MGT on the CD (n=5) and HRD (n=4). Unpaired two-tailed t-test. **(C)** Tumour volume of mice on the CD (n=25) and HRD (n=25). Data are presented as mean ± s.d.; repeated measures two-way ANOVA with Geisser-Greenhouse correction and Šídák for multiple comparisons. **(D)** Images of representative tumours. **(E)** Tumour weight at collection and **(F)** Tumour weight normalized to grams bodyweight. Data are presented as mean ± s.d.; unpaired two-tailed t-test. **p≤0.01, ***p≤0.001, ****p≤0.0001.